

PROTEINOPATHIES, PROTEOTOXICITY AND TRIAGING IN NEURODEGENERATIVE DISORDERS

**A Thesis Submitted in The Partial Fulfillment of
The Requirement for The Degree of**

DOCTOR OF PHILOSOPHY

By

MEHAR SAHU

(2K21/PHDBT/03)

Under The Supervision of

PROF. PRAVIR KUMAR

**Professor and Former Head
Department of Biotechnology
Delhi Technological University, Delhi**



Department of Biotechnology

**DELHI TECHNOLOGICAL UNIVERSITY
(Formerly Delhi College of Engineering)
Shahbad Daulatpur, Bawana Road, Delhi – 110042, India**

November 2024



DELHI TECHNOLOGICAL UNIVERSITY
(Formerly Delhi College of Engineering)
Shahbad Daulatpur, Main Bawana Road, Delhi-42

CANDIDATE'S DECLARATION

I Mehar Sahu, hereby certify that the work which is being presented in the thesis entitled “Proteinopathies, Proteotoxicity and Triaging in Neurodegenerative Disorders” in partial fulfillment of the requirements for the award of the Degree of Doctor of Philosophy, submitted in the Department of Biotechnology, Delhi Technological University is an authentic record of my own work carried out during the period from 02.08.2021 to 06.08.2024 under the supervision of Prof. Pravir Kumar, Department of Biotechnology, Delhi Technological University.

The matter presented in the thesis has not been submitted by me for the award of any other degree from this or any other institute.

Candidate's Signature
Mehar Sahu
2K21/PHDBT/03

This is to certify that the student has incorporated all the corrections suggested by the examiners in the thesis and statement made by the candidate is correct to the best of our knowledge.

Signature of Supervisor
25/11/2024

Signature of External Examiners



DELHI TECHNOLOGICAL UNIVERSITY
(Formerly Delhi College of Engineering)
Shahbad Daulatpur, Main Bawana Road, Delhi-42

CERTIFICATE BY THE SUPERVISOR

Certified that **Mehar Sahu** (2K21/PHDBT/03) has carried out her search work presented in this thesis entitled “**Proteinopathies, Proteotoxicity and Triaging in Neurodegenerative Disorders**” for the award of Doctor of Philosophy from the Department of Biotechnology, Delhi Technological University, Delhi, under my supervision. The thesis embodies the results of the original work, and studies are carried out by the student herself. The contents of the thesis do not form the basis for the award of any other degree to the candidate or to anybody else from this or any other University/Institution.

Date: 21-10-2024

Yashaswini
21.10.24

Prof. Yasha Hasija
Head of Department & DRC Chairperson
Department of Biotechnology
Delhi Technological University
Delhi - 110042

Pravir Kumar
21/10/2024

Prof. Pravir Kumar
Professor and Dean International Affairs
Department of Biotechnology
Delhi Technological University
Delhi - 110042

ACKNOWLEDGEMENTS

First and foremost, I bow down to **God**, the Almighty for his grace, blessings, and countless love from the inception to the completion of this research work. During the complete course of this work, I have felt the grace of God which enlightens my knowledge and thoughts. This thesis appears in its current form due to the motivation and guidance of many people. I would therefore like to acknowledge all of them.

I would like to express my gratitude to **Prof. Prateek Sharma**, Vice-Chancellor, Delhi Technological University, Delhi for providing me the opportunity to carry out this work in this prestigious institute. Further, I express my gratitude to **Prof. Indu Sreedevi**, **Prof. Jai Prakash Saini**, and **Prof. Yogesh Singh**, Former Vice-Chancellors of Delhi Technological University, Delhi for providing me the opportunity and infrastructure to complete this work.

With pleasure, I am deeply grateful to **Prof. Pravir Kumar**, Dean of International Affairs, Former Head of the Department of Biotechnology, and Former DRC Chairman at Delhi Technological University, Delhi for admitting me under his sole supervision. His enlightening guidance, intelligent approach, constructive critique, and wholehearted and ever-available help have been the primary motivation behind my research. Without his wise advice and guidance, it would have been impossible to complete the thesis in this manner.

The unwavering guidance and support from **Dr. Rashmi Ambasta**, Associate Professor at SRM University, Haryana, and former CSIR Scientist at Delhi Technological University, Delhi, has been pivotal in shaping my research direction and elevating the quality of my work. I am appreciative of the invaluable discussions, insightful feedback, and the autonomy she afforded me to innovate and explore novel ideas.

I would like to thank my fellow lab mates **Neetu Rani**, **Rahul Tripathi**, **Shrutikirti Vashishth**, and **Shefali Kardam** for their invaluable help and unwavering encouragement throughout my research. I also extend my heartfelt thanks to my seniors, **Dr. Rohan Gupta**, **Dr. Smita Kumari**, **Dr. Sudhanshu Sharma**, and **Dr. Dia Advani**, for their genuine support.

Special shoutout and big thanks to **Dr. Rohan Gupta**, **Neetu Rani**, **Rahul Tripathi**, and **Devesh Srivastava**. They were my rock-solid support system throughout this amazing journey.

This journey's success is attributed to the unwavering positivity and hope brought by my mother, **Mrs. Rekha Sahu**, and my aunt, **Dr. Neelima Thakur**.

Finally, I dedicate my thesis to my late father, **Mr. Satya Narayan Sahu**, whose words of wisdom continue to guide me and have shaped me into the person I am today. I know he is celebrating my success in the heavenly kingdom.



Dedication

*This thesis is dedicated to my beloved father,
Late Satya Narayan Sahu,
Who always said I am a Fighter and a Child of God.*



PROTEINOPATHIES, PROTEOTOXICITY AND TRIAGING IN NEURODEGENERATIVE DISORDERS

Mehar Sahu

(2K21/PHDBT/03)

ABSTRACT

Lysine-based post-translational modifications (PTMs) such as acylation, acetylation, deamination, methylation, SUMOylation, and ubiquitination have proven to be major regulators of gene expression, chromatin structure, protein stability, protein-protein interaction, protein degradation, and cellular localization. However, besides all the PTMs, ubiquitination stands as the second most common PTM after phosphorylation that is involved in the etiology of neurodegenerative diseases (NDDs) namely, Alzheimer's disease (AD) and Parkinson's disease (PD). NDDs are characterized by the accumulation of misfolded protein aggregates in the brain that lead to disease-related gene mutation and irregular protein homeostasis. The ubiquitin-proteasome system (UPS) is in charge of degrading these misfolded proteins, which involve an interplay of E1, E2, E3, and deubiquitinase enzymes. Impaired UPS has been commonly observed in NDDs and E3 ligases are the key members of the UPS, thus, dysfunction of the same can accelerate the neurodegeneration process. Therefore, this study explores the impact of point mutation on BRCA1, BARD1, RNF8, and RNF168. All these E3 ligases are involved in the DNA repair mechanism following a complex ubiquitination cascade. The first study concludes BRCA1, a potential E3 ligase common in both AD and PD, and RING domain mutation at sites K32 and K45 possibly disturbs its interaction with its E2, Ube2k. BRCA1 is mostly found in a heterodimeric state, tightly bonded with BARD1. BRCA1 operates its DNA repair mechanism primarily in the nucleus and any DNA repair deficiencies result in neurodegeneration, particularly AD. Therefore, the second study investigates the impact of BARD1 mutation on the binding affinity of BRCA1 with UbcH5c, H2A, and Tau. The result concludes, L44A mutation significantly destabilizes BARD1 and its interaction with BRCA1, although no significant deviations were observed in BRCA1-BARD1

(L44A) docked with UbcH5c. However, destabilization of BRCA1-BARD1(L44A) with H2A and stabilization with Tau are noted, underscoring the importance of the RING domain mutation of BARD1 on BRCA1 and its interactions with UbcH5c, H2A, and Tau. However, RNF8 and RNF168 are crucial E3 ligases that are recruited first to the site of DNA damage. RNF8 initiates the conjugation of ubiquitin with H2A and H2AX, subsequently, RNF168 is employed to amplify the K-63-linked ubiquitin chain. These two E3 ligases are necessary for the downstream signaling where 53BP1 and BRCA1 are recruited. RNF168 directs 53BP1 involvement in non-homologous end joining (NHEJ) but is unable to save BRCA1 which is involved in homologous recombination (HR); therefore, RNF8 plays a huge role in the recruitment of BRCA1. Thus, the third and fourth studies are on assessing the impact of mutagenesis of RNF8 and RNF168 on its binding with E2 conjugating enzyme, UBE2N and UbcH5c, respectively. The RING domain of RNF8 was taken and its interacting sites with UBE2N were carefully studied. The result depicted that I405, S407, E408, E429, R433, P438, I439, and R441 could be possible sites that affect the binding of RNF8 with UBE2N and thereby hampering its E3 ligase activity. Likewise, mutagenesis on RNF168 at C31G and C50G stood as potential sites that could hamper its E3 ligase activity. However, this study was further continued where warheads of PROTACs were screened and docked with these mutants so that they could be marked for degradation by UPS. The inclusive result inferred that Warhead 4 (Ligand 4) (UniProt ID: Q86U86) and Warhead 13 (Ligand 11) (UniProt ID: P51531) were potential ligands that represented better binding and stability than the wild-type structure. C31G with warhead 11 showed exceptional binding and stability. Overall, the study tries to identify potential mutants that can affect the binding affinity of E3 ligases, BRCA1, BARD1, RNF8, and RNF168 with their corresponding E2-conjugating enzymes, disturbing its E3 ligase activity.

LIST OF PUBLICATIONS

1. **Sahu, M.**, Rani, N., Kumar, P. (2024). Simulation and Computational Study of RING Domain Mutants of BRCA1 and Ube2k in AD/PD Pathophysiology. *Molecular Biotechnology*, 1–21. <https://doi.org/10.1007/S12033-023-01006-4/METRICS> [SCIE, IF: 2.4]
2. **Sahu, M.**, Gupta, R., Ambasta, R. K., Kumar, P. (2024). IoT-driven augmented reality and virtual reality systems in neurological sciences. *Internet of Things*, 25, 101098. <https://doi.org/10.1016/J.IOT.2024.101098> [SCIE, IF: 6.0]
3. **Sahu, M.**, Ambasta, R. K., Das R. S, Mishra K. M., Shanker A., & Kumar, P. (2024). Harnessing Brainwave Entrainment: A Non-Invasive Strategy to Alleviate Neurological Disorder Symptoms. *Ageing Research Reviews*, 102547. <https://doi.org/10.1016/j.arr.2024.102547> [SCIE, IF: 12.5]
4. **Sahu, M.**, Tripathi, R., Jha, N. K., Jha, S. K., Ambasta, R. K., & Kumar, P. (2022). Cross talk mechanism of disturbed sleep patterns in neurological and psychological disorders. *Neuroscience & Biobehavioral Reviews*, 140, 104767. <https://doi.org/10.1016/J.NEUBIOREV.2022.104767> [SCIE, IF: 7.5]
5. **Sahu, M.**, Vashishth, S., Kukreti, N., Gulia, A., Russell, A., Ambasta, R. K., & Kumar, P. (2024). Synergizing drug repurposing and target identification for neurodegenerative diseases. *Progress in Molecular Biology and Translational Science*, 205, 111–169. <https://doi.org/10.1016/BS.PMBTS.2024.03.023> [IF: 3.6]
6. **Sahu, M.**, Gupta, R., Ambasta, R. K., & Kumar, P. (2022). Artificial intelligence and machine learning in precision medicine: A paradigm shift in big data analysis. *Progress in Molecular Biology and Translational Science*. <https://doi.org/10.1016/BS.PMBTS.2022.03.002> [IF: 3.6]
7. **Sahu, M.**, & Kumar, P. (2023a). E3 ligase activity of RNF168 at stake on ring domain mutation. *Journal of the Neurological Sciences*, 455, 121447. <https://doi.org/10.1016/j.jns.2023.121447> [SCIE, IF: 3.6]
8. **Sahu, M.**, & Kumar, P. (2023b). RING Domain Mutation Hinders the E3 Ligase Activity of RNF8 and Affects UBE2N Binding. 2023 International Conference on Network, Multimedia and Information Technology, NMITCON 2023. <https://doi.org/10.1109/NMITCON58196.2023.10276155>

9. Rani, N., **Sahu, M.**, Ambasta, R. K., & Kumar, P. (2024). Triaging between post-translational modification of cell cycle regulators and their therapeutics in neurodegenerative diseases. *Ageing Research Reviews*, 94, 102174. <https://doi.org/10.1016/J.ARR.2023.102174> [SCIE, IF: 12.5]
10. Gupta, R., **Sahu, M.**, Srivastava, D., Tiwari, S., Ambasta, R. K., & Kumar, P. (2021). Post-translational modifications: Regulators of neurodegenerative proteinopathies. In *Ageing Research Reviews* (Vol. 68). Elsevier Ireland Ltd. <https://doi.org/10.1016/j.arr.2021.101336> [SCIE, IF: 12.5]
11. Gupta, R., **Sahu, M.**, Tripathi, R., Ambasta, R. K., & Kumar, P. (2022). Protein S-sulfhydration: Unraveling the prospective of hydrogen sulfide in the brain, vasculature and neurological manifestations. *Ageing Research Reviews*, 76, 101579. <https://doi.org/10.1016/J.ARR.2022.101579> [SCIE, IF: 12.5]
12. Gupta, R., Srivastava, D., **Sahu, M.**, Tiwari, S., Ambasta, R. K., & Kumar, P. (2021). Artificial intelligence to deep learning: machine intelligence approach for drug discovery. *Molecular Diversity*. <https://doi.org/10.1007/s11030-021-10217-3> [SCIE, IF: 3.9]
13. Tripathi, R., Gupta, R., **Sahu, M.**, Srivastava, D., Das, A., Ambasta, R. K., & Kumar, P. (2021). Free radical biology in neurological manifestations: mechanisms to therapeutics interventions. *Environmental Science and Pollution Research* 2021, 1–48. <https://doi.org/10.1007/S11356-021-16693-2> [SCIE]

LIST OF TABLES

S. NO.	TITLE	PAGE NO.
CHAPTER 4		
Table 4.1.	Top ten hub genes and their involvement in various pathways	38
Table 4.2.	Comparative result of lysine residues of wild-type BRCA1 and their mutants based on size, charge, and hydrophobicity	48
Table 4.3.	Active and passive sites of BRCA1-BARD1 and Ube2k identified using CPORT	50
Table 4.4.	Topological features of the binding site of BRCA1 and UbCH5c on BARD1	59
Table 4.5.	Physio-chemical properties of potential residues	60
Table 4.6.	Pocket prediction for PDB ID:1JM7 and 8GRQ	62
Table 4.7.	Average RMSD of wild-type and mutants	78
Table 4.8.	Pocket prediction for PDB ID: 8SN2	81
Table 4.9.	Structure stability analysis of top mutants of RNF168	83
Table 4.10.	Protein-Peptide docking results of RNF168	84
Table 4.11.	Potential warheads screened out to dock with mutant RNF168	86
Table 4.12.	Molecular docking results of RNF168 (WT/Mutants) with warheads	87

LIST OF FIGURES

S. NO.	TITLE	PAGE NO.
CHAPTER 1		
Fig. 1.1.	The study revolves around the key E3 ligases, BRCA1, BRCA1-BARD1, RNF8, and RNF168	6
CHAPTER 2		
Fig. 2.1.	Sequence of E3 ligases involved in double-stranded break repair	11
Fig. 2.2.	Schematic representation of BRCA1 illustrating its involvement in neurodegeneration	12
Fig. 2.3.	Two scenarios depicting normal and Alzheimer's disease case to illustrate the functioning of BRCA1-BARD1 in the event of a point mutation in BARD1	13
Fig. 2.4.	RNF8 and RNF168 mediated ubiquitination at double-stranded	15
Fig. 2.5.	Diagrammatic representation of PROTAC molecule's core structure and its action mechanism in promoting target degradation	17
CHAPTER 3		
Fig. 3.1.	Methodology for identifying BRCA1	19
Fig. 3.2.	Methodology for identifying BRCA1-BARD1	24
Fig. 3.3.	Methodology for identifying RNF8	29
Fig. 3.4.	Methodology for identifying RNF168	31
CHAPTER 4		
Fig. 4.1.	Steps involved in identifying E3 ligases that are common in both AD and PD	36
Fig. 4.2.	Protein-protein interaction network of 74 genes and highlighting top 10 hub genes	37
Fig. 4.3.	Gene enrichment analysis of hub genes	41
Fig. 4.4.	Evolutionary conservation studies and pocket prediction of BRCA1, PML, and TRIM33	44
Fig. 4.5.	Steps involved in studying mutation in the RING domain of BRCA1	45
Fig. 4.6.	Prediction of disease-related mutations by PredictSNP, PhD-SNP, PolyPhen-1, PolyPhen-2, SIFT, SNAP, and PANTHER	47
Fig. 4.7.	Diagrammatic view of 3 active sites observed in the RING domain of BRCA1	51
Fig. 4.8.	Molecular dynamics simulation of wild-type and mutants of BRCA1 – K32Y, K32L, K32C, K45V, K45Y, and K45G at 20 ns	53

Fig. 4.9.	Molecular dynamics simulation of wild-type and mutants K32L and K45Y at 50 ns	54
Fig. 4.10.	Visual representation of how BRCA1-BARD1 interacts with E2-UbcH5c and the nucleosome core protein-H2A	56
Fig. 4.11.	Predicted Alignment Error (PAE) plot of BARD1	58
Fig. 4.12.	Docking performed for both wild-type and mutant structures of BRCA1-BARD1, BRCA1-BARD1-UbcH5c, BRCA1-BARD1-H2A, and BRCA1-BARD1-Tau	66
Fig. 4.13.	Molecular dynamics simulations conducted for both wild-type and mutant structures of BARD1, including S37G, A40H, L44A, L47A, and M104K, over a period of 50 ns	68
Fig. 4.14.	Illustration of RMSF and RG of both wild-type and mutant structures of BARD1, including S37G, A40H, L44A, L47A, and M104K	69
Fig. 4.15.	Molecular dynamic simulation conducted for both wild-type and mutant structures of BRCA1-BARD1 (L44A) and BRCA1-BARD1 (L44A)-UbcH5c for 50 ns	70
Fig. 4.16.	Molecular dynamic simulation carried out for both wild-type and mutant structures of BRCA1-BARD1 (L44A)-H2A and BRCA1-BARD1 (L44A)-Tau over a 50 ns period	72
Fig. 4.17.	Protein-protein interaction network, gene co-expression, and domain structures of RNF8 and its other interacting partners	73
Fig. 4.18.	Predicted Aligned Error (PAE) plot to demarcate FHA and RING domain of RNF8	74
Fig. 4.19.	Topology of predicted residues using ConSurf and I-TASSER	75
Fig. 4.20.	Evolutionary conservation score of each predicted site using AlphaFold and ConSurf	76
Fig. 4.21.	Comparison of Z-score between wild-type and mutants of RNF8 using HADDOCK	77
Fig. 4.22.	Result of protein-peptide docking of wild-type and their mutants of RNF8 using CABS-dock	77
Fig. 4.23.	STRING analysis depicting a close relationship of RNF168 with the E2-conjugating enzyme UBE2D3 and the E3 ligase complex BRCA1-BARD1	79
Fig. 4.24.	Secondary structure prediction of RNF168	80
Fig. 4.25.	Protein-Protein docking results of RNF168	85
Fig. 4.26.	Molecular dynamic simulation results: Comparison of RMSD between wild-type and mutants of RNF168	89
Fig. 4.27.	Molecular dynamic simulation results: Comparison of RMSF between wild-type and mutants of RNF168	90

Fig. 4.28.	Molecular dynamic simulation results: Comparison of RG between wild-type and mutants of RNF168	91
Fig. 4.29.	Molecular dynamic simulation results: Comparison of RMSD, RMSF, and RG between wild-type and mutants of RNF168 when docked with E2-conjugating enzyme, UbcH5c	93
Fig. 4.30.	Molecular dynamic simulation results: Comparison of RMSD, RMSF, RG, RMSD_LIG, RG_LIG, and H-BONDS between wild-type and mutants (C31G and C50G) of RNF168 when docked with Ligand 4	95
Fig. 4.31.	Molecular dynamic simulation results: Comparison of RMSD, RMSF, RG, RMSD_LIG, RG_LIG, and H-BONDS between wild-type and mutants (C31G and C50G) of RNF168 when docked with Ligand 11	96

CHAPTER 5

Fig. 5.1.	The illustration depicting the hypothesis regarding the normal and aberrant behavior of the BRCA1-BARD1 heterodimer upon the BARD1 mutation at L44A	102
Fig. 5.2.	The major finding of the entire study	105

LIST OF SYMBOLS AND ABBREVIATIONS

PTM	Post-Translational Modification
Ub	Ubiquitin
E1	Ub-Activating Enzyme
E2	Ub-Conjugating Enzyme
E3	Ub-Ligase
DUBs	Deubiquitinase
UPS	Ubiquitin-Proteasome System
NDDs	Neurodegenerative Diseases
AD	Alzheimer's Disease
PD	Parkinson's Disease
HD	Huntington's Disease
ALS	Amyotrophic Lateral Sclerosis
RING	Really Interesting New Gene
HECT	Homologous with E6 Associated Protein C Terminus
RBR	RING Between RING
PRC1	Polycomb Repressive Complex 1
NFTs	Neurofibrillary Tangles
BBB	Blood-Brain Barrier
ROS	Reactive Oxygen Species
SSBs	Single-Stranded Breaks
DSBs	Double-Stranded Breaks
BRCA1	Breast Cancer Gene 1
BARD1	BRCA1-associated RING domain protein
RNF8	Ring Finger Protein 8
RNF168	Ring Finger Protein 168
PROTACs	Proteolysis Targeting Chimeras
GEO	Gene Expression Omnibus
NCBI	National Centre For Biotechnology Information
DEGs	Differentially Expressed Genes
ESBL	Epithelial Systems Biology Library
PAE	Predicted Alignment Error
PDBe-KB	Protein Data Bank in Europe–Knowledge Base
JNK	c-Jun N-terminal kinase
ASK1	Signal-Regulating Kinase 1
MDS	Molecular Dynamics Simulation
RMSD	Root Mean Square Deviation
RMSF	Root Mean Square Fluctuation
RG	Radius Of Gyration
GO	Gene Ontology
HMMER	Hidden Markov Model Method
IR	Ionizing Radiation
POI	Protein Of Interest
$\Delta\Delta G$	Folding Free Energy

CONTENTS

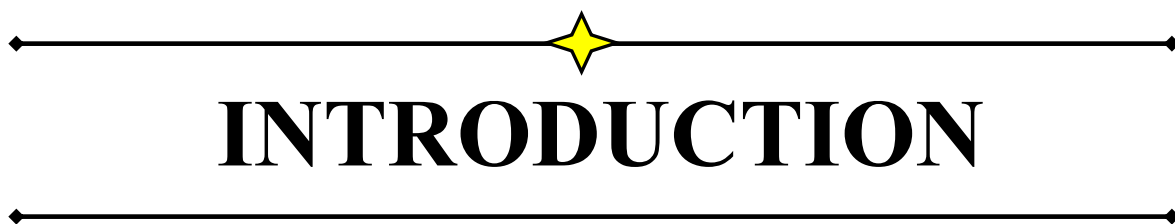
TITLE	PAGE NO.
<i>Certificates</i>	ii
<i>Acknowledgments</i>	iv
<i>Declaration</i>	v
<i>Abstract</i>	vi
<i>List of Publications</i>	viii
<i>List of Tables</i>	x
<i>List of Figures</i>	xi
<i>List of Symbols and Abbreviations</i>	xiv
CHAPTER 1	INTRODUCTION
1.1.	Overview
1.2.	Research Motivation
1.3.	Objectives
1.4.	Summary of the Thesis
CHAPTER 2	REVIEW OF LITERATURE
2.1.	Neurodegenerative Diseases
2.2.	PTM: Ubiquitination
2.3.	Crucial Role of E3 Ligases
2.4.	DNA Damage and Complexes Involved in the DNA Repair
2.5.	BRCA1
2.6.	BARD1
2.7.	RNF8 and RNF168
2.8.	PROTACs
CHAPTER 3	MATERIALS AND METHODS
3.1.	Methodology – BRCA1
3.1.1.	Data Retrieval
3.1.2.	Data Pre-Processing and Screening of Differentially Expressed Genes
3.1.3.	Screening of Common Ubiquitin E3 Ligase and DEGs Through Venn Analysis
3.1.4.	Protein-Protein Interaction (PPI) Analysis
3.1.5.	Pathway Enrichment Analysis of E3 Ubiquitin Ligases
3.1.6.	Domain and Motif Analysis
3.1.7.	Prediction of Post-translational Modification Sites
3.1.8.	Prediction of Deleterious Mutations and Their Impact on Structural and Functional Stability
3.1.9.	Structure Preparation
3.1.10.	Molecular Docking
3.1.11.	Molecular Dynamics Simulation

3.2.	Methodology – BRCA1-BARD1	24
3.2.1.	Extraction of Structures: BRCA1-BARD1, UbcH5c, H2A, and Tau	24
3.2.2.	Screening and Assessment of Potential Sites in the RING Domain of BARD1	25
3.2.3.	Structural and Functional Topology Studies of Qualified Residues	25
3.2.4.	Mutagenesis of BARD1	26
3.2.5.	Visualization and Preparation of Structures	26
3.2.6.	Pocket Prediction and Molecular Docking Studies	27
3.2.7.	Molecular Dynamics Simulation	28
3.3.	Methodology – RNF8	29
3.3.1.	Network Analysis of RNF8	29
3.3.2.	Structure Retrieval and Preparation of RNF8 and UBE2N	29
3.3.3.	Domain Analysis	30
3.3.4.	Screening of Site of Interaction of UBE2N on RNF8	30
3.3.5.	Evolutionary Conservation Of Interacting Sites	30
3.3.6.	Mutational Studies of RNF8	30
3.3.7.	Protein-Protein and Protein-Peptide Docking	30
3.4.	Methodology – RNF168	31
3.4.1.	Extraction and Preparation of Structures: RNF168 and UbcH5c	32
3.4.2.	Secondary Structure Prediction of RNF168	32
3.4.3.	Domain Structure Analysis of RNF168	32
3.4.4.	Pocket Prediction of RNF168	32
3.4.5.	Mutagenesis and Domain Mapping of Disease Mutation in RNF168	33
3.4.6.	Disease Tolerability and Stability Analysis of Mutated Structures	33
3.4.7.	Obtaining, Screening, and Preparing Warheads for Therapeutics: A Unique Part of PROTACs	33
3.4.8.	Molecular Docking Studies (E3-E2 and Mutant E3-Warhead)	34
3.4.9.	Molecular Dynamics Studies to Assess the Functionality of RNF168	34
CHAPTER 4	RESULTS	35
4.1.	Results I (Objective I)	36
4.1.1.	Common E3 Ligase in AD and PD	37
4.1.2.	Functional Enrichment Analysis of E3 Ligases in AD-PD Crosstalk	38
4.1.3.	Protein Motif Discovery and RING Domain Analysis	39

	4.1.4.	Structure Characterization of BRCA1, PML and TRIM33	43
4.2.		Results I (Objective II)	45
	4.2.1.	Mutagenesis and its Stability Analysis on RING Domain of BRCA1	46
	4.2.2.	BRCA1-BARD1 Docking with Ube2k	49
	4.2.3.	Molecular Dynamics Simulation of Protein-Protein Docked Structure	52
4.3.		Results II (Objective II)	55
	4.3.1.	Recruitment, Visualization, and Preparation of Structures: BRCA1-BARD1, UbcH5c, H2A, and Tau	55
	4.3.2.	Unraveling the Interacting Residues of RING Domain of BARD1	57
	4.3.3.	Structural and Functional Characterization of Interacting Sites	60
	4.3.4.	Mutagenesis Findings of BARD1 Disrupting E3 Ligase Activity of BRCA1	61
	4.3.5.	Predicted Pocket Intervention	62
	4.3.6.	BARD1 Mutants' Impact on BRCA1 Binding with UbcH5c, H2A, Tau	64
	4.3.7.	MDS of Docked Structures	67
4.4.		Results III (Objective II)	73
	4.4.1.	Protein-Protein Interaction and Gene Co-expression of RNF8	73
	4.4.2.	Structural Analysis of RNF8 and UBE2N	74
	4.4.3.	Analysis of RING Domain of RNF8	74
	4.4.4.	Interface Prediction of RNF8 with UBE2N	75
	4.4.5.	Evolutionary Conservation Analysis	75
	4.4.6.	Mutagenesis of Qualified Sites and its Preparation	76
	4.4.7.	Docking Analysis	76
4.5.		Results IV (Objective II)	78
	4.5.1.	Structure Recruitment of E3 and E2: RNF168 and UbcH5c	78
	4.5.2.	Breakdown of Secondary Structure, Domain, and Pockets of RNF168	79
	4.5.3.	Search for Top Mutants of RNF168	83
	4.5.4.	Tolerability and Stability of Top Mutants	83
	4.5.5.	Impact of RNF168 Mutagenesis on Binding Affinity with UbcH5c	84
4.6.		Results I (Objective III)	86
	4.6.1.	Extraction, Drug Likelihood, and ADME Check of Warheads	86
	4.6.2.	Molecular Docking Analysis of RNF168 (WT/Mutant) with Warheads	87
	4.6.3.	Results of MD Simulation	88

4.6.4.	Control and Mutants of RNF168	88
4.6.5.	E3-E2: RNF168-UbcH5c	92
4.6.6.	RNF168 (Mutant)-Warhead	94
CHAPTER 5	DISCUSSION, CONCLUSION, AND FUTURE PERSPECTIVE	97
5.1.	Discussion	98
5.2.	Conclusion	103
5.3.	Future Perspective	105
REFERENCES		107
LIST OF PUBLICATIONS		121
CURRICULUM VITAE		123

CHAPTER 1



INTRODUCTION

CHAPTER 1

INTRODUCTION

1.1. Overview

Ubiquitination is a post-translational modification (PTM) where ubiquitin (Ub) is covalently attached to a specific protein target, exerting significant influence over protein functionality, stability, and localization. The regulation of this modification involves a series of enzymes, comprising Ub-activating enzyme (E1), Ub-conjugating enzyme (E2), and Ub-ligase (E3). It entails the formation of an isopeptide linkage between the C-terminal glycine residue of Ub and the lysine residue of the targeted protein, leading to mono-ubiquitination, di-ubiquitination, multi-ubiquitination, or poly-ubiquitination [1]. Contrastingly, deubiquitinating enzymes (DUBs) possess the ability to detach the conjugated ubiquitin molecules from the target protein by cleaving either the isopeptide bond or peptide bond which helps in connecting Ub to the N-terminal methionine of the target protein [2]. The ubiquitin-proteasome system (UPS) holds vital significance in the breakdown of targeted proteins, overseeing various facets of cellular functions such as DNA repair, endocytosis, metabolism, signal transduction, immune response, protein quality control, cell proliferation, and cell death [3]. As the regulation of ubiquitination is multifaceted, hence, several factors like the structure of the target protein, availability of ubiquitin molecules, and structural and functional alterations in E3 ligases can greatly influence the efficiency of ubiquitination. Therefore, ubiquitination is a critical PTM, and any changes in it can lead to severe diseases. The exploration of ubiquitination's role in neurodegenerative diseases (NDDs), such as Alzheimer's disease (AD), Parkinson's disease (PD), and Huntington's disease (HD), has gathered significant attention over the past two decades. Evidence suggests that alterations in E3 ligase are associated with the pathophysiology of NDDs, for instance, it has been observed that the implication of mutation in E3 ligases directly affects the ubiquitin signaling cascade [4]. E3 ubiquitin ligases play a vital role in developmental processes and their maintenance is necessary which involves cell signaling, metabolism, transcriptional control, protein sorting, trafficking, and degradation of cellular components. E3 ligases are broadly classified based on their catalytic activities: homologous with E6 associated protein C terminus (HECT), U-Box, really interesting new gene (RING), and RING between RING (RBR) [5]. HECT and RBR type E3 enzymes transfer ubiquitin from the E2-Ub complex to the target whereas, RING and U-Box directly transfer ubiquitin to the substrate [6].

Double-stranded breaks (DSBs) are one of the most lethal types of DNA damage. Where ATM initiates the response to DSBs which results in the

phosphorylation of H2AX. Secondly, MDC1 directly interacts with γ -H2AX and amplifies the signal of DDR. Thereafter, RNF8 and RNF168 E3 ligases are recruited via MDC1. Chromatin bounded RNF8 attaches with E2 conjugating enzyme, UBE2N/UBC13 to ubiquitinate damaged chromatin. On the other hand, a ubiquitinated target X is identified by RNF168 at monoubiquitinates K13-15 on H2A [7]. Both the E3 ligases orchestrate to extend the ubiquitin chain on H2A and maintain genome integrity. Nonetheless, the ubiquitination of H2A is governed by three major E3 ligases namely, RNF8 and RNF168, polycomb repressive complex 1 (PRC1), and BRCA1-BARD1 heterodimer complex. These E3 ligases modify the site of H2A and enable DNA repair that further enhances chromatin compaction [8]. It has been observed that in AD, BRCA1 mislocates to cytoplasmic neurofibrillary tangles (NFTs) which results in DNA fragmentation, however, BARD1 prevents BRCA1 from leaving the nuclear compartment as BRCA1 contributes to DNA repair [9], [10]. The purpose here is to study the impact of mutation in the E3 ligases, BRCA1, BARD1, RNF8, and RNF168 which are called upon to take part in a complex ubiquitination cascade and repair DSBs.

1.2. Research Motivation

- ▶ Post-translational modifications such as acylation, acetylation, deamination, methylation, SUMOylation, and ubiquitination have proven to be major regulators of gene expression, chromatin structure, protein stability, protein-protein interaction, protein degradation, and cellular localization.
- ▶ Ubiquitination stands as the second most common PTM after phosphorylation that is involved in the etiology of neurodegenerative diseases namely, Alzheimer's disease and Parkinson's disease.
- ▶ The ubiquitin-proteasome system removes the toxic metabolites from the cellular milieu by orchestrating a cascade of E1, E2, and E3 enzymes. Missense mutation on E3 can hamper this cascade.
- ▶ Past studies suggest that there is a strong inverse association between cancer and AD that has resulted in increased morbidity and mortality rates. Interestingly, such studies point to one common fact there is a potential link between molecular mechanisms involved in both such that in today's scenario, many anti-cancer treatments are being used against AD.
- ▶ BRCA1 is a tumor suppressor gene that plays a significant role in DNA damage response. Mutations in BRCA1 mark 80% of Breast cancer and ovarian cancer cases in females. Moreover, a study highlights increased cases of BC-AD with age in BC patients.
- ▶ The integral role of BRCA1 as E3 ligase involves the repair of double-stranded breaks and it is evident from past research that BRCA1 carries out ubiquitination of H2A and H2A variants at K125/K127/K129 residues.

- ▶ BARD1 helps BRCA1 to attach with nucleosomes, however, impairment in BARD1 releases BRCA1 from the nucleosome core protein and binds with tau lesion in the cytosol which is a hallmark feature in AD.
- ▶ The unique ubiquitination cascade that initiates DSBs involving several E3 ligases has turned out a crucial signaling pathway that regulates DNA repair.
- ▶ RNF8 is one of the first E3 ligases called upon during DSBs. Its deficiency is enough to cause cognitive decline, whereas, its loss potentially leads to neurodegeneration.
- ▶ RNF168 amplifies RNF8 ubiquitin activity and co-operates in extending the K-63-linked polyubiquitin chain that further recruits RAP80, BRCA1, and 53BP1 which altogether assists in DSB repair.

1.3. Objectives

- ▶ **Objective I** - To dissect the molecular mechanism of ubiquitination and explore the cross-talk mechanism between Alzheimer's and Parkinson's disease at the protein level
- ▶ **Objective II** - To investigate the implication of mutation on E3 ligase activity
- ▶ **Objective III** - To identify the biomolecules involved in the recovery or elimination of mutated protective proteins

1.4. Summary of the Thesis

The thesis is structured into five chapters. **Chapter 1** serves as an introductory section, offering a comprehensive overview of the study. It delves into the underlying motivation driving the research and outlines the specific objectives that have been formulated to guide the study's execution. **Chapter 2** introduces the etiology of neurodegenerative diseases that jeopardize human society and stand as a challenge. It further talks about how post-translational modifications play a crucial role in the pathogenesis of NDDs. There are many PTMs, however, this study focuses on ubiquitination which is a multistep ATP-dependent mechanism involving ubiquitin-activating (E1), conjugating (E2), and ligase (E3) enzymes. The chapter also throws light upon how mutations on E3 ligases can hamper the process of ubiquitination. Double-stranded breaks (DSBs) are one of the most lethal types of DNA damage. The unique ubiquitination cascade initiated on DSBs involves several E3 ligases which is an important signaling pathway that regulates DNA repair. The impact of mutation has been studied on four E3 ligases, namely, BRCA1, BRCA1-BARD1, RNF8, and RNF168. Hence, the detailed operation of each E3 ligase has been discussed in this chapter. In **Chapter 3**, four different methodologies have been described to govern the materials and methods used for mutagenesis in each E3 ligase (BRCA1, BRCA1-BARD1, RNF8, and RNF168) and to assess the impact of mutations on their

functioning. The key steps employed are extraction, screening, domain analysis, pocket prediction, mutational analysis, stability and tolerability investigation, varied docking studies, and molecular dynamic simulation. **Chapter 4** discusses the in-depth results behind each methodology. The results have been described based on the objectives given above. **Result I (Objective I)** stated that 74 E3 ligases were common in both AD and PD. The top10 hub genes were PML, BRCA1, TRIM23, TRIM32, RNF11, TRIM27, UBR2, TRIM37, MID2, and TRIM33. After gene enrichment, evolutionary conservation, and lysine site investigation, the top 3 E3 ligases observed were BRCA1, PML, and TRIM33. The literature survey confirmed BRCA1 as the most influential E3 ligase common in AD and PD. **Result I (Objective II)** specified that in neurodegeneration, BRCA1 acts as a key DNA repair protein. Mutagenesis of K32 and K45 on BRCA1 has a significant impact on its binding with Ube2k. Molecular dynamics simulation validated K32L as the most potential mutant. The broader implication of this result is to elucidate the functional mechanistic insights behind lysine mutation in the RING domain of BRCA1 to find therapeutic interventions for NDDs. **Result II (Objective II)** concludes that mutation (L44A) on the first α -helix bundle of BARD1 not only destabilizes its own structure but also disturbs its heterodimeric conformation with BRCA1. The impact of the L44A mutation on the interaction of BRCA1-BARD1 with UbcH5c appears to be minimal, likely due to UbcH5c's exclusive binding with BRCA1 rather than BARD1. However, the same mutation disrupts the interaction of BRCA1-BARD1 with H2A. Consequently, they fail to interact with H2A and instead become colocalized with tau protein in the cytoplasm. This result concludes with two hypotheses: Hypothesis I - BRCA1 dissociates from BARD1 during the export and subsequently coaggregates with tau. Hypothesis II - Dissociation of BRCA1 from BARD1 happens during coaggregation with tau in the cytoplasm. **Result III (Objective II)** highlights the importance of RNF8 which binds with UBE2N and forms a K-63 linked ubiquitin chain that acts as a framework for other proteins carrying ubiquitin-binding motifs. Both E3 ligases, RNF8 and RNF168 are wanted at the site of DNA damage. RNF168 amplifies RNF8 ubiquitin activity and co-operates in extending the K-63-linked polyubiquitin chain that further recruits RAP80, BRCA1, and 53BP1 which altogether assists in DSB repair. This result states that mutagenesis of RNF8 hampers its binding with E2 conjugating enzyme, UBE2N; possibly compromising the functioning of further E3 ligases involved in the cascade. The top mutants observed on RNF8 are I405, S407, E408, E429, R433, P438, I439, and R441. **Result IV (Objective II)** emphasizes mutational studies on RNF168, the potential mutants observed are C16G, C19G, C31G, H33G, C36G, C39G, C50G, C51G, and C54G. These mutants show poor binding with UbcH5c indicating poor E3 ligase activity. Based on stability and tolerability analysis, C16G, C31G, C39G, C50G, and C51G were studied further. Further, MDS studies filtered out C31 G and C50G as the most potential mutants. **Result I (Objective III)** targets therapeutics primarily focusing on proteolysis

targeting chimeras (PROTACs). Warheads of PROTACs were taken to show strong binding with mutants of RNF168 so that it can be marked for degradation by UPS. Warheads 1, 2, 3, 4, 8, 9, 10, 11, 12, 13, 14, and 15 depicted better binding with mutants. However, Warhead 4 (Ligand 4) and Warhead 13 (Ligand 11) are promising warheads that show better binding with mutants C31G and C50G compared to the wild-type. **Chapter 5**, delves into the discussion, conclusions, and future perspectives surrounding each E3 ligase, including BRCA1, BRCA1-BARD1, RNF8, and RNF168 (**Fig. 1.1**). This is a crucial section that sheds light on the exciting possibilities and implications within this domain.

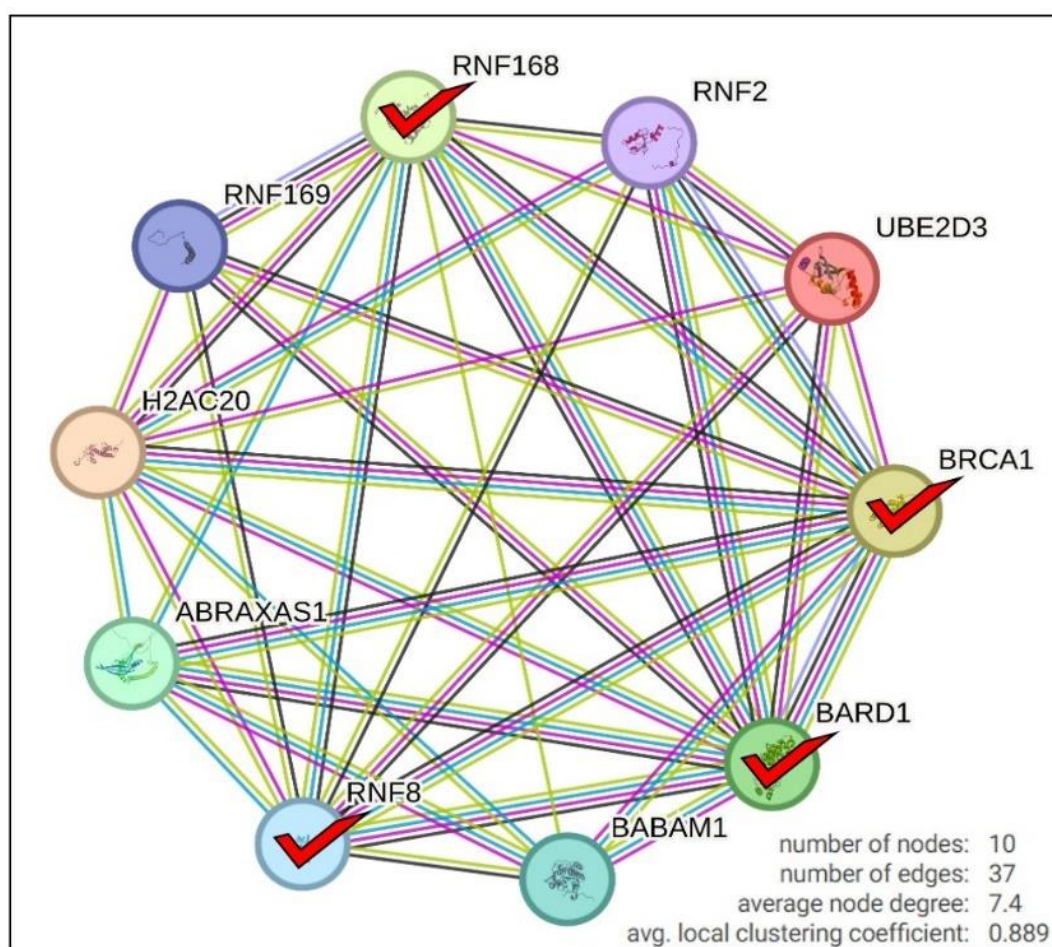


Fig. 1.1. The study revolves around BRCA1, BRCA1-BARD1, RNF8, and RNF168, which are the key E3 ligases.

CHAPTER 2



**LITERATURE OF
REVIEW**



CHAPTER 2

LITERATURE OF REVIEW

2.1. Neurodegenerative Diseases

Despite dedicated research efforts, the absence of disease-curing remedies for neurodegenerative diseases (NDDs) continues to jeopardize human society and stands as a challenge. Scientists and researchers have been focusing on specific genes, a particular site in DNA, a protein, or a molecule that might be involved in the pathogenesis of the disease. However, the new era discusses directing the signaling mechanism involved in the disease progression, where receptors, ion channels, enzymes, and other carrier molecules play a huge role. Neurons play a central role in brain functioning as they have a critical part in neuronal communication. They originate in the brain and are present throughout the body. Neural stem cells produce many neurons during the phase of childhood but are significantly reduced during adulthood. The progressive loss of neurons' structural and functional characteristics leads to neurodegeneration which is a central case in many neurodegenerative diseases such as Alzheimer's disease (AD), Parkinson's disease (PD), Huntington's disease (HD), and Amyotrophic lateral sclerosis (ALS). The pathophysiology of these NDDs is linked with impairment of neural networks, synaptic dysfunction, or accumulation of pathological protein deposits [11]. Various factors predispose to NDDs, for instance, aging, genetic mutations, environmental influences, gut microbiota, and issues related to the blood-brain barrier (BBB) microvascular complications [12].

2.2. PTM: Ubiquitination

Many studies have demonstrated post-translational modifications (PTMs) to play a crucial role in the pathogenesis of NDDs. There are more than fifty types of PTMs and phosphorylation, ubiquitination, acetylation, SUMOylation and methylation are some of the common PTMs. These PTMs are responsible for transcriptional alterations that further leads to mitochondrial dysfunctions, DNA damage, autophagy and apoptosis of the cell [13]. PTMs are crucial in the regulation of many biological processes and their alterations disrupt the genetic regulation that hamper the protein quality control [14]. After phosphorylation, ubiquitination is the second most important PTM linked to several NDDs as it regulates virtually all events in cells [15]. Ubiquitination is a multistep ATP-dependent mechanism involving ubiquitin-activating (E1), conjugating (E2), and ligase (E3) enzymes, which ubiquitinate the misfolded proteins [16]. The Ubiquitin tag is attached to the lysine of the target protein under the regulation of these enzymes which is further marked to the ubiquitin-proteasome system (UPS) for its degradation. The aberration in the

regulatory mechanism of ubiquitination results in the abnormal accumulation of toxic proteins which is a key characteristic feature of many NDDs.

2.3. Crucial Role of E3 Ligases

It entails the formation of an isopeptide linkage between the C-terminal glycine residue of Ub and the lysine residue of the targeted protein, leading to mono-ubiquitination, di-ubiquitination, multi-ubiquitination, or poly-ubiquitination [1]. Contrastingly, deubiquitinating enzymes (DUBs) possess the ability to detach the conjugated ubiquitin molecules from the target protein by cleaving either the isopeptide bond or peptide bond which helps in connecting Ub to the N-terminal methionine of the target protein [2]. The ubiquitin-proteasome system (UPS) holds vital significance in the breakdown of targeted proteins, overseeing various facets of cellular functions such as DNA repair, endocytosis, metabolism, signal transduction, immune response, protein quality control, cell proliferation, and cell death [3]. As the regulation of ubiquitination is multifaceted, hence, several factors like the structure of the target protein, availability of ubiquitin molecules, and structural and functional alterations in E3 ligases can greatly influence the efficiency of ubiquitination. Therefore, ubiquitination is a critical PTM, and any changes in it can lead to severe diseases. The exploration of ubiquitination's role in NDDs, such as Alzheimer's disease, Parkinson's disease, and Huntington's disease, has gathered significant attention over the past two decades.

Evidence suggests that alterations in E3 ligase are associated with the pathophysiology of NDDs, for instance, it has been observed that the implication of mutation in E3 ligases directly affects the ubiquitin signaling cascade [4]. Presently, 2 E1, 35-40 E2, and 600 E3 enzymes have been reported in humans [17]. E3 ubiquitin ligases play a vital role in developmental processes and their maintenance is necessary which involves cell signaling, metabolism, transcriptional control, protein sorting, trafficking, and degradation of cellular components. E3 ligases are broadly classified based on their catalytic activities: homologous with E6 associated protein C terminus (HECT), U-Box, really interesting new gene (RING), and RING between RING (RBR) [5]. HECT and RBR type E3 enzymes transfer ubiquitin from the E2-Ub complex to the target whereas, RING and U-Box directly transfer ubiquitin to the substrate [6]. Nedd4, a HECT-type E3 ligase has been observed to be upregulated in AD, PD, and HD which further ubiquitinates several neuronal receptors to enhance their lysosomal degradation mechanism [18]. Contrarily, Parkin is an RBR-type E3 ligase that has been extensively studied in PD; mutation in the same can lead to the accumulation of damaged mitochondria which contributes to the progression of PD [19]. An example of U-Box-type E3 ligase is the carboxyl terminus of Hsp70-interacting protein (CHIP) that maintains the protein folding homeostasis by refolding or dephosphorylating the pathological proteins, hence, once CHIP becomes

dysfunctional, the degradation process is severely compromised as proteasomal and lysosomal machinery are overburdened [20]. RING-type E3 ligases constitute the largest class of ubiquitin ligases, however, due to the lack of a catalytic center, it becomes difficult to target [21]. For survival, genome stability is of the utmost importance, however, it is constantly being challenged by various endogenous and exogenous processes, such as reactive oxygen species (ROS) and ultraviolet light exposure [22]. If genomic instability persists, it results in single-stranded breaks (SSBs) and double-stranded breaks (DSBs) causing faulty DNA replication and transcription. Past studies have encoded that mutation in E3 ligase genes often results in neurodegenerative and neurodevelopment disorders, for instance, epilepsy, regionalized neuropathies, and intellectual disability [23]. The study of mutations in E3 ligases has considerably increased in the last five years.

2.4. DNA Damage and Complexes Involved in the DNA Repair

Eukaryotic cells have developed a very delicate mechanism to spot and repair different types of DNA damage, jointly known as DNA damage response (DDR). This in turn triggers cell cycle checkpoints to stop further development of cells and activate the DNA damage repair mechanism. DSBs are one of the most lethal types of DNA damage (**Fig. 2.1.**). Where ATM initiates the response to DSBs which results in the phosphorylation of H2AX. Secondly, MDC1 directly interacts with γ -H2AX and amplifies the signal of DDR. Thereafter, RNF8 and RNF168 E3 ligases are recruited via MDC1. Chromatin bounded RNF8 attaches with E2 conjugating enzyme, UBE2N/UBC13 to ubiquitinate damaged chromatin. On the other hand, a ubiquitinated target X is identified by RNF168 that monoubiquitinates K13-15 on H2A [24]. Both the E3 ligases orchestrate to extend the ubiquitin chain on H2A and maintain genome integrity. RNF8 is that it is the first E3 ligase that cooperates with UBE2N and is recruited to the site of DSB to start ubiquitination of H2AX, whereas, RNF168 recognizes the by-now ubiquitinated H2AX by RNF8. Later, RAP80 binds with the elongated chain created by RNF8 and RNF168 and forms a complex with BRCA1. Shreds of evidence suggest that BARD1 helps BRCA1 to attach with nucleosomes, however, impairment in BARD1 releases BRCA1 from the nucleosome core protein and binds with tau lesion in the cytosol which is a hallmark feature in AD.

At the DNA damage site, RNF8 and RNF168 E3 ligases are required for the recruitment of 53BP1 and BRCA1-BARD1 that will further repair non-homologous DNA end joining (NHEJ) and homologous recombination (HR), respectively. Moreover, BRCA1 E3 ligase undergoes resection further loading RAD51 on ssDNA which is important for HR. RNF8, RNF168, and BRCA1 work directly on DSBs; other E3 ligases that indirectly impact is TRIP12, UBR5, and APC [22].

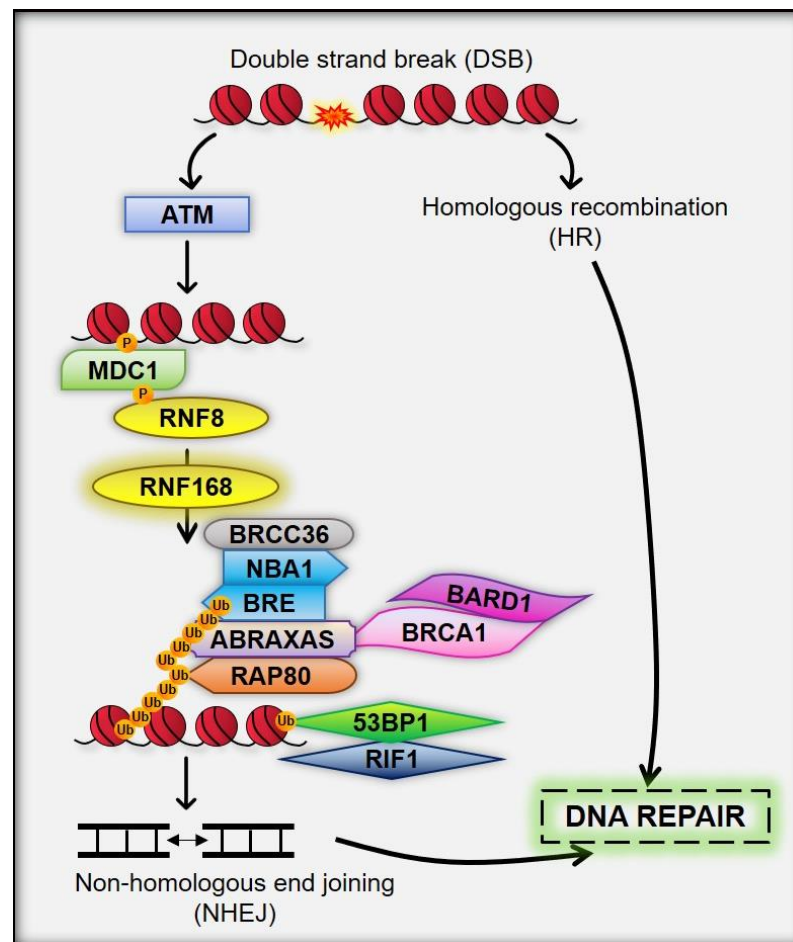


Fig. 2.1. Sequence of E3 ligases involved in double-stranded break repair.

2.5. BRCA1

BRCA1 (RNF53), located on chromosome 17q21 is an incomplete recessive gene encoding 220 kD protein carrying multi-domains. It consists of 24 exons, with exons 2-5 encoding the RING domain at the N-terminal, and exons 15-23 encoding the BRCA1 C-terminal (BRCT) domain [25], [26]. Many studies done in the past suggest that there is a strong inverse association between cancer and AD that has resulted in increased morbidity and mortality rates. Interestingly, such studies point to one common fact there is a potential link between molecular mechanisms involved in both such that in today's scenario, many anti-cancer treatments are being used against AD [27]. BRCA1 is the major DNA repair protein and its mutation marks 80% of breast cancer (BC) and ovarian cancer (OC) cases in females, however, some studies highlight the increasing cases of BC-AD with age in BC patients, therefore, there is a direct association between cancer and neurodegeneration and the potential link behind them is their molecular mechanism [28] (Fig. 2.2.). Previous studies demonstrate that as per neuron-specific methylome analysis in AD brains, BRCA1, a major DNA repair protein that once dysfunctional is mislocalized to the cytoplasm of neuronal cells and co-localized with tau proteins [29], [30].

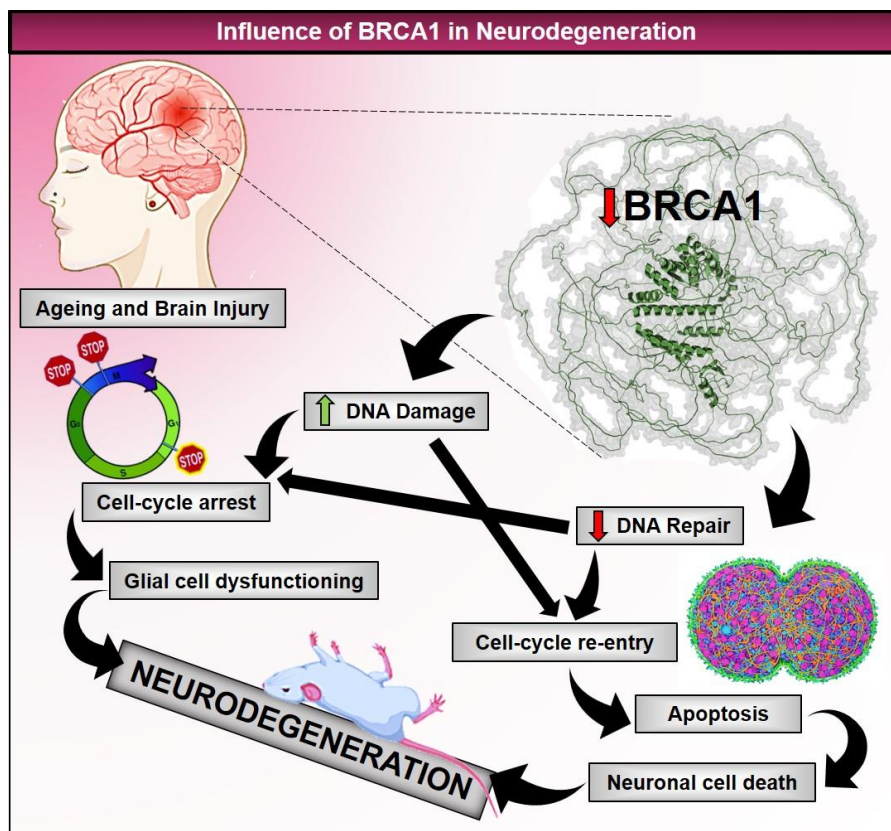


Fig. 2.2. Schematic representation of BRCA1 illustrating its involvement in neurodegeneration known to affect DNA repair mechanism, disturbing cell-cycle leading to apoptosis and ultimately neuronal death.

2.6. BARD1

A critical protein partner of BRCA1 is BRCA1-associated RING domain protein (BARD1), which possesses its RING domain at the N-terminal region [31]. BARD1 forms a tightly bound heterodimeric complex with BRCA1. Interestingly, BRCA1 and BARD1 do not directly interact via their RING domains. Instead, their interaction occurs through a four-helix bundle formed by the helices of BRCA1 and BARD1 that flank each RING domain [32]. An *in vitro* study suggests that BRCA1-BARD1 heterodimer exhibits significantly higher E3 ligase activity compared to BRCA1 alone [33]. To evaluate the importance of the RING domain of BARD1, mutations were introduced that altered the Zn^{2+} coordinating cysteine (C53A or C71A) within its RING domain. The findings revealed that while BRCA1 maintained its ability to bind Zn^{2+} , structural changes occurred resulting in the loss of E3 ligase activity. In another study, a RINGless BARD1 construct was generated, wherein a five-residue linker connected the helices that typically flank the RING domain. Surprisingly, the results confirmed that even in the absence of the RING domain, the helices of BARD1 retained both the binding capability and E3 ligase activity of BRCA1 [32].

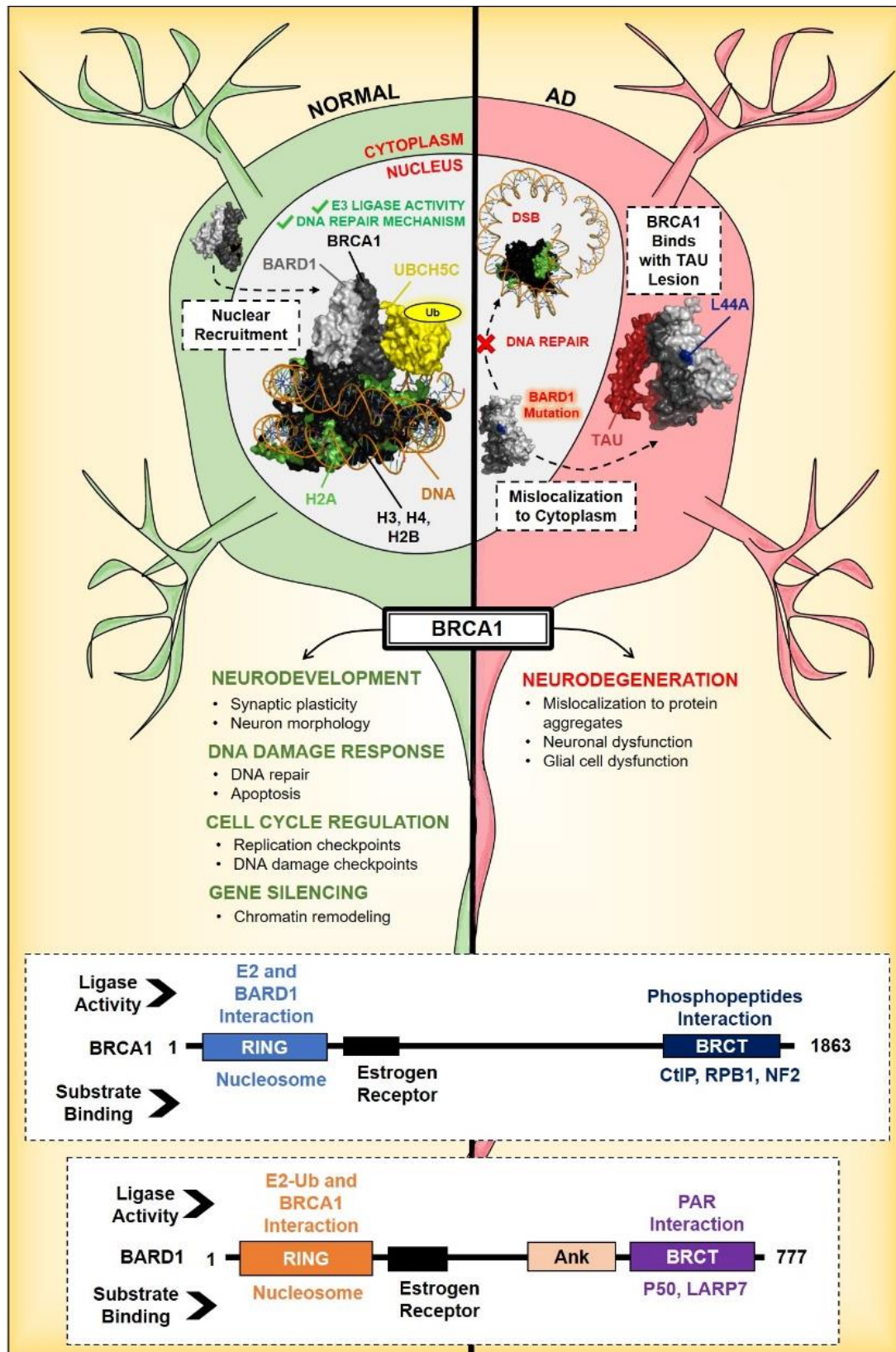


Fig. 2.3. Two scenarios depicting normal and Alzheimer's disease case to illustrate the functioning of BRCA1-BARD1 in the event of a point mutation in BARD1. In the normal scenario, BRCA1-BARD1 are recruited in the nuclear compartment to perform E3 ligase

activity and DNA repair, where the heterodimeric partner BRCA1 binds with UbcH5c, an E2-conjugating enzyme, and simultaneously interacts with the histone protein H2A. BARD1 plays a critical role in tethering BRCA1 to the nucleosome core protein (NCP). In Alzheimer's disease, any impairment in BARD1 leads to the release of BRCA1 from NCP, resulting in its mislocalization from the nucleus to the cytoplasm, where it colocalizes with tau protein. Observations indicate that the point mutation of L44A on the first α -helix of BARD1 disrupts the structure and function of BRCA1, resulting in reduced binding with H2A and increased stability with tau protein. At the bottom of the figure, domain structures, ligase activity, and substrate binding regions of BRCA1 and BARD1 are depicted

BRCA1 engages in various cellular complexes to fulfill its functions and uphold stability. Additionally, studies have noted that owing to BRCA1's RING finger domain, it possesses the ability to conduct diverse forms of ubiquitination, contingent upon the specific E2-conjugating enzyme it interacts with. BRCA1 forms specific interactions with E2-conjugating enzymes to facilitate Ub transfer, while BARD1 significantly aids BRCA1 in executing its E3 ligase activity. BRCA1-BARD1 has been demonstrated to interact with 9 E2-conjugating enzymes; however, many studies predominantly focus on the Ube2D family of E2s [34]. BRCA1-BARD1 facilitates the formation of mono-Ub linkages to lysine sidechains and N-termini of substrates in collaboration with E2s, Ube2E1/2/3, and Ube2W, respectively [35]. Conversely, it is involved in the generation of poly-Ub chain types with E2s such as Ube2D1/2/3, Ube2K, and Ube2N [36]. In *in vitro* investigations, it is noted that for BRCA1-BARD1 to attach its initial Ub to the substrate, it necessitates the participation of various E2s, a process often referred to as the priming step. However, when paired with Ube2D, no priming step is required. For example, the coupling of BRCA1-BARD1 with Ube2D1/2/3 generates K6-linked chains during auto-ubiquitination, yet it also has the capability to mono-ubiquitinate nucleosome H2A and estrogen receptors- α (ER α) [32], [37]. A study mapped the binding site on the BRCA1-BARD1 for Ube2D3 (UbcH5c) and the result demonstrates that UbcH5c only binds with the RING domain of BRCA1 and not BARD1, however, Ube2L3 (UbcH7) binds with BRCA1 but was found inactive in Ub ligase activity assay [38], [39]. Nucleosome H2A stands out as the sole BRCA1-BARD1 substrate for which atomic-level structural information is presently available [40]. Furthermore, a cryo-EM structure of BRCA1-BARD1-UbcH5c-H2A revealed that the C-terminal domains of BARD1, namely ankyrin-repeat domain (Ank) and BRCA1 C-terminal (BRCTs), distinctly recognize nucleosomes harboring H4K20me0 and H2A K15 Ub, binding to a histone surface that fully overlaps with the one utilized by the RING heterodimer [41], [42], [43]. Studies highlight the role of BRCA1 in the pathology of AD and may be one of the major players in neurodegeneration [44], [45]. Under pathological conditions, the Ub-ligase activity of BRCA1-BARD1 has been associated with the ubiquitination of γ -tubulin in the cytosol. This activity is essential for the concentration of proteins involved in the cell cycle regulation at the centrosome complex, therefore, indicating

impairment of BRCA1 in ubiquitination and subcellular mislocalization of a large portion of BRCA1 protein in neurons during neurodegeneration [46] (**Fig. 2.3.**). In AD, extracellular A β triggers the DNA damage response (DDR) by upregulating the BRCA1 protein in neurons. BRCA1 then co-localizes with tau aggregates in the cytoplasm leading to the accumulation of DNA fragments and becoming insoluble in a manner dependent on tau [47]. It is BARD1 that favors BRCA1 to be in the nucleus and this fact has been proved by some studies where the researchers blocked the nuclear export signal of BRCA1 and observed that the heterodimer retained in the nuclear compartment and contributed to DNA repair and transcription activation.

2.7. RNF8 and RNF168

The ubiquitination of H2A is governed by three major E3 ligases namely, RNF8 and RNF168, polycomb repressive complex 1 (PRC1), and BRCA1-BARD1 heterodimer complex. These E3 ligases modify the site of H2A and enable DNA repair that further enhances chromatin compaction [8].

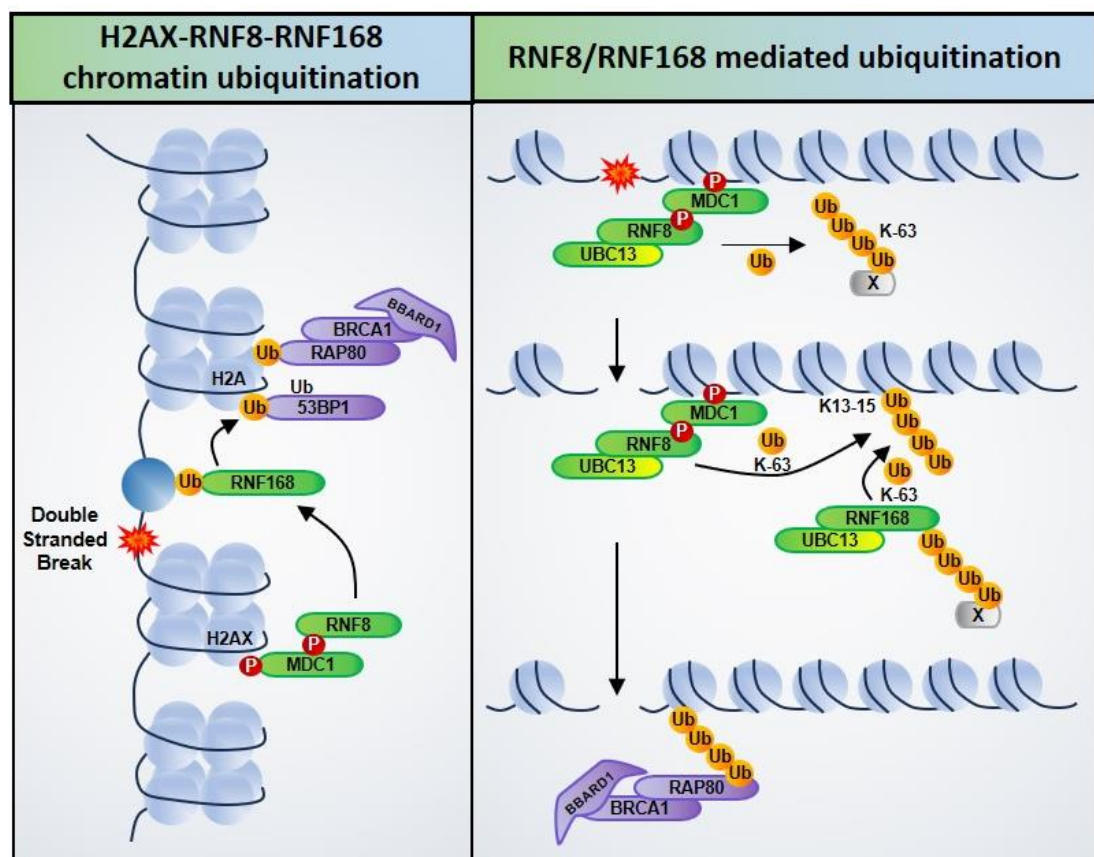


Fig. 2.4. RNF8 and RNF168 mediated ubiquitination at double-stranded.

RNF8 is the first E3 ligase called upon during DSBs following ionizing radiation (IR) or neocarzinostatin (NCS). Auto-activated ATM phosphorylates γ H2A

at S139 which further recruits MDC1. RNF8 and RNF168, together built K63 -linked polyubiquitin chain on γ H2A at K13 and K15. Moreover, ubiquitinated RNF8 mediates NBS1 at K435, crucial for HR. It has been well stated that deficiency of RNF8 is enough to cause cognitive decline, whereas, its loss potentially leads to neurodegeneration [48]. Mutation in the same might affect the forthcoming ubiquitin cascade which is to be taken forward by other E3 ligases as mentioned above. Therefore, RNF8 plays a very crucial role and could be a new therapeutic target to bring a cure to two most complicated diseases i.e., AD and BC. According to cBioPortal, 3.97% of point mutation has been observed in RNF8 [49]. Similarly, RNF168, which is being called upon to amplify the ubiquitin chain first formed by RNF8 stands equally important (**Fig. 2.4.**). Studies suggest that in many cancers, RNF168 is abnormally expressed and its mutation has been a persistent reason behind influencing DNA repair. Rather overexpression of RNF168 results in mutations in NHEJ and HR repair, thereby, greatly impacting genome stability [49]. Therefore, mutations in RNF8 or RNF168 could potentially hamper the entire ubiquitination cascade along with the DNA repair mechanism.

2.8. PROTACs

Proteolysis targeting chimeras (PROTACs) are an emerging approach for developing treatments for previously undruggable protein targets. PROTACs hijack the UPS for targeted protein degradation. NDDs are the largest class of CNS diseases. Lately, PROTACs have shown significant potential in treating AD, PD, HD, and ALS. For degrading tau protein in AD, a PROTAC has been designed using Keap1-Cul3 ubiquitin E3 ligase. This PROTAC could cross the blood-brain barrier (BBB) and degrade 95% of pathogenic tau [50]. In PD, a PROTAC has been designed that carries an α -synuclein binding domain, a cell-penetrating domain, and a motif to target UPS. This PROTAC's potential was recognized when there was decreased mitochondrial dysfunction due to decreased α -synuclein production [51]. Two PROTACs have also been designed to reduce the levels of huntingtin protein in HD [52]. The rational design of PROTACs involves three components, namely, warhead, E3 ligand, and linker [53]. PROTACs work by inducing proximity between E3 ligase and substrate/protein of interest (POI) such that the ubiquitin molecule is transferred from E3 to POI. A single PROTAC can undergo multiple ubiquitination, resulting in the formation of a polyubiquitin chain on the POI. This ubiquitin chain is then recognized by the UPS, resulting in the degradation of the POI [54] (**Fig. 2.5.**). There are certain limitations, firstly, its molecular weight which is often greater than 700, preventing it from crossing BBB. Secondly, it causes drug resistance as playing with the core component of E3 ligases can change the genome. Thirdly, PROTACs exhibits the "hook effect", where using a higher concentration of a drug can result in self-inhibition. Lastly, "off-target effect", where PROTACs may accidentally injure

normal protein. Since not much time has passed in exploring PROTACs, there is nonetheless great therapeutic potential with unique advantages.

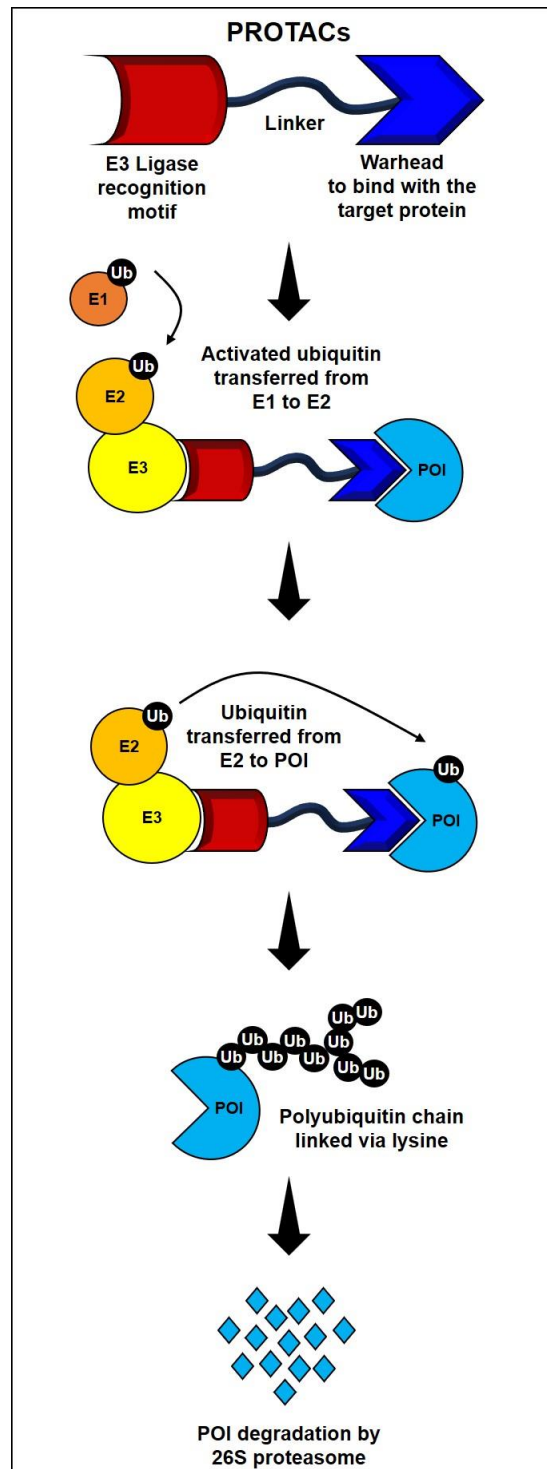


Fig. 2.5. The diagram depicts a PROTAC molecule's core structure and its action mechanism in promoting target degradation. By binding to a target protein and an E3 ligase, the PROTAC enables repeated cycles of target protein ubiquitylation. This ultimately leads to the target's degradation by the 26S proteasome.

CHAPTER 3



CHAPTER 3

MATERIALS AND METHODS

3.1. METHODOLOGY I ► BRCA1

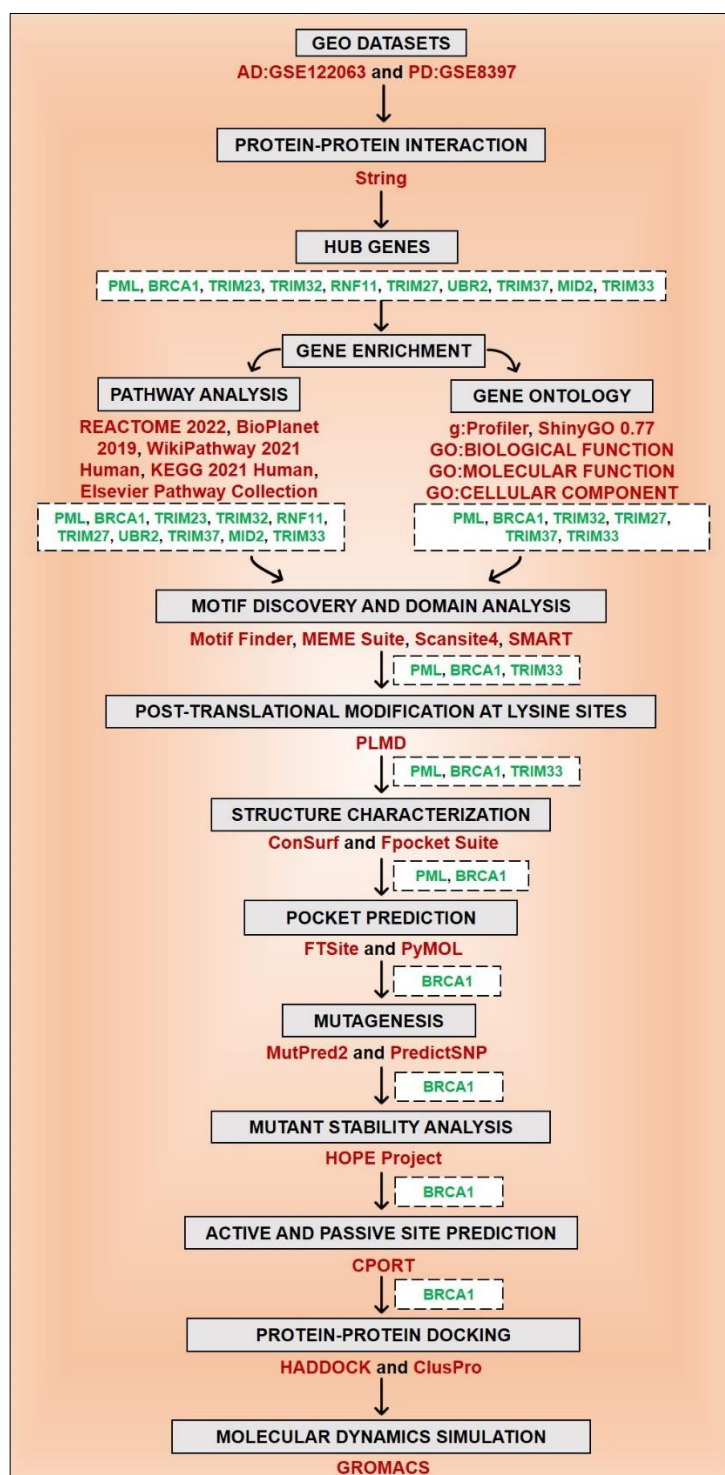


Fig. 3.1. The methodology for identifying BRCA1 as the most potential E3 ligase common in both AD and PD, along with the steps involved in assessing the impact of point mutation on its E3 ligase activity.

3.1.1. Data Retrieval

The expression profiling of genes was carried out by high throughput screening. The AD and PD datasets were downloaded from the Gene Expression Omnibus (GEO) of the National Centre for Biotechnology Information (NCBI) [55], [56]. The microarray dataset GSE8397 carries genes from post-mortem brain samples of Parkinson's Disease comprising 47 individual samples from substantia nigra which was further divided into lateral, medial parts, and the frontal cortex. In this study, 30 diseased samples and 17 control samples were used. The study was based on the platform data Affymetrix HG_U133 array set A for Parkinson's Disease. The 2nd dataset GSE122063 consists of 36 samples of Vascular Dementia, 18 each from frontal and temporal cortex, and 56 samples of Alzheimer's Disease, 28 each from frontal and temporal cortex i.e., 92 diseased samples, and 44 control samples were selected. The study was based on Agilent-039494 SurePrint G3 Human GE v2 8x60K Microarray 039381.

3.1.2. Data Pre-Processing and Screening of Differentially Expressed Genes

GEO2R tool is a web-based program using GEOQuery and Limma packages of R from Bioconductor projects. It can be utilized to compare datasets and analyze Differentially Expressed Genes (DEGs) from GEO series datasets. In this study, GEO2R was used to predict the role of DEGs in cellular, molecular, and biological functions [57], [58]. The Benjamini-Hochberg correction method was used to calculate the adjusted P value of the false discovery rate (FDR) [59]. The DEGs were categorized significantly based on the cut-off limit applied on the GEO2R tool which was an adjusted P value < 0.05 and Pvalue < 0.05 . The adjusted P value is the smallest familywise significance level at which a particular comparison will be declared statistically significant as part of the multiple comparison testing.

3.1.3. Screening of Common Ubiquitin E3 Ligase and DEGs Through Venn Analysis

The E3 ligase list was collected from the Epithelial Systems Biology Library (ESBL) database consisting of 377 E3 ligases [60]. The DEGs screened based on adjusted P value were significant by nature, these significant DEGs of the above two datasets were analyzed for the ubiquitin E3 ligase list using InteractiVenn analysis [61] It is a web-based tool used to generate a Venn diagram illustrating common DEGs of AD and PD that were overlapping with the Ubiquitin E3 ligase list. These significantly common DEGs that are also E3 Ubiquitin ligases were further analyzed to interpret their involvement in the pathogenesis of AD and PD.

3.1.4. Protein-Protein Interaction (PPI) Analysis

Various protein-protein interaction tools were explored, namely, BIOGRID which is a public database that contains curated proteins and their genetic interaction data for model organism species – yeast, nematode, fly, zebrafish, mouse, and human, whereas, STRING is another freely available database that helps assess the physical and functional associations between two proteins [62], [63]. STRING v 11.5 was used to generate PPI network of the overlapping DEGs. The gene symbol of common DEGs was uploaded on the multiple protein module available on the server and was screened for the PPI in the *Homo sapiens* category with adjusted P value < 0.05 and confidence score of 0.40 [64]. The high throughput labs experiment and knowledge were used by the STRING database to analyze the PPI network with a score ≥ 0.4 [65], [66]. The PPI STRING network was exported to CytoScape v.3.9.1 [67] to visualize and acquire the PPI network. There are three methods to obtain 10 hub genes, namely, maximal clique centrality (MCC), maximum neighborhood component (MCN), and degree method [68]. Here, 10 hub genes with the highest node degree score were screened out as the degree of the node signifies the number of connections with other nodes.

3.1.5. Pathway Enrichment Analysis of E3 Ubiquitin Ligases

Numerous databases are available for gene information extraction consisting of three major domains (1) Biological Processes (BP), (2) Cellular Processes (CP), and (3) Molecular Function (MF). Widely used software for gene set enrichment analysis like g:Profiler that maps genes to know functional information and detect statically significant enriched terms [69]; Enricher provides various types of visualization summaries of collective functions of gene lists [70] and ShinyGO 0.77 which is an intuitive graphical web application that aids researchers in gaining actionable insights from gene sets [71] were used for gene set enrichment and pathway analysis. The threshold parameters were set on P value < 0.05 for significantly enriched genes, thereby, the functional enrichment was calculated.

3.1.6. Domain and Motif Analysis

For the Domain architecture and motif analysis, we used several web-based tools such as SMART which uses profile-hidden Markov models built from multiple sequence alignments (MSA) to detect protein domains [72]; MEME Suite allows to identify novel motifs in protein sequences and performs other motif-based analysis [73]; similarly, Scansite 4 uses accession number of protein to identify its motifs [74]. We submitted the FASTA sequences of our key proteins on these servers to analyze their domains. For structure analysis of common genes, we used Consurf [75].

3.1.7. Prediction of Post-translational Modification Sites

Various datasets were explored for screening PTMs effect on the selected genes. Protein lysine modification database (PLMD) [76] was used to extract the ubiquitination, acetylation, and sumoylation sites of the selected gene. As the data was deduced, the duplicate PTM sites were removed manually as there are some sites that undergo two different functions when ubiquitinated. Finally, the PTM sites were arranged according to their PTM types happening on the different motifs of genes.

3.1.8. Prediction of Deleterious Mutations and their Impact on Structural and Functional Stability

We used PredictSNP web-based tool to predict the mutation. PredictSNP consists of several other tools such as PhD-SNP, SNAP, SIFT, PolyPhen-1, PolyPhen-2, and PANTHER [77]. We also used another web-based tool MutPred [78], that associates molecular and genetic data to ascertain the pathogenicity by substituting different amino acids. It can also anticipate the molecular origin of pathogenicity. Further, we used the Project HOPE tool [79] that helped in assessing the effect of mutation on the structure and function of the protein sequence. We submitted the FASTA sequences of our key proteins to this server to analyze the impact of the mutation.

3.1.9. Structure Preparation

We extracted the three-dimensional structure of the BRCA1-BARD1 complex (PDB ID - 1JM7) with resolution 0.45Å to 0.95Å [80] and Ube2k (PDB ID - 6IF1) with resolution 2.47Å from RCBS protein databank [81]. The FTSite server was used to predict the active sites on BRCA1 domain [82]. Furthermore, mutation was incorporated in BRCA1 using the mutagenesis built-in wizards in PyMOL software. CPORT tool was used to determine the active-passive sites of selected domain [83]

3.1.10. Molecular Docking

Protein-protein docking tool was used to analyze the complexity of the BRCA1-BARD1 and Ube2k binding. Wild-type (Control) and mutant (Variable-K32Y, K32L, K32C, K45V, K45Y, and K45G) structures of BRCA1-BARD1 were prepared using PyMOL and were docked with Ube2k using ClusPro [84], [85], [86], [87], [88] that gave the cluster size and lowest binding energy which does not directly report energy value in kcal/mol or kJ/mol but predicts the most favorable spatial arrangement between two proteins and focuses on the relative ranking of predicted binding structures; HADDOCK [89], [90] was used which is based on z-score parameters; and lastly, in LZerD the models are assessed based on four scores, namely GOAP, DFIRE, ITScore, and Ranksum. GOAP, DFIRE, and ITScore are statistical potentials, whereas, Ranksum is used to rank the models and is the sum of all three

scores. As Ranksum score is the recommended score for interpreting the result, hence, the Ranksum score for wild-type and mutant structures was studied [91] (Figure S1). The purpose behind using three different docking tools was the specificity behind their functioning, for instance, ClusPro uses the Fast Fourier Transforms (FFT) based program PIPER which generates 1000 lowest energy structures that are clustered using pairwise RMSD and centers of the largest cluster; HADDOCK is a semi-flexible docking algorithm which used experimental data and bioinformatics interface predictions, whereas, LZerD uses 3D Zernike descriptors which depends on mathematical series expansion of protein surface [92].

3.1.11. Molecular Dynamics Simulation

The GROMACS 2022 package [93] was applied for molecular dynamic (MD) simulations with the OPLS-AA/L force field [94]. The OPLS-AA/L force field was selected, as its parameters are public and can be used in wide range of MD simulations. The docked complex structures were prepared in the pdb2gmx format and converted it into the gromacs format i.e., ighn to prepare the clean file after removing the hydrogen atoms from the docked structures. The orthorhombic cubic complex was centered at least 10 Å and filled with the solvent SPCE molecule in the middle of cubic box to perform the process of solvation. The genion file was used to neutralize the system by replacing the solvent ions with 5 sodium molecules. The energy minimization was performed for 50,000 nsteps with a maximum force of 1000.0 KJ/mol/nm to ensure that there are no steric clashes in the system. The next phase was equilibration to avoid the uncontrolled dynamics. The NVT ensemble was the first phase of equilibration where temperature was kept 300 K with 1ps constant time. In the next phase pressure was equilibrated at 1 atm by NVT. After attaining desired equilibration, the system was ready to run the MD simulation for 20 ns and 50 ns. The frames have been examined using the MD simulation results which helped in determining the root mean square deviation (RMSD), root mean square fluctuation (RMSF), and radius of gyration (RG) of wild-type and mutant structures.

3.2. METHODOLOGY II ► BRCA1-BARD1

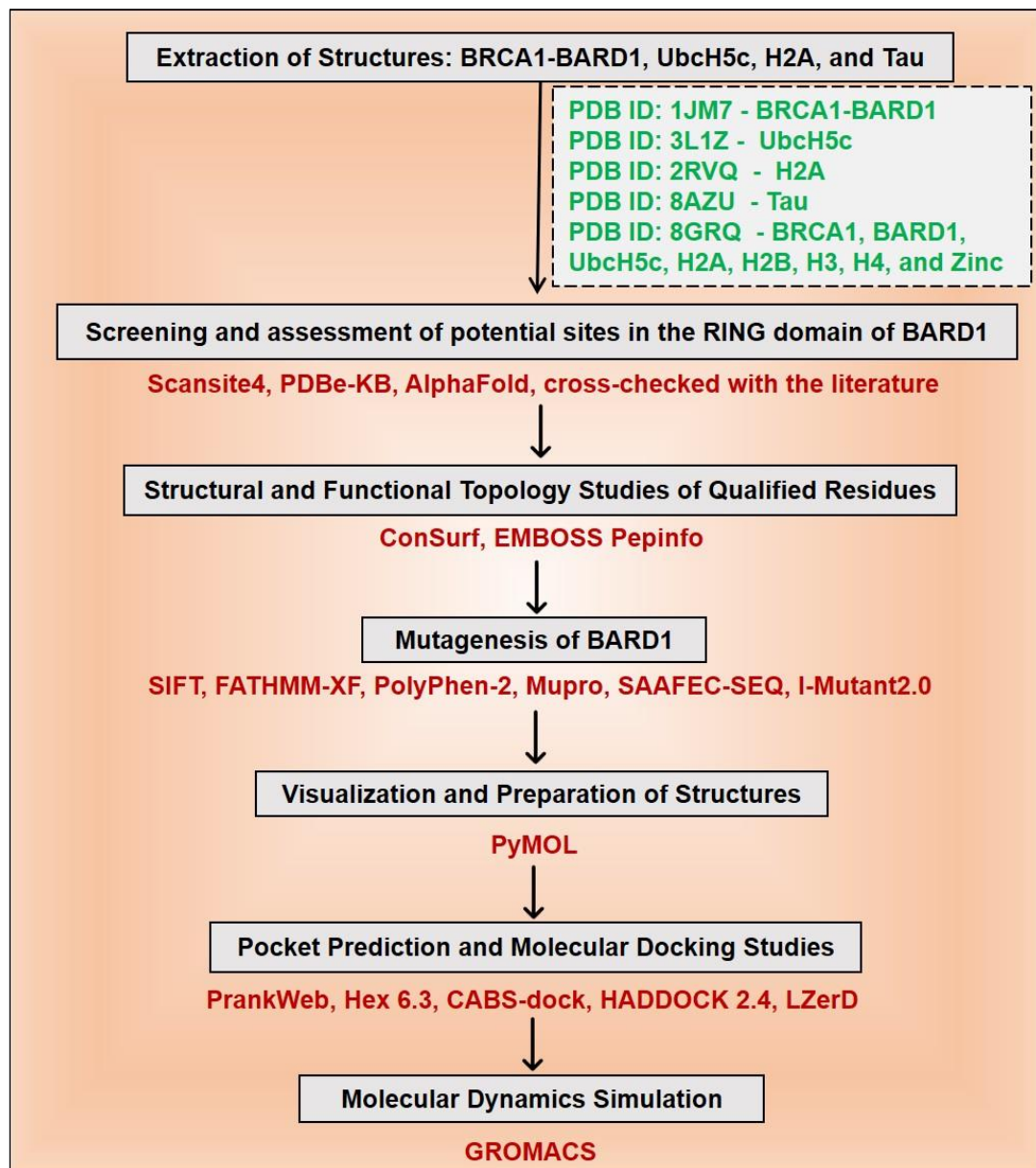


Fig. 3.2. The methodology for identifying BRCA1-BARD1 as a key E3 ligase in DNA repair and evaluating the effects of point mutations in BARD1 on BRCA1's E3 ligase activity.

3.2.1. Extraction of Structures: BRCA1-BARD1, UbcH5c, H2A, and Tau

The structures of BRCA1-BARD1, UbcH5c, H2A, and Tau were retrieved from the Protein Data Bank (PDB) of the Research Collaboratory for Structural Bioinformatics (RCSB) which is one of the biggest archives of structural data [95], [96]. The following structures were extracted PDB ID: 1JM7 (<https://doi.org/10.2210/pdb1jm7/pdb>) for BRCA1-BARD1 [97], PDB ID: 3L1Z

(<https://doi.org/10.2210/pdb311z/pdb>) for UbcH5c [98], PDB ID: 2RVQ (<https://doi.org/10.2210/pdb2rvq/pdb>) for H2A [99], and PDB ID: 8AZU (<https://doi.org/10.2210/pdb8azu/pdb>) for Tau protein [100]. For template-based docking, PDB ID: 8GRQ (<https://doi.org/10.2210/pdb8grq/pdb>) was also retrieved which is a structure composed of BRCA1, BARD1, UbcH5c, H2A, H2B, H3, H4, and Zinc [101].

3.2.2. Screening and Assessment of Potential Sites in the RING Domain of BARD1

Before screening and assessing sites, the localization of BRCA1 and BARD1 was studied using Scansite4 which helps predict the localization of a protein utilizing the LocTree3 data source [102]. Sub-cellular localization is a crucial step in understanding the function of a protein. LocTree3 applies machine learning (profile kernel SVM) along with annotated localization by PSI-BLAST and gene ontology results [103]. Firstly, Protein Data Bank in Europe–Knowledge Base (PDBe-KB) was explored in search of potential residues or sites on the RING domain of BARD1 where BRCA1, UbcH5c, H2A, and Tau possibly interacts. However, in the case of UbcH5c, H2A, and Tau, BRCA1-BARD1 were taken together. PDBe-KB is an open consortium augmented with structural and functional annotations of proteins managed by EMBL–EBI [104]. The screened residues were assessed using AlphaFold where per-residue model confidence score (pLDDT) was observed for each residue along with predicted alignment error (PAE). AlphaFold is an artificial intelligence system developed by DeepMind that uses a novel machine learning approach to predict the physical and biological nature of protein and leverages multi-sequence alignments into a deep learning algorithm [105], [106]. Later, the screened sites were cross-checked with the literature to get the qualified residues.

3.2.3. Structural and Functional Topology Studies of Qualified Residues

Evolutionary conservation of all qualified sites was done through ConSurf to analyze the pattern of evolution of each amino acid in the protein BARD1 (UniProt ID: Q99728) to help decipher the regions that carry structural and/or functional importance. Unlike other approaches, where consensus and relative entropy are measured; ConSurf estimates evolutionary rates by phylogenetic analysis of homologs and progressive probabilistic evolutionary models that accurately predict active sites [107]. Later, the physicochemical properties of qualified sites were carefully studied using EMBOSS Pepinfo which includes tiny, small, aliphatic, aromatic, non-polar, polar, charged, positive, and negative features [108]. The input protein sequence used in EMBOSS Pepinfo was BARD1 (UniProt ID: Q99728) with hydropathy window size 9.

3.2.4. Mutagenesis of BARD1

Missense substitutions greatly impact the structure and function of a protein such that it helps detect disease-causing mutations. Considering the RING domain site of BARD1, firstly, we predicted each substitution of the potential site as tolerated or non-tolerated, deleterious or neutral, and disease-causing or benign using SIFT, FATHMM-XF, and PolyPhen-2. Sorts intolerant from tolerant substitutions (SIFT) is a sequence homology-based tool [109]. The sequence of BARD1 (UniProt ID: Q99728) was taken as input to predict tolerated and deleterious substitutions for every residue in the protein based on multiple alignment information. Functional analysis through hidden Markov models – eXtended feature (FATHMM-XF) uses supervised machine learning to predict functional consequences of both non-synonymous single nucleotide variants (nsSNVs) and non-coding variants in the human genome. The tool uses Platt scaling which gives a p-score to each prediction to assess pathogenic SNV [110]. Polymorphism Phenotyping v2 (PolyPhen-2) is an automated prediction tool that focuses on non-synonymous single nucleotide polymorphism (nsSNPs) [111]. It uses dictionary of secondary structure in protein (DSSP) database to get structural parameters for mapping amino acid residues which is further taken to the MSA pipeline and supervised machine learning based on the Naïve Bayes classifier [112]. Proteins adopt a particular 3D conformation to exhibit their function, therefore, its ability to fold into a desired structure is administered by folding free energy (delta delta G, $\Delta\Delta G$) and to assess the effect of single site mutation on protein stability becomes essential. Thus, $\Delta\Delta G$ was calculated by using MUpro, SAAFEC-SEQ, and I-Mutant2.0. MUpro utilizes two machine learning approaches namely, support vector machine and neural networks to predict relative stability and give a confidence score between -1 and 1; a score <0 indicates decreased stability [113]. SAAFEC-SEQ uses machine learning based on gradient-boosting decision tree and physiochemical features, sequence properties, and evolutionary information to predict $\Delta\Delta G$ caused by amino acid substitution [114]. I-Mutant2.0 is a support vector machine-based tool that is trained with the data from ProTherm, a comprehensive database of protein mutations, and automatically predicts the protein stability upon a single substitution mutation [115]. Later, the average of $\Delta\Delta G$ was taken which highlighted the potential mutants to be studied further.

3.2.5. Visualization and Preparation of Structures

The PyMOL molecular graphics system, v1.2r3pre, Schrödinger, LLC, a cross-platform molecular graphics tool was used for 3D visualization and preparation of the structure. All the retrieved PDB structures were prepared before molecular docking. Hydrogen atoms were added to examine the H-bond interactions and binding affinity of the interacting protein. Moreover, in experimental structures, hydrogen atoms are often absent, therefore, by adding hydrogen atoms H-bonds were optimized

in the structures. Other preparatory steps involve removing atomic clashes and co-crystallized ligands. Further, water molecules were also removed as it makes the computation easier and clears the binding pockets [116]. In mutant structures the aforementioned preparatory steps were followed, however, the mutations were created using the Wizard tab > Mutagenesis > Protein in the taskbar of PyMOL.

3.2.6. Pocket Prediction and Molecular Docking Studies

In prior docking studies, PrankWeb, a webserver for P2Rank was used to predict the binding sites in the protein structure. Alongside interacting residues or ligand binding sites, PrankWeb offers visualization and gives a ligandability score to each pocket which helps elucidate docking prioritization [117]. P2Rank, the backend of PrankWeb, is a template-free machine learning method that employs a random forest algorithm [118]. For docking studies various tools were explored based on different algorithms, namely, Hex 6.3, CABS-dock, HADDOCK 2.4, and LZerD. Regarding template-based docking, Hex 6.3 was used which offers superposition and docking programs based on the Spherical Polar Fourier (SPF) correlation approach. Three files were uploaded separately, namely, receptor, ligand, and complex. The complex file contains the information of both receptor and ligand in the docked orientation which helps the Hex software to identify and superimpose/match corresponding pairs of α -carbon atoms from each chain to calculate root mean square (RMS) deviations between the docked position of the ligand and its position in the known complex. Superimposition calculations are controlled by the Matching Control panel [119], [120]. For protein-peptide docking, CABS-dock was used which relies on a global docking method designed to search for both binding sites in the protein and the peptide pose [121]. The protein and peptide sequence goes through a robust protocol, where, at first random structures are generated for the peptide sequence that are randomly placed on the surface of the protein considering its center. Subsequent steps involve the production of 10 trajectories which pass through initial filtering and K-medoid structural clustering. Finally, 10 consensus medoids are picked as final models [122]. Thereafter, docking was performed using HADDOCK 2.4 (High ambiguity driven protein-protein docking) which utilizes ambiguous experimental data such as NMR chemical shift perturbation (CSP) and information on mutations. It helps transform the data into ambiguous interaction restraint (AIR) that further aids in predicting the distance between binding residues and hence, accomplishes the docking process [123]. Lastly, LZerD (Local 3D Zernike descriptor-based docking algorithm) was used to complete the docking studies which depends on geometric hashing to produce different orientations of the ligand via 3D Zernike descriptors such as shape-matching. The models generated are assessed by 4 different scores, namely, GOAP, DFIRE, ITScore, and Ranksum. Ranksum score is the sum of the former three scores, consequently, are considered for assessing the models, thus, the smaller the score, the better it is [91]. The other strong reason for using LZerD is that LZerD12, 13, 14, 15

webservers have been performing unswervingly among the top in the CAPRI16 and 17 blind communitywide competition of protein docking [124].

3.2.7. Molecular Dynamics Simulation

The deleterious consequences of mutation on BARD1 protein were analyzed by performing molecular dynamics simulation (MDS) using GROMACS version 2023.3 [93]. The OPLS-AA/L force field was used for the generation of the protein parameters. Initially, the docked structure was made ready in the pdb2gmx file format which was later converted into ignh to get the clean file. This step is necessary in order to remove hydrogen atoms from the docked structure. By using gmx editconf module, the cubic box was defined and centered the protein 1 nm away from the edges of the box. Later, the box was filled with SPCE solvent for the process of solvation. The system was electro-neutralized via gmx genion module which aided in removing steric clashes. After assembling solvation and electro-neutral system, the structure was optimized through the process of energy minimization. Further, the equilibration step was performed by NVT and NPT ensemble. NVT equilibration was executed for 1 ns where the system was heated to 300 K temperature and NPT ensemble was also done for another 1 ns to stabilize the pressure. After equilibrating the whole system, the density was also set using gmx energy module and later each structure was directed towards MDS for 20 ns and 50 ns. After running the MDS, molecular dynamics trajectories such as root mean square deviation (RMSD), root mean square fluctuation (RMSF), and radius of gyration (RG) were analyzed. The expression for RMSD, RMSF, and RG are formulas (3.1), (3.2), and (3.3), respectively [125]. This helped in carefully assessing the structural deviation in mutants compared to their wild-type.

$$RMSD(t_1, t_2) = \left(\frac{1}{M}\right) \sum_{i=1}^N m_i \|r_i(t_1) - r_i(t_2)\|^2 \quad (3.1)$$

In this equation, $M = \sum_{i=1}^N m_i$ and $r_i(t)$ is the position of atom i at time t . N specifies the number of atoms.

$$\rho_i^{RMSF} = \sqrt{\langle (r_i - \langle r_i \rangle)^2 \rangle} \quad (3.2)$$

The equation calculates the fluctuation variance of the C α atom for each residue, simplifying it to the square root of this variance around the average position.

$$Rg = \sqrt{\frac{\sum_i m_i (R_i(y)^2 + R_i(z)^2)}{\sum_i m_i}} \quad (3.3)$$

In this equation, i indicates the atom and m_i represents the mass of atom i . $R_i(y)$ and $R_i(z)$ direct the positions of atom i along the axes y and z .

3.3. METHODOLOGY III ► RNF8

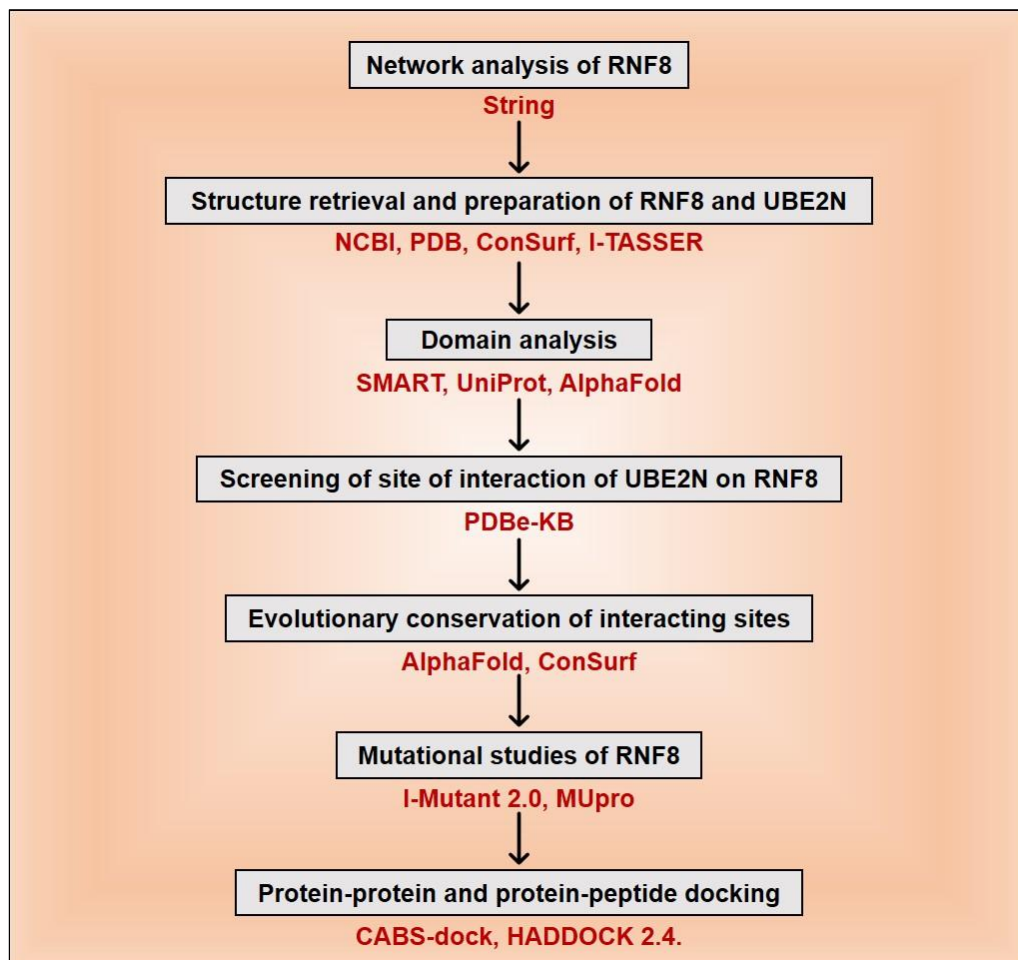


Fig. 3.3. The methodology for identifying RNF8 as the first E3 ligase involved in DNA repair mechanism and evaluating the effects of point mutations in its functionality.

3.3.1. Network Analysis of RNF8

The protein-protein interaction of RNF8 was performed using STRING (version 11.5) [126], where a single protein name and organism were specified as RNF8 and Homo sapiens respectively. It gave a network that summarised the association of RNF8 with other interacting partners with a confidence score. Later, gene co-expression was also studied using STRING where the intense colour of the square represents a higher association.

3.3.2. Structure Retrieval and Preparation of RNF8 and UBE2N

The complete structure of RNF8 is not yet available, therefore, the FASTA sequence of RNF8 was retrieved from NCBI and was submitted to ConSurf to prepare the high-resolution structure with conservation grade mapped on it [127]. RNF8 structure was validated using I-TASSER that gives top-ranked structures, estimated by C-score which is defined by equation (3.4) [128]. The structure of UBE2N was taken from the PDB database, 4whv.

$$C - \text{score} = \ln \left(\frac{M/M_{\text{tot}}}{\langle \text{RMSD} \rangle} * \frac{1}{N} \sum_{i=1}^N \frac{z_i}{z_{\text{cut},i}} \right) \quad (3.4)$$

3.3.3. Domain Analysis

In order to understand the domain structure of RNF8 and its interacting partners, a Simple Modular Architecture Research Tool (SMART) was used that helped to understand genetically mobile domains on the basis of phyletic distribution, functional class, tertiary structure, and vital residues involved [129]. Particularly, for RNF8, its domain structure was cross-checked through UniProt (O76064). Moreover, AlphaFold which is an AI system developed by DeepMind prepared a Predicted Aligned Error (PAE) plot that further assisted in understanding useful inter-domain and intra-domain predictions [130].

3.3.4. Screening of Site of Interaction of UBE2N on RNF8

RNF8 is an E3 ligase and one of its potential E2 conjugating enzymes is UBE2N, therefore, it is evident that they interact with each other. Thus, the macromolecular interaction interfaces of UBE2N on RNF8 were analyzed on PDBe-KB which helped in predicting the key sites of their interaction.

3.3.5. Evolutionary Conservation of Interacting Sites

The conservation score of each predicted site was retrieved from AlphaFold and ConSurf. The AlphaFold gave the confidence measure in the form of per-residue confidence score (pLDDT), whereas ConSurf calculated the evolutionary rates based on Multiple Sequence Alignment (MSA) which are constructed using alignment algorithms, namely, MAFFT, PRANK, T-COFFEE, MUSCLE, and CLUSTALW [131].

3.3.6. Mutational Studies of RNF8

Mutagenesis of predicated sites was performed using I-Mutant 2.0 and MUpro. I-Mutant 2.0, a support vector machine-based tool assisted in predicting protein stability upon point mutation [132]. Similarly, MUpro, based on two machine learning programs namely support vector machine and neural network helped in predicting protein stability on single-site amino acid substitution [133]. Both tools gave delta G (DDG) values.

3.3.7. Protein-Protein and Protein-Peptide Docking

Two separate tools were used to understand RNF8 and UBE2N binding, namely, CABS-dock and HADDOCK 2.4. Protein-peptide docking was performed using CABS-dock where the targeted peptide (Wild-Type and Mutants) was uploaded separately with UBE2N

that further gave cluster density, average RMSD, and Max RMSD values [134]. The CABS energy of protein-peptide contact is given by the equation (3.5).

$$E_{contact}(d) = \begin{cases} 0 & \text{if } d \leq D_0 \\ s(d - D_0) & \text{if } d > D_0, \end{cases} \quad (3.5)$$

HADDOCK was used to dock two full-structure proteins and their binding affinity was judged based on Z-score which was calculated by equation (3.6) where E_{elec} is the electrostatic energy, E_{vdw} is the van der Waals energy, $E_{desolvation}$ is the desolvation energy and E_{AIR} restraints (i.e., distance) violation energies [135].

$$HADDOCK_{SCORE} = 0.2 * E_{elec} + 1.0 * E_{LJ} + 1.0 * E_{AIR} \quad (3.6)$$

3.4. METHODOLOGY IV ► RNF168

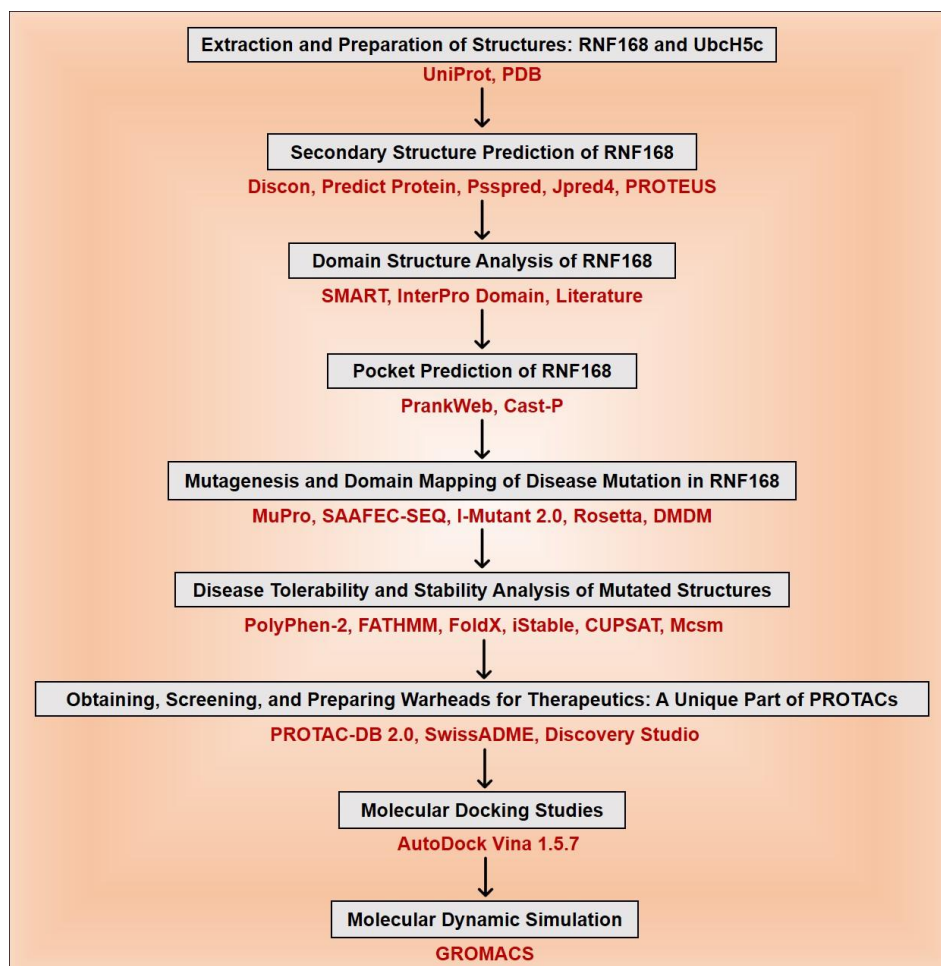


Fig. 3.4. The methodology for identifying RNF168 as the second E3 ligase involved in the DNA repair mechanism, responsible for amplifying the ubiquitin chain initiated by RNF8. Additionally, it includes steps for evaluating the effects of point mutations on its E3 ligase activity.

3.4.1. Extraction and Preparation of Structures: RNF168 and UbcH5c

The structures of RNF168 and its E2 conjugating partner, UbcH5c were retrieved from the Protein Data Bank (PDB) with the PDB ID: 8SN2 (<https://doi.org/10.2210/pdb8SN2/pdb>) [95], [96]. It is a Cryo-EM structure of human nucleosome core particle in complex with RNF168 and UbcH5c. RNF168 plays a central role in regulating DNA damage response by ubiquitinating H2A. Moreover, it performs its E3 ligase activity by conjugating with UbcH5c. Therefore, Hu. Q. et al., 2024 have chemically conjugated UbcH5c with H2A. Often, many computational tools demand UniProt ID, hence, the UniProt ID of RNF168 is Q8IYW5.

3.4.2. Secondary Structure Prediction of RNF168

Various tools were explored to predict the secondary structure of RNF168, such as DisCon, JPred 4, and PROTEUS2. Disorder Content Predictor (DisCon) is designed to predict a disordered percentage in a protein structure [136]. JPred is based on Jnet algorithm which predicts the secondary structure of the protein on solvent accessibility and coiled-coil regions [137]. PROTEUS is designed for comprehensive structure prediction and structure-based annotation [138]. All these tools took the UniProt sequence and helped predicting the coil and helix regions in the structure of RNF168.

3.4.3. Domain Structure Analysis of RNF168

To analyze the domain structure of RNF168, a literature survey was performed. Along with that, some tools were also explored, for instance, SMART and InterPro Domain (Version 90.0). SMART utilizes profile-hidden Markov models built from multiple sequence alignments (MSA) to detect protein domains [139]. InterPro domain uses predictive models called as signatures to predict domains and important sites on the protein [140].

3.4.4. Pocket Prediction of RNF168

Two tools were used to predict the pockets in PDB ID: 8SN2, namely, PrankWeb and CASTp. PrankWeb was used to predict the binding sites in the protein structure. Alongside interacting residues or ligand binding sites, PrankWeb offers visualization and gives a ligandability score to each pocket which helps elucidate docking prioritization [117]. Computed Atlas of Surface Topography of Proteins (CASTp) is based on the computational geometry of Voronoi diagram, Delaunay triangulation, and Alpha shape which aids in predicting empty concavities in protein [141].

3.4.5. Mutagenesis and Domain Mapping of Disease Mutation in RNF168

The ability of a protein to fold into a desired structure is judged by its folding free energy ($\Delta\Delta G$). Therefore, $\Delta\Delta G$ was calculated for wild-type and mutant structures of RNF168 by using MUpro, SAAFEC-SEQ, I-Mutant2.0, and Rosetta. The concept behind MUpro, SAAFEC-SEQ, and I-Mutant 2.0 are explained above. Rosetta performs point mutation and gives a score for each mutant compared to the wild-type, further generating a heatmap of those scores [142].

3.4.6. Disease Tolerability and Stability Analysis of Mutated Structures

To assess disease tolerability, SIFT, PolyPhen-2, and FATHMM-XF were used, the detailed protocol of the same has been explained in the earlier steps of the methodology. FoldX, iStable, CUPSAT, and mCSM were used for stability analysis. FoldX Suite was downloaded and given commands were followed. FoldX predicts the stability of wild-type and mutant proteins by calculating the free energy of unfolding (ΔG) [143]. Later, $\Delta\Delta G$ was calculated as the difference between ΔG of the wild-type and ΔG of the mutant protein, i.e., $\Delta\Delta G = \Delta G \text{ Mutant} - \Delta G \text{ WT}$. The positive and negative values represented destabilizing and stabilizing mutations, respectively. Similarly, iStable 2.0 is based on a support vector machine that takes the sequence information and predicts the protein stability changes ($\Delta\Delta G$) by assessing different predictors [144]. CUPSAT predicts the stability of the protein by assessing its environment utilizing solvent availability, secondary structure specificity, and torsion angles [145]. mCSM predicts the protein stability by relying on graph-based signatures that assess the impact of mutation with atomic-distance pattern surrounding the main aa residue [146]. All of these tools proved invaluable in evaluating how point mutations can affect the stability of a structure.

3.4.7. Obtaining, Screening, and Preparing Warheads for Therapeutics: A Unique Part of PROTACs

PROTACs comprise three components, namely, E3 ligand, linker, and warhead. PROTAC-DB 2.0 is an online database, a repository of structural and experimental data about PROTACs [147]. Here, we specifically considered warheads which are small molecules targeting the protein of interest for degradation. Also, warheads are that portion of the PROTACs that directly binds with the protein of interest. PROTAC-DB is highly cited and is a growing database that provides effective structural information on PROTACs. For screening out potential warheads, SwissADME was used, which is a website that allows one to predict ADME parameters, pharmacokinetic properties, and drug likeliness [148].

3.4.8. Molecular Docking Studies

3.4.8.1. E3-E2

Protein-protein and protein-peptide molecular docking was performed to understand the interaction between E3 ligase and E2-conjugating enzymes. Here, E3 denotes RNF168 and E2 represents UbcH5c. The docking studies utilize the CABS-dock and LZeroD tools, each of which is explained in detail above, including their working principles and methodology.

3.4.8.2. Mutant E3-Warhead

Molecular docking was also performed between wild-type/mutants and potential warheads using AutoDock Vina 1.5.7 [149]. It is an open-source program to perform molecular docking. Other features include its ease of use, high accuracy, and implementation quality. First, the PDB file of protein structure was exported and water molecules were deleted from it. Missing atoms were checked and repaired in the protein structure. Later, polar hydrogens and Kollman charges were added to the structure. Lastly, grid selection was done by setting the parameters (center_x = 206.913; center_y = 167; center_z = 163.691) and (size_x = 28; size_y = 34; size_z = 34). These parameters were prior computed from the Cast-P pocket prediction tool.

3.4.9. Molecular Dynamics Studies to Assess the Functionality of RNF168

MD simulation was performed for three cases: (1) RNF168 and its mutants, (2) RNF168 and its mutants docked with UbcH5c, and (3) RNF168 and its top two mutants docked with potential warheads. MDS was performed using GROMACS of which the steps are given above. For the first and second scenarios, steps of lysozyme in water (explained in the above sections) were followed, however, for the third scenario, steps of protein-ligand interaction were followed. Charmm27 forcefield was used to perform MDS of the protein-ligand complex, and the structure was solvated with three-point transferable intermolecular potential (TIP3P). The addition of Na and Cl neutralized the charge, and the LINCS algorithm controlled the bond length. Energy minimization was performed with a force of 1000 kJ/mol/nm. Temperature and pressure were equilibrated at 300K and 1 atm, respectively. After achieving the desired equilibration, MDS was done for 100 ns from which RMSD (protein), RMSD_LIG (protein-ligand), RG (protein), RG_LIG (protein-ligand), RMSF, and Hydrogen bonds were calculated for wild-type and mutant structures docked with warheads.

CHAPTER 4



RESULTS

CHAPTER 4

RESULTS

- **Objective I** - To dissect the molecular mechanism of ubiquitination and explore the cross-talk mechanism between Alzheimer's and Parkinson's disease at the protein level

4.1. Results I (Objective I)

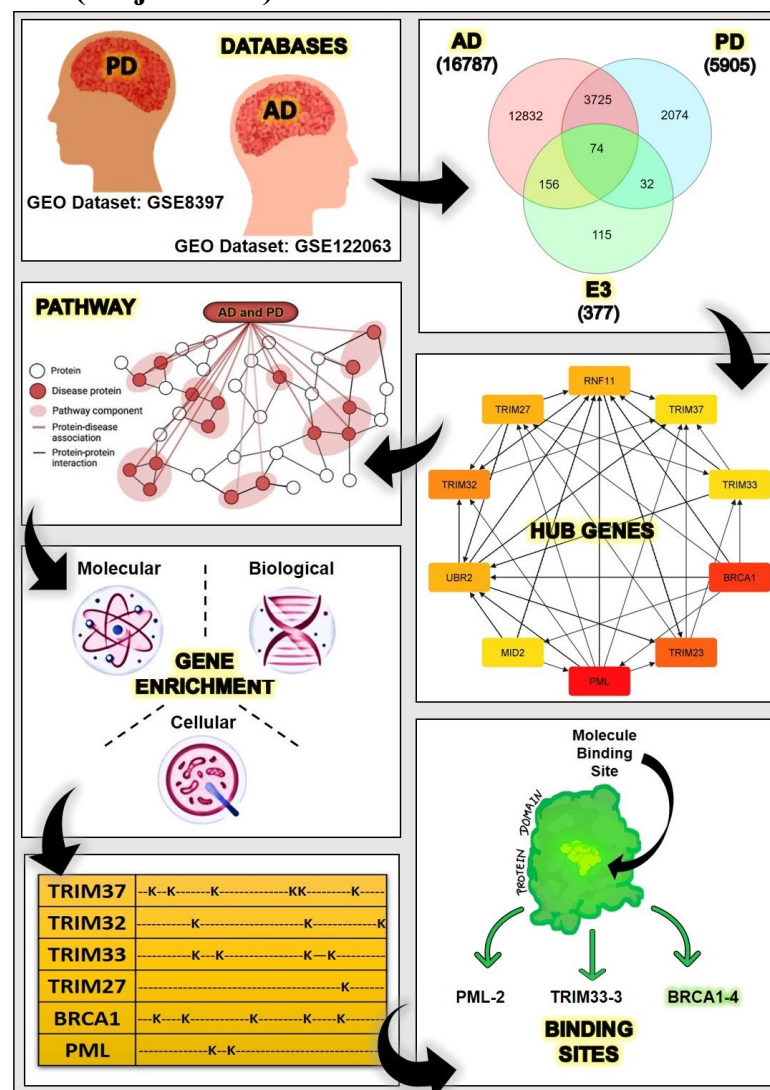


Fig. 4.1. The following are the steps involved in identifying E3 ligases that are commonly associated with both Alzheimer's disease (AD) and Parkinson's disease (PD), as well as determining the hub genes, conducting gene enrichment analysis for the hub genes, and predicting potential lysine sites for ubiquitination. Furthermore, the task involves the prediction of binding sites within the top three E3 ligases.

4.1.1. Common E3 Ligase in AD and PD

The list of E3 ubiquitin ligase enzymes from ESBL and all the significant DEGs of AD (GSE122063) and PD (GSE8397) datasets which were screened based on adjusted P value < 0.05 were extracted. All the genes were intersected ($A \cap B \cap C$) using InteractiVenn that gave 74 genes which were common E3 ligase enzymes in both AD and PD datasets (Figure 2). These genes were further analyzed on the STRING database to predict their protein-protein interactions and understand their direct and indirect functional associations. The network was then shared with CytoScape to run CytoHubba interface to do the topological analysis of these genes. Based on the degree method which calculated the highest degree score and gave the top 10 hub genes, namely PML, BRCA1, TRIM23, TRIM32, RNF11, TRIM27, UBR2, TRIM37, MID2 and TRIM33. The network of these hub genes was also analyzed on CytoScape plug-in, CentiScaPe for performing the network centrality analysis to identify the most relevant nodes for experimental prioritization [150]. As there are six centralities, namely, bottleneck, eccentricity, closeness, radiality, betweenness, and stress [151]. Here, based on betweenness the nodes were identified and were marked red and yellow based on high and low degree scores, respectively (Fig. 4.2.).

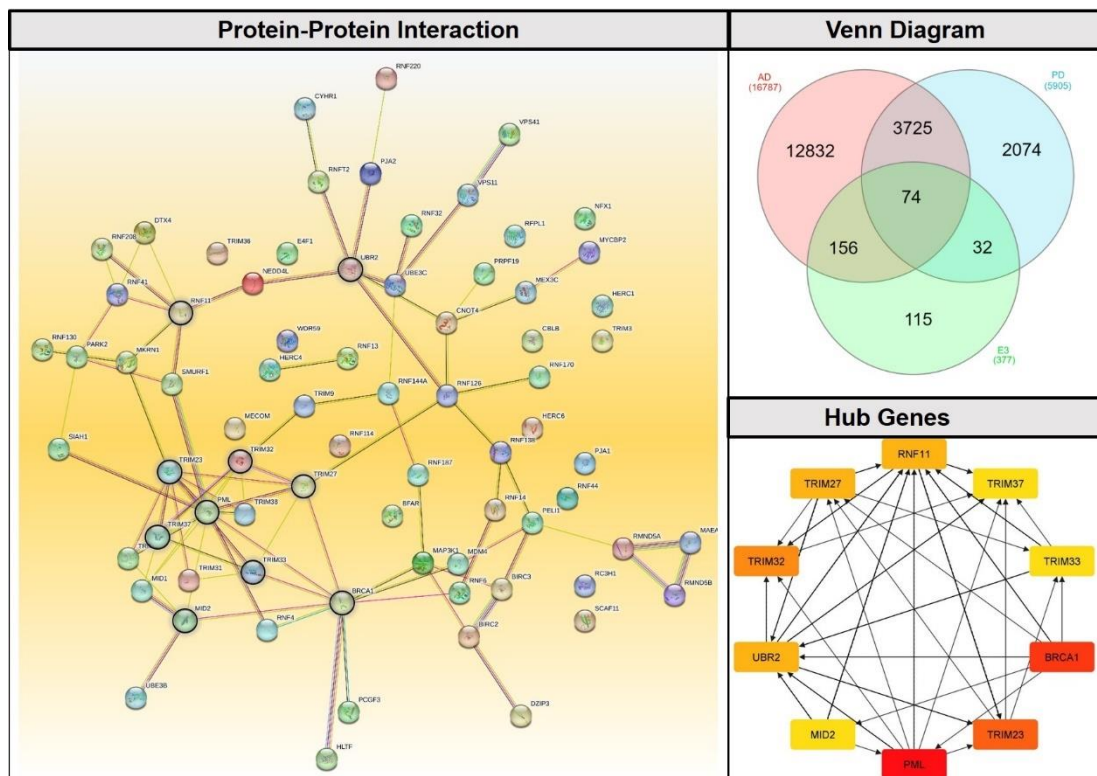


Fig. 4.2. Protein-protein interaction network of 74 genes that are common E3 ligase enzymes in both AD and PD. Out of the 74 genes, the top 10 hub genes were selected based on degree topological analysis which are also highlighted in protein-protein interaction.

4.1.2. Functional Enrichment Analysis of E3 Ligases in AD-PD Crosstalk

To understand the connection between these hub genes and identify the key genes involved, pathway analysis was performed that helped in analyzing the involvement of these hub genes in different pathways. A web-based tool, Enrichr was used to access different pathway databases such as REACTOME 2022, BioPlanet 2019, WikiPathway 2021 Human, KEGG 2021 Human, and Elsevier Pathway Collection (Table 4.1).

Table 4.1. Top ten hub genes and their involvement in various pathways

PATHWAYS			
REACTOME 2022	P Value	Genes	Total
SUMO E3 Ligases SUMOylate Target Proteins R-HSA-3108232	6.69E-05	BRCA1; TRIM27; PML	PML - 8 BRCA1 - 16
SUMOylation Of Ubiquitylation Proteins R-HSA-3232142	1.65E-04	TRIM27; PML	TRIM23 - 0
Antigen Processing: Ubiquitination and Proteasome Degradation R-HSA-983168	3.97E-04	UBR2; TRIM37; TRIM32	TRIM32 - 1 RNF11 - 0
SUMOylation Of DNA Damage Response and Repair Proteins R-HSA-3108214	6.29E-04	BRCA1; PML	TRIM27 - 4 UBR2 - 1
Regulation Of TP53 Activity R-HSA-5633007	0.00264381	BRCA1; PML	TRIM37 - 1 MID2 - 0
PIP3 Activates AKT Signaling R-HSA-1257604	0.00749871	TRIM27; PML	TRIM33 - 3
Impaired BRCA2 Binding to PALB2 R-HSA-9709603	0.01193796	BRCA1	
Impaired BRCA2 Binding to RAD51 R-HSA-9709570	0.01736657	BRCA1	
Transcriptional Activity of SMAD2/SMAD3:SMAD4 Heterotrimer R-HSA-2173793	0.02521481	TRIM33	
Diseases Of DNA Repair R-HSA-9675135	0.02521481	BRCA1	
Post-translational Protein Modification R-HSA-597592	0.02741189	BRCA1; TRIM27; PML	
Meiotic Recombination R-HSA-912446	0.02765579	BRCA1	
Recruitment And ATM-mediated Phosphorylation of Repair And Signal Proteins At DNA Double Strand Breaks R-HSA-5693565	0.02960461	BRCA1	
DNA Double Strand Break Response R-HSA-5693606	0.03009127	BRCA1	
TP53 Regulates Transcription of DNA Repair Genes R-HSA-6796648	0.0305777	BRCA1	
Gene Expression (Transcription) R-HSA-74160	0.03097182	BRCA1; PML; TRIM33	
G2/M DNA Damage Checkpoint R-HSA-69473	0.03784795	BRCA1	
Processing Of DNA Double-Strand Break Ends R-HSA-5693607	0.0392961	BRCA1	
Meiosis R-HSA-1500620	0.04314824	BRCA1	
Interferon Gamma Signaling R-HSA-877300	0.04362878	PML	
Regulation Of TP53 Activity Thru Phosphorylation R-HSA-6804756	0.0441091	BRCA1	
Signaling By TGF-beta Receptor Complex R-HSA-170834	0.0445892	TRIM33	
BioPlanet 2019	P Value	Genes	Total
Ubiquitin-mediated proteolysis	4.16E-07	TRIM37; BRCA1; TRIM32; PML	PML - 8 BRCA1 - 13 TRIM23 - 0
MicroRNA regulation of DNA damage response	5.34E-04	BRCA1; PML	TRIM32 - 1 RNF11 - 0
ATM-mediated phosphorylation of repair proteins	0.00249771	BRCA1	

BRCA1-dependent ubiquitin ligase activity	0.00399365	BRCA1	TRIM27 - 0 UBR2 - 0 TRIM37 - 1 MID2 - 0 TRIM33 - 1
Double-strand break repair	0.01094805	BRCA1	
C-Myc pathway	0.01243259	PML	
Cell cycle: G2/M checkpoint	0.01342116	BRCA1	
BARD1 signaling events	0.01440885	BRCA1	
ATM pathway	0.02374757	BRCA1	
TAp63 pathway	0.02716803	PML	
Signaling by TGF-beta receptor complex	0.03252125	TRIM33	
Myc repressed pathway	0.03591403	BRCA1	
E2F transcription factor network	0.03639784	BRCA1	
p73 transcription factor network	0.0388136	PML	
Meiosis	0.04074228	BRCA1	
DNA repair	0.05128792	BRCA1	
mTOR signaling pathway	0.05509675	PML	
p53 signaling pathway	0.06738061	PML	
TGF-beta signaling pathway	0.08876199	PML	
Cell cycle	0.20479564	BRCA1	
WikiPathway 2021 Human	P Value	Genes	Total
DNA damage response WP707	5.04E-04	BRCA1; PML	PML - 3 BRCA1 - 4 TRIM23 - 0 TRIM32 - 0 RNF11 - 0 TRIM27 - 0 UBR2 - 0 TRIM37 - 0 MID2 - 0 TRIM33 - 0
ATM Signaling Pathway WP2516	0.01982523	BRCA1	
p53 transcriptional gene network WP4963	0.03300659	PML	
DNA Repair Pathways Full Network WP4946	0.05841819	BRCA1	
TGF-beta Signaling Pathway WP366	0.06408763	PML	
PI3K-Akt signaling pathway WP4172	0.15759978	BRCA1	
KEGG 2021 Human	P Value	Genes	Total
Ubiquitin mediated proteolysis	4.67E-07	TRIM37; BRCA1; TRIM32; PML	PML - 1 BRCA1 - 2 TRIM23 - 0 TRIM32 - 1 RNF11 - 0 TRIM27 - 0 UBR2 - 0 TRIM37 - 1 MID2 - 0 TRIM33 - 0
PI3K-Akt signaling pathway	0.16358073	BRCA1	
Elsevier Pathway Collection	P Value	Genes	Total
SIRT1 Signaling in Aging	1.74E-04	BRCA1; PML	PML - 3 BRCA1 - 5 TRIM23 - 0 TRIM32 - 0 RNF11 - 0 TRIM27 - 0 UBR2 - 0 TRIM37 - 0 MID2 - 0 TRIM33 - 0
Histone Ubiquitylation	0.00498982	BRCA1	
Histone Sumoylation	0.00946151	PML	
Histone Acetylation	0.00995725	BRCA1	
ERK5/MAPK7 Signaling	0.01835069	PML	
Proteins Involved in Stem Cell Exhaustion in Aging	0.01933394	PML	
DNA Persistent Repair Inhibits mTOR Signaling	0.02031629	BRCA1	
Cell Cycle Overview	0.05224142	BRCA1	

Those pathways were selected that were involved in post-translational modifications and cell signaling having a P value < 0.5 . Ubiquitin mediated-proteolysis pathway involves maximum number of genes including TRIM37, BRCA1, TRIM32, and PML. The result of pathway analysis showed that BRCA1 was involved in the maximum number of pathways followed by PML, TRIM27, TRIM33, TRIM32, and TRIM37 depicting its biological significance in AD and PD. Further, to decipher the relationship between biological processes, molecular phenotypes, environmental factors, and adaptive functions among the selected genes, gene ontology study was performed for BRCA1, PML, TRIM27, TRIM33, TRIM32, and TRIM37 using g:Profiler. It was observed that according to GO Biological Process 2021, Protein ubiquitination (GO:0016567) was involved in all the genes with adjusted P value 2.766×10^{-9} . Regarding GO Molecular Function 2021, Ubiquitin-protein transferase activity (GO:0004842) was common in all the genes with adjusted P value 6.381×10^{-11} whereas, as per GO Cellular Component 2021, all genes except TRIM32 and TRIM33 were observed in Nucleoplasm (GO:0005654) and Intracellular non-membrane-bounded organelle (GO:0043232) with adjusted P value 2.0×10^{-3} and 1.8×10^{-2} , respectively. Moreover, as per ShinyGO 0.77, all 6 genes showed Zinc ion binding site that confers ligase functionality (**Fig. 4.3.**).

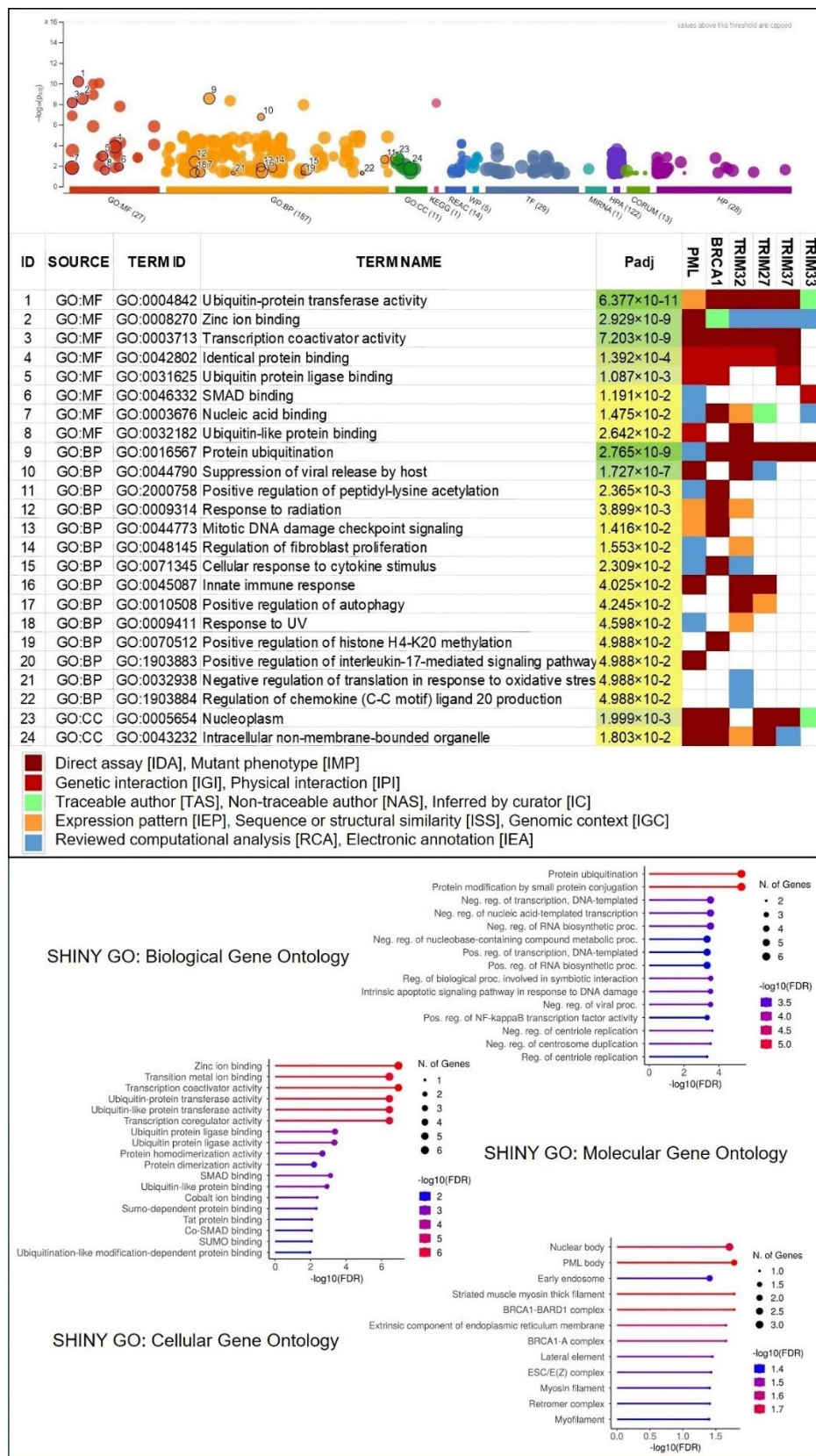


Fig. 4.3. The first half of the figure displays the results of g:Profiler used to perform gene ontology studies. BRCA1, PML, TRIM27, TRIM33, TRIM32, and TRIM37 genes were

uploaded that gave top 24 enriched functions comprising of 8 molecular functions, 14 biological processes, and 2 cellular components. The latter half of the figure represents the results of SHINY GO which was used to validate the results and it suggested that protein ubiquitination and protein modification by small protein conjugation are the two processes in which all 6 genes are highly involved. Whereas, all 6 genes showed zinc ion binding sites which is necessary for E2 enzyme to bind successfully and according to the cellular component, all were found in nuclear bodies.

4.1.3. Protein Motif Discovery and RING Domain Analysis

The binding site of the motif provides more information about protein function, therefore, we tried to find motifs of our selected genes (BRCA1, PML, TRIM27, TRIM33, TRIM32, and TRIM37) using MotifFinder considering Pfam and NCBI-CDD databases, respectively. We got 15 and 235 motifs for BRCA1, 7 and 115 motifs for PML, 12 and 250 motifs for TRIM27, 8 and 250 motifs for TRIM33, 17 and 228 motifs for TRIM32, 8 and 160 motifs for TRIM37. However, to narrow down our selection process we went forward with motifs from Pfam database. As these selected genes are also E3 ligases thus, E3 ligases can be divided into four types: Homologous to the E6-AP Carboxyl Terminus (HECT) type, U-box type, Really Interesting New Gene (RING-finger) type and RING Between RING (RBR) type. The motifs of our selected genes were only limited to U-box and RING-finger type. Moreover, as E3 ligase activity is intrinsic to RING domains having a RING finger-containing protein (AO7) that attaches with E2 that is necessary for the process of ubiquitination. Perhaps, there are other RING finger-associated proteins, namely BRCA1, Siah-1, TRC8, NF-X1, kf-1, and Praja1 which also enable E2 dependent ubiquitination [152]. For our selected genes, different RING domain superfamilies were also observed like C3HC4, C3H2C3, C4HC3, and U-box as they display similar protein folding and functional similarity however, their sequence identity is less than 30% depicting that they are poorly conserved. Hence, such domains were not taken forward for further analysis. Based on this observation, the potential genes having the desired domain were BRCA1, PML, TRIM33, and TRIM32 [153]. To produce an alignment of each significant match we run our query motif on MEME-Suite TOMTOM to get the list of target motifs ranked by P value and total overall matches. For BRCA1, PML, and TRIM33 the overall matches were more than 15, however, this was not the case for TRIM32. The target motif of BRCA1 is Zf RING Ubox (24-62) – CPICLELIKEPVSTKCDHIFCKFCMLKLLNQKKGPSQCP, target motif of PML is Zf B-box (127-223) – AVCTRCKESADFWCFECEQLLCAKCFEAHQWFLKHEARPLAELRNQSVREFLDGTRKTNNIFCSNPNHRTPTLTSIYCRGCSKPLCCSCALLDSSHS and target motif of TRIM33 is Zf RING Ubox (125-182) – CAVCQQLQSRREAEPKLLPCLHSFCLRCLPEPERQLSVPIPGGSNGDIQQVG VIRCP. Once the E2 conjugated ubiquitin is ready, it has four possibilities that it might form a thioester bond with Cys or oxy ester bond through Ser/Thr or form peptide

bond on N-terminal or have an isopeptide bond with Lys residue of substrate/E3. Our further study extensively involved Lysine residues (Lys/K), so the total number of lysine residues was counted for the target motifs of BRCA1, PML, and TRIM33 using Scansite 4. 6K residues were found in the target motif of BRCA1 (K32; K38; K45; K50; K55; K56;), 5K residues were found for PML (K133; K150; K160; K183; K209) and 1K site was observed in TRIM33 i.e. (K141). Later, post-translational modification sites were checked for these lysine residues using PLMD and SMART. Results states that in BRCA1, K32 undergoes ubiquitination and sumoylation, K55 undergoes ubiquitination and acetylation, whereas, the remaining lysine residues, K38, K45, K50, K56 only undergo ubiquitination. When it comes to PML, ubiquitination takes place on all the residues, namely, K133, K150, K183, K209 except K160 as it undergoes sumoylation and acetylation. However, K141 of TRIM33 only undergo ubiquitination.

4.1.4. Structure Characterization of BRCA1, PML and TRIM33

As BRCA1, PML, and TRIM33 were found to be the most potent E3 ligases which were common in both AD and PD, thus, it becomes important to study in depth their structures. To study the functional regions in the protein domain, ConSurf server was used, where, the FASTA sequence was uploaded for all three genes simultaneously. ConSurf is a bioinformatics tool that helps to estimate the evolutionary conservation of amino acid positions based on phylogenetic analysis among homologous sequences and then grading them 1-through-9 with a color code cyan-through-purple, where, 1 indicates the most rapidly evolving position, 5 stands for intermediate results, and 9 depicts most evolutionarily conserved position [154]. In the domain structure of BRCA1, K32, K50, K55, and K56 are exposed as well as functional, however, K38 and K45 are only exposed, and based on the conservation analysis there is no revelation of whether K38 and K45 are structural or functional. Similarly, in PML, K183 and K209 are exposed and functional, while, K133 and K150 are only exposed. Interestingly, in TRIM33, K141 is buried and structural (**Fig. 4.4.**). Therefore, it becomes evident that a site must be functional in order to bind with E2 conjugating enzyme. Further, we performed the pocket detection using Fpocket suite which helped us to find possible cavities where E2 conjugating enzyme might fit in E3 ligase enzyme [155]. We performed pocket detection of wild-type full structures as well as domain structure of all three genes, BRCA1, PML, and TRIM33. The observation describes that the pockets of wild-type BRCA1, PML, and TRIM33 are 113, 67, and 83, respectively, although, for their domains, it is 4, 2, and 3. Ubiquitination is distinct from sumoylation which happens more commonly in PML as it has four SUMO family proteins, including SUMO1, SUMO2, SUMO3, and SUMO5 which are known to modify PML at different lysine sites [156], [157], [158]. Interestingly, it has been found that PIAS1 and PIAS α promote sumoylation in PML, moreover, PIAS1-dependent PML sumoylation further governs PML ubiquitination,

- **Objective II** - To investigate the implication of mutation on E3 ligase activity

4.2. Results I (Objective II)

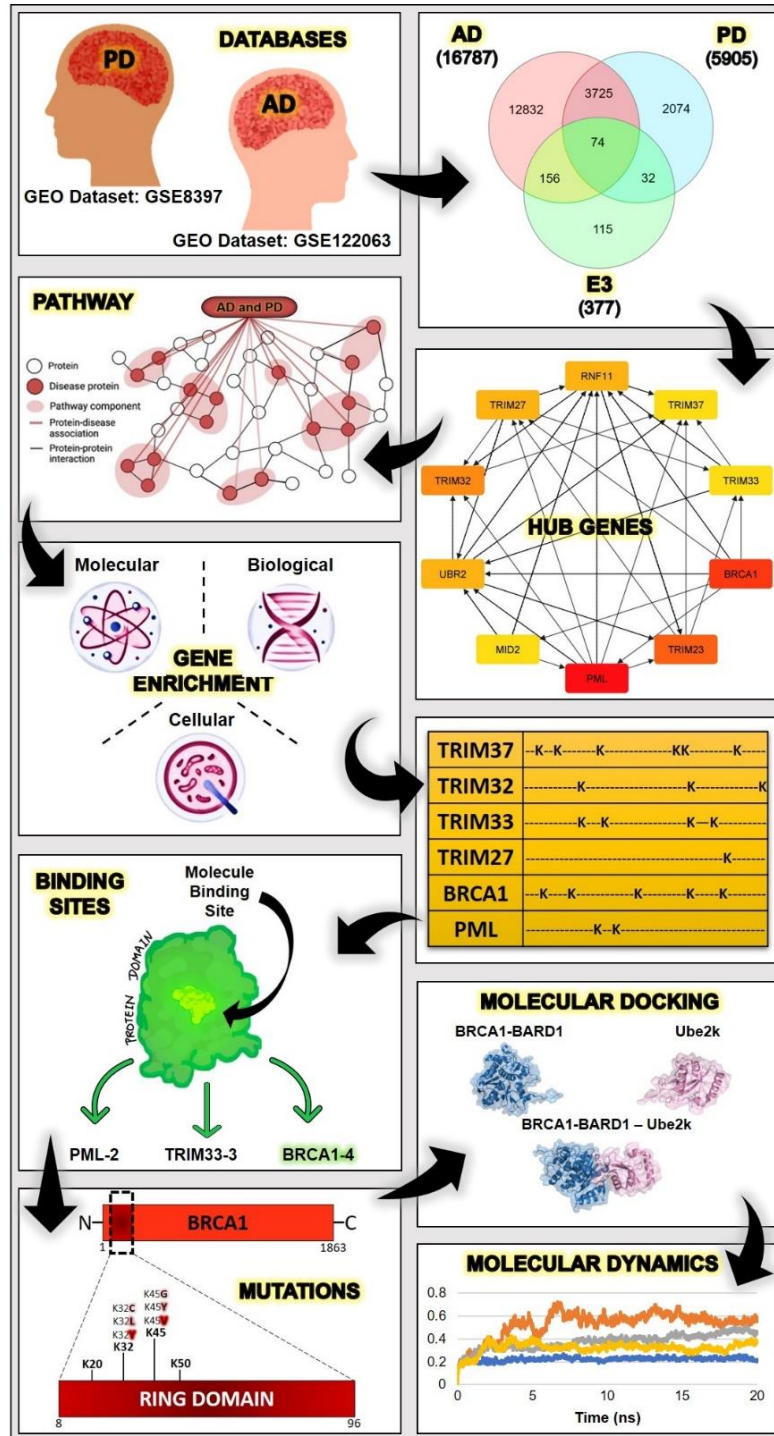


Fig. 4.5. The figure represents all the steps involved to study mutation in the RING domain of BRCA1 which is a common E3 ligase observed in Alzheimer's disease and Parkinson's disease.


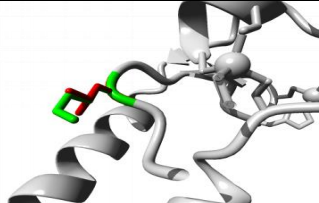

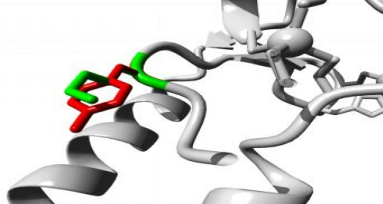

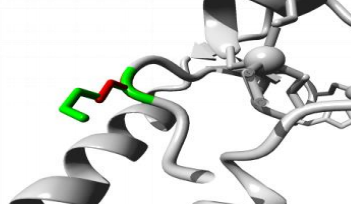

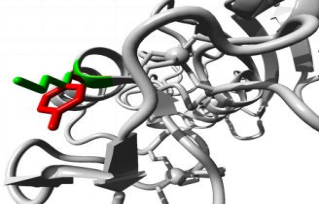
4.2.1. Mutagenesis and its Stability Analysis on RING Domain of BRCA1

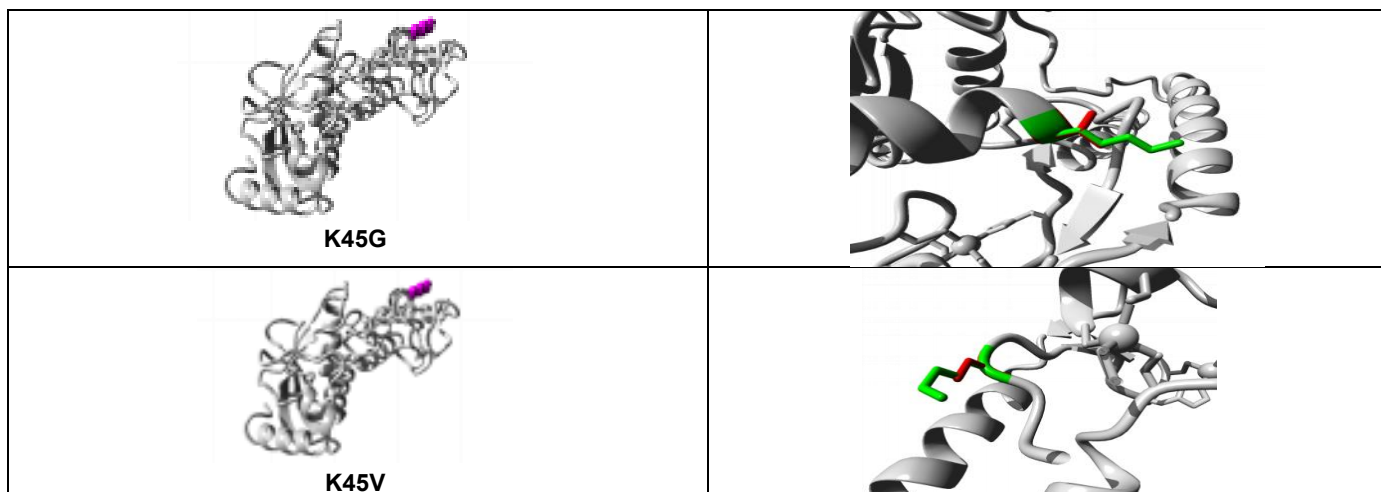
Studies done on the amino acids of BRCA1 have not deciphered much about its function, nonetheless, it is quite evident from the literature that there are two potential motifs in BRCA1, BRCT domain and zinc RING-finger domain [160], [161], [162]. The RING domain is necessary for E2 binding, whereas, the rest of the complex takes part in substrate binding. Interestingly, in the human proteome, BRCA1 and BARD1 are the only two proteins that have the RING domain at N-terminal, BRCT domain at C-terminal, and flanking α -helices that make BRCA1-BARD1 complex a heterodimer. Though both have RING domains, still only the BRCA1 RING domain binds with E2 [163]. Yet, how ubiquitination of BRCA1-BARD1 directly affects its ligase activity stands unsolved. Several BRCA1 missense variants occur in the N-terminus and have the potential to disrupt E3 ligase activity. To get to the depth of that, firstly, the structure of BRCA1-BARD1 was retrieved from the PDB database, 1JM7, and active sites was studied for the same using FTSite. Three active sites were visualized using PyMOL, namely, Active Site 1: (KILECP--L--I-----DHIF----...---L---...---RF) (20-79), Active Site 2: (IC---...---FC--KL) (26-51) and Active Site 3: (ELIKE---...---CKF) (29-46). Moreover, as the growing characterization of BRCA1-dependent ubiquitination is widely studied on lysine residues, thus, we targeted lysine residues from these three active sites. Four lysine residues were observed, namely, K20 from Active Site 1, K50 from Active Site 2, and K32 and K45 from Active Site 3. Later, pathogenic variants of these lysine residues were analyzed using MutPred2 which gave a general score with a threshold of 0.5 suggesting whether the amino acid substitution is pathogenic or not [164]. Intriguingly, K20 and K50 showed no score >0.5 . Moreover, as K20 does not come in the selected motif of BRCA1 as well as ubiquitination does not affect this site, as verified by PLMD and SMART, thus, this residue was dropped for further mutational analysis. Similarly, K50 was also dropped though it undergoes ubiquitination yet no pathogenic variant was observed from its MutPred2 analysis. MutPred2 analysis of K32 showed 8 variants with pathogenicity score >0.5 , where, the top three in increasing order were K32C, K32L, and K32Y. Likewise, for K45, 17 mutants were found pathogenic out of which K45G, K45V, and K45Y were the top three in increasing order. The result was validated using other mutational tools including, PredictSNP, PHD-SNP, PolyPhen-1, PolyPhen-2, SIFT, SNAP, and PANTHER (**Fig. 4.6.**). Therefore, Active Site 3 carrying K32 and K45 sites was considered as it displays strong mutagenesis. Lastly, stability analysis was performed for the variants of K32 and K45 using ProjectHOPE that compared mutants with the wild type based on size, charge, and hydrophobicity. Results suggested that all mutants were variable in size, neutral in charge, and more hydrophobic than the wild type. The green color represents the wild-type while the red color represents the mutant (**Table 4.2.**).

Mutation	PredictSNP	PhD-SNP	Poly-Phen-1	Poly-Phen-2	SIFT	SNAP	PANTHER
K32A	61 %	66 %	59 %	81 %	79 %	50 %	66 %
K32C	61 %	66 %	74 %	81 %	79 %	50 %	74 %
K32D	72 %	58 %	74 %	81 %	79 %	62 %	69 %
K32E	55 %	68 %	59 %	81 %	79 %	50 %	61 %
K32F	65 %	68 %	74 %	81 %	79 %	56 %	76 %
K32G	65 %	66 %	74 %	81 %	79 %	62 %	69 %
K32H	72 %	58 %	74 %	81 %	79 %	56 %	69 %
K32I	61 %	51 %	74 %	81 %	79 %	58 %	74 %
K32L	55 %	68 %	74 %	81 %	79 %	61 %	68 %
K32M	55 %	72 %	74 %	81 %	79 %	58 %	74 %
K32N	64 %	78 %	74 %	81 %	79 %	56 %	65 %
K32P	76 %	51 %	74 %	81 %	79 %	62 %	72 %
K32Q	65 %	72 %	74 %	81 %	79 %	62 %	56 %
K32R	51 %	83 %	67 %	65 %	79 %	56 %	47 %
K32S	65 %	68 %	74 %	81 %	79 %	56 %	66 %
K32T	61 %	68 %	74 %	81 %	79 %	50 %	49 %
K32V	65 %	68 %	74 %	81 %	79 %	56 %	72 %
K32W	72 %	66 %	74 %	81 %	79 %	72 %	78 %
K32Y	72 %	55 %	74 %	81 %	79 %	62 %	74 %
K45A	65 %	58 %	59 %	40 %	79 %	62 %	57 %
K45C	76 %	45 %	74 %	60 %	79 %	81 %	77 %
K45D	87 %	58 %	74 %	43 %	79 %	85 %	67 %
K45E	55 %	58 %	59 %	61 %	79 %	81 %	48 %
K45F	72 %	58 %	74 %	56 %	79 %	56 %	74 %
K45G	72 %	51 %	59 %	43 %	79 %	72 %	65 %
K45H	72 %	58 %	74 %	56 %	79 %	81 %	65 %
K45I	87 %	61 %	74 %	47 %	79 %	72 %	72 %
K45L	72 %	58 %	74 %	45 %	79 %	72 %	65 %
K45M	65 %	66 %	74 %	60 %	79 %	81 %	71 %
K45N	61 %	68 %	67 %	72 %	79 %	56 %	65 %
K45P	87 %	68 %	74 %	50 %	79 %	85 %	69 %
K45Q	65 %	66 %	74 %	45 %	79 %	72 %	47 %
K45R	83 %	78 %	67 %	75 %	73 %	55 %	68 %
K45S	52 %	68 %	59 %	61 %	79 %	62 %	48 %
K45T	65 %	68 %	74 %	45 %	79 %	72 %	61 %
K45V	65 %	66 %	74 %	45 %	79 %	72 %	70 %
K45W	72 %	55 %	74 %	60 %	79 %	85 %	74 %
K45Y	76 %	51 %	74 %	56 %	79 %	81 %	71 %

Fig. 4.6. Prediction of disease-related mutations by PredictSNP, PhD-SNP, PolyPhen-1, PolyPhen-2, SIFT, SNAP, and PANTHER. The green and red color indicate neutral and deleterious pathogenicity, respectively, whereas, the percentage indicates the expected accuracy or confidence score of each tool.

Table 4.2. Comparative result of lysine residues of wild-type BRCA1 and their mutants based on size, charge, and hydrophobicity

Amino acid substitution	Wild-type amino acid			Mutant-type amino acid			Domain
	Size	Charge	Hydrophobicity	Size	Charge	Hydrophobicity	
K32L	Larger	Positive	less	Smaller	Neutral	More	Highly conserved
K32Y	Smaller	Positive	less	Larger	Neutral	More	Highly conserved
K32C	Larger	Positive	less	Smaller	Neutral	More	Highly conserved
K45Y	Smaller	Positive	less	Larger	Neutral	More	Highly conserved
K45G	Larger	Positive	less	Smaller	Neutral	More	Highly conserved
K45V	Larger	Positive	less	Smaller	Neutral	More	Highly conserved
Modeled ribbon structure of BRCA1-BARD1 mutant				Close-up structure of BRCA1-BARD1 mutant			
 <p>K32L</p>							
 <p>K32Y</p>							
 <p>K32C</p>							
 <p>K45Y</p>							



4.2.2. BRCA1-BARD1 Docking with Ube2k

As BRCA1-BARD1 likely acts as E3 ligase in most cellular complexes and leads to ubiquitination of different substrates in each complex, it becomes necessary to identify which all E2 conjugating enzymes are bringing ubiquitin to it. Many studies state that the RING domain of BRCA1 has the ability to bind with the following E2 conjugating enzymes, UbcH6, UbcH7, Ube2e2, UbcM2, Ube2w, Ubc13, Ube2k and UbcH5 [165], [166], [167]. However, in one study it was further clarified that for BRCA1, Ubc13, and Ube2k are ubiquitin-specific E2s which means that E2 conjugates ubiquitin to another ubiquitin while UbcH6, Ube2e2, UbcM2, and Ube2w are substrate specific E2s suggesting that they transfer ubiquitin directly to the substrate [166]. UbcH7, Ube2w, Ubc13, and UbcH5 are class I E2s as they only have ubiquitin-conjugating (UBC) core domain. Ube2k is a class II E2, having a C-terminal extension from UBC core domain containing a ubiquitin associated (UBA) domain that attaches ubiquitin molecule and helps to dispense its transfer *in vitro* [168]. UbcH6, Ube2e2, and UbcM2 own an exclusive N-terminal extension from their closely-related UBC core domain [166]. Although, there are different classes of E2s, yet they all share many conserved features along with the same core domains and their ability to bind with E1s. Nonetheless, in our study, we picked Ube2k (PDB:6IF1) to dock with BRCA1-BARD1 because, firstly, Ube2k explicitly shapes a ubiquitin chain that is degradative in function such that whenever it binds with its suitable substrate, it gets degraded. Secondly, Ube2k is the only E2 that has a ubiquitin-binding domain that may lead to an increased local concentration of enzymes which further encourages to quickly build a ubiquitin chain for degradation [169]. Lastly, pieces of evidence suggest that Ube2k plays a crucial role in different neurodegenerative diseases, for instance, its involvement in Huntington's disease and Polyglutamine diseases [170], [171]. Elevated levels of Ube2k in the whole blood of individuals with schizophrenia show its surge in the brain indicating UPS dysfunction [172]. Moreover, Ube2k response is proapoptotic to the amyloid- β neurotoxicity as it upregulates signal-

regulating kinase 1 (ASK1) and c-Jun N-terminal kinase (JNK) signaling pathway, thereby inhibiting proteasome activity [173]. Furthermore, reduced expression of Ube2k contributes to dopaminergic neuronal death and motor deficits in patients with Parkinson's disease [174]. Before docking analysis, the active/attraction and passive/repulsion sites for both BRCA1-BARD1 (PDB:1JM7) and Ube2k (PDB:6IF1) were identified using CPORT. Active and passive sites of BRCA1-BARD1 and Ube2k are given in (Table 4.3.). Three protein-protein docking tools, HADDOCK, ClusPro, and LZerD were used to understand the binding of Ube2k with the mutants of BRCA1-BARD1 namely, K32Y, K32L, K32C, K45V, K45Y, and K45G. HADDOCK results were compiled based on the top cluster found and its z-score, which signifies the total number of standard deviations from the average, the more negative the better. Contrarily, ClusPro results were evaluated on the basis of highly populated clusters and low energy conformation of balance structures, suggesting that the cluster size should be more positive and energy should be more negative. Moreover, LZerD results were assessed on the basis of ranksum score, indicating smaller the ranksum score, better is the result (Fig. 4.7.).

Table 4.3. Active and passive sites of BRCA1-BARD1 and Ube2k identified using CPORT

	Active Sites	Passive Sites
BRCA1-BARD1 (E3 ligase enzyme)	19, 20, 21, 23, 25, 26, 27, 28, 29, 30, 32, 33, 36, 40, 41, 42, 44, 45, 46, 49, 50, 51, 54, 60, 62, 63, 64, 65, 66	14, 16, 17, 18, 24, 38, 39, 52, 53, 55, 56, 57, 58, 67, 69, 70, 72, 73, 74, 75, 76, 77, 78, 79, 82, 84, 87, 101, 102
Ube2k (E2 conjugating enzyme)	1, 2, 3, 4, 6, 7, 8, 10, 11, 13, 15, 35, 36, 63, 65, 68, 69, 94, 98, 99, 100, 101, 102, 103, 104, 105, 107, 108, 112	14, 17, 18, 19, 20, 21, 22, 30, 31, 33, 34, 37, 38, 61, 62, 64, 70, 72, 92, 93, 96, 97, 111, 114, 115, 117, 124

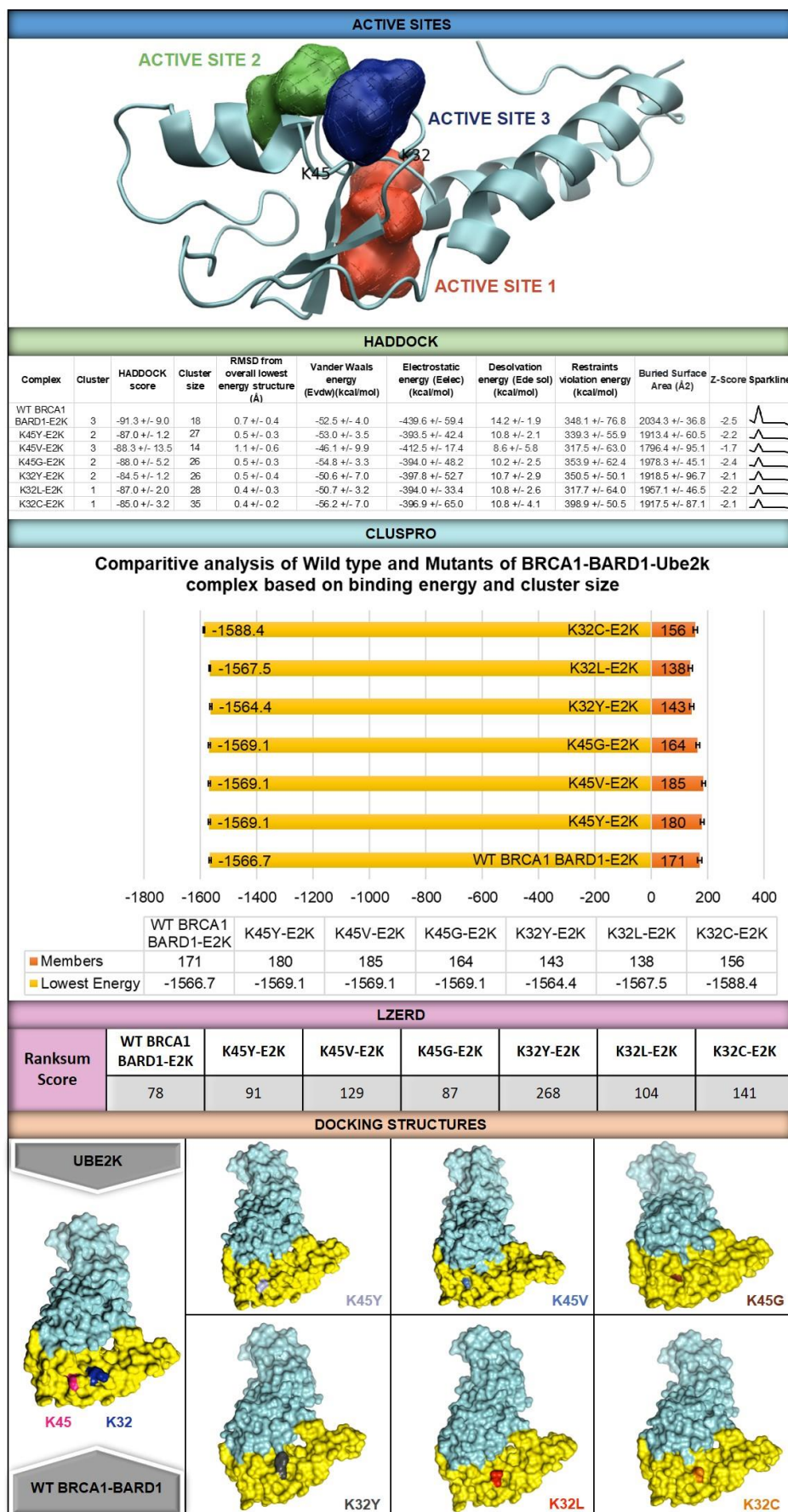


Fig. 4.7. Diagrammatic view of 3 active sites observed in the RING domain of BRCA1. The 2 potential lysine sites i.e., K32 and K45 lie in the blue-colored active site. The docking results of HADDOCK suggests that the z-score for all the mutant were less than the wild type suggesting that the mutants have a significant impact on E2-E3 binding while the ClusPro results indicate the lowest energy and the cluster size of each mutant (balanced model). LZerD gave a Ranksum for wild-type and each mutant which is calculated as the sum of GOAP, DFIRE, and ITScore, therefore, smaller Ranksum score suggests better result. Lastly, docking structures of BRCA1-BARD1 with Ube2k reveal structural changes detected in each case.

4.2.3. Molecular Dynamics Simulation of Protein-Protein Docked Structure

Molecular dynamics simulation (MDS) was performed for 20 nanoseconds (ns) for wild-type and all the mutants using an open-source software, GROMACS, following the steps of lysozyme in water to apprehend the conformational variations in BRCA1 owing to mutations K32Y, K32L, K32C, K45V, K45Y, and K45G (**Fig. 4.8.**). The top mutants i.e., K32L and K45Y were further analysed for 50 ns (**Fig. 4.9.**). RMSD, RMSF, and RG have been investigated throughout the simulation trajectory of the protein with time-dependent function. The RMSD value for the backbone residue of wild-type and mutants of BRCA1 was observed for all the atoms from the initial structure (1-103aa) to decipher the impact of mutation on protein stability. It has been observed that the RMSD value of all the mutants is highly unstable compared to the wild-type, however, the maximum deviation showed up in mutant K32L ranging from ~ 0.25 nm (wild-type) to ~ 0.7 nm (mutant), respectively. The second most unstable mutant observed was K45Y with deviation ranging from ~ 0.25 (wild-type) nm to ~ 0.6 nm (mutant) correspondingly (Figures 6 and 7). Later, RMSF of C α atom of wild-type and mutants were calculated to assess the fluctuation in each residue after mutation. The result depicted high residue level fluctuations in mutants compared to wild-type, exclusively for residues located between 40 to 70 positions. However, residue flexibility was not much affected in Ube2k docked with mutants of K45, nonetheless, in case of mutants of K32, noticeable fluctuations were observed, especially for Ube2k docked with mutant K32L. Lastly, the analysis of RG revealed that only the mutant K32L had least compactness in its structure with ~ 2.38 nm compared to wild-type with compactness ~ 2.28 nm, however, RG of K32C and K32Y had the highest compactness in structure with ~ 2.15 nm and ~ 2.2 nm, respectively. Whereas, in case of mutants of K45, K45Y showed least compactness with ~ 2.36 compared to wild-type with compactness ~ 2.28 nm.

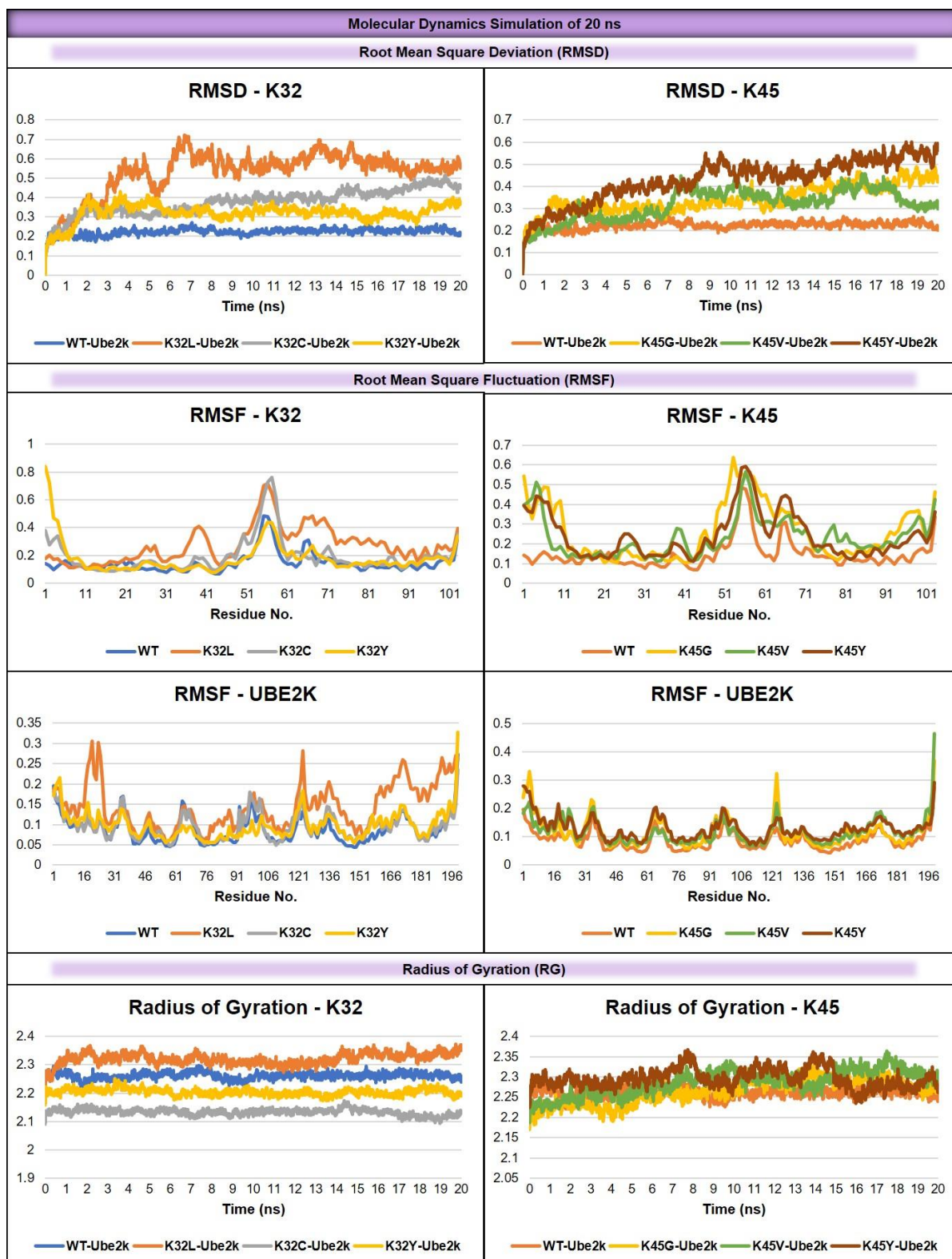


Fig. 4.8. Molecular dynamics simulation of wild-type and mutants K32Y, K32L, K32C, K45V, K45Y, and K45G at 20 ns, where several parameters were analysed including root mean square deviation (RMSD), root mean square fluctuation (RMSF), and radius of gyration (RG). The results suggest K32L as the most potential mutant that affects the E2-E3 binding.

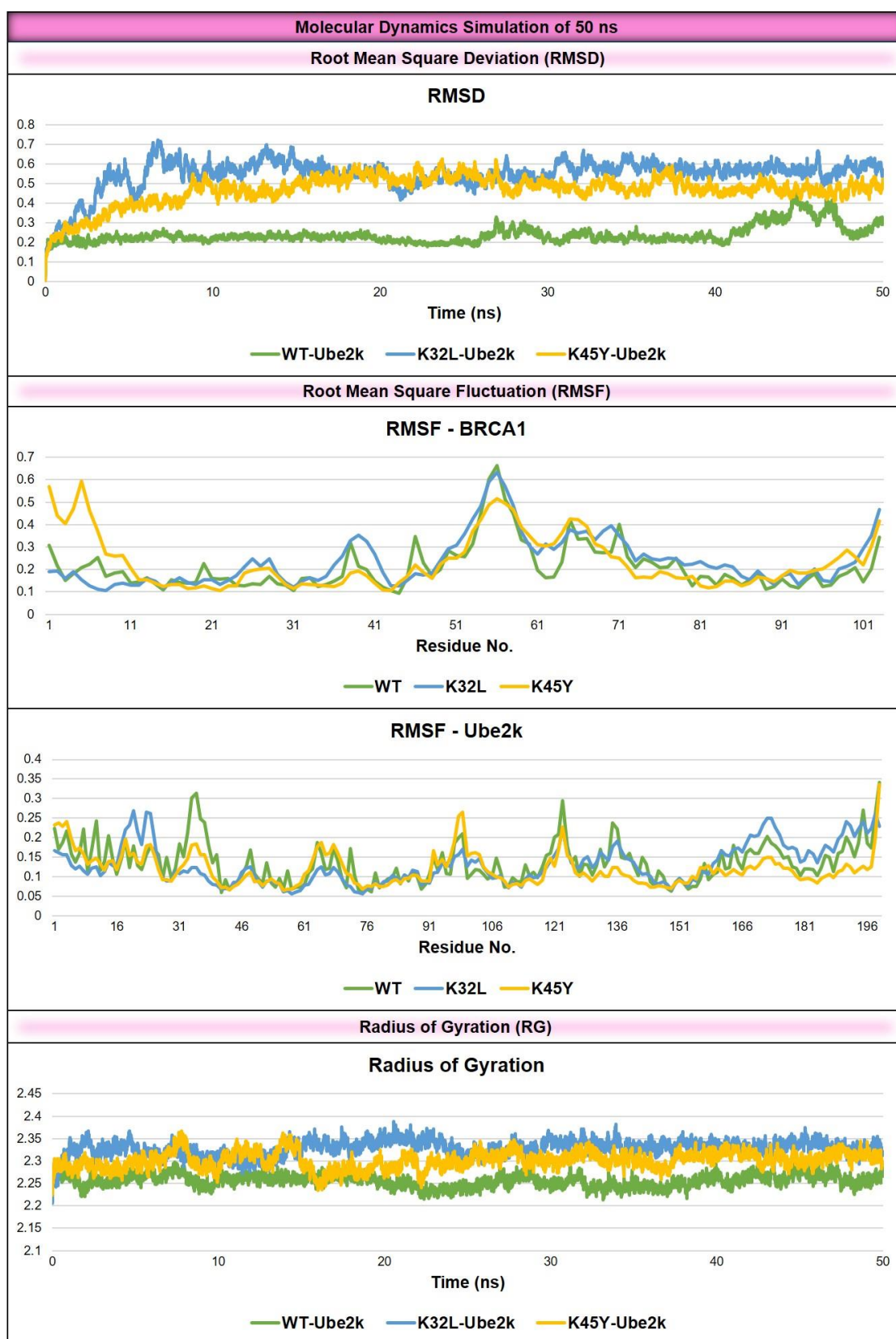


Fig. 4.9. Molecular dynamics simulation of wild-type and mutants K32L and K45Y at 50 ns, where K32L found to be most probable mutant that could affect the binding of BRCA1-Ube2k.

4.3. Results II (Objective II)

4.3.1. Recruitment, Visualization, and Preparation of Structures: BRCA1-BARD1, UbcH5c, H2A, and Tau

The architecture of the solution structure of BRCA1-BARD1 RING domain heterodimer (PDB ID: 1JM7) is composed of two chains: chain A representing BRCA1 (1-103aa) and chain B representing BARD1 (26-122aa). Both chains comprise two Zn^{2+} molecules flanking the helical bundle and pointing toward the surface of the nucleosome core protein. For the structure of the E2-conjugating enzyme, the crystal structure of E4B ubiquitin ligase in complex with UbcH5c (PDB ID: 3L1Z) was selected. It comprises two chains, namely, chain A of UbcH5c (1-147aa) and chain B of Ub-conjugating factor E4B (1226-1300aa) which is also a microRNA-9 gene that promotes autophagy-mediated tau degradation. Solution structure of histone protein (PDB ID: 2RVQ) composed of chain A of histone H2A (1-129aa) and chain B of Histone H2B (1-125). Paired helical tau filaments (306-379aa) from high-spin supernatants of aqueous extracts from AD brains were retrieved from (PDB ID: 8AZU). A reference structure of the complex having BRCA1-BARD1, UbcH5c, and H2A was taken from (PDB ID: 8GRQ) to comprehend the rightful placing of each component (**Fig. 4.10.**). The structure contains eleven chains namely, chain K of BRCA1 (6-97aa), chain M of BARD1 (34-117aa), chain N of UbcH5c (1-147aa), chain A & E of histone H3 (37-134), chain B & F of histone H4 (22-101aa), chain C & G of histone H2A (10-119aa), chain D & H of histone H2B (31-124aa), and two pairs of small molecules of Zn^{2+} attached with BRCA1 and BARD1, respectively. The same structure was also used for template-based docking carried out in later steps. The structures were downloaded in PDB format from the respective PDB identifier and were visualized in PyMol. It was made sure that all the structures retrieved were of the organism *Homo sapiens*.

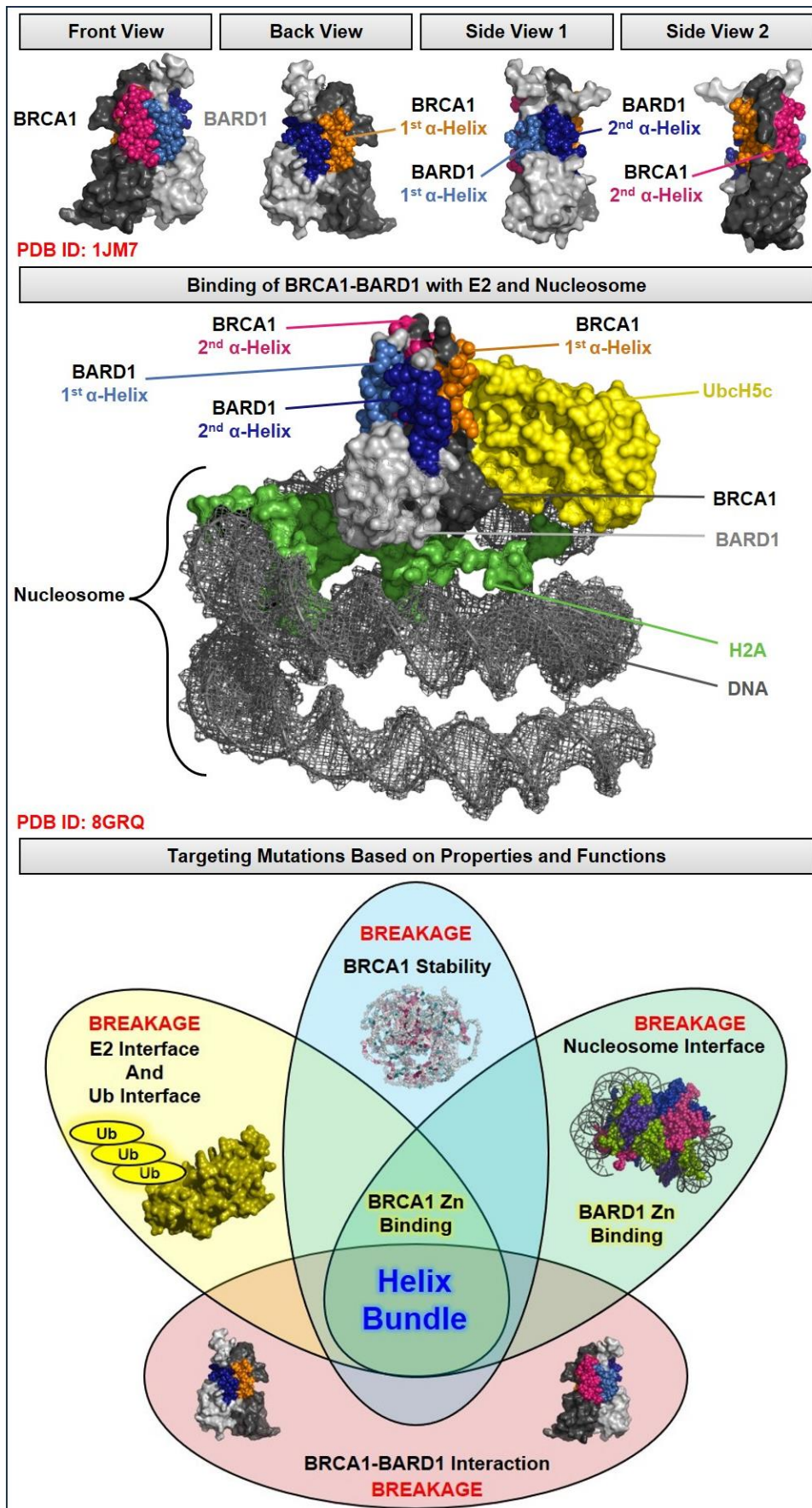


Fig. 4.10. At the top of the figure, the front view, back view, and lateral views of the α -helix bundle of the heterodimer BRCA1-BARD1 are depicted. In the middle portion, there is a visual representation of how BRCA1-BARD1 interacts with E2-UbcH5c and the nucleosome core protein-H2A. Finally, the bottom of the figure features a Venn diagram directing how to categorize mutations based on the properties and functions of BRCA1-BARD1.

4.3.2. Unraveling the Interacting Residues of RING Domain of BARD1

Prior to finding interacting residues, Scansite4 was used to predict the localization of BRCA1 and BARD1. The result suggested that for protein identifier BRCA1_HUMAN (UniProtKB/Swiss-Prot), it is majorly localized in cytoplasm with a prediction score of 29. The gene ontology (GO) terms associated with it are GO: 0005737 (Cytoplasm) and GO: 0005634 (Nucleus). It also stated the isoelectric point and molecular weight of BRCA1 as 5.294 and 207.75 kDa, respectively. Similarly, for protein identifier BARD1_HUMAN (UniProtKB/Swiss-Prot), its major localization lies in the nucleus with a prediction score of 100. The GO terms allied to BARD1 are GO: 0070531 (BRCA1-A complex), GO: 0031436 (BRCA1-BARD1 complex), and GO: 0005737 (Cytoplasm). Moreover, the isoelectric point and molecular weight of BARD1 are 8.988 and 86.66 kDa, respectively. Later, 12 interacting partners were observed for BARD1 (UniProtQ ID: Q99728) on PDBe-KB, namely, BRCA1 (P38398), UbcH5c (P61077), Histone H4 (P62805), Polyubiquitin-B (P0CG47), Histone H2B type 1-J (P06899), Histone H2B 1.1 (P02281), Histone H3.2 (Q71DI3), Histone H2B type 1-K (O60814), Histone H2A type 1-B/E (P04908), Histone H2A type 1 (P06897), Histone H3.1 (P68431), and DNA. Under the column of interaction interfaces, interacting residues of all these 12 interacting partners with BARD1 were noted, and manually selected the common residues that participate in binding with BRCA1 and UbcH5c, thus, 8 sites/residues were excluded as they were not common. BARD1 presented 37 and 28 interacting sites with BRCA1 and UbcH5c, respectively (**Table 4.4.**). Each common residue was assessed on AlphaFold that gave per residue confidence score (pLDDT) between 0 to 100. Those residues with pLDDT > 90 and >70 were selected for further evaluation as they suggest very high and high confidence scores, respectively. The inter-domain accuracy was also checked through a predicted alignment error (PAE) plot made through AlphaFold that aids in establishing the relative positioning of two residues that further assists in contemplating the location of two distinct domains. Hence, the dark green portion indicates good prediction with low error while light green corresponds to poor prediction with high error (**Fig. 4.11.**). The search was not limited to this, further, literature review was done to identify and filter out potential qualified sites. The BRCA1-BARD1 heterodimer is a stabilized conformation as it binds with each other through a hydrophobic core of four-helix bundles that comprise of two α -helices in both BRCA1 (8-22 and 81-96) and BARD1 (36-48 and 101-116). At the flanking end of the helix bundle carrying RING domains lies the Zn^{2+} binding regions in BRCA1 (23-76) and BARD1 (49-100) that point towards nucleosome core complex [38], [80], [175]. Since most of the cellular functions of BRCA1 are found in association with BARD1, thus, the heterodimeric conformation becomes an essential mediator of BRCA1 [176]. Therefore, the qualified residues that share binding with both BRCA1 and UbcH5c and lies within the range of two α -helices of BARD1 are H36, S37, A40, R43, L44, L47, L101, S103,

M104, L107, C108, L111, L114, and L115. That is to say 6 out of 7 qualified sites from the 1st α -helix and 8 out of 10 from the 2nd α -helix of BARD1 were taken forward for structural and functional analysis.

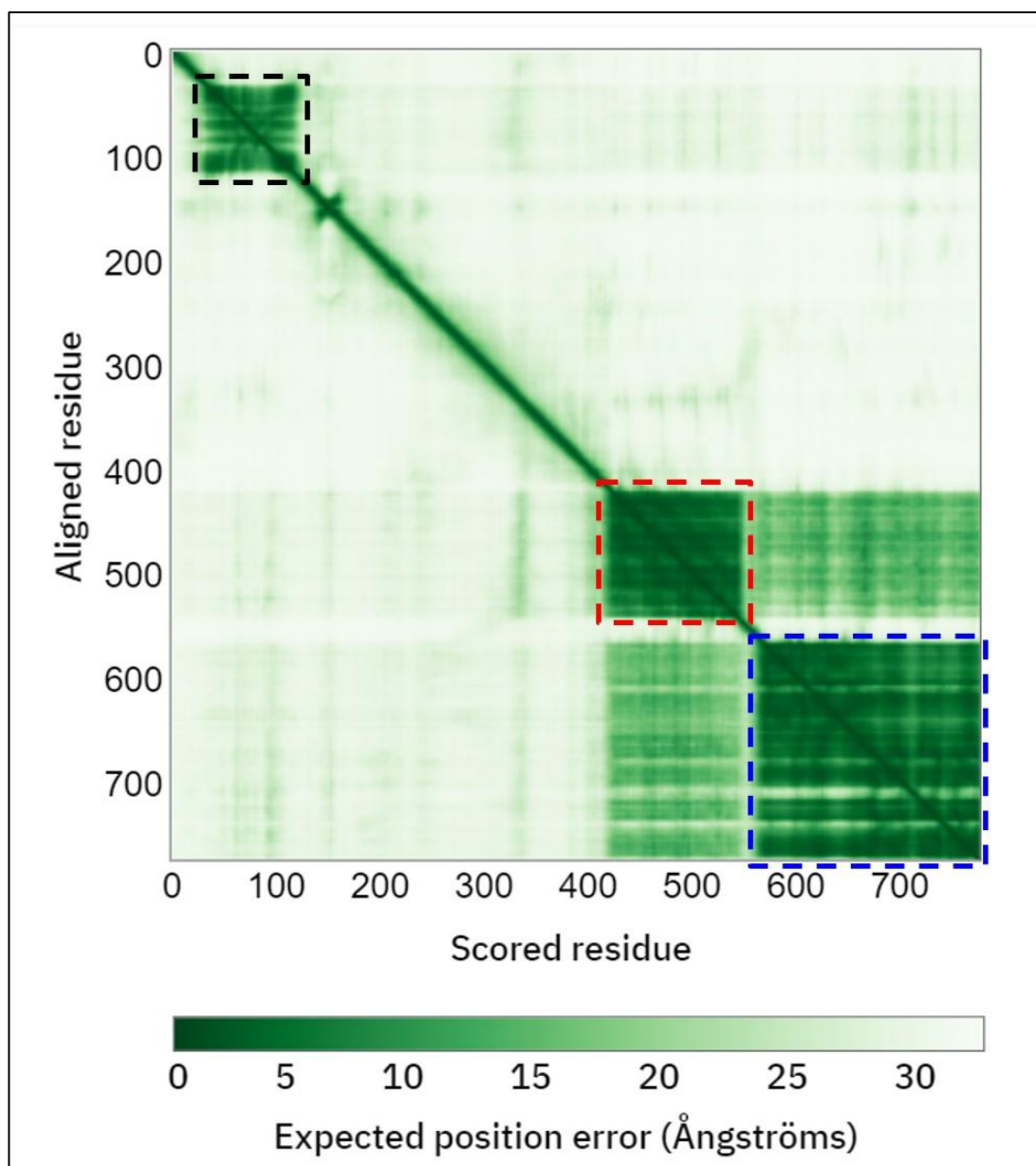


Fig. 4.11. Predicted Alignment Error (PAE) plot of BARD1. The plot is made through AlphaFold which predicts the inter-domain accuracy. The region marked in black, red, and blue are RING, Ank, and BRCT domains, respectively.

Table 4.4. Topological features of the binding site of BRCA1 and UbcH5c on BARD1

BARD1	PDBe-KB BRCA1 and UbcH5c Common Binding Sites on BARD1	AlphaFold (pLDDT)	ConSurf				
			Evolutionary Conservation Score	Structural or Functional	Buried or Exposed		
RING	33 aa	D29	46.51	4	-	Exposed	
		G30	53.16	2	-	Exposed	
		A33	71.5	3	-	Exposed	
	36 aa 1 st α -Helix	W34	81.8	9	Functional	Exposed	
		H36	80.78	5	-	Exposed	
		S37	85.94	9	Functional	Exposed	
		A40	87.15	9	Functional	Exposed	
		R43	89.34	5	-	Exposed	
		L44	88.53	7	-	Exposed	
		48 aa	G64	63.52	8	Functional	Exposed
			G65	67.82	4	-	Exposed
			E67	81.32	7	-	Exposed
			K96	71.97	8	Functional	Exposed
	I97		81.58	8	Functional	Exposed	
	N98		82.8	9	Functional	Exposed	
	R99		86.78	9	Functional	Exposed	
	101 aa 2 nd α -Helix	Q100	85.49	9	Functional	Exposed	
		L101	87.38	9	Structural	Buried	
		S103	87.85	5	-	Exposed	
		M104	88.77	7	-	Exposed	
		L107	89.16	9	Functional	Exposed	
		C108	87.97	8	-	Buried	
		K110	88.48	6	-	Exposed	
L111		86.88	9	Functional	Exposed		
L114		84.12	8	Functional	Exposed		
L115		79.22	8	-	Buried		
116 aa	N118	51	2	-	Exposed		
	S121	37.32	5	-	Exposed		
118 aa							

4.3.3. Structural and Functional Characterization of Interacting Sites

The topological feature intervention of qualified sites was first done through ConSurf where the query sequence of BARD1 (UniProt ID: Q99728) was uploaded. ConSurf utilizes its own database to find amino acid sequences similar to the query sequence and performs Multiple Sequence Alignment (MSA) using the Hidden Markov Model Method (HMMER), Multiple Alignment using Fast Fourier Transform (MAFFT), and Cluster Database at High Identity with Tolerance (CD-HIT) based on Rate4Site algorithm. The algorithm considers the phylogenetic relationship and stochastic behavior of evolution; therefore, it provides the pre-calculated evolutionary conservation profiles for every amino acid by using the Bayesian method. These conservation profiles range from 1 to 9 indicating highly variable to highly conserved sites, visually represented as turquoise to maroon color scale (**Table 4.4.**). The algorithm also helps in identifying functional and structural regions by mapping the evolutionary determinants. S37, A40, L44, L101, M104, L107, C108, L111, L114, and L115 residues are highly conserved, whereas, residues H36, R43, L47, and S103 are intermediately conserved. However, there were no highly variable residues observed. Based on an algorithm by NACSES, buried and exposed residues were identified indicating H36, S37, A40, R43, L44, L47, S103, M104, L107, L111, and L114 as exposed, while L101, C108, and L115 are buried. Moreover, some of the highly conserved residues were also predicted for their structural or functional significance. Thus, it was observed that residues S37, A40, L107, L111, and L114 are involved functionally, whereas, L101 participates structurally. Later, physicochemical properties such as tiny residues, small residues, aliphatic residues, aromatic residues, non-polar residues, polar residues, charged residues, positive residues, and negative residues were interpreted using EMBOSS Pepinfo as shown in (**Table 4.5.**). These properties can be termed as group potentials as those amino acids that share similar properties are put into one group. This helps to understand the number of occurrences of different amino acids of the same group in a particular segment of protein, for instance, here, is this case of RING domain of BARD1 which is also the part of α -helices.

Table 4.5. Physio-chemical properties of potential residues

Physico-Chemical Properties	Tiny Residues	Small Residues	Aliphatic Residues	Aromatic Residues	Non-Polar Residues	Polar Residues	Charged Residues	Positive Residues
1st α-Helix								
H36				✓		✓	✓	✓
S37	✓	✓				✓		
A40	✓	✓			✓			
R43						✓	✓	✓

L44			✓		✓			
L47			✓		✓			
L48 (Only in BRCA1)			✓		✓			
2nd α-Helix								
L101			✓		✓			
S103	✓	✓				✓		
M104					✓			
L107			✓		✓			
C108	✓	✓			✓			
K110 (Only in BRCA1)						✓	✓	✓
L111			✓		✓			
N113 (Only in BRCA1)		✓				✓		
L114			✓		✓			
L115			✓		✓			

4.3.4. Mutagenesis Findings of BARD1 Disrupting E3 Ligase Activity of BRCA1

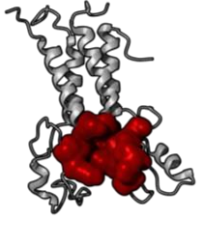
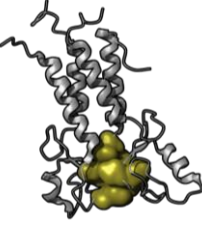
As majority of cellular functions of BRCA1 are done along with its heterodimeric partner, BARD1, therefore, there are high possibilities that any structural or functional changes or deviation in BARD1 could greatly affect the functionality of BRCA1. Missense mutation is one such possibility that if caused on BARD1 then it is likely going to have an impact on BRCA1 and its other interacting partners. Therefore, all the potential sites were studied for tolerated and deleterious substitutions using SIFT, FATHMM-XF, and PolyPhen-2. The result of SIFT suggested that nearly all the sites were predicted as not tolerated for all the substitutions, however, for C108, only C108H, C108Q, C108R, C108M, C108K, C108E, and C108I were projected as not tolerated. On the contrary, the outcome of FATHMM-XF depicted all substitutions of H36, S37, A40, R43, L44, L47, S103, M104, L107, C108, L111, L114, and L115 to be tolerated, except for L101 which was not tolerated. According to PolyPhen-2 results, all the substitutions of A40, L44, L101, M104, L107, L111, L114, and L115 exhibited probably damaging, whereas, for H36 (H36R and H36E), S37 (S37A and S37T), R43 (R43E and R43L), L47 (L47A, L47N, L47E, L47Q, L47K, and L47S), S103 (S103N and S103D), and C108 (C108A, C108G, C108L, C108S, C108T, C108Y, and C108V) predicted benign. Later, folding

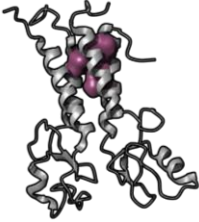
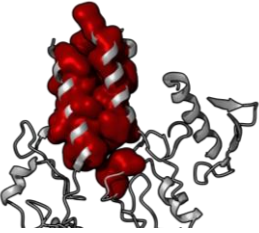
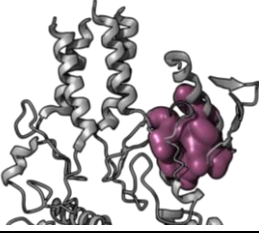
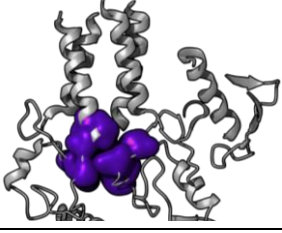
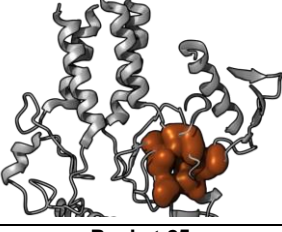
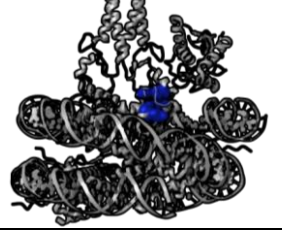
free energy ($\Delta\Delta G$) was calculated for every substitution mutation of the potential sites using MUpro, SAAFEC-SEQ, and I-Mutant2.0. The $\Delta\Delta G$ calculated from these three tools was averaged to decipher the top three mutants of all the qualified sites. Thus, the top three mutants are- H36 (H36N, H36T, and H36D); S37 (S37G, S37D, and S37H); A40 (A40G, A40H, and A40K); R43 (R43K, R43G, and R43S); L44 (L44G, L44D, and L44A); L47 (L47G, L47D, and L47A); L101 (L101G, L101T, L101A); S103 (S103G, S103H, S103P); M104 (M104G, M104K, M104A); L107 (L107G, L107T, L107A); C108 (C108G, C108T, C108K); L111 (L111G, L111T, L111A); L114 (L114G, L114T, L114D); and L115 (L115G, L115T, L115A).

4.3.5. Predicted Pocket Intervention

Predicting binding pockets helps to explicate docking prioritization, therefore, by using PrankWeb, binding pockets were assessed for two PDB structures, namely, 1JM7 and 8GRQ. These two structures were assessed simultaneously to get the binding residues between the two chains. The result projects that in structure 1JM7 which comprises of BRCA1 (Chain A) and BARD1 (Chain B), a total of 7 binding pockets were observed of which 3 showed inter-binding residues and the rest showed intra-binding residues. The 3 pockets that show the interaction between BRCA1 and BARD1 are Pockets 1, 2, and 7. Similarly, in structure 8GRQ, 28 pockets were observed, out of which only 5 were considered to support the study involving chains of BRCA1, BARD1, UbcH5c, and H2A. The 5 pockets selected were Pocket 1, 7, 8, 12, and 25. Where Pocket 1 and 8 showed interaction between BRCA1 and BARD1; Pocket 7 and 12 indicated residues between BRCA1 and UbcH5c; and Pocket 25 gave binding residues between BRCA1 and H2A. Along with binding residues, the tool also provided rank, score, probability, number of residues, and average evolutionary conservation score (Table 4.6).

Table 4.6. Pocket prediction for PDB ID:1JM7 and 8GRQ

PDB ID: 1JM7						
Pockets	Binding Partners	Rank	Score	Probability	Avg. Conservation Score	Residues
 <p>Pocket 1</p>	BRCA1(A)- BARD1(B)	1	9.25	0.541	1.723	A_25 A_39 A_40 A_41 A_42 A_63 A_64 A_65 A_67 A_78 A_79 B_100 B_96 B_97 B_98 B_99
 <p>Pocket 2</p>	BRCA1(A)- BARD1(B)	2	4.78	0.223	0.877	A_36 A_37 A_40 A_74 A_76 A_78 B_62 B_64 B_65 B_91

Pocket 7 	BRCA1(A)- BARD1(B)	7	1.02	0.007	0	A_89 A_93 B_36 B_37
PDB ID: 8GRQ						
Pockets	Binding Partners	Rank	Score	Probability	Avg. Conservation Score	Residues
Pocket 1 	BRCA1(K)- BARD1(M)	1	29.07	0.912	0.636	K_11 K_15 K_18 K_21 K_22 K_36 K_42 K_6 K_76 K_78 K_79 K_8 K_82 K_86 K_89 K_90 K_93 M_100 M_101 M_104 M_105 M_107 M_108 M_111 M_114 M_115 M_34 M_36 M_37 M_40 M_41 M_44 M_47 M_48
Pocket 7 	BRCA1(K)- UbcH5c(N)	7	4.25	0.187	1.689	K_26 K_27 K_29 K_46 K_47 K_50 N_1 N_4 N_5 N_59 N_60 N_61 N_62 N_8
Pocket 8 	BRCA1(K)- BARD1(M)	8	4.15	0.18	1.168	K_36 K_40 K_42 K_74 K_76 K_78 M_100 M_101 M_62 M_64 M_67 M_96 M_98
Pocket 12 	BRCA1(K)- UbcH5c(N)	12	2.41	0.065	2.35	K_26 K_43 K_47 K_51 K_60 K_62 N_62 N_95
Pocket 25 	BRCA1(K)- H2A(C)	25	1.12	0.01	1.981	C_65 C_68 C_86 C_89 C_90 K_52 K_70

4.3.6. BARD1 Mutants' Impact on BRCA1 Binding with UbcH5c, H2A, Tau

The technique of docking aids in understanding the effect of BARD1 mutagenesis on BRCA1 and its immediate interacting partners, UbcH5c, H2A, and Tau. Initially, template-based docking was conducted using Hex 6.3, wherein ETotal and RMS were computed for both wild-type and top three mutant structures of each potential residue, prepared using Pymol. For docking in Hex 6.3, three structures were uploaded separately: the receptor, the ligand, and the complex. For example, in the initial scenario, BRCA1 and BARD1 were uploaded as the receptor and ligand, respectively, while their pre-defined structure from PDB ID: 8GRQ served as the complex (Chain K and Chain M) to facilitate template-based docking. Prior to docking, structure matching was performed, which entailed superimposition calculations resulting in a grey tinge overlaying the structures. During docking, the correlation type parameter selected was shape + electrostatics, facilitating the computation of ETotal and RMS for both wild-type and mutant structures. Subsequently, in the second scenario, UbcH5c was designated as the receptor, while BRCA1-BARD1 served as the ligand, and their complex (Chain K, Chain M, and Chain N) was retrieved from PDB ID: 8GRQ to facilitate docking, utilizing the same parameters as outlined previously. In the third and fourth instances, H2A and Tau were designated as the receptor, with BRCA1-BARD1 serving as the ligand. For H2A, the complex (Chain K, Chain M, Chain C) was sourced from PDB ID: 8GRQ. However, concerning Tau, a docked structure of BRCA1-BARD1-Tau was retrieved from LZerD and employed as the complex. The results revealed varied outcomes regarding the interactions of BARD1 mutants with these complexes. Nonetheless, the primary aim of this study is to identify BARD1 mutants that destabilize the complexes with BRCA1, UbcH5c, and H2A, while simultaneously stabilizing the complex with Tau. The observations suggest that mutants H36D, S37G, A40H, L44G, L44D, L44A, L47G, L47D, L47A, M104K, L107G, K110G, and N113H significantly destabilize the complexes with BRCA1, UbcH5c, and H2A, while concurrently stabilizing the complex with Tau. Interestingly, mutants A40K, R43G, L114G, and L114D showcased destabilization not only with BRCA1, UbcH5c, and H2A, but also with Tau. The mutants that satisfy the aim were taken forward to CABS-dock for further analysis. The binding between BARD1 and BRCA1 was studied through CABS-dock which is a protein-peptide docking tool. The structure of BARD1 (1JM7, Chain B) was uploaded in the column for protein structure and the peptide sequence of BRCA1 was uploaded in the field provided for peptide sequence. The peptide sequence was designed to feature the mutated residue positioned centrally, surrounded by 10 residues on each side. Two peptide sequences were synthesized to assess the impact of each mutant: one representing the wild-type sequence, and the other featuring the mutation. The results were interpreted based on Average RMSD, aiming for structures closer to 5 Å. Thus, the smaller the RMSD, the better the structure. Consequently, the

results indicated greater deviation in the following mutant structures compared to their wild-type counterparts: S37G, A40H, L44A, M104K, and L107G. The resultant mutants derived from Hex 6.3 were tested with HADDOCK2.4 and LZerD. The HADDOCK2.4 results included the HADDOCK score, cluster size, RMSD from the overall lowest energy structure, van der Waals energy, electrostatic energy, desolvation energy, restraints violation energy, buried surface area, and Z-score for both wild-type and mutant structures. However, interpretations were primarily guided by the Z-score, where a smaller Z-score indicates a better structure. The following mutants were identified as destabilizing with BRCA1, UbcH5c, and H2A while stabilizing with Tau, arranged in decreasing order based on the sharper distinction in their values compared to the wild-type: L47G, L47D, A40H, L44A, and H36D. Similarly, the results of LZerD gave GOAP, DFIRE, and IT scores with their respective ranks, however, the model was assessed based on the Ranksum score which is the total of all three scores. The observed outcomes indicate that mutants M104K, S37G, A40H, and L47A exhibited destabilized complexes with BRCA1; mutants L44G, H36D, L44A, L47D, K110G, L47A, L47G, and S37G showed destabilized complexes with UbcH5c; mutants M104K and L44D displayed destabilized complexes with H2A; and mutants S37G, H36D, K110G, L44A, L47G, A40H, M104K, and L44D demonstrated stabilized complexes with Tau. Hence, S37G, A40H, L44A, L47A, and M104K are promising mutants that have recurrently occurred in CABS-dock, HADDOCK2.4, and LZerD (**Fig. 4.12.**).

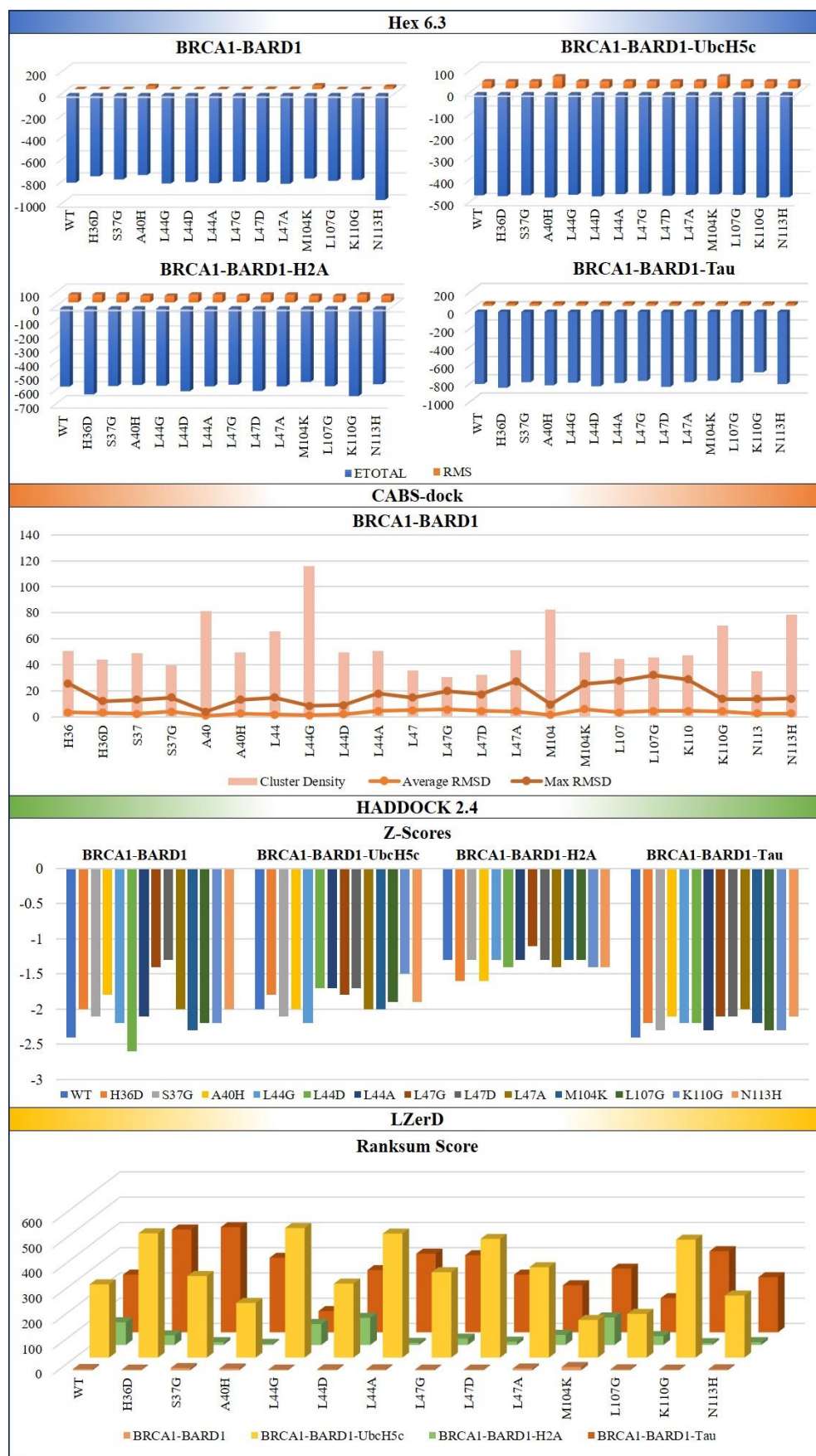


Fig. 4.12. The docking was performed for both wild-type and mutant structures of BRCA1-BARD1, BRCA1-BARD1-UbcH5c, BRCA1-BARD1-H2A, and BRCA1-BARD1-Tau. The first section of the figure presents the results of Hex 6.3, displaying the ETotal value and RMS of all the docked structures. In the second section, the findings of CABS-dock are presented in the form of a clustered chart illustrating cluster density, average RMSD, and maximum RMSD of all the docked structures. The third and fourth sections of the figure depict the outcomes of HADDOCK 2.4 and LZerD docking tools.

4.3.7. MDS of Docked Structures

Molecular dynamic simulations were conducted on both wild-type and mutant structures for 50 ns using the GROMACS software. By emulating the steps of lysozyme in water, conformational variations in BARD1 were elucidated, revealing the impact of mutations S37G, A40H, L44A, L47A, and M104K on BRCA1 and their direct binding partners UbcH5c, H2A, and Tau. RMSD, RMSF, and RG were analyzed throughout the simulation trajectory of the protein/complexes using a time-dependent function. Five distinct scenarios were investigated independently to comprehend the impact of BARD1 mutation. In the initial case, MD simulation of both wild-type and mutant structures of the BARD1 protein encompassed all atoms from the initial structure (26-122aa) to decipher the mutation's effect on protein stability. It has been observed that out of all potential mutants, RMSD values of mutants L44A and L47A were unstable compared to wild-type, however, the maximum deviation was observed in L44A that ranged from ~0.62 nm (wild-type) to ~0.81 nm (mutant), respectively. Nevertheless, in L47A the deviation went to a maximum of 0.73 nm (**Fig. 4.13.**).

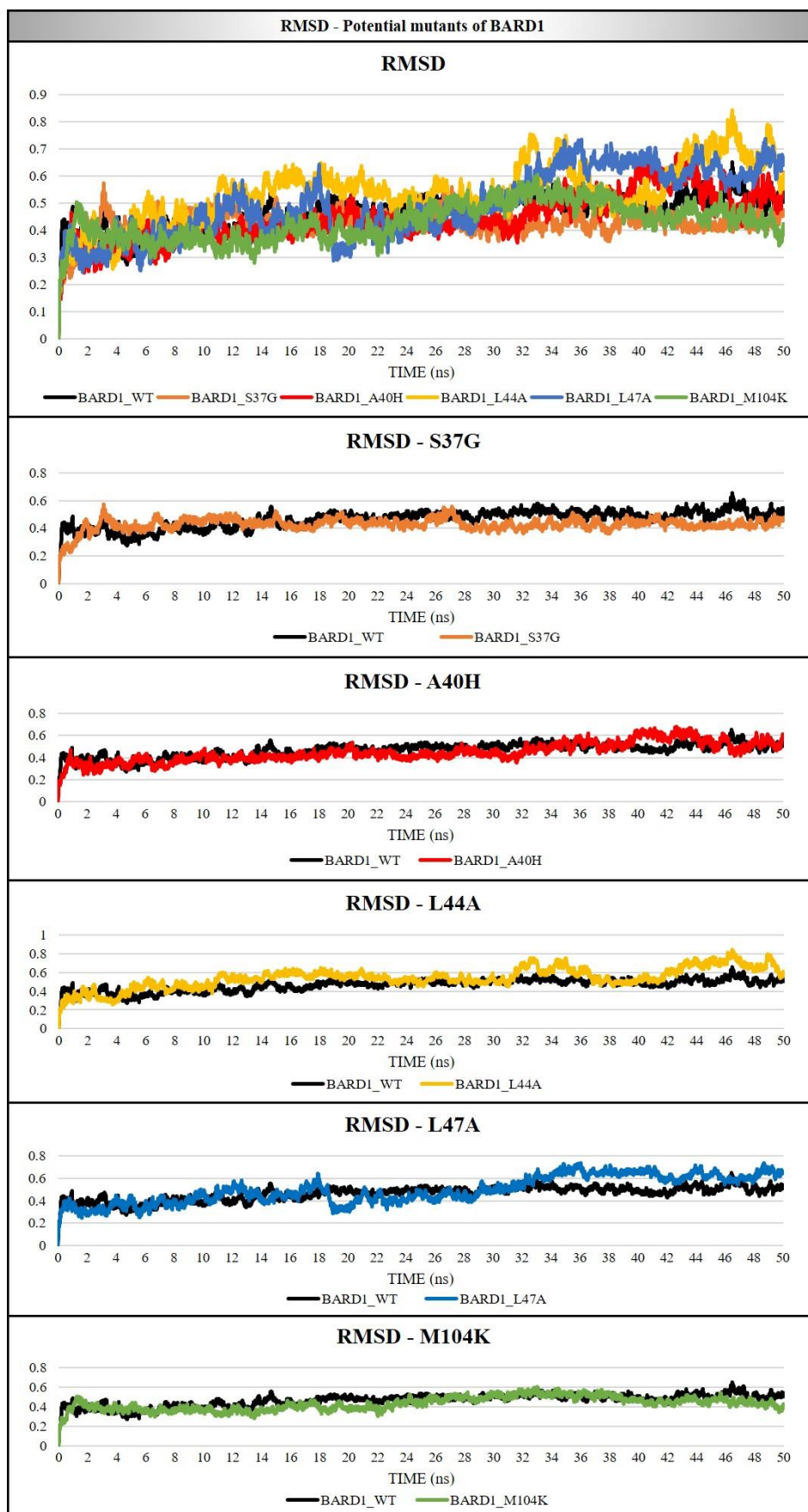


Fig. 4.13. MDS were conducted for both wild-type and mutant structures of BARD1, including S37G, A40H, L44A, L47A, and M104K, over a period of 50 ns. The findings indicate that the L44A mutation exhibited the highest root mean square deviation (RMSD) compared to the other mutants, suggesting its potential impact on the structure and dynamics of BARD1.

The RMSF of the C α atom was calculated for both the wild-type and mutants to assess the fluctuation in each residue following mutation. The results described high fluctuations in mutant L44A throughout all the positions; however, in mutant L47A the fluctuations positioned between 35 to 50 and 70 to 90 positions. For the rest of the mutants, the residual fluctuations were not that greatly significant compared to the wild-type. Interestingly, the analysis of RG revealed that mutant S37G, L44A, and M104K depicted nearly similar compactness in their structures with respect to wild-type. i.e., around 1.81 nm. However, mutants A40H and L47A demonstrated lower compactness in their structures, measuring around ~1.84 nm, compared to the wild-type (**Fig. 4.14.**). As BARD1 mutant L44A showed maximum deviation and fluctuations in its structure compared to wild-type, therefore, its impact on other binding partners were studied in the following four scenarios.

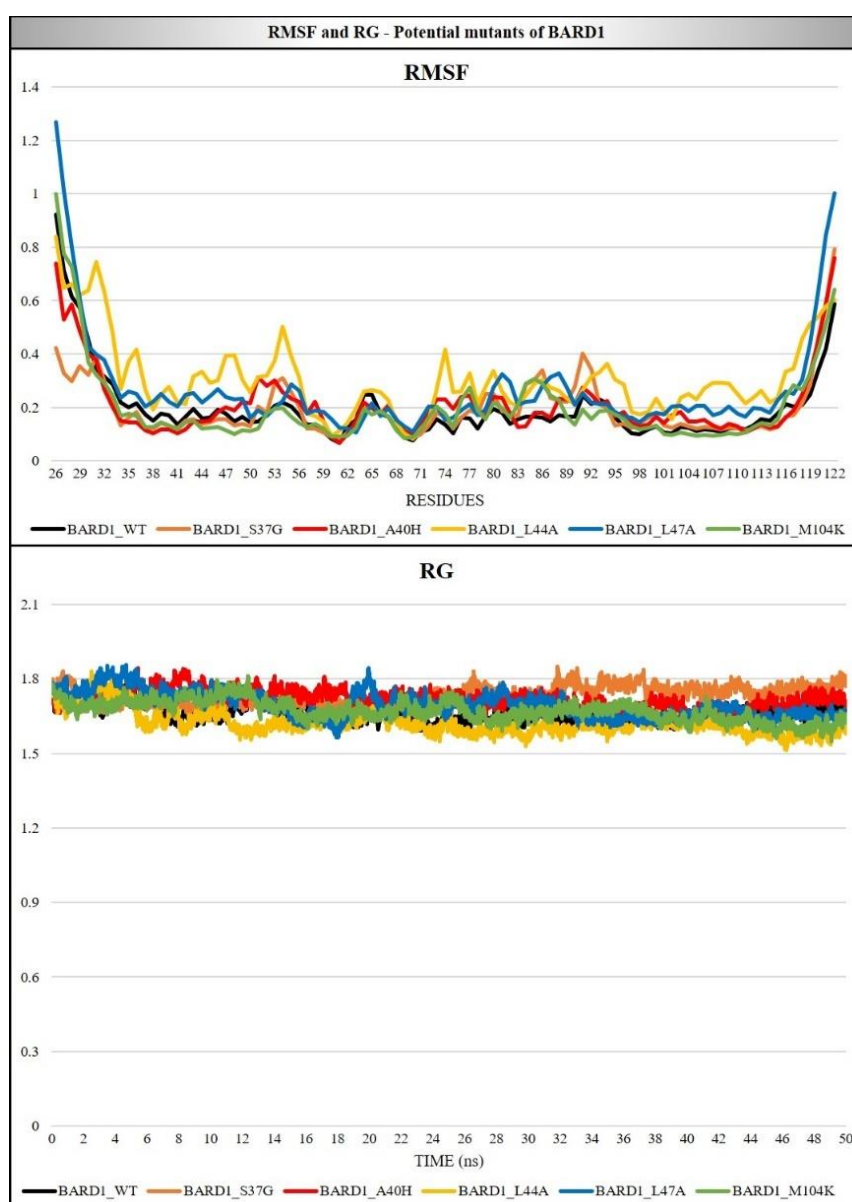


Fig. 4.14. The figure illustrates the root mean square fluctuation (RMSF) and radius of gyration (RG) of both wild-type and mutant structures of BARD1, including S37G, A40H, L44A, L47A, and M104K. The results indicate that the L44A mutant displayed the highest fluctuations in residues, while simultaneously exhibiting the least compactness in its structure.

In the second scenario, the interaction between BRCA1 and BARD1 was examined to evaluate the impact of BARD1 mutation on its heterodimeric partner, BRCA1. All atoms were extracted from the primary structures of BRCA1 (1-103aa) and BARD1 (26-122aa) for analysis. The RMSD value of the mutant L44A observed was ~ 0.49 nm, whereas for wild-type, it was ~ 0.43 nm. Similarly, when RG was compared between the mutant and wild-type structures, the results suggested poorer compactness in the mutant L44A, measuring around 2.04 nm compared to the wild-type, which measured around 2.02 nm. Surprisingly, in this instance, the RMSF values revealed significant differences, with the wild-type structure exhibiting more fluctuations across all positions compared to the mutant BARD1 structure carrying the L44A missense mutation. Likewise, the residue flexibility of BRCA1 docked with mutant BARD1 noted very less fluctuations compared to the wild-type structure (Fig. 4.15.).

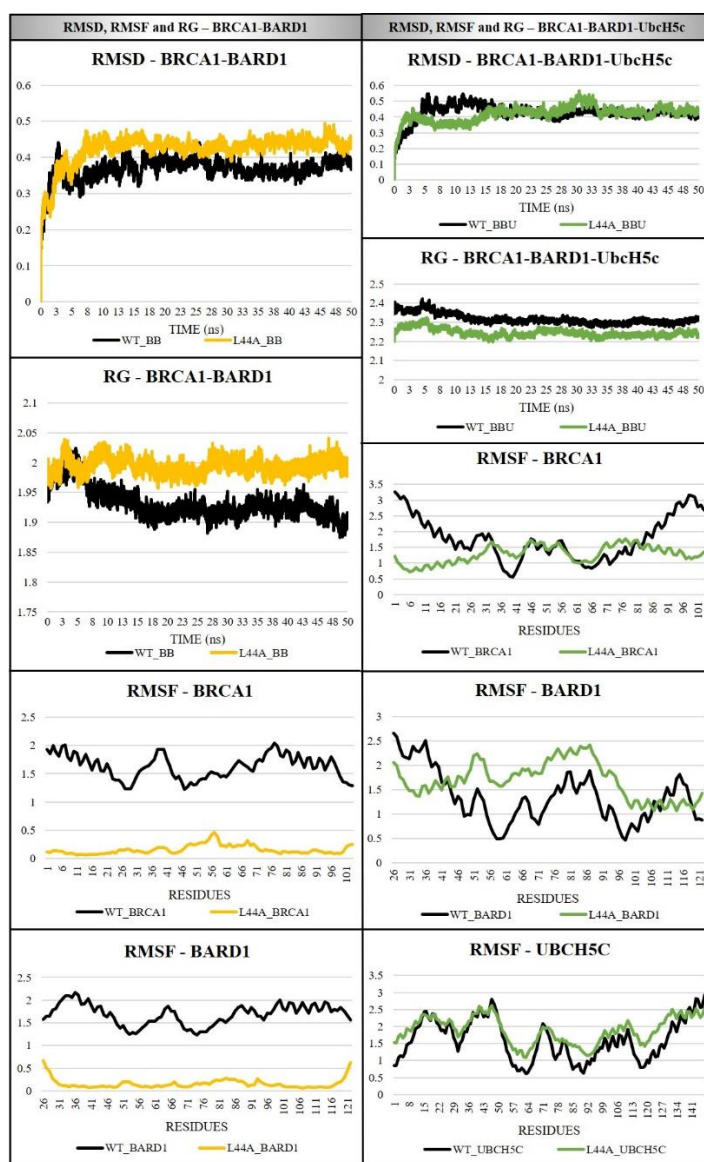


Fig. 4.15. The molecular dynamic simulation was conducted for both wild-type and mutant structures of BRCA1-BARD1 (L44A) and BRCA1-BARD1 (L44A)-UbcH5c for 50 ns. The results indicate a higher deviation in the mutant structure of BARD1 when docked with BRCA1, whereas no significant deviation was observed in the case of BRCA1-BARD1 docked with UbcH5c. Regarding the radius of gyration (RG), BRCA1-BARD1 (L44A) exhibited less compactness compared to the wild-type, whereas in BRCA1-BARD1 (L44A)-UbcH5c, the opposite trend was observed. Furthermore, the root mean square fluctuation (RMSF) analysis revealed higher residue fluctuations of BARD1 in BRCA1-BARD1 (L44A)-UbcH5c compared to BRCA1-BARD1 (L44A).

In the third instance, the interaction between BRCA1-BARD1 and an E2 conjugating enzyme, UbcH5c, was explored. UbcH5c serves as an immediate binding partner of BRCA1. However, since BRCA1 predominantly functions in its heterodimeric state, coupled with BARD1, any alteration in the conformational state of BARD1 will inevitably influence the conformation of BRCA1. Consequently, this change will impact the binding of BRCA1 with UbcH5c. The observed RMSD of the backbone residues of wild-type and mutant protein of BRCA1-BARD1-UbcH5c was detected for all the atoms from the initial structure of BRCA1 (1-103aa), BARD1 (26-122aa), and UbcH5c (1-147aa). The result suggested that after 50 ns, there was a negligible difference in RMSD values of wild-type and mutant structures i.e., around 0.53 nm. The result of RG suggests that the compactness of the wild-type structure is ~2.41 nm, whereas the compactness of the mutant structure is ~2.31 nm, indicating the mutant structure to be more stable than the wild-type. Later, RMSF of the C α atom of BARD1 deciphered higher fluctuations in BARD1 (L44A) than wild-type for residues located between 43-106 positions. However, the flexibility of BRCA1 docked with mutated BARD1 showed fluctuations for the residues located between 34-40 and 62-77 positions. Similarly, UbcH5c docked with BRCA1-BARD1 (L44A) showed fluctuations for the residues between 1-10, 57-65, and 74-130 positions.

In the fourth and fifth scenarios, RMSD, RMSF, and RG were calculated for both mutant and wild-type structures of BRCA1-BARD1 docked with H2A (1-129aa) and Tau (306-379aa), respectively. The RMSD value of the BRCA1-BARD1-H2A docked structure carrying the L44A mutation in BARD1 was ~1.95 nm, whereas the RMSD of the wild-type structure was around 1.87 nm. Conversely, when BRCA1-BARD1 was docked with Tau, the RMSD of the wild-type structure was ~1.54 nm compared to the mutant structure, which was approximately 1.03 nm. These findings suggest that the BARD1 mutation destabilizes the BRCA1-BARD1 interaction with H2A. However, interestingly, the same mutation stabilizes the interaction of BRCA1-BARD1 with Tau. The RG results indicate that the mutant structures of BRCA1-BARD1-H2A and BRCA1-BARD1-Tau had the least compactness, with a value of ~3.29 nm and ~2.39 nm, respectively, compared to the compactness of their respective wild-type structures i.e., ~2.81 nm and ~2.53nm. The RMSF analysis of the C α atoms of the mutant BARD1 in BRCA1-BARD1-H2A revealed high fluctuations between residues 49-105. Moreover, for BRCA1 bonded to BARD1, the most significant fluctuations were observed between positions 20-30. Similarly, H2A docked with BRCA1-BARD1 carrying the L44A mutation exhibited increased fluctuation between positions 2-16 and 56-105. Specifically, the RMSF of the C α atoms of BARD1 with the L44A mutation in BRCA1-BARD1-Tau showed heightened fluctuations primarily at position 51 compared to the wild-type. For BRCA1, maximum fluctuation was observed at position 56 and between positions 65-68. Furthermore, when Tau was

docked with BRCA1-BARD1, peaked fluctuations were noted between positions 344-348 only (Fig. 4.16.).

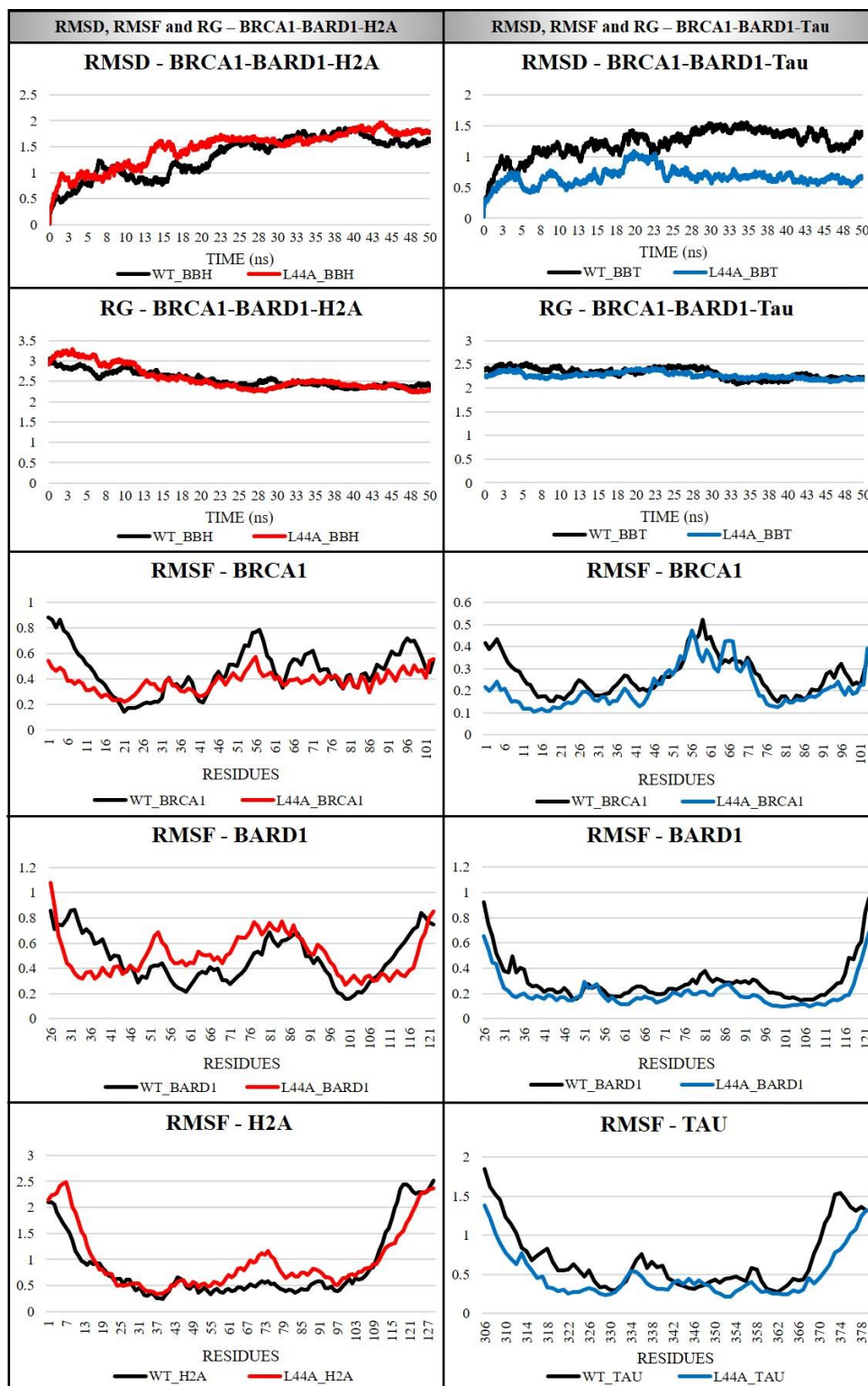


Fig. 4.16. The molecular dynamic simulation was carried out for both wild-type and mutant structures of BRCA1-BARD1 (L44A)-H2A and BRCA1-BARD1 (L44A)-Tau over a 50 ns period. The results indicated greater deviation in BRCA1-BARD1 (L44A)-H2A, while the opposite trend was observed in BRCA1-BARD1 (L44A)-Tau. The radius of gyration (RG) showed similar values for both wild-type and mutant structures in both scenarios. Additionally, the root mean square fluctuation (RMSF) analysis demonstrated higher residue fluctuations of BARD1 in BRCA1-BARD1 (L44A)-H2A compared to BRCA1-BARD1 (L44A)-Tau.

4.4. Results III (Objective II)

4.4.1. Protein-Protein Interaction and Gene Co-expression of RNF8

Interaction between E3 ligase, RNF8, and E2 conjugating enzyme, UBE2N is indispensable for DSB and recruitment of BRCA1. However, it becomes necessary to understand other interacting partners that support this association and the STRING network analysis represented 10 networking partners of RNF8 namely UBE2N, MDC1, TP53BP1, H2AFX, RNF168, BRCA1, ATM, UIMC1, NBN, and HERC2 (Fig. 4.17.). The p-value of this enriched network is $5.55e-16$. Moreover, the number of nodes, edges, and avg. node degree of this network is 11, 55, and 10 respectively. The functional enrichment gene ontology of RNF8 suggests that it is highly involved in the histone H2A K63-linked ubiquitination biological process (GO:0070535). Molecular function suggests its direct involvement in K63-linked polyubiquitin modification-dependent protein binding (GO:0070530) and cellular component states engrossment of RNF8 in the BRCA1-A complex (GO:0070531). KEGG and Reactome pathways suggested that RNF8 is hugely involved in homologous recombination (hsa03440) and DSBs (HSA-5693548). Additionally, the subcellular localization study describes the cellular entity of RNF8 is BRCA1-BARD1 complex (GOCC:0031436). Gene co-expression analysis of RNF8 and its other interacting partners also suggested a close interaction among themselves.

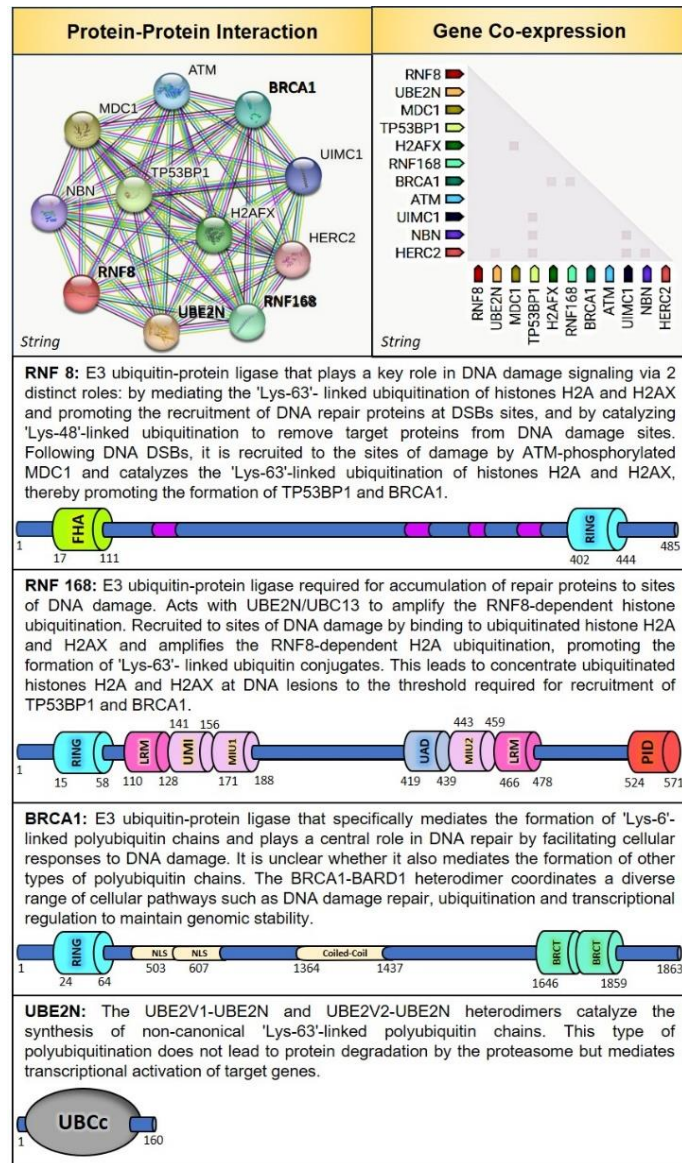


Fig. 4.17. Protein-protein interaction network, gene co-expression, and domain structures of RNF8 and its other interacting partners.

Gene co-expression analysis of RNF8 and its other interacting partners also suggested a close interaction among themselves.

4.4.2. Structural Analysis of RNF8 and UBE2N

The FASTA sequence of RNF8 (485aa) was retrieved from NCBI (Accession: O76064.1 GI: 21362894), thereafter the sequence was submitted to ConSurf which gave a 3D structure of the protein. The derived 3D structure was verified through I-TASSER (Model 4, C-score -3.19). The structure of UBE2N (160aa) was retrieved from PDB (4WHV), chain B. Both the proteins are of the organism, *Homo sapiens*.

4.4.3. Analysis of RING Domain of RNF8

The domain architecture of RNF8, RNF168, BRCA1, and UBE2N was extracted from SMART which showed the presence of the RING domain in each one of them (Fig. 2). However, keeping RNF8 as the target protein, it becomes necessary to intensely understand the domain structure of the same. Therefore, it was first checked on UniProt (O76064), where under the section of family and domain it was observed that a Zinc finger RING-type domain of RNF8 lies between 403-441aa. Later, with AlphaFold, inter and intra domains were predicted for accuracy which showed 2 distinct domains namely FHA (marked in red) (37-109aa) and RING (marked in yellow) (403-441aa) (**Fig. 4.18.**). Some low-complexity regions were also observed; however, they require further validation.

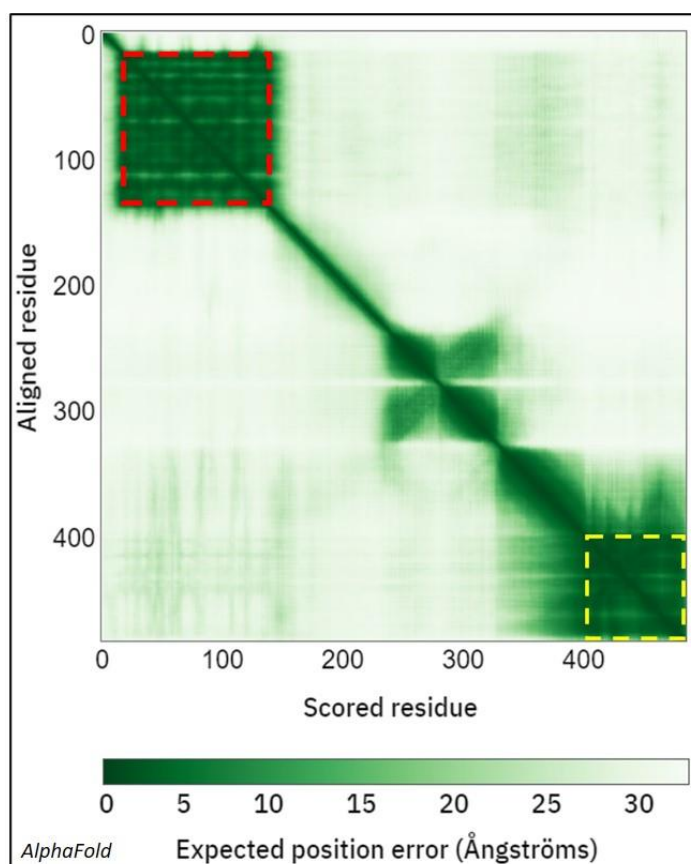


Fig. 4.18. Predicted Aligned Error (PAE) plot to demarcate FHA and RING domain of RNF8.

4.4.4. Interface Prediction of RNF8 with UBE2N

The UniProt Id of RNF8, O76064 was searched on PDBe-KB which gave 14 interaction sites of UBE2N on RNF8 namely Q402, I404, I405, C406, S407, E408, E429, W430, R433, K434, P438, I439, R441 and R471. However, Q402 and R471 were not further analyzed as they do not lie in the RING domain. Under flexibility prediction, the results of WEBnma and DynaMine showed very less fluctuations in the residues of the RING domain as according to DynaMine, all residues have values above 0.8 suggesting a rigid conformation. Moreover, early folding residue prediction by EFoldMine depicted all key sites except R441 to have a value greater than 0.169 indicating all residues to start the early folding process. Further, through ConSurf and I-TASSER, predicted solvent accessibility of key residues exhibited whether they are structural, functional, buried, or exposed (**Fig. 4.19.**). However, as for I404, it was not clear whether it is structurally or functionally involved, therefore, it was dropped for further analysis.

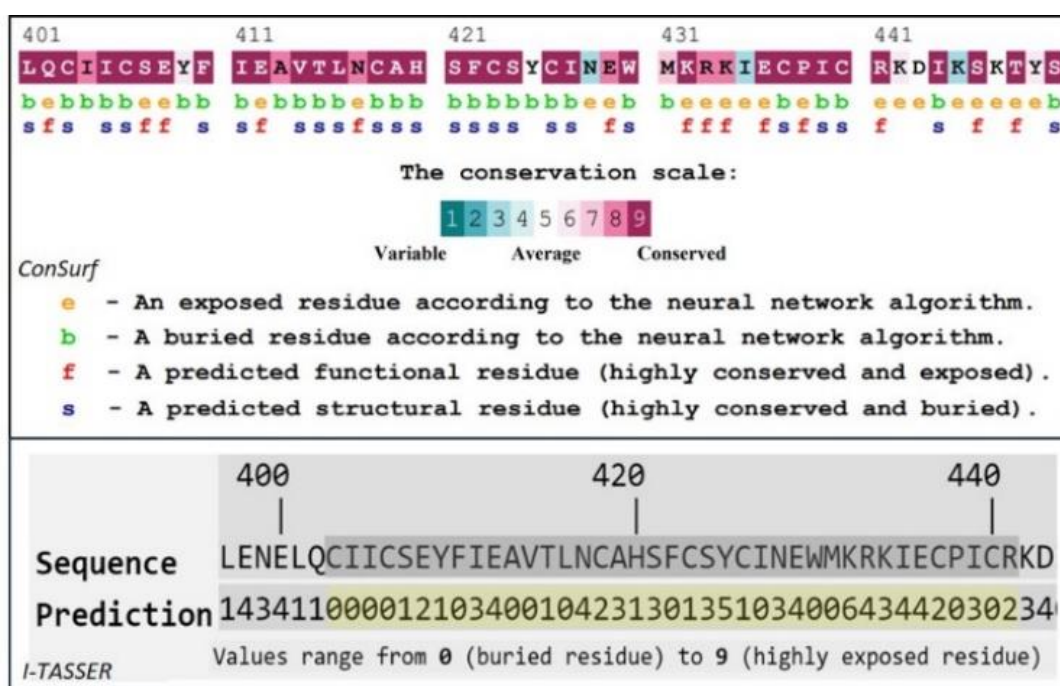


Fig. 4.19. Topology of predicted residues using ConSurf and I-TASSER.

4.4.5. Evolutionary Conservation Analysis

The evolutionary conservation score of each predicted site namely I405, C406, S407, E408, E429, W430, R433, K434, P438, I439, and R441 was first analyzed using AlphaFold which gave pLDDT score for each residue indicating that all are highly conserved. Whereas, the results of ConSurf stated that all the residues were highly conserved except for E429 and K434 which had scored a little less than the other residues (**Fig. 4.20.**).

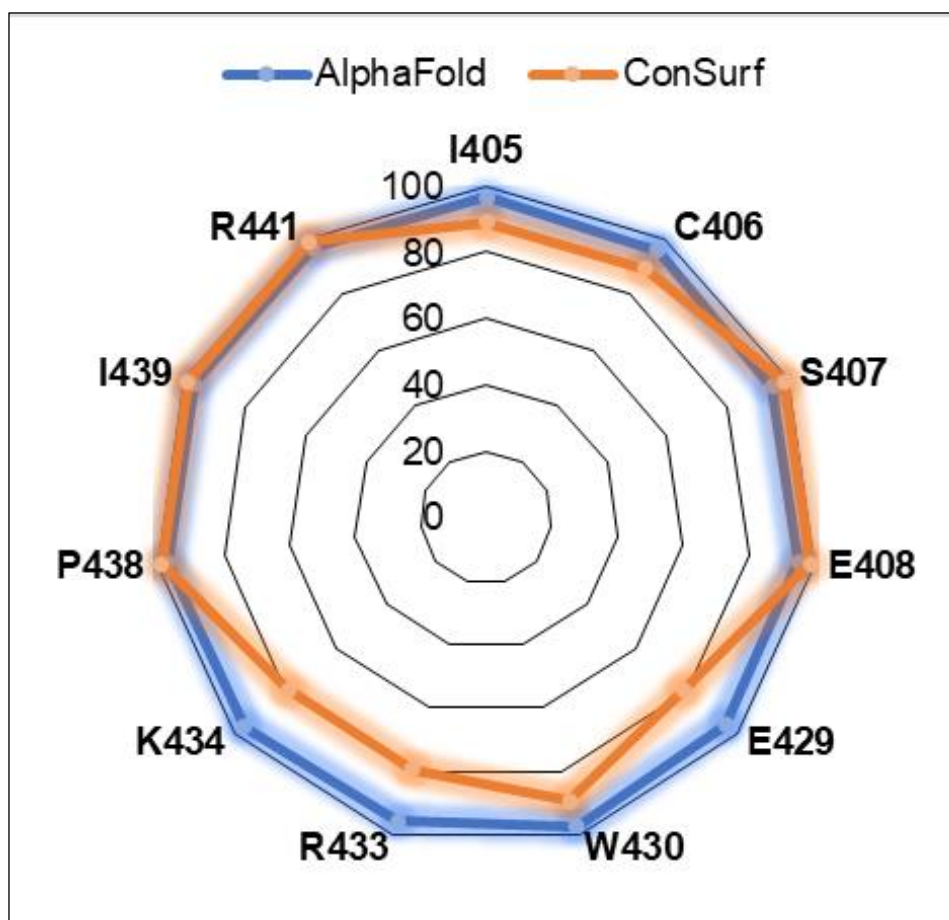


Fig. 4.20. Evolutionary conservation score of each predicted site using AlphaFold and ConSurf.

4.4.6. Mutagenesis of Qualified Sites and its Preparation

Despite the fluctuations in the evolutionary conservation score, all the residues were taken forth for mutational studies. The DDG values were estimated for each residue using I-Mutant 2.0 and MUpro. The average DDG value was further calculated to indicate the top mutant of each predicted site, I405 (I405G, -3.09), C406 (C406T, -1.51), S407 (S407G, -1.19), E408 (E408G, -1.34), E429 (E429G, -0.96), W430 (W430G, -2.425), R433 (R433P, -1.34), K434 (K434G, -0.95), P438 (P438A, -0.99), I439 (I439G, -1.74) and R441 (R441P, -1.61). Later, the mutant structures were prepared using PyMOL.

4.4.7. Docking Analysis

HADDOCK2.4 (Calculation of Z-score): HADDOCK2.4 server was used for protein-protein docking which gave the Z-score for each mutant of RNF8 docked with UBE2N. According to Z-score, all the mutants except P438A and R441P had Z-score less than the wild-type. P438A had similar while R441P had greater Z-score than the wild-type (Fig. 4.21).

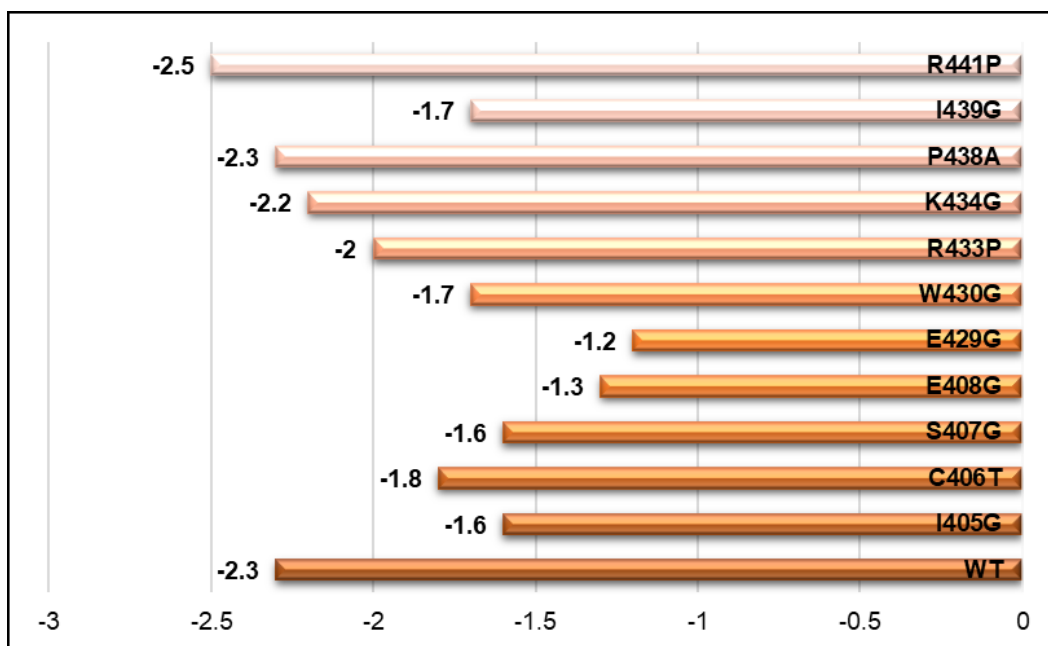


Fig. 4.21. Comparison of Z-score between wild-type and mutants using HADDOCK.

CABS-dock (Calculation of RMSD): As CABS-dock provides the platform for protein-peptide docking, therefore, the wild-type and mutant peptide sequences were prepared for each predicted residue, where the key residue was flanked by 10 residues on both sides. Contrarily, the protein structure of UBE2N was taken to be docked. The values of avg. RMSD, max RMSD, and cluster density were noted for every wild-type and mutant peptide sequence (Fig. 4.22.). However, here the minimal avg. RMSD suggested the best binding affinity, therefore, those mutants that had avg. RMSD values less than its wild-type were dropped. Hence, suggesting that I405, S407, E408, E429, R433, P438, I439, and R441 could be potential motifs that affected the binding of UBE2N and also might hamper the E3 ligase activity of RNF8 (Table 4.7.).

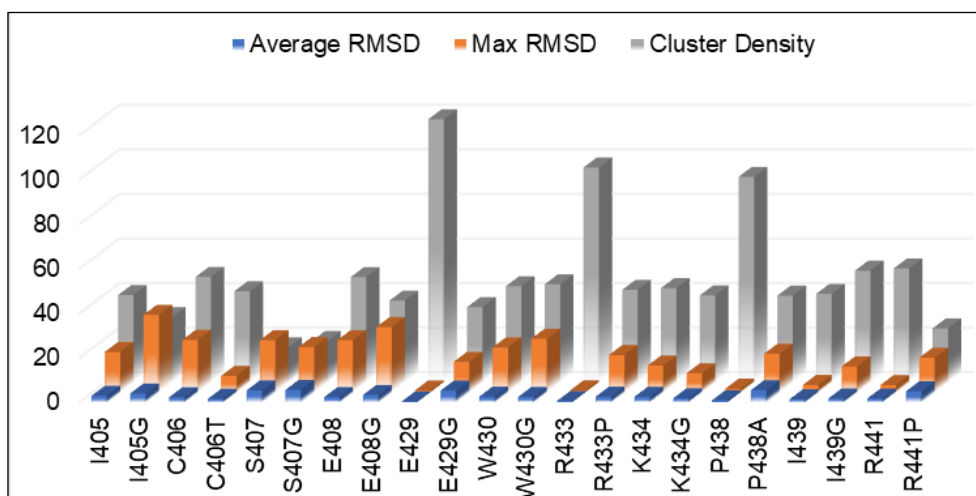


Fig. 4.22. Result of protein-peptide docking of wild-type and their mutants using CABS-dock.

Table 4.7. Average RMSD of wild-type and mutants

Sites	WT/M	Targeted Residues	Average RMSD	Max RMSD	Cluster Density
I405	Wild Type	DVLENELQCIICSEYFIEAVT	2.79215	18.0271	39.038
I405G	Mutant	DVLENELQCIGCSEYFIEAVT	3.87994	34.6759	29.1242
C406	Wild Type	VLENELQCIICSEYFIEAVTL	2.16142	23.4241	47.1911
C406T	Mutant	VLENELQCIITSEYFIEAVTL	1.47072	7.26077	40.7964
S407	Wild Type	LENELQCIICSEYFIEAVTLN	5.2558	23.2859	15.6018
S407G	Mutant	LENELQCIICGEYFIEAVTLN	5.472	20.252	18.4576
E408	Wild Type	ENELQCIICSEYFIEAVTLNC	2.24924	23.339	47.127
E408G	Mutant	ENELQCIICSGYFIEAVTLNC	3.1999	29.1583	36.5636
E429	Wild Type	AHSFCSYCYNEWMKRRIECPIC	0.305078	0.769314	118.003
E429G	Mutant	AHSFCSYCYINGWMKRRIECPIC	5.17444	13.5865	33.6268
W430	Wild Type	HSFCSYCYNEWMKRRIECPIC	2.48757	20.0762	43.0138
W430G	Mutant	HSFCSYCYNEGWMKRRIECPIC	2.30179	23.9917	43.879
R433	Wild Type	CSYCYNEWMKRRIECPICRDK	0.477527	0.789012	96.3295
R433P	Mutant	CSYCYNEWMKPKIECPICRDK	2.4398	16.632	41.3968
K434	Wild Type	SYCYNEWMKRRIECPICRDKI	2.3946	11.9272	42.1783
K434G	Mutant	SYCYNEWMKRRIECPICRDKI	1.72293	8.44531	38.8873
P438	Wild Type	NEWMKRRIECPICRDKIKSKT	0.835786	1.52559	92.1289
P438A	Mutant	NEWMKRRIECAICRDKIKSKT	5.33359	17.1949	38.8106
I439	Wild Type	EWMKRRIECPICRDKIKSKTY	1.28767	3.23257	39.6065
I439G	Mutant	EWMKRRIECPGCRDKIKSKTY	1.63978	11.5038	50.0066
R441	Wild Type	MKRRIECPICRDKIKSKTYSL	1.60781	3.17365	51.001
R441P	Mutant	MKRRIECPICPKDKIKSKTYSL	4.86235	15.3933	24.0624

4.5. Results IV (Objective II)

4.5.1. Structure Recruitment of E3 and E2: RNF168 and UbcH5c

The structure of RNF168 and UbcH5c retrieved from PDB ID: 8SN2 comprises 12 chains, namely, Chain A and E: Histone H3.1 (140 aa), Chain B and F: Histone H4 (107 aa), Chain C and G: Histone H2A type 1-B/E (119 aa), Chain D and H: Histone H2B type 1-J (128 aa), Chain K: RNF168 (103 aa), Chain L: UbcH5c (151 aa), and Chain I and J: DNA. One pair of Zn²⁺ is attached to RNF168. According to UniProt, the structure of RNF168 comprises of 571 aa. The STRING analysis of RNF168 shows that it is closely involved with BRCA1-BARD1 (Fig. 4.23.).

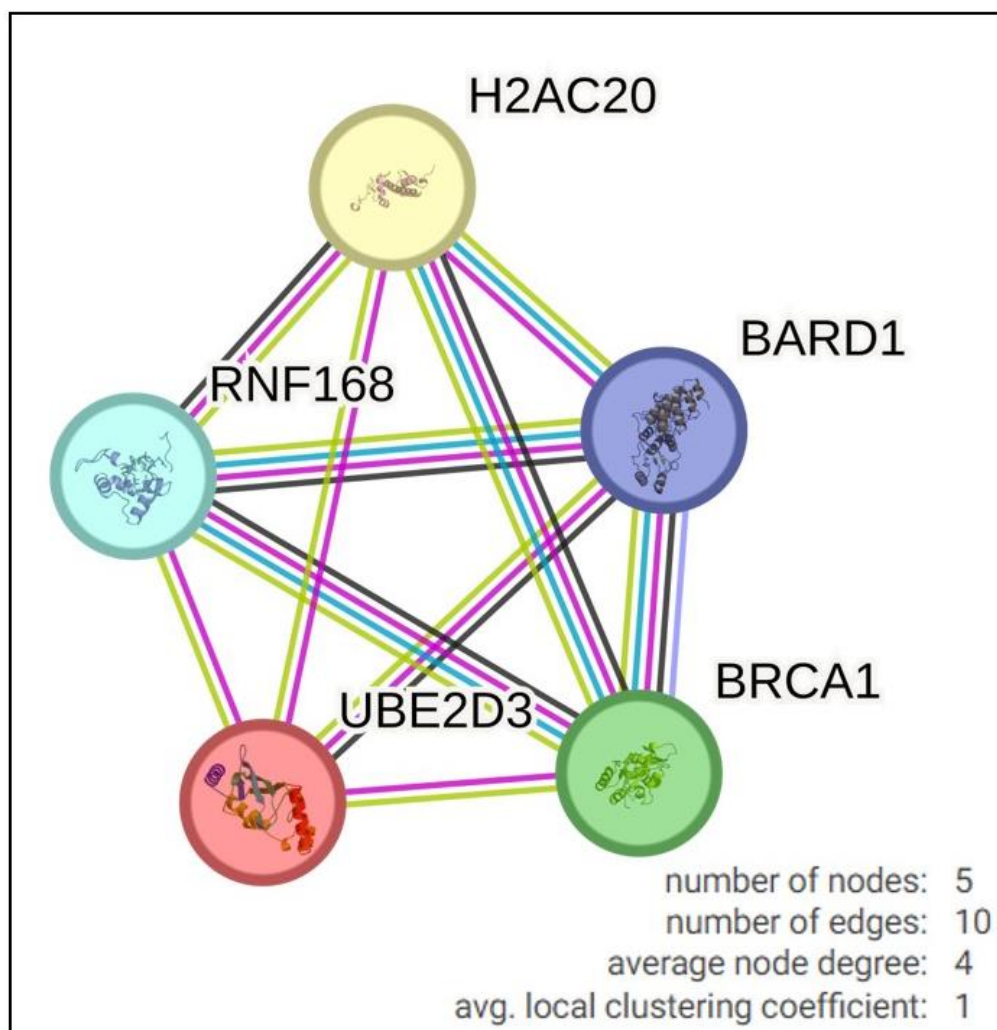


Fig. 4.23. STRING analysis depicting a close relationship of RNF168 with the E2-conjugating enzyme UBE2D3 and the E3 ligase complex BRCA1-BARD1.

4.5.2. Breakdown of Secondary Structure, Domain, and Pockets of RNF168

The results observed on DisCon suggest 24 disordered residues out of 103 aa of RNF168, indicating 23.301% disordered regions. Results of JPred directed towards various annotation bars, for instance, JNetPRED which marks helices with red tubes and sheets with green arrows; JNetCONF which gives confidence scores where a high value indicates high confidence prediction; JNetHMM which performs HMM profile-based prediction representing helices and sheets as red tubes and green arrows respectively; and JNetPSSM is similar to JNetHMM. The results from PROTEUS 2 suggest 23% helix (24 residues), 8% sheets (8 residues), and 69% coil (71 residues). Along with this PROTEUS 2 also gave results from other tools like PSIPRED, JNET, TRANSSEC, and Jury of Expert Prediction that indicated the minute differences arising from each tool (Fig. 4.24.).

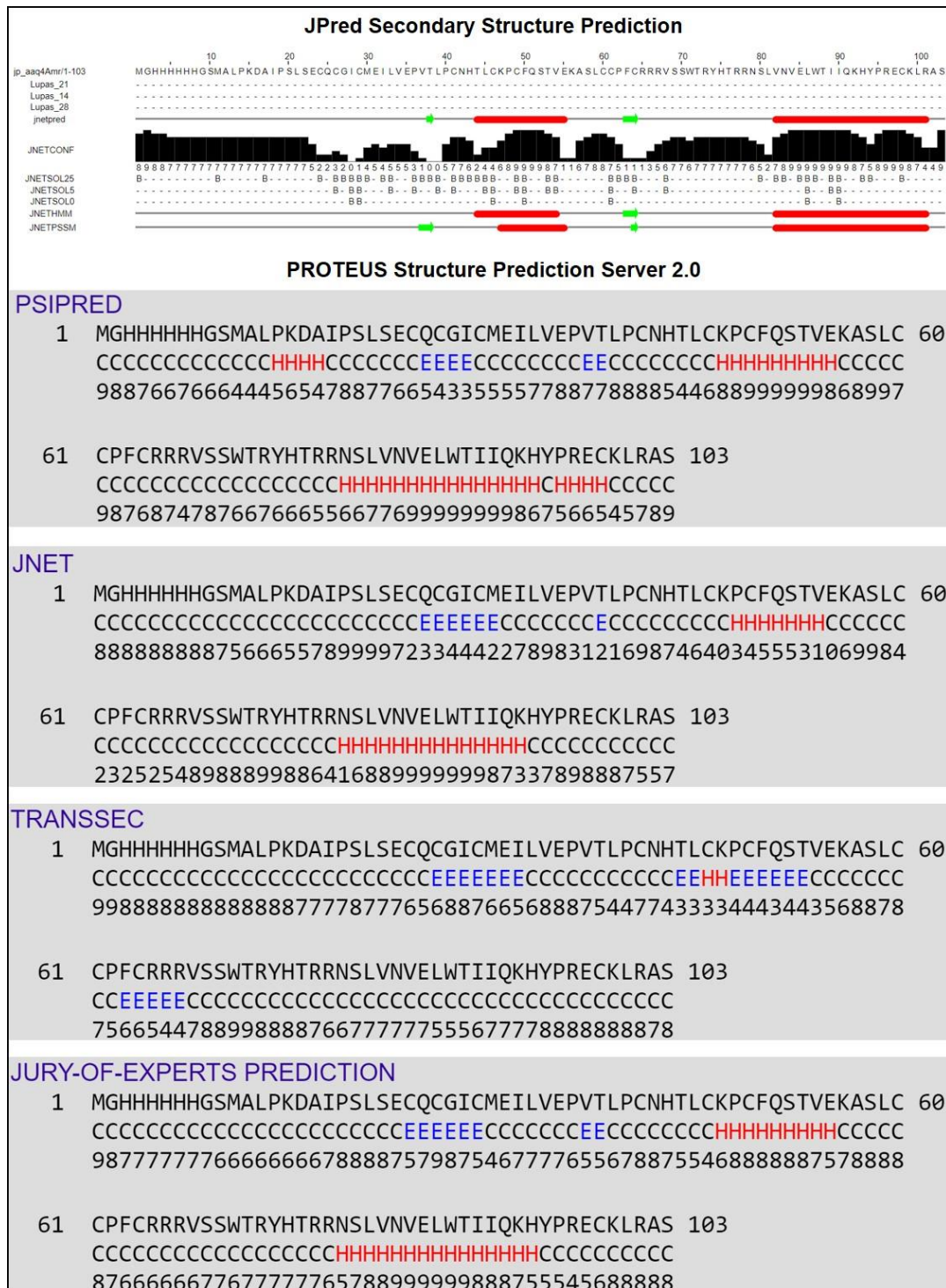


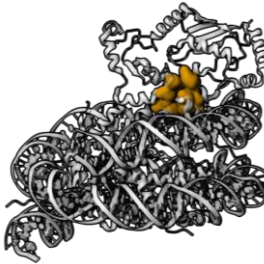



Fig. 4.24. Secondary structure prediction of RNF168.

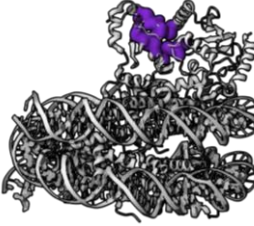
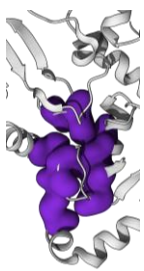
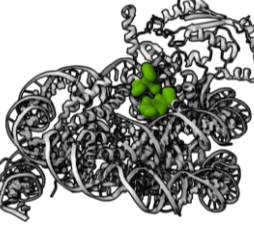
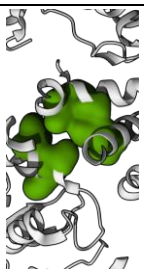
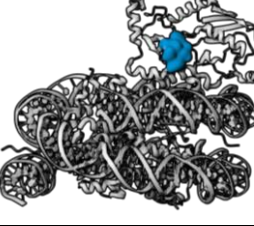
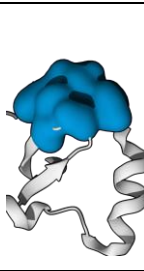
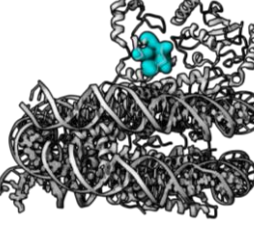
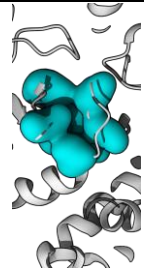
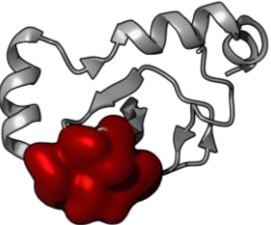
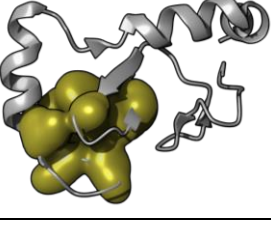
RNF168 domain structure comprises of a catalytic RING domain (15-58 aa) and two ubiquitin-dependent double-stranded break recruitment modules (UDMs), where UDM1 is composed of LR motif (LRM) (110-128 aa), ubiquitin-interacting motif-related (UMI) (141-156 aa), and motif interacting with ubiquitin (MIU1) (171-188 aa). Similarly, UDM2 comprises ubiquitin-associated domain (UAD) (419-439

aa), MIU2 (443-459 aa), and LRM (466- 478 aa) [177]. There is an arginine anchor for substrate identification and a PALB2 interacting domain which is also known as PID domain. However, the RING domain was the primary focus to assess the E3 ligase activity of RNF168. Therefore, according to UniProt, the RING domain of RNF168 is from 16-55 aa. Moreover, as per the tools, namely, SMART and InterPro domain, the RING domain is from 16-54 aa. Histidine and Cysteine are two crucial amino acids required for E2-E3 interaction; therefore, it was found that there are 1 Histidine and 8 Cysteine residues in the RING domain of RNF168, namely, C16, C19, C31, H33, C36, C39, C50, C51, and C54.

Before performing docking, pockets were predicted for RNF168 using PrankWeb and Cast-P. The structure was assessed to get the binding residues between H2A (Chain C), H2B (Chain D), RNF168 (Chain K), and UbcH5c (Chain L). For complete structure, 6 pockets were observed, whereas, for only RNF168, 2 pockets were observed (**Table 4.8.**). From the results of Cast-P, the highest values of the x-axis, y-axis, and z-axis were taken which were 206.9133, 167, and 163. 6913 respectively. These values assisted further in setting the grid box for docking.

Table 4.8. Pocket prediction for PDB ID: 8SN2

FULL STRUCTURE						
Pockets	Close-Up	Binding Partners	Rank	Score	Probability	Residues
<p>Pocket 3</p> 		H2A(C)- H2B(D)- RNF168(K)- UBCH5C(L)	3	11.66	0.647	C_21 C_22 C_23 C_24 C_53 C_56 C_57 C_60 D_113 D_116 D_117 D_120 D_44 D_47 K_48 K_57 L_91 L_92
<p>Pocket 12</p> 		H2B(D)- RNF168(K)	12	3.18	0.111	D_105 D_108 D_109 D_112 K_41 K_44 K_45 K_62 K_66

Pocket 14 		RNF168(K)- UBCH5C(L)	14	2.41	0.065	K_19 K_21 K_24 K_36 K_38 K_39 K_42 K_91 L_1 L_59 L_62
Pocket 17 		H2A(C)- RNF168(K)-	17	1.86	0.035	C_65 C_68 C_86 C_89 C_90 K_60 K_61 K_64
Pocket 22 		RNF168(K)	22	1.43	0.019	K_31 K_33 K_53 K_54 K_56
Pocket 27 		RNF168(K)	27	0.89	0.005	K_29 K_35 K_40 K_43 K_44 K_50 K_52 K_58
ONLY CHAIN K						
Pockets	Binding Partners	Rank	Score	Probability	Residues	
Pocket 1 	RNF168(K)	1	1.42	0.018	K_31 K_33 K_53 K_54 K_56	
Pocket 2 	RNF168(K)	2	1.1	0.009	K_29 K_35 K_40 K_43 K_44 K_50 K_52 K_58	

4.5.3. Search for Top Mutants of RNF168

The mutational analysis was performed for the key sites involved in E2-E3 interaction, namely, C16, C19, C31, H33, C36, C39, C50, C51, and C54. The results of MUpro, SAAFEC-SEQ, I-Mutant 2.0, and Rosetta gave $\Delta\Delta G/DDG$ value for wild-type and all the mutants. The average $\Delta\Delta G/DDG$ was calculated. The top 3 mutants were predicted for all 9 sites: C16 (C16G, C16R, C16T), C19 (C19G, C19H, C19T), C31 (C31G, C31T, C31H), H33 (H33G, H33D, H33Q), C36 (C36G, C36K, C36D), C39 (C39G, C39K, C39T), C50 (C50G, C50K, C50H), C51 (C51G, C51K, C51N), and C54 (C54G, C54K, C54N).

4.5.4. Tolerability and Stability of Top Mutants

The mutant tolerability test by SIFT suggested that besides C50, all the residues showed no tolerable mutants. Similarly, the mutant tolerability results of PolyPhen-2 and FATHMM observed that all the mutants of all the sites except C50 indicated damaging results. In the case of C50, it was observed, that the mutants showed varied results, such that, some were probably damaging, some were possibly damaging and even some were benign. Later, stability prediction was done; the results of FoldX suggested that C16G, C16R, C19H, C31H, H33Q, C36G, C36K, C39T, C50K, C50H, C51K, and C54K are destabilizing mutations. Nonetheless, C16R, C31H, and C51K were highly destabilizing. The top three mutants of all 9 sites were run on iStable, which indicated C16G, C19G, C31G, H33G, C36G, C39G, C50G, C51G, and C54G have decreased stability. According to CUPSAT, the following mutants depicted destabilizing and unfavorable mutations: C16G (-5.48), C19G (-2.35), C31G (-2.98), H33G (-1.68), C36K (-20.44), C36G (-19.72), C39G (-5.99), C50G (-13.86), C51K (-10.26), C51G (-9.44), and C54G (-2.31). As per mCSM, C16G, C31G, C39G, and C51G were highly destabilizing mutations (**Table 4.9**). From the overall analysis, C16G, C31G, C36G, C39G, C50G, and C51G were taken forward for further analysis.

Table 4.9. Structure stability analysis of top mutants

iStable	CUPSAT	Mcsm
C16G (Decrease) (0.764)	Destabilizing, Unfavourable (-5.48)	Highly Destabilizing (-2.005)
C19G (Decrease) (0.787)	Destabilizing, Unfavourable (-2.35)	Destabilizing (-1.18)
C31G (Decrease) (0.705)	Destabilizing, Unfavourable (-2.98)	Highly Destabilizing (-2.033)
H33G (Decrease) (0.755)	Destabilizing, Unfavourable (-1.68)	Destabilizing (-0.633)
C36G (Decrease) (0.731)	Destabilizing, Unfavourable (-19.72)	Destabilizing (-1.942)
C39G (Decrease) (0.792)	Destabilizing, Unfavourable (-5.99)	Highly Destabilizing (-2.124)
C50G (Decrease) (0.653)	Destabilizing, Unfavourable (-13.86)	Destabilizing (-1.446)
C51G (Decrease) (0.647)	Destabilizing, Unfavourable (-9.44)	Highly Destabilizing (-2.802)
C54G (Decrease) (0.745)	Destabilizing, Unfavourable (-2.31)	Destabilizing (-1.998)

4.5.5. Impact of RNF168 Mutagenesis on Binding Affinity with UbcH5c

To understand the binding affinity between RNF168 and UbcH5c, two approaches were used: protein-peptide docking and protein-protein docking. This step was performed to comprehend the impact of mutations on the binding affinity, therefore, the wild-type and mutant RNF168 were docked with UbcH5c. For protein-peptide docking, CABS-dock was used, where the wild-type and mutant RNF168 sequences were prepared for each target residue such that the key residue was flanked by 10 residues on both sides. Later, these sequences were docked with UbcH5c, which in turn gave three results, namely, cluster density, average RMSD, and maximum RMSD. Here, the results were interpreted based on average RMSD suggesting higher the deviation, the poorer the binding affinity. It was observed, that C31G, C31H, C31T, H33G, H33D, C36G, C39K, C50K, and C54N showed high deviation compared to their respective wild-type sequence (Table 4.10.).

Table 4.10. Protein-Peptide docking results of RNF168

RNF168_E2	Peptide Sequences	Cluster Density	Average RMSD	Max RMSD
WT_C16	DAIPSLSECQCGICMEILVEP	29.6801	5.79513	28.3731
E2_C16G	DAIPSLSECQGGICMEILVEP	31.4502	3.27502	7.73342
E2_C16R	DAIPSLSECQRGICMEILVEP	37.926	3.19043	23.1871
E2_C16T	DAIPSLSECQTGICMEILVEP	19.5233	3.99523	26.5469
WT_C19	PSLSECQCGICMEILVEPVTL	28.7872	3.57798	16.8824
E2_C19G	PSLSECQCGIGMEILVEPVTL	36.1567	2.84872	27.4171
E2_C19H	PSLSECQCGIHMEILVEPVTL	33.4115	3.23242	22.6609
E2_C19T	PSLSECQCGITMEILVEPVTL	130.109	0.768585	1.33059
WT_C31	EILVEPVTLPCNHTLCKPCFQ	69.5308	1.09304	14.9289
E2_C31G	EILVEPVTLPGNHTLCKPCFQ	38.3186	5.74133	23.289
E2_C31H	EILVEPVTLPHNHTLCKPCFQ	37.2616	3.97192	13.2955
E2_C31T	EILVEPVTLPTNHTLCKPCFQ	23.7407	5.2231	35.4159
WT_H33	LVEPVTLPCNHTLCKPCFQST	41.5247	2.74535	11.6659
E2_H33G	LVEPVTLPCNGLTCKPCFQST	20.3023	8.12716	26.9661
E2_H33D	LVEPVTLPCNDTLCKPCFQST	22.9793	8.4859	21.745
E2_H33Q	LVEPVTLPCNQTLCKPCFQST	21.7612	2.52744	9.26924
WT_C36	PVTLPCNHTLCKPCFQSTVEK	20.4633	6.89038	20.4058
E2_C36G	PVTLPCNHTLGGKPCFQSTVEK	24.8449	4.42747	18.7443
E2_C36K	PVTLPCNHTLKKPCFQSTVEK	25.011	3.51845	21.8829
E2_C36D	PVTLPCNHTLDKPCFQSTVEK	31.6218	3.25725	30.358
WT_C39	LPCNHTLCKPCFQSTVEKASL	43.9253	3.32382	14.5965
E2_C39G	LPCNHTLCKPGFQSTVEKASL	31.4917	3.33422	22.5658
E2_C39K	LPCNHTLCKPKFQSTVEKASL	28.2562	4.56538	20.5622
E2_C39T	LPCNHTLCKPTFQSTVEKASL	24.4473	3.31324	15.7113
WT_C50	FQSTVEKASLCCPFCRRRVSS	36.2553	2.42723	10.8798
E2_C50G	FQSTVEKASLGCPCRRRVSS	38.4477	1.76864	14.0442

E2_C50K	FQSTVEKASLKPCFCRRRVSS	26.8377	4.13597	21.2918
E2_C50H	FQSTVEKASLHPCFCRRRVSS	69.9213	0.614977	1.3522
WT_C51	QSTVEKASLCCPFRRRVSSW	43.9316	4.68911	27.3088
E2_C51G	QSTVEKASLCGPFRRRVSSW	21.385	4.67617	21.4129
E2_C51K	QSTVEKASLCKPFRRRVSSW	23.1955	8.88102	23.9609
E2_C51N	QSTVEKASLCPNPFRRRVSSW	56.4774	1.85915	17.1356
WT_C54	VEKASLCCPFRRRVSSWTRY	22.4342	7.31027	29.7985
E2_C54G	VEKASLCCPFGRRRVSSWTRY	25.7153	5.2498	20.3205
E2_C54K	VEKASLCCPFKRRRVSSWTRY	22.7858	6.1003	31.0293
E2_C54N	VEKASLCCPFNRRRVSSWTRY	24.2647	8.69576	33.5399

The results of LZerD were assessed based on the Ranksum score, where the higher the Ranksum score, the poorer the binding. Therefore, the result inferred that C16G, C16T, C19G, C19H, C31H, C31T, H33D, H33Q, C36G, C36D, C39G, C39K, C39T, C50G, C50K, C50H, C51G, C51N, C54G, C54K, and C54N have high Ranksum score compared to wild-type (**Fig. 4.25.**). Overall, docking results suggested C16G, C31G, C36G, C39G, C50G, and C51G as key mutants that not only hamper the structural stability but also the E3 ligase activity of RNF168.

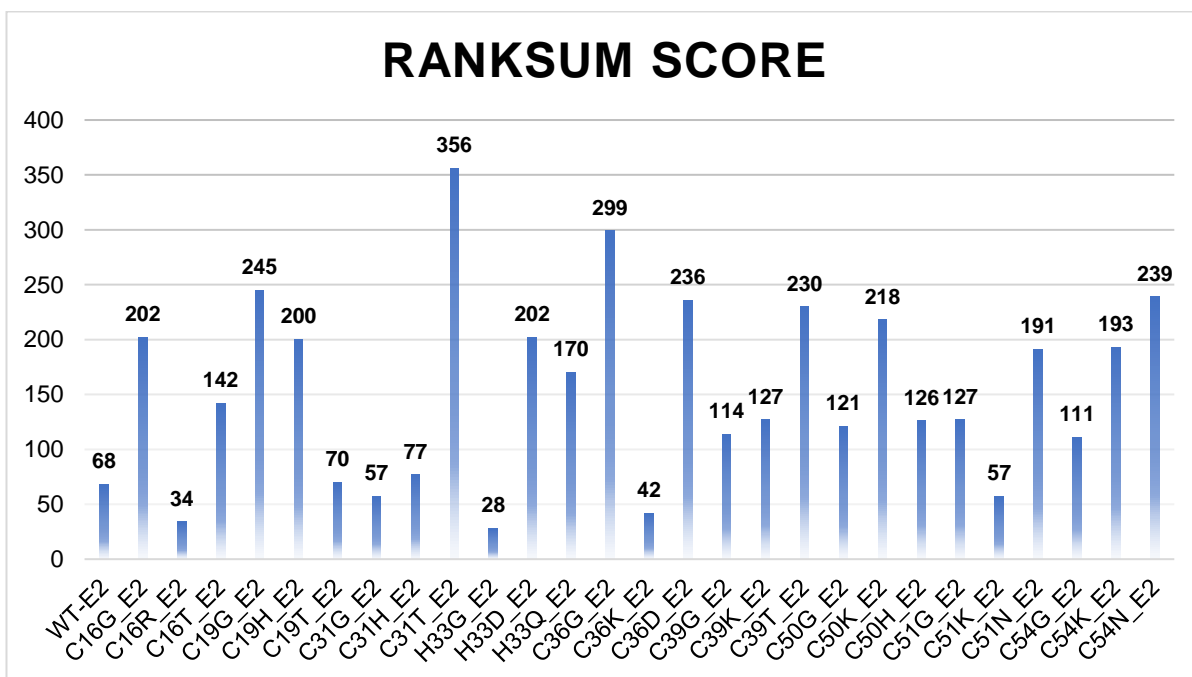


Fig. 4.25. Protein-Protein docking results of RNF168.

- **Objective III** - To identify the biomolecules involved in the recovery or elimination of mutated protective proteins

4.6. Results I (Objective III)

4.6.1. Extraction, Drug Likelihood, and ADME Check of Warheads

PROTAC-DB 2.0 database was used to extract all the details regarding warheads. The CSV file downloaded contained 1167 warheads, which were then filtered using SwissADME. In the first filtration process, by applying all filters, 99 warheads showed up. However, later, warheads were manually filtered out by applying filters like Lipinski (0), PAINS (0), Brenks (0), Muegge (0), Veber (0), Egan (0), Ghose (0), Lead likelihood (0), and Rotatable bonds (≤ 10). This gave 24 potential warheads (**Table 4.11.**) that were later docked with wild-type and top mutants (C16G, C31G, C36G, C39G, C50G, and C51G).

Table 4.11. Potential warheads screened out to dock with mutant RNF168

Warheads	UniProt	Target	Name	Canonical SMILES	
W1	LIG1	P50750	CDK9	Wogonin	<chem>COc1c(O)cc(c2c1oc(cc2=O)c1cccc1)O</chem>
W2	LIG2	P50750	CDK9	-	<chem>COc1ccc(cc1)CC(=O)Nc1n[nH]c(c1)C1CCC1</chem>
W3	LIG3	P03372	ER	Estrone	<chem>Oc1ccc2c(c1)CC[C@@H]1[C@@H]2CC[C@]2([C@H]1CCC2=O)C</chem>
W4	LIG4	Q86U86	PBRM1	-	<chem>Nc1nnc(cc1N1CCNCC1)c1cccc1O</chem>
W5		P51531	SMARCA2	-	<chem>Nc1nnc(cc1N1CCNCC1)c1cccc1O</chem>
W6		P51532	SMARCA4	-	<chem>Nc1nnc(cc1N1CCNCC1)c1cccc1O</chem>
W7	LIG5	P10275	AR	-	<chem>N#Cc1ccc(cc1Cl)O[C@@H]1C[C@@H]2CC[C@H](C1)N2</chem>
W8	LIG6	P10275	AR	-	<chem>N#Cc1ccc(cc1Cl)N1CC2(C[C@@H]1C)CCNCC2</chem>
W9	LIG7	Q9H8M2	BRD9	-	<chem>COc1cc(cc(c1C)OC)c1cn(C)c(=O)c(c1C)C</chem>
W10	LIG8	P51531	SMARCA2	-	<chem>Nc1nnc(cc1N1CCNCC2(C1)CC2)c1cccc1O</chem>
W11	LIG9	P51531	SMARCA2	-	<chem>Nc1nnc(cc1N1CC2CCC(C1)N2)c1cccc1O</chem>
W12	LIG10	Q16342	PDCD2	-	<chem>C[C@@H](c1ccccn1)NC(=O)c1ccc2c(c1)cccc2</chem>
W13	LIG11	P62937	CypA	CypA-L1	<chem>O=C(NC(=O)c1c(O)cccc1O)NC1CCCCC1</chem>
W14	LIG12	O15379	HDAC3	-	<chem>CCCNCC(=O)c1ccc(cc1)N1CCN(CC1)C</chem>
W15		Q9BY41	HDAC8	-	<chem>CCCNCC(=O)c1ccc(cc1)N1CCN(CC1)C</chem>
W16	LIG13	P51531	SMARCA2	-	<chem>Cn1ncc(c1)c1cc(nnc1N)c1cccc1O</chem>
W17		P51532	SMARCA4	-	<chem>Cn1ncc(c1)c1cc(nnc1N)c1cccc1O</chem>
W18	LIG14	Q12830	BPTF BD	-	<chem>Cn1ncc(c(c1=O)Cl)Nc1ccc2c(c1)CCNC2</chem>
W19		Q9H8M2	BRD9 BD	-	<chem>Cn1ncc(c(c1=O)Cl)Nc1ccc2c(c1)CCNC2</chem>
W20		Q9BXF3	CECR2 BD	-	<chem>Cn1ncc(c(c1=O)Cl)Nc1ccc2c(c1)CCNC2</chem>
W21	LIG15	Q12830	BPTF BD	-	<chem>Cn1ncc(c(c1=O)Cl)Nc1ccc2c(c1)CNCC2</chem>
W22		Q9H8M2	BRD9 BD	-	<chem>Cn1ncc(c(c1=O)Cl)Nc1ccc2c(c1)CNCC2</chem>
W23		Q9BXF3	CECR2 BD	-	<chem>Cn1ncc(c(c1=O)Cl)Nc1ccc2c(c1)CNCC2</chem>
W24	LIG16	P00918	CA2	-	<chem>COCCNC(=O)c1ccc(cc1)S(=O)(=O)N</chem>

*Warheads sharing the same SMILES were considered as one.

4.6.2. Molecular Docking Analysis of RNF168 (WT/Mutant) with Warheads

Molecular docking was performed using AutoDock Vina, where wild-type and mutant structures of RNF168 were docked with 16 potential warheads. The results were interpreted by comparing the binding affinity score of wild-type with the top five mutants. As per AutoDock Vina, a more negative value indicates greater binding affinity. Hence, the results depicted that for LIG4 and LIG11, the mutants showed greater binding affinity than the wild-type, i.e., a difference of 0.9 (Table 4.12.).

Table 4.12. Molecular docking results of RNF168 (WT/Mutants) with warheads

LIGANDS	WT	C16G	C31G	C36G	C39G	C50G	C51G
LIG1	-5.5	-5.9	-5.9	-5.8	-5.9	-6.2	-5.8
LIG2	-4.6	-5.4	-5.6	-5.7	-5.1	-5.3	-5.2
LIG3	-6.1	-6.4	-6.3	-6.4	-6.4	-6.4	-6.4
LIG4	-4.7	-5.7	-5.6	-5.6	-5.8	-5.6	-5.7
LIG5	-4.7	-4.8	-4.8	-4.8	-4.9	-4.9	-5.2
LIG6	-5.5	-5.5	-5.5	-5.5	-5.5	-5.5	-5.5
LIG7	-5	-5	-4.9	-5	-5	-4.9	-5
LIG8	-5.2	-5.9	-5.8	-5.7	-5.9	-5.7	-5.6
LIG9	-5.3	-5.8	-5.8	-5.8	-5.8	-5.7	-5.8
LIG10	-5.9	-6.1	-6.1	-6.2	-6.1	-6.2	-6.1
LIG11	-5.7	-6.6	-6.6	-6.6	-6.6	-6.6	-6.6
LIG12	-4.5	-5	-4.9	-4.9	-5.4	-5.2	-5.4
LIG13	-4.9	-5.7	-5.8	-5.8	-5.7	-5.6	-5.7
LIG14	-4.7	-5	-5.1	-5.3	-5.2	-5.3	-5.3
LIG15	-4.9	-4.9	-5.1	-5.2	-5.2	-5.2	-5.2
LIG16	-4	-4.6	-4.5	-4.4	-4.1	-4.6	-4.5

4.6.3. Results of MD Simulation

Molecular dynamic simulations were performed for three cases: first, for the protein structure of RNF168 and its mutants. This helped in finding the most unstable mutant to be further worked upon. Second, for the docked structure of RNF168 and UbcH5c, which aided in predicting which mutants show poor binding with E2-conjugating enzymes and thus render the E3 ligase activity of RNF168. Lastly, for the docked structure of RNF168 with warheads, to conclude which warhead can easily bind with the top mutant, which could be taken to UPS for further degradation.

4.6.4. Control and Mutants of RNF168

MDS was carried out for wild-type and mutant (C16G, C31G, C36G, C39G, C50G, and C51G) structures of RNF168. RMSD, RMSF, and RG were computed throughout the trajectory of protein structure using a time-dependent function, and later results were compared between wild-type and mutant structures. It was observed that the RMSD values of all six mutants showed higher deviation than the wild-type. In addition, the highest deviation was observed in C50G, ranging from ~0.37 nm (wild-type) to ~0.55 nm (mutant). The deviation observed for other mutants were C16G (~0.55 nm), C31G (~0.44 nm), C36G (~0.55 nm), C39G (~0.52), and C51G (~0.42) (**Fig. 4.26.**). RMSF of the C α atom was calculated for both wild-type and mutants, and it was observed that fluctuation was observed throughout the structure in C16G, however, for the rest of the mutants, it was C31G (1-7 position, 58-87 position), C36G (15-57 position), C39G (40-44 position, 57-61 position), C50G (1-9 position), and C51G (21-27 position, 59-73 position, 89-91 position) (**Fig. 4.27.**). The analysis of RG revealed mutation C16G showed less compactness than the wild-type, measuring around ~1.55 nm. Mutants C36G, C39G, and C50G exhibit similar compactness in their structure. However, structures with mutation C31G and C51G are more compact than the wild-type, measuring ~1.4 nm and ~1.38 nm, respectively (**Fig. 4.28.**).

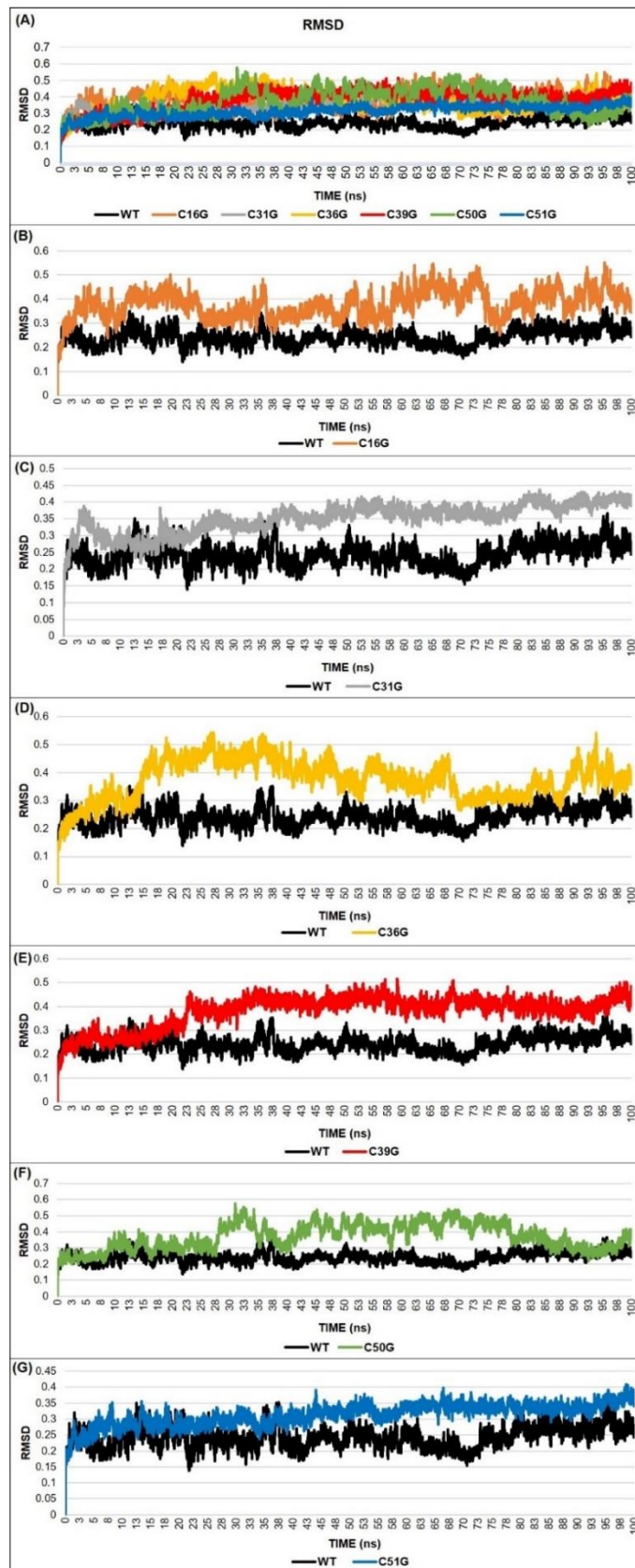


Fig. 4.26. Molecular dynamic simulation results: Comparison of RMSD between wild-type and mutants of RNF168.

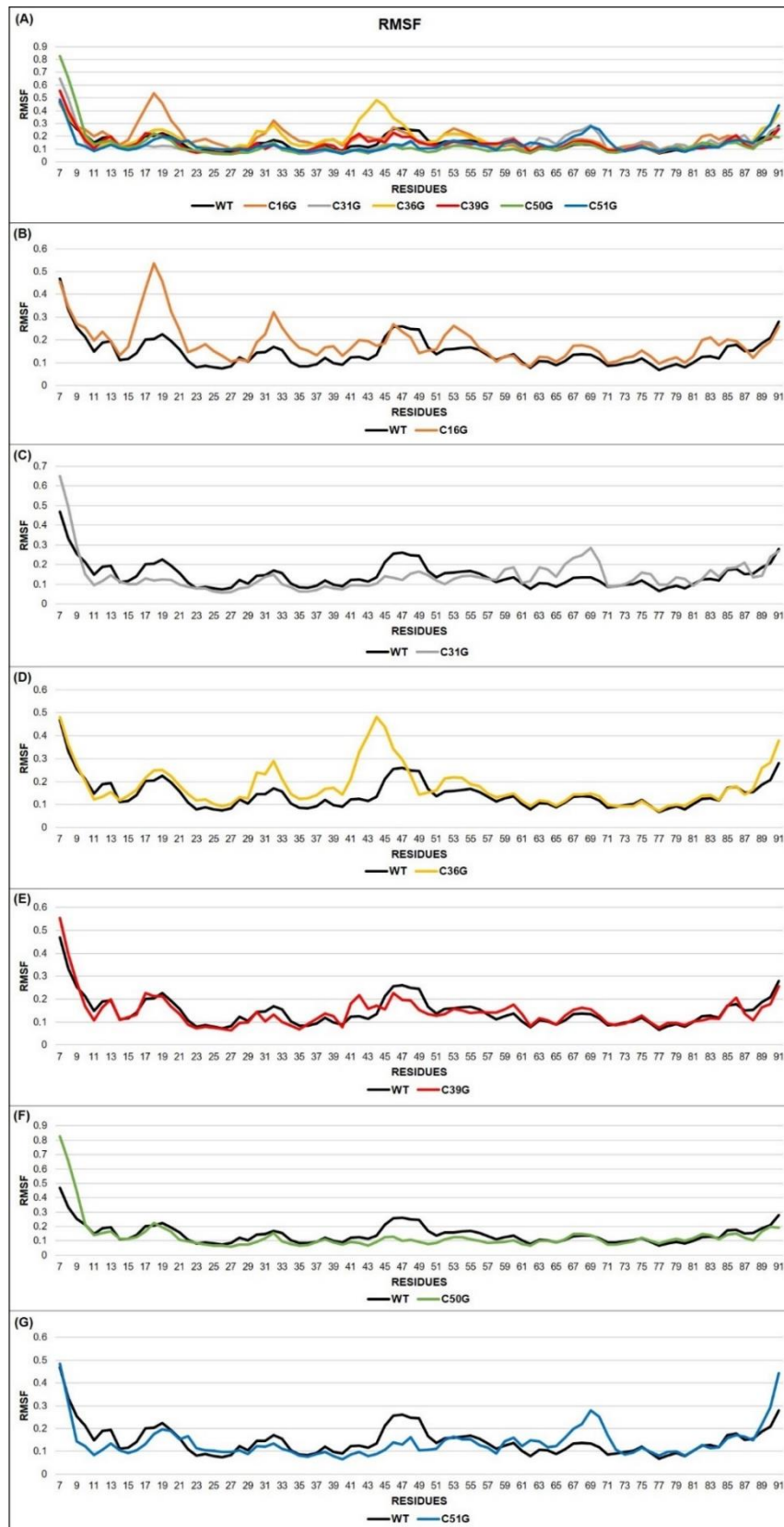


Fig. 4.27. Molecular dynamic simulation results: Comparison of RMSF between wild-type and mutants of RNF168.

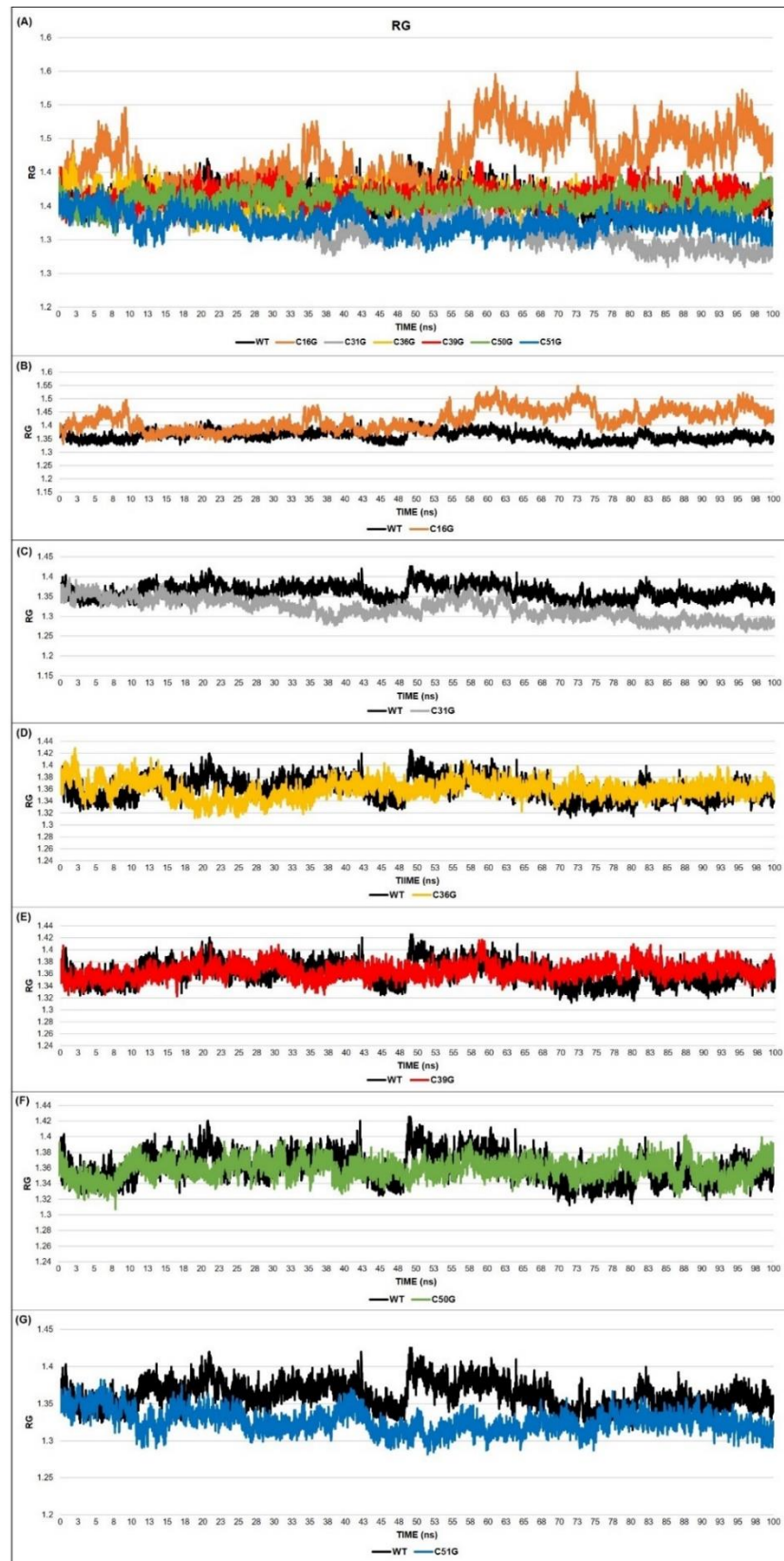


Fig. 4.28. Molecular dynamic simulation results: Comparison of RG between wild-type and mutants of RNF168.

4.6.5. E3-E2: RNF168-UbcH5c

MDS was performed for wild-type and mutant structures docked with UbcH5c for 100 ns. As per the RMSD analysis, all mutants except C31G and C50G observed more deviation in their structure compared to the wild-type. The highest deviation observed for C31G and C50G was ~0.57 nm and ~0.65 nm, respectively. RG analysis suggests that the least compactness was recorded with mutant C50G (~2.1 nm), whereas, C51G showed similar compactness compared to wild-type structure. For the rest of the mutants, the compactness was, C16G (~1.96 nm), C31G (~1.98 nm), C36G (~1.96 nm), and C39G (~1.99 nm) which showed a little less compactness than the wild-type. The results of RMSF suggest that less residual fluctuation was observed in UbcH5c docked with mutants C16G, C36G, C39G, and C51G, however, in C31G, high fluctuations were observed from position 7-80 and in C50G, from positions 7-29, 31-40, and 73-91 (**Fig. 4.29.**). As C31G and C50G depicted more deviation, more residual fluctuation, and least compactness, therefore, they were taken forward for further analysis.

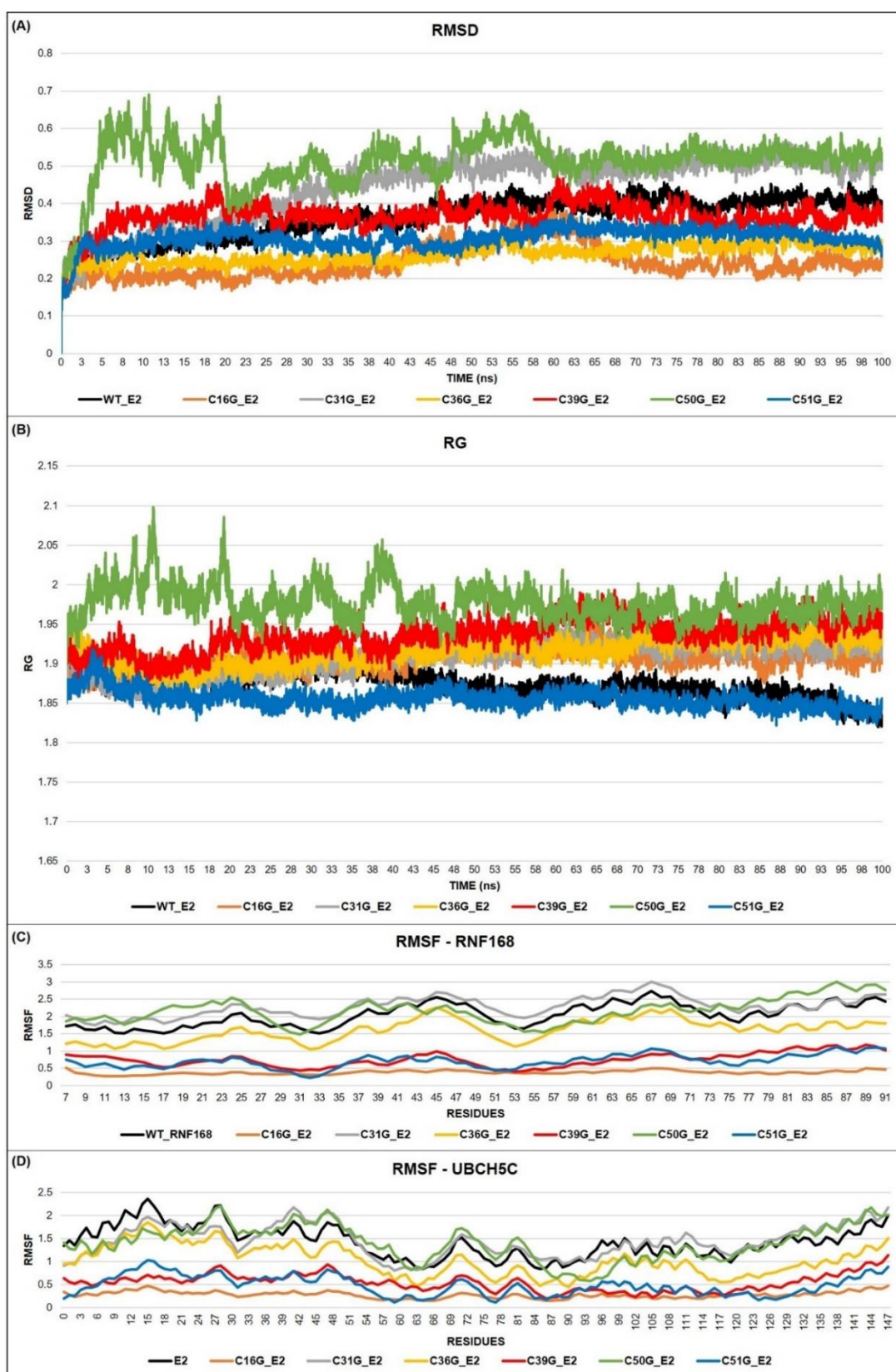


Fig. 4.29. Molecular dynamic simulation results: Comparison of RMSD, RMSF, and RG between wild-type and mutants of RNF168 when docked with E2-conjugating enzyme, Ubh5c.

4.6.6. RNF168 (Mutant)-Warhead

C31G and C50G are two key mutants that hamper the binding of RNF168 with its E2-conjugating enzyme, UbcH5c, and thereby preventing the E3 ligase activity of RNF168. Therefore, either repairing or degrading the faulty mutant becomes a crucial step. MDS of mutants docked with warheads were assessed and compared with wild-type, such that, the mutants must show greater stability than wild-type so that it can be further tagged and taken further to the UPS system for its degradation. MDS was performed for wild-type and mutants, C31G and C50G docked with Ligand 4 and Ligand 11 simultaneously.

The results of the wild-type, C31G, and C50G docked with Ligand 4 suggest that both the mutant structures showed negligible deviation compared to the wild-type structure. Moreover, in the case of RMSD_LIG, C50G was comparatively less deviated than the wild-type, however, C31G exhibited a similar deviation to the wild-type structure. For C31G, high residual fluctuation was observed from 27-46 and 61-89 positions. Nevertheless, for C50G, residual fluctuation was observed from position 13-91. RG analysis suggests, C31G depicted more compactness in its structure than wild-type. Contrarily, C50G observed less compactness of around ~ 1.54 nm than the wild-type. However, RG_LIG suggests that both the mutants exhibited similar compactness to wild-type structure. The number of hydrogen bonds reflects the degree of binding between the ligand and RNF168 (wild-type/ mutant). In the C31G-LIG4 complex, 5 hydrogen bonds were observed for a short duration and 3 hydrogen bonds were observed for a longer duration. In contrast, the C50G-LIG4 complex showed 6 hydrogen bonds for a short duration and 4 hydrogen bonds for a longer duration; overall, indicating better binding than the wild-type (**Fig. 4.30.**).

The results of the wild-type, C31G, and C50G docked with Ligand 11 suggest that less deviation was observed in mutant structure C31G compared to the wild-type, however, the highest deviation of ~ 0.72 nm was observed in C50G than the wild-type of ~ 0.55 nm. Later, both the mutant structures become more stable than the wild-type. In the case of RMSD_LIG, all three cases showed high deviation, however, C31G showed high stability throughout the time. RG results suggest that C31G depicted more compactness than the wild-type, however, C50G showed slightly less compactness than the wild-type of around ~ 1.55 nm in the initial time, later exhibited similar compactness to the wild-type. RG_LIG result suggests that both the mutants are more compacted than the wild-type. In the C31G-LIG11 and C50G-LIG11 complexes, 5 hydrogen bonds and 4 hydrogen bonds were observed for a longer duration of time than that of the wild-type (**Fig. 4.31.**).

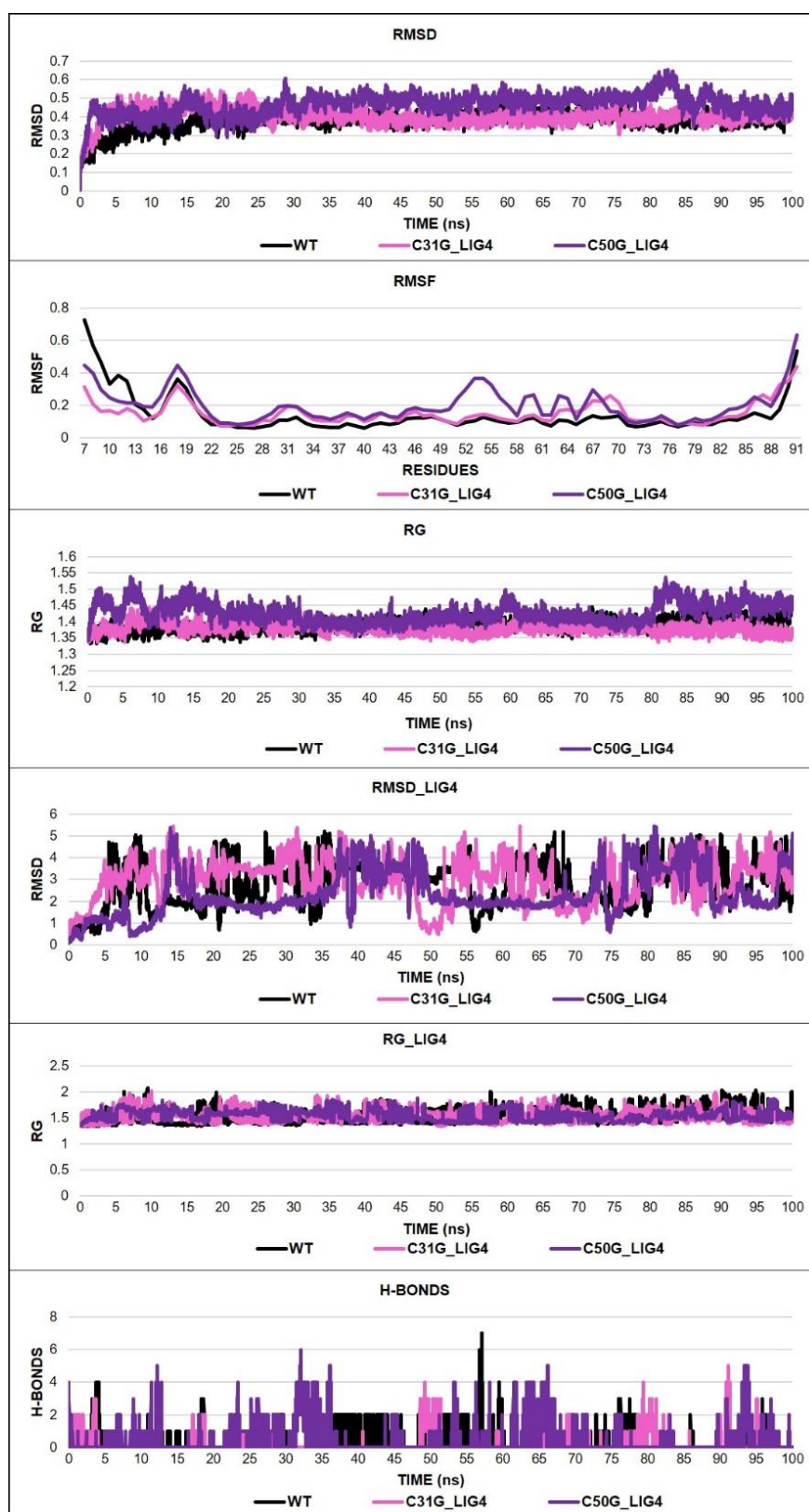


Fig. 4.30. Molecular dynamic simulation results: Comparison of RMSD, RMSF, RG, RMSD_LIG, RG_LIG, and H-BONDS between wild-type and mutants (C31G and C50G) of RNF168 when docked with Ligand 4.

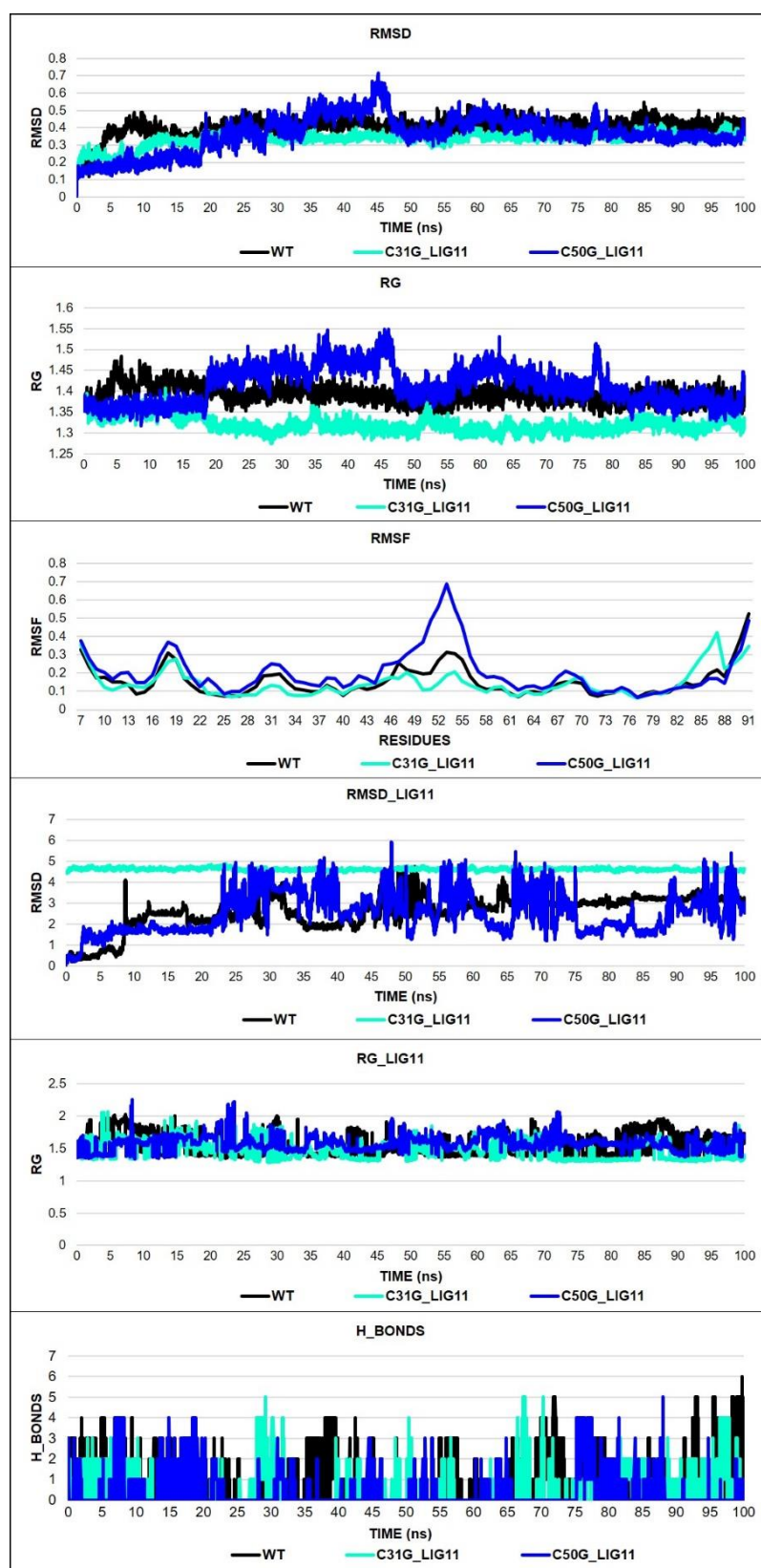


Fig. 4.31. Molecular dynamic simulation results: Comparison of RMSD, RMSF, RG, RMSD_LIG, RG_LIG, and H-BONDS between wild-type and mutants (C31G and C50G) of RNF168 when docked with Ligand 11.

CHAPTER 5



CHAPTER 5

DISCUSSION, CONCLUSION AND FUTURE PERSPECTIVE

5.1. Discussion

BRCA1 ► The hallmark feature of NDDs is the accumulation of non-functional proteins in the cellular milieu and PTMs play a very crucial role in regulating these non-functional protein aggregates in the pathogenesis of NDDs [178]. Alzheimer's disease and Parkinson's disease are two such NDDs that are characterized by progressive neuronal cell death that further causes memory and motor impairment. Ubiquitination is a prevalent pathway that degrades or modifies proteins, controls many cellular complexes, and is majorly involved whenever there is growth and development [179], [180]. Therefore, ubiquitination is a more important modification than phosphorylation because of its high involvement in numerous functions. In this modification, E2 plays a vital role in transferring ubiquitin from E1 to E3 to the substrate. One of the ways by which ubiquitin is conjugated to the target protein is by forming an isopeptide bond between its glycine and ϵ -amino group of a lysine residue. Nonetheless, more observations and analysis are demanded to completely understand the role of E2. In this study, the binding of E2, Ube2k with E3, BRCA1-BARD1 are primarily discussed, with a focus, particularly on Ube2k binding with the mutants of BRCA1-BARD1.

Firstly, Venn analysis of the AD dataset (GSE122063), PD dataset (GSE8397), and E3 dataset (ESBL) gave a list of 74 E3 ligases that were common in both AD and PD from which we computed 10 hub genes namely, PML, BRCA1, TRIM23, TRIM32, RNF11, TRIM27, UBR2, TRIM37, MID2 and TRIM33. Gene enrichment analysis of these 10 genes demonstrated that the majority of the genes took part in the Ubiquitin mediated-proteolysis pathway. Afterward, by using MotifFinder, total number of motifs were observed for the genes: BRCA1-15, PML-7, TRIM27-12, TRIM33-8, TRIM32-17, and TRIM37-8. Later, it was observed that only three genes i.e., BRCA1, PML, and TRIM33 have more than 15 overlap matches. As aforementioned, lysine is the key amino acid on which the attachment takes place, therefore, for BRCA1, PML, and TRIM33, 6, 5, and 1 lysine hotspot sites were observed, respectively. In BRCA1 and TRIM33, all lysine sites undergo at least ubiquitination, however, in PML, 4/5 lysine sites undergo ubiquitination. Using ConSurf, the role of these lysine residues in the protein was checked and it was found that all these hotspot sites of BRCA1 and PML were exposed and functional, whereas, in TRIM33, it was structural and buried. The binding pockets for BRCA1, PML, and

TRIM33 were 4, 3, and 2, respectively. Furthermore, ubiquitination in PML is often dependent on other post-translational modifications like sumoylation, phosphorylation, and poly-isomerization indicating that PML ubiquitination is highly complex by nature [181]. Therefore, BRCA1 was further taken forward for mutational analysis.

BRCA1 plays a crucial role in many cellular processes, however, here we target one of its well-established functions as a ubiquitin E3 ligase. Although, BRCA1 has its own RING domain for E2 binding, despite that its E3 ligase activity necessitates both BRCA1 and BARD1 protein. The putative substrates identified so far of BRCA1-BARD1 to carry out its E3 ligase activity are nucleophosmin 1 (NPM1), RNA Polymerase II Subunit A (RPB1), RNA polymerase core subunit (RPB8), progesterone receptor-A (PR-A), transcription factor IIE (TFIIE), Topoisomerase IIa, Estrogen receptor alpha (ER α), progesterone receptor, γ -tubulin, histones, H2A, macroH2A1, p50, neurofibromatosis type 2 (NF2), organic cation/carnitine transporter 1 (Oct1), la ribonucleoprotein 7 (LARP7), Claspin and Aurora Kinase which could possibly have diverse involvement in AD and PD. E3 ligase activity of BRCA1 has been extensively studied in cancer, however, in neurodegeneration, BRCA1 acts as a key DNA repair protein which is associated with cell senescence, transcriptional regulation, cell-cycle checkpoint, apoptosis, chromatic remodeling, and centrosome replication [182]. BARD1 forms a heterodimer with BRCA1 through its RING domain and supports its migration into the nucleus. In AD, it has been reported that BRCA1 colocalizes with tau protein in a diseased brain, whereas in PD, BRCA1 does not colocalize with α -synuclein [183].

In BRCA1, it has been observed that all the known missense substitutions due to missense dysfunction either on RING domain or BRCT domain are pathogenic [184]. A study observed that missense mutation in the RING domain alters the region of BRCA1 that is required for interaction with ubiquitin-conjugating enzymes [185]. Although, increased level of BRCA1-BARD1 complex is vital for ubiquitin E3 ligase activity of BRCA1, however, under pathological conditions BRCA1-BARD1 ubiquitin ligase activity results in the ubiquitination of γ -tubulin in the cytosol, a process important for centrosomal complex concentration of proteins involved in cell cycle; this directs towards dysfunctioning of BRCA1 in ubiquitination and results in subcellular mislocalization of a large portion of BRCA1 protein in neurons during neurodegeneration. Therefore, this also suggests that inflection in BRCA1 levels and activity is significant for different brain conditions [186].

The mutagenesis studies were performed on the target motif of BRCA1 - Zf RING Ubox, position 24-62. Also, out of the three active sites, Active Site 3 was considered because the lysine residues of Active Site 1 and Active Site 2 did not show

pathogenicity on different amino acid substitutions. However, lysine sites K32 and K45 of Active Site 3 showed high pathogenicity on substituting with other amino acids. The top three mutants for both hotspots were K32Y, K32L, K32C, and K45Y, K45V, K45G, respectively. To further decipher the impact of these mutants on the E3 ligase activity of BRCA1-BARD1, protein-protein docking was carried out with one of its potential E2, Ube2k using HADDOCK and ClusPro. According to HADDOCK results, there was a considerable difference observed in the z-score of the wild-type and the other six variants. Moreover, as per ClusPro results, all the mutants of K32, namely K32Y, K32L, and K32C exhibited smaller cluster size compared to the wild-type. Out of the three variants of K45, only K45G displayed a smaller cluster size. However, the lowest binding energies of all the variants did not show any significant changes in their values in comparison to the wild-type. As per the LZerD, all mutants had Ranksum score higher than the wild-type, thereby, suggesting substitution mutation has a significant impact on protein structure.

MD simulation analysis facilitated in investigation of the impact of mutation on the structure of the protein. RMSD data suggested a significant deviation in mutants as compared to wild-type throughout the simulation time, hence it clearly indicates that the mutation has a destabilizing effect on the protein. The results were substantiated by RMSF data which represented high residue level fluctuations for variant protein thereby directing that mutation affects the flexibility of the protein. RG plot revealed that variant K32L destabilizes the structure resulting in loss of protein compactness.

BRCA1-BARD1 ► Impairment of the DNA repair protein BRCA1 leads to cellular senescence, which in turn contributes to brain dysfunction and neurodegeneration. However, the precise mechanism underlying this process remains unclear. Therefore, this study aims to address this longstanding question, with a specific focus on mutagenesis on BARD1, the heterodimeric partner of BRCA1, as a significant contributor to this process. BRCA1 has been widely conferred for Breast Cancer, where its primary function is in the nuclear compartment as a tumor suppressor that participates in multiple cellular processes. However, BRCA1 commonly exists as a heterodimer to ensure its stability, yet it can participate in several complexes via the RING domain and BRCT domain at N- and C-termini, respectively [187]. As research increasingly emphasizes neurodegeneration caused by DNA repair deficiencies resulting from DNA damage-induced senescence in the brain, BRCA1 has become a subject of particular interest. Shreds of evidence observed that concertation of BRCA1 in the AD mouse model is low in contrast to the wild-type. A similar result is observed in post-mortem brain samples of AD patients. Moreover, mice with BRCA1 knockdown displayed high neuronal double-stranded breaks [188]. Even embryos with BRCA1 knockdown exhibited DNA damage accumulation

because of BRCA1 deficiency [189]. Two plausible reasons for the decrease in BRCA1 levels include aberrant activation of N-methyl-D-aspartate (NMDA) receptors [190], which prompts the proteasome system to degrade BRCA1, and mislocalization of BRCA1 from the nucleus to the cytoplasm, where it colocalizes with tau [191]. Interestingly, BRCA1 does not colocalize with α -synuclein or TAR DNA-binding protein associated with Parkinson's disease (PD) and Amyotrophic Lateral Sclerosis (ALS) [192]. Building upon this potential explanation, the study investigated the effects of point mutations on the BARD1 RING domain on BRCA1 and its immediate binding partners, namely, UbcH5c, H2A, and Tau.

Firstly, the structures of BRCA1-BARD1, UbcH5c, H2A, and Tau were extracted from PDB. Secondly, screening and assessment of common sites were conducted to identify potential residues on the BARD1 RING domain where BRCA1, UbcH5c, and H2A interact. The findings indicated that residues H36, S37, A40, R43, L44, L47, L101, S103, M104, L107, C108, L111, L114, and L115 are not only shared between BRCA1 and UbcH5c but also reside within the two α -helices of BARD1. Evolutionary conservation and physiochemical properties were examined for all these potential sites. Subsequently, disease tolerability was evaluated through SIFT, FATHMM, and Polyphen-2, while mutagenesis was conducted using MUpro, SAAFEC-SEQ, and I-Mutant2.0, which provided $\Delta\Delta G$ values. The average $\Delta\Delta G$ was calculated to identify the top three mutants among all the potential sites. Before docking, binding pockets were predicted to determine the inter- and intra-binding residues, aiding in the precise localization of the docking sites. A variety of docking algorithms and tools were utilized to investigate and compare the interaction of mutant and wild-type structures. For template-based docking, Hex 6.3 was employed, while CABS-dock was used for protein-peptide docking. Additionally, flexible docking was conducted using HADDOCK and LZerD. The results identified the top five mutants as S37G, A40H, L44A, L47A, and M104K, which were further validated using GROMACS. Molecular dynamic simulation revealed L44A as the potential mutant that destabilizes not only BARD1 but also the docked structure BRCA1. However, no significant results were observed with the docking of BRCA1-BARD1(L44A) with UbcH5c. Nevertheless, consistent with the hypothesis, BRCA1-BARD1(L44A) adversely affected the stability of H2A, while conversely exhibiting stabilization with tau. Hence, the result indicates that mutation of L44A on BARD1 α -helices has a destabilizing effect on itself and other binding proteins (**Fig. 5.1.**). However, further experimentations are required to validate the result. The prospects of this study suggest that there may be mutations other than those disrupting the RING domain yet to be discovered, which could compromise the functionality of BRCA1-BARD1, rendering it ineffective. Moreover, the E2 enzymes that bind to BRCA1 recognize a comparable binding surface on the RING domain, making it exceedingly challenging to identify mutations that selectively disrupt the interaction with one E2 while preserving others.

Lately, numerous computational studies have attempted to unveil the role of BRCA1-BARD1 mutations in understanding the progression of breast cancer. For instance, mutation of BRCA1 (C61G, C64Y, C39Y, and C24R) and BARD1 (C53W, C71Y, and C83R) exhibits loss of hotspot residues necessary for other interactions [193]. Moreover, mutation on BRCA1 (L51W and K65R) and BARD1 (C53W) severely impacts the ubiquitination of histones in NCP, affecting DNA repair and resulting in cancer [194]. Furthermore, mutations positioned in the PPI regions of BRCA1-BARD1 (V11G, M18K, L22S, and T97R) are identified as the most significant [195]. However, in our previous study [196], we deeply studied the E3 ligase activity of BRCA1 in Alzheimer's disease, keeping that in mind, the present study bridges the gap between BRCA1 and Alzheimer's disease by targeting BARD1, a heterodimeric partner of BRCA1.

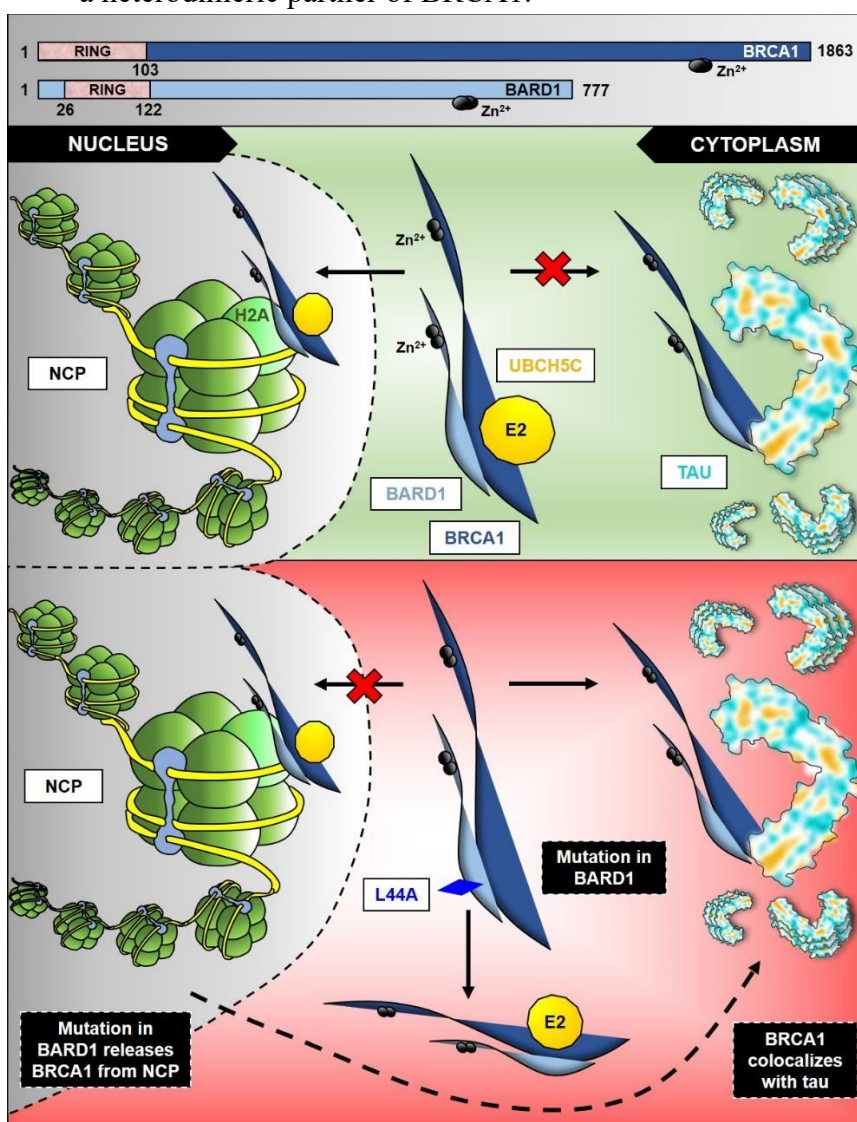


Fig. 5.1. The illustration depicts the hypothesis regarding the normal and aberrant behavior of the BRCA1-BARD1 heterodimer upon the BARD1 mutation at L44A. In the upper half, BRCA1-BARD1 interacts with histone H2A and the E2-conjugating enzyme, Ubch5c, displaying proper E3 ligase activity. In the lower half, the L44A point mutation on the RING domain of BARD1 results in the improper E3 ligase activity of BRCA1. Consequently, BRCA1 is mislocalized from the nucleus to the cytoplasm, where it colocalizes with tau lesions.

RNF8 ► The present study focused on a small segment of this huge ubiquitination cascade i.e., the impact of mutagenesis of RNF8 on its binding with E2 conjugating enzyme, UBE2N. The RING domain of RNF8 was taken and its interacting sites with UBE2N were carefully studied. After scrutinizing every site, few qualified for mutational studies. The result depicted that I405, S407, E408, E429, R433, P438, I439, and R441 could be possible sites that affect the binding of RNF8 with UBE2N and thereby hampering its E3 ligase activity. Further, validation is required to concrete the reliability of the results. Nevertheless, the limitation of this study is the impact of the mutation on other diverse functions of RNF8, added, γ H2AX foci do not always represent DSB formation; in such cases how would RNF8 initiate ubiquitination?

RNF168 ► It is the second E3 ligase that comes to amplify the ubiquitin chain initiated by RNF8. The impact of a point mutation in the RING domain of RNF168 was studied, where the E2-conjugating enzyme UbcH5c comes and binds. The results suggested that C16G, C31G, C36G, C39G, C50G, and C51G were key mutants that destabilized the structure of RNF168. However, when the same mutants were studied in the docking studies, the results inferred that mutants C31G and C50G depicted more deviation. To find a therapeutic potential for taming such mutants, PROTACs were introduced. PROTACs comprise three domains, namely, substrate binding motif, linker, and E3 ligase binding motif. The E3 ligase binding motif is also known as warheads. The dataset of warheads was downloaded from the database, PROTAC-DB 2.0 which was further screened out and docked with all the mutants. However, as the top two mutants observed from E3-E2 docking were C31G and C50G, therefore, MDS was performed for them. The overall result concluded that Ligand 4 and Ligand 11 when docked with mutants showed better stability than the wild-type. Hence, the mutants can be marked for degradation by UPS.

5.2. Conclusion

BRCA1 ► BRCA1 has been extensively studied in breast and ovarian cancer however, in neurodegeneration, BRCA1 acts as a key DNA repair protein. BRCA1 acts as an E3 in many cellular complexes that ubiquitinates different substrates. There is a potential link between cellular senescence and neurodegeneration where a deficient DNA repair mechanism leads to structural and functional impairment of BRCA1 that contributes to the pathogenesis of neurodegeneration. Here, we studied the E3 ligase activity of BRCA1 with its E2 conjugating partner, Ube2k. Results suggest mutagenesis of K32 and K45 has a significant impact on their binding. Thereby, giving an insight into how Ube2k binding is affected at the RING domain of BRCA1, impacting its ability to do E3 ligase activity and resulting in detrimental ubiquitination events. Molecular dynamics simulation validated K32L as the most

potential mutant. However, more *in vivo* studies and experiments are required for further validation. The broader implication of this work is to elucidate the functional mechanistic insights behind lysine mutation in the RING domain of BRCA1 to find therapeutic interventions for NDDs.

BRCA1-BARD1 ► The principal discoveries and implications of this study indicate that the point mutation (L44A) on the first α -helix bundle of BARD1 not only destabilizes its own structure but also disturbs its heterodimeric conformation with BRCA1. This underscores the importance of BRCA1-BARD1 heterodimer stability and its E3 ligase functionality within the cellular system. The impact of the L44A mutation on the interaction of BRCA1-BARD1 with UbcH5c appears to be minimal, likely due to UbcH5c's exclusive binding with BRCA1 rather than BARD1. However, the same mutation disrupts the interaction of BRCA1-BARD1 with H2A. Given that BARD1, along with the RING domain of BRCA1, interacts with H2A, this suggests that the L44A mutation alters the conformation and E3 ligase activity of both BARD1 and BRCA1. Consequently, they fail to interact with H2A and instead become colocalized with tau protein in the cytoplasm, exhibiting higher stability than the wild-type. Since heterodimeric formation with BARD1 is crucial for the nuclear localization of BRCA1, thus, one hypothesis suggests that BRCA1 dissociates from BARD1 during the export and subsequently co-aggregates with tau, whereas, another hypothesis suggests dissociation of BRCA1 from BARD1 happens during coaggregation with tau in the cytoplasm [47].

RNF8-RNF168 ► Studies in the past suggest, that BRCA1 plays a vital role in AD pathology and dysfunctioning of the same can worsen the symptoms. BRCA1 and BARD1 form a heterodimer RING that facilitates E3 ligase activity. This heterodimer RING is involved in the ubiquitination of γ -tubulin in the cytosol which is important for the centrosome complex concentration of various proteins involved in the cell cycle [197]. Dysfunction of BARD1 results in the subcellular mislocalization of BRCA1 which is highly insoluble and binds to tau lesion. BARD1 plays a vital role in binding BRCA1 with nucleosome core protein. However, before this happens, there is a huge possibility that the other interacting partners may not be functioning properly. One of the significant E3 ligase during DSBs is RNF8 which binds with UBE2N and forms a K-63 linked ubiquitin chain that in turn acts as a framework for other proteins carrying ubiquitin-binding motifs such as RAP80 and another E3 ligase, RNF168. It is well stated in the literature that both E3 ligases, RNF8 and RNF168 are wanted at the site of DNA damage. RNF168 amplifies RNF8 ubiquitin activity and co-operates in extending the K-63-linked polyubiquitin chain that further recruits RAP80, BRCA1, and 53BP1 which altogether assists in DSB repair. I405, S407, E408, E429, R433, P438, I439, and R441 could be possible sites that affect the binding of RNF8

with UBE2N and thereby hampering its E3 ligase activity, whereas, in RNF168, C16G, C31G, C36G, C39G, C50G, and C51G are the key sites.

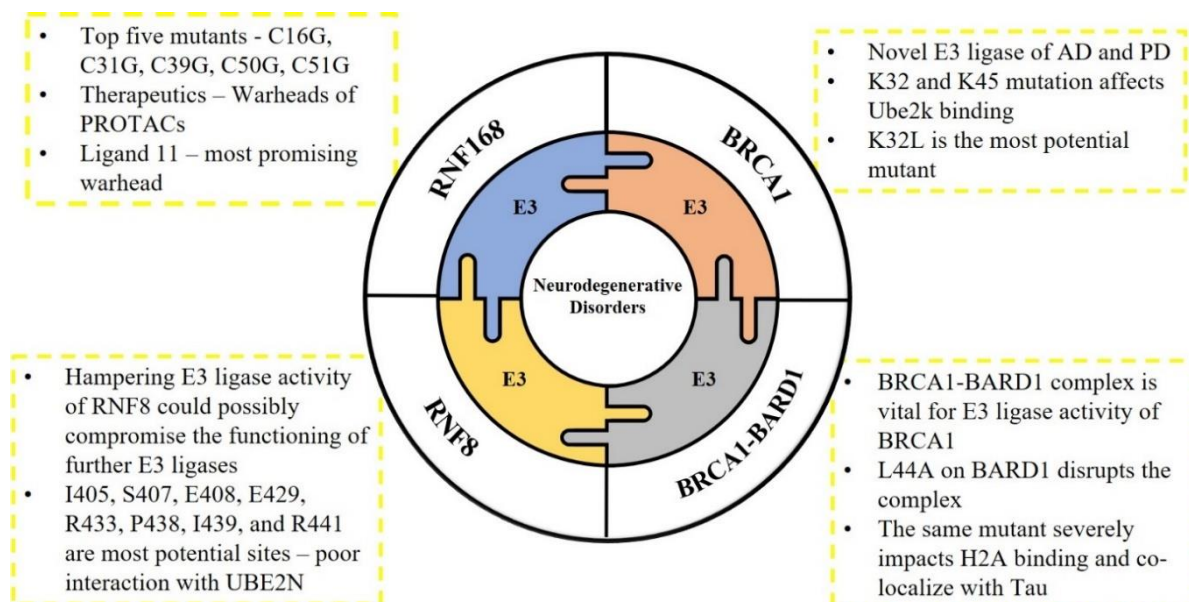


Fig. 5.2. The major finding of the entire study.

5.3. Future Perspective

BRCA1 ► Future prospects of this study address that mutation in the RING domain of BRCA1 could decrease its co-localization with BARD1 and BACH1. Moreover, histidine and cysteine are two key residues involved in many E2-E3 interactions, therefore mutation of these amino acids could be explored in BRCA1 as well.

BRCA1-BARD1 ► This study underscores that besides A β accumulation, mutations in BARD1 can also lead to the mislocalization of the complex from the nucleus to the cytoplasm, resulting in the loss of its E3 ligase activity and DNA repair mechanism. Nonetheless, further *in vitro* and *in vivo* experiments are necessary for additional validation.

RNF8-RNF168 ► Multiple regulation of RNF8 and RNF168 represents potential therapeutic target, for instance, here it states that by hampering the E3 ligase activity of RNF8 could possibly compromise the functioning of further E3 ligases involved in the cascade. In such a case, reversing the reaction by a deubiquitinating enzyme signifies a workable therapeutic solution.

This research holds significant societal implications, especially in the context of the increasing prevalence of neurodegenerative diseases such as Alzheimer's and Parkinson's, which are expected to rise with global aging populations. These conditions not only cause a loss of independence and quality of life for patients but also place a tremendous burden on families, caregivers, and healthcare systems. By identifying key molecular mechanisms—specifically the role of E3 ligase dysfunction in protein aggregation and neurodegeneration—this work has the potential to shift current therapeutic approaches. The development of targeted therapies, like PROTACs, aimed at eliminating or correcting faulty proteins, can lead to more effective treatments that slow disease progression.

Such advances could result in reduced hospitalizations, a decline in the need for long-term care facilities, and decreased reliance on caregivers, directly impacting public health costs. Moreover, by addressing these diseases at the molecular level, this research contributes to the broader goals of personalized medicine, offering targeted treatment strategies that could improve not only individual patient outcomes but also reduce the broader societal and economic burden of neurodegenerative diseases. This progress has the potential to reshape aging-related healthcare and alleviate the strain on social welfare systems globally.

Lastly, this research not only deepens the understanding of neurodegenerative diseases but also has broader implications for diseases like cancer, particularly breast cancer, due to the shared molecular mechanisms involving BRCA1. This cross-disease insight opens the possibility of developing chemical assays that can simultaneously detect early signs of disease progression in both neurodegenerative diseases and cancers. Such assays could be designed to monitor key biomarkers, including BRCA1 mutations, offering a dual benefit by catching early-stage neurodegeneration and cancer in patients.

REFERENCES

- [1] S. Zafar, S. I. Fatima, M. Schmitz, and I. Zerr, “Current Technologies Unraveling the Significance of Post-Translational Modifications (PTMs) as Crucial Players in Neurodegeneration,” *Biomolecules*, vol. 14, no. 1, Jan. 2024, doi: 10.3390/BIOM14010118.
- [2] L. L. Zheng, L. T. Wang, Y. W. Pang, L. P. Sun, and L. Shi, “Recent advances in the development of deubiquitinases inhibitors as antitumor agents,” *Eur J Med Chem*, vol. 266, p. 116161, Feb. 2024, doi: 10.1016/J.EJMECH.2024.116161.
- [3] H. Xie and C. Zhang, “Potential of the nanoplatform and PROTAC interface to achieve targeted protein degradation through the Ubiquitin–Proteasome system,” *Eur J Med Chem*, vol. 267, p. 116168, Mar. 2024, doi: 10.1016/J.EJMECH.2024.116168.
- [4] A. Jaishankar *et al.*, “A Comprehensive Atlas of E3 Ubiquitin Ligase Mutations in Neurological Disorders,” *Frontiers in Genetics* | www.frontiersin.org, vol. 9, p. 29, 2018, doi: 10.3389/fgene.2018.00029.
- [5] N. LeBlanc, E. Mallette, and W. Zhang, “Targeted modulation of E3 ligases using engineered ubiquitin variants,” *FEBS J*, vol. 288, no. 7, pp. 2143–2165, Apr. 2021, doi: 10.1111/FEBS.15536.
- [6] Q. Yang, J. Zhao, D. Chen, and Y. Wang, “E3 ubiquitin ligases: styles, structures and functions,” *Molecular Biomedicine*, vol. 2, no. 1, Dec. 2021, doi: 10.1186/S43556-021-00043-2.
- [7] C. Bartocci and E. L. Denchi, “Put a RING on it: Regulation and inhibition of RNF8 and RNF168 RING finger E3 ligases at DNA damage sites,” *Frontiers in Genetics*, vol. 4, no. JUL, p. 51975, Jul. 2013, doi: 10.3389/FGENE.2013.00128/BIBTEX.
- [8] Y. Guo *et al.*, “Histone H2A ubiquitination resulting from Brap loss of function connects multiple aging hallmarks and accelerates neurodegeneration,” *iScience*, vol. 25, no. 7, Jul. 2022, doi: 10.1016/J.ISCI.2022.104519.
- [9] M. M. Authiat *et al.*, “Preferential Involvement of BRCA1/BARD1, Not Tip60/Fe65, in DNA Double-Strand Break Repair in Presenilin-1 P117L Alzheimer Models,” 2022, doi: 10.1155/2022/3172861.
- [10] T. A. Evans *et al.*, “BRCA1 May Modulate Neuronal Cell Cycle Re-Entry in Alzheimer Disease,” *Int J Med Sci*, vol. 4, no. 3, pp. 140–145, 2007.
- [11] R. N. L. Lamptey, B. Chaulagain, R. Trivedi, A. Gothwal, B. Layek, and J. Singh, “A Review of the Common Neurodegenerative Disorders: Current Therapeutic Approaches and the Potential Role of Nanotherapeutics,” *Int J Mol Sci*, vol. 23, no. 3, Feb. 2022, doi: 10.3390/IJMS23031851.
- [12] D. K. Khatri *et al.*, “Gauging the role and impact of drug interactions and repurposing in neurodegenerative disorders,” *Current Research in Pharmacology and Drug Discovery*, vol. 2, Jan. 2021, doi: 10.1016/J.CRP HAR.2021.100022.
- [13] Y. Hou *et al.*, “Ageing as a risk factor for neurodegenerative disease,” *Nature Reviews Neurology* 2019 15:10, vol. 15, no. 10, pp. 565–581, Sep. 2019, doi: 10.1038/s41582-019-0244-7.

- [14] L. Chen, S. Liu, and Y. Tao, "Regulating tumor suppressor genes: post-translational modifications," *Signal Transduction and Targeted Therapy* 2020 5:1, vol. 5, no. 1, pp. 1–25, Jun. 2020, doi: 10.1038/s41392-020-0196-9.
- [15] D. Salas-Lloret and R. González-Prieto, "Insights in Post-Translational Modifications: Ubiquitin and SUMO," *International Journal of Molecular Sciences* 2022, Vol. 23, Page 3281, vol. 23, no. 6, p. 3281, Mar. 2022, doi: 10.3390/IJMS23063281.
- [16] V. S. Kumar and A. Vellaichamy, "Sequence and structure-based characterization of ubiquitination sites in human and yeast proteins using Chou's sample formulation," *Proteins: Structure, Function, and Bioinformatics*, vol. 87, no. 8, pp. 646–657, Aug. 2019, doi: 10.1002/PROT.25689.
- [17] A. Upadhyay *et al.*, "E3 ubiquitin ligases neurobiological mechanisms: Development to degeneration," *Front Mol Neurosci*, vol. 10, p. 151, May 2017, doi: 10.3389/FNMOL.2017.00151/BIBTEX.
- [18] M. F. Schmidt, Z. Y. Gan, D. Komander, and G. Dewson, "Ubiquitin signalling in neurodegeneration: mechanisms and therapeutic opportunities," *Cell Death & Differentiation* 2021 28:2, vol. 28, no. 2, pp. 570–590, Jan. 2021, doi: 10.1038/s41418-020-00706-7.
- [19] N. D. Roverato, C. Sailer, N. Catone, A. Aiche, F. Stengel, and M. Groettrup, "Parkin is an E3 ligase for the ubiquitin-like modifier FAT10, which inhibits Parkin activation and mitophagy," *Cell Rep*, vol. 34, no. 11, Mar. 2021, doi: 10.1016/J.CELREP.2021.108857.
- [20] T. Wang, W. Wang, Q. Wang, R. Xie, A. Landay, and D. Chen, "The E3 ubiquitin ligase CHIP in normal cell function and in disease conditions," *Ann N Y Acad Sci*, vol. 1460, no. 1, pp. 3–10, Jan. 2020, doi: 10.1111/NYAS.14206.
- [21] M. B. Metzger, J. N. Pruneda, R. E. Klevit, and A. M. Weissman, "RING-type E3 ligases: Master manipulators of E2 ubiquitin-conjugating enzymes and ubiquitination," *Biochimica et Biophysica Acta (BBA) - Molecular Cell Research*, vol. 1843, no. 1, pp. 47–60, Jan. 2014, doi: 10.1016/J.BBAMCR.2013.05.026.
- [22] A. S. Chauhan, S. S. Jhujh, and G. S. Stewart, "E3 ligases: a ubiquitous link between DNA repair, DNA replication and human disease," *Biochemical Journal*, vol. 481, no. 14, pp. 923–944, Jul. 2024, doi: 10.1042/BCJ20240124.
- [23] L. Lescouzères and P. Bomont, "E3 Ubiquitin Ligases in Neurological Diseases: Focus on Gigaxonin and Autophagy," 2020. doi: 10.3389/fphys.2020.01022.
- [24] C. Bartocci and E. L. Denchi, "Put a RING on it: Regulation and inhibition of RNF8 and RNF168 RING finger E3 ligases at DNA damage sites," *Front Genet*, vol. 4, no. JUL, p. 51975, Jul. 2013, doi: 10.3389/FGENE.2013.00128/BIBTEX.
- [25] X. Fu, W. Tan, Q. Song, H. Pei, and J. Li, "BRCA1 and Breast Cancer: Molecular Mechanisms and Therapeutic Strategies," *Front Cell Dev Biol*, vol. 10, p. 813457, Mar. 2022, doi: 10.3389/FCELL.2022.813457/BIBTEX.
- [26] S. Azrak, "upQMPSF, a Method for the Detection of BRCA1 Exon Copy Number Variants," *Biochem Genet*, vol. 53, no. 4–6, pp. 141–157, Jun. 2015, doi: 10.1007/S10528-015-9681-1/FIGURES/8.
- [27] R. Mezencev and Y. O. Chernoff, "Risk of Alzheimer's Disease in Cancer Patients: Analysis of Mortality Data from the US SEER Population-Based Registries," *Cancers (Basel)*, vol. 12, no. 4, Apr. 2020, doi: 10.3390/CANCERS12040796.

- [28] R. Mezencev and Y. O. Chernoff, "Risk of Alzheimer's Disease in Cancer Patients: Analysis of Mortality Data from the US SEER Population-Based Registries," *Cancers* 2020, Vol. 12, Page 796, vol. 12, no. 4, p. 796, Mar. 2020, doi: 10.3390/CANCERS12040796.
- [29] T. Mano *et al.*, "Tau-related dysfunction of BRCA1 leads to reduced neuronal plasticity in Alzheimer's disease," *Alzheimer's & Dementia*, vol. 14, no. 7S_Part_18, Jul. 2018, doi: 10.1016/J.JALZ.2018.06.2771.
- [30] T. A. Evans *et al.*, "BRCA1 May Modulate Neuronal Cell Cycle Re-Entry in Alzheimer Disease," *Int J Med Sci*, vol. 4, no. 3, p. 140, May 2007, doi: 10.7150/IJMS.4.140.
- [31] S. Arshad, I. Ishaque, S. Mumtaz, M. U. Rashid, and N. Malkani, "In-Silico Analyses of Nonsynonymous Variants in the BRCA1 Gene," *Biochem Genet*, vol. 59, no. 6, pp. 1506–1526, Dec. 2021, doi: 10.1007/S10528-021-10074-7/FIGURES/4.
- [32] M. D. Stewart *et al.*, "Tuning BRCA1 and BARD1 activity to investigate RING ubiquitin ligase mechanisms," *Protein Science*, vol. 26, no. 3, 2017, doi: 10.1002/pro.3091.
- [33] R. Hashizume *et al.*, "The RING Heterodimer BRCA1-BARD1 Is a Ubiquitin Ligase Inactivated by a Breast Cancer-derived Mutation," *Journal of Biological Chemistry*, vol. 276, no. 18, 2001, doi: 10.1074/jbc.C000881200.
- [34] S. R. Witus, M. D. Stewart, and R. E. Klevit, "The BRCA1/BARD1 ubiquitin ligase and its substrates," *Biochem J*, vol. 478, no. 18, p. 3467, Sep. 2021, doi: 10.1042/BCJ20200864.
- [35] V. Vittal *et al.*, "Intrinsic disorder drives N-terminal ubiquitination by Ube2w," *Nat Chem Biol*, vol. 11, no. 1, 2015, doi: 10.1038/nchembio.1700.
- [36] D. E. Christensen, P. S. Brzovic, and R. E. Klevit, "E2-BRCA1 RING interactions dictate synthesis of mono- or specific polyubiquitin chain linkages," *Nature Structural & Molecular Biology* 2007 14:10, vol. 14, no. 10, pp. 941–948, Sep. 2007, doi: 10.1038/nsmb1295.
- [37] M. D. Stewart *et al.*, "BARD1 is necessary for ubiquitylation of nucleosomal histone H2A and for transcriptional regulation of estrogen metabolism genes," *Proc Natl Acad Sci U S A*, vol. 115, no. 6, 2018, doi: 10.1073/pnas.1715467115.
- [38] P. S. Brzovic *et al.*, "Binding and recognition in the assembly of an active BRCA1/BARD1 ubiquitin-ligase complex," *Proc Natl Acad Sci U S A*, vol. 100, no. 10, 2003, doi: 10.1073/pnas.0836054100.
- [39] X. Zhang, C. Huo, Y. Liu, R. Su, Y. Zhao, and Y. Li, "Mechanism and Disease Association With a Ubiquitin Conjugating E2 Enzyme: UBE2L3," 2022. doi: 10.3389/fimmu.2022.793610.
- [40] S. R. Witus *et al.*, "BRCA1/BARD1 site-specific ubiquitylation of nucleosomal H2A is directed by BARD1," *Nat Struct Mol Biol*, vol. 28, no. 3, 2021, doi: 10.1038/s41594-020-00556-4.
- [41] L. Dai *et al.*, "Structural insight into BRCA1-BARD1 complex recruitment to damaged chromatin," *Mol Cell*, vol. 81, no. 13, 2021, doi: 10.1016/j.molcel.2021.05.010.
- [42] J. Becker, C. Bonnet, G. Clifford, A. Groth, M. Wilson, and J. R. Chapman, "BARD1 links histone H2A Lysine-15 ubiquitination to initiation of BRCA1-dependent homologous recombination," *bioRxiv*, vol. 20, 2020.

- [43] K. Nakamura *et al.*, “H4K20me0 recognition by BRCA1–BARD1 directs homologous recombination to sister chromatids,” 2019. doi: 10.1038/s41556-019-0282-9.
- [44] M. Wezyk *et al.*, “Overactive BRCA1 Affects Presenilin 1 in Induced Pluripotent Stem Cell-Derived Neurons in Alzheimer’s Disease,” *Journal of Alzheimer’s Disease*, vol. 62, no. 1, 2018, doi: 10.3233/JAD-170830.
- [45] T. Mano *et al.*, “Neuron-specific methylome analysis reveals epigenetic regulation and tau-related dysfunction of BRCA1 in Alzheimer’s disease,” *Proc Natl Acad Sci U S A*, vol. 114, no. 45, 2017, doi: 10.1073/pnas.1707151114.
- [46] M. Wezyk and C. Zekanowski, “Role of BRCA1 in Neuronal Death in Alzheimer’s Disease,” *ACS Chem Neurosci*, vol. 9, no. 5, pp. 870–872, May 2018, doi: 10.1021/ACSCHENNEURO.8B00149/ASSET/IMAGES/LARGE/CN-2018-00149N_0001.JPEG.
- [47] M. Kurihara, T. Mano, Y. Saito, S. Murayama, T. Toda, and A. Iwata, “Colocalization of BRCA1 with Tau Aggregates in Human Tauopathies,” *Brain Sci*, vol. 10, no. 1, Jan. 2020, doi: 10.3390/BRAINSCI10010007.
- [48] S. Ouyang, Y. Song, Y. Tian, Y. Chen, X. Yu, and D. Wang, “RNF8 deficiency results in neurodegeneration in mice,” *Neurobiol Aging*, vol. 36, no. 10, p. 2850, Oct. 2015, doi: 10.1016/J.NEUROBIOLAGING.2015.07.010.
- [49] E. H. Jo, M. Y. Kim, H. J. Lee, and H. S. Park, “Ubiquitin E3 ligases in cancer: somatic mutation and amplification,” 2023. doi: 10.5483/BMBRep.2023-0037.
- [50] K. Farrell and T. J. Jarome, “Is PROTAC technology really a game changer for central nervous system drug discovery?,” *Expert Opin Drug Discov*, vol. 16, no. 8, 2021, doi: 10.1080/17460441.2021.1915979.
- [51] J. Qu *et al.*, “Specific Knockdown of α -Synuclein by Peptide-Directed Proteasome Degradation Rescued Its Associated Neurotoxicity,” *Cell Chem Biol*, vol. 27, no. 6, 2020, doi: 10.1016/j.chembiol.2020.03.010.
- [52] S. Tomoshige, S. Nomura, K. Ohgane, Y. Hashimoto, and M. Ishikawa, “Discovery of Small Molecules that Induce the Degradation of Huntingtin,” *Angewandte Chemie - International Edition*, vol. 56, no. 38, 2017, doi: 10.1002/anie.201706529.
- [53] Z. Liu *et al.*, “An overview of PROTACs: a promising drug discovery paradigm,” 2022. doi: 10.1186/s43556-022-00112-0.
- [54] M. Békés, D. R. Langley, and C. M. Crews, “PROTAC targeted protein degraders: the past is prologue,” 2022. doi: 10.1038/s41573-021-00371-6.
- [55] T. Barrett *et al.*, “NCBI GEO: archive for functional genomics data sets--update,” *Nucleic Acids Res*, vol. 41, no. Database issue, Jan. 2013, doi: 10.1093/NAR/GKS1193.
- [56] R. Edgar, M. Domrachev, and A. E. Lash, “Gene Expression Omnibus: NCBI gene expression and hybridization array data repository,” *Nucleic Acids Res*, vol. 30, no. 1, pp. 207–210, Jan. 2002, doi: 10.1093/NAR/30.1.207.
- [57] G. P. Hunt *et al.*, “GEOexplorer: a webserver for gene expression analysis and visualisation,” *Nucleic Acids Res*, vol. 50, no. W1, pp. W367–W374, Jul. 2022, doi: 10.1093/NAR/GKAC364.
- [58] S. Udhaya Kumar *et al.*, “Analysis of differentially expressed genes and molecular pathways in familial hypercholesterolemia involved in atherosclerosis: A systematic

- and bioinformatics approach,” *Front Genet*, vol. 11, pp. 1–16, Jul. 2020, doi: 10.3389/FGENE.2020.00734/BIBTEX.
- [59] A. T. H. Wu, B. Lawal, L. Wei, Y. T. Wen, D. T. W. Tzeng, and W. C. Lo, “Multiomics Identification of Potential Targets for Alzheimer Disease and Antrocin as a Therapeutic Candidate,” *Pharmaceutics 2021, Vol. 13, Page 1555*, vol. 13, no. 10, p. 1555, Sep. 2021, doi: 10.3390/PHARMACEUTICS13101555.
- [60] W. Li *et al.*, “Genome-Wide and Functional Annotation of Human E3 Ubiquitin Ligases Identifies MULAN, a Mitochondrial E3 that Regulates the Organelle’s Dynamics and Signaling,” *PLoS One*, vol. 3, no. 1, p. e1487, Jan. 2008, doi: 10.1371/JOURNAL.PONE.0001487.
- [61] H. Heberle, V. G. Meirelles, F. R. da Silva, G. P. Telles, and R. Minghim, “InteractiVenn: A web-based tool for the analysis of sets through Venn diagrams,” *BMC Bioinformatics*, vol. 16, no. 1, pp. 1–7, May 2015, doi: 10.1186/S12859-015-0611-3/FIGURES/4.
- [62] D. Szklarczyk *et al.*, “STRING v10: Protein-protein interaction networks, integrated over the tree of life,” *Nucleic Acids Res*, vol. 43, no. D1, pp. D447–D452, 2015, doi: 10.1093/nar/gku1003.
- [63] R. Oughtred *et al.*, “BioGRID: A Tool for Studying Biological Interactions in Yeast,” *Cold Spring Harb Protoc*, vol. 2016, no. 1, p. pdb.top080754, Jan. 2016, doi: 10.1101/PDB.TOP080754.
- [64] D. Szklarczyk *et al.*, “The STRING database in 2021: customizable protein–protein networks, and functional characterization of user-uploaded gene/measurement sets,” *Nucleic Acids Res*, vol. 49, no. D1, pp. D605–D612, Jan. 2021, doi: 10.1093/NAR/GKAA1074.
- [65] M. Cao *et al.*, “New directions for diffusion-based network prediction of protein function: incorporating pathways with confidence,” *Bioinformatics*, vol. 30, no. 12, Jun. 2014, doi: 10.1093/BIOINFORMATICS/BTU263.
- [66] M. Cao *et al.*, “Going the distance for protein function prediction: a new distance metric for protein interaction networks,” *PLoS One*, vol. 8, no. 10, Oct. 2013, doi: 10.1371/JOURNAL.PONE.0076339.
- [67] P. Shannon *et al.*, “Cytoscape: A Software Environment for Integrated Models of Biomolecular Interaction Networks,” *Genome Res*, vol. 13, no. 11, p. 2498, Nov. 2003, doi: 10.1101/GR.1239303.
- [68] M. K. Elbashir, M. Mohammed, H. Mwambi, and B. Omolo, “Identification of Hub Genes Associated with Breast Cancer Using Integrated Gene Expression Data with Protein-Protein Interaction Network,” *Applied Sciences (Switzerland)*, vol. 13, no. 4, p. 2403, Feb. 2023, doi: 10.3390/APP13042403/S1.
- [69] J. Reimand, T. Arak, and J. Vilo, “g:Profiler—a web server for functional interpretation of gene lists (2011 update),” *Nucleic Acids Res*, vol. 39, no. suppl_2, pp. W307–W315, Jul. 2011, doi: 10.1093/NAR/GKR378.
- [70] Z. Xie *et al.*, “Gene Set Knowledge Discovery with Enrichr,” *Curr Protoc*, vol. 1, no. 3, p. e90, Mar. 2021, doi: 10.1002/CPZ1.90.
- [71] S. X. Ge, D. Jung, D. Jung, and R. Yao, “ShinyGO: a graphical gene-set enrichment tool for animals and plants,” *Bioinformatics*, vol. 36, no. 8, pp. 2628–2629, Apr. 2020, doi: 10.1093/BIOINFORMATICS/BTZ931.

- [72] I. Letunic and P. Bork, “20 years of the SMART protein domain annotation resource,” *Nucleic Acids Res*, vol. 46, no. D1, pp. D493–D496, Jan. 2018, doi: 10.1093/NAR/GKX922.
- [73] T. L. Bailey, J. Johnson, C. E. Grant, and W. S. Noble, “The MEME Suite,” *Nucleic Acids Res*, vol. 43, no. W1, pp. W39–W49, Jul. 2015, doi: 10.1093/NAR/GKV416.
- [74] J. C. Obenauer, L. C. Cantley, and M. B. Yaffe, “Scansite 2.0: Proteome-wide prediction of cell signaling interactions using short sequence motifs,” *Nucleic Acids Res*, vol. 31, no. 13, pp. 3635–3641, Jul. 2003, doi: 10.1093/NAR/GKG584.
- [75] H. Ashkenazy *et al.*, “ConSurf 2016: an improved methodology to estimate and visualize evolutionary conservation in macromolecules,” *Nucleic Acids Res*, vol. 44, 2016, doi: 10.1093/nar/gkw408.
- [76] H. Xu, J. Zhou, S. Lin, W. Deng, Y. Zhang, and Y. Xue, “PLMD: An updated data resource of protein lysine modifications,” *J Genet Genomics*, vol. 44, no. 5, pp. 243–250, May 2017, doi: 10.1016/J.JGG.2017.03.007.
- [77] J. Bendl *et al.*, “PredictSNP: Robust and Accurate Consensus Classifier for Prediction of Disease-Related Mutations,” *PLoS Comput Biol*, vol. 10, no. 1, 2014, doi: 10.1371/JOURNAL.PCBI.1003440.
- [78] V. Pejaver *et al.*, “Inferring the molecular and phenotypic impact of amino acid variants with MutPred2,” *Nat Commun*, vol. 11, no. 1, Dec. 2020, doi: 10.1038/S41467-020-19669-X.
- [79] H. Venselaar, T. A. H. te Beek, R. K. P. Kuipers, M. L. Hekkelman, and G. Vriend, “Protein structure analysis of mutations causing inheritable diseases. An e-Science approach with life scientist friendly interfaces,” *BMC Bioinformatics*, vol. 11, no. 1, pp. 1–10, Nov. 2010, doi: 10.1186/1471-2105-11-548/FIGURES/5.
- [80] P. S. Brzovic, P. Rajagopal, D. W. Hoyt, M. C. King, and R. E. Klevit, “Structure of a BRCA1-BARD1 heterodimeric RING-RING complex,” *Nat Struct Biol*, vol. 8, no. 10, pp. 833–837, 2001, doi: 10.1038/nsb1001-833.
- [81] S. K. Burley *et al.*, “RCSB Protein Data Bank (RCSB.org): delivery of experimentally-determined PDB structures alongside one million computed structure models of proteins from artificial intelligence/machine learning,” *Nucleic Acids Res*, vol. 51, no. D1, pp. D488–D508, Jan. 2023, doi: 10.1093/NAR/GKAC1077.
- [82] D. Kozakov *et al.*, “The FTMap family of web servers for determining and characterizing ligand-binding hot spots of proteins,” *Nature Protocols 2015 10:5*, vol. 10, no. 5, pp. 733–755, Apr. 2015, doi: 10.1038/nprot.2015.043.
- [83] S. J. de Vries and A. M. J. J. Bonvin, “CPORT: a consensus interface predictor and its performance in prediction-driven docking with HADDOCK,” *PLoS One*, vol. 6, no. 3, 2011, doi: 10.1371/JOURNAL.PONE.0017695.
- [84] I. T. Desta, K. A. Porter, B. Xia, D. Kozakov, and S. Vajda, “Performance and Its Limits in Rigid Body Protein-Protein Docking,” *Structure*, vol. 28, no. 9, pp. 1071–1081.e3, Sep. 2020, doi: 10.1016/j.str.2020.06.006.
- [85] S. Vajda *et al.*, “New Additions to the ClusPro Server Motivated by CAPRI,” 2017, doi: 10.1002/prot.25219.
- [86] D. Kozakov *et al.*, “How good is automated protein docking?,” *Proteins: Structure, Function, and Bioinformatics*, vol. 81, no. 12, pp. 2159–2166, Dec. 2013, doi: 10.1002/prot.24403.

- [87] D. Kozakov *et al.*, “The ClusPro web server for protein–protein docking,” *Nat Protoc*, vol. 12, no. 2, pp. 255–278, Feb. 2017, doi: 10.1038/nprot.2016.169.
- [88] K. A. Porter *et al.*, “ClusPro PeptiDock: efficient global docking of peptide recognition motifs using FFT,” *Bioinformatics*, vol. 33, no. 20, pp. 3299–3301, Oct. 2017, doi: 10.1093/bioinformatics/btx216.
- [89] G. C. P. Van Zundert *et al.*, “The HADDOCK2.2 Web Server: User-Friendly Integrative Modeling of Biomolecular Complexes,” *J Mol Biol*, vol. 428, no. 4, pp. 720–725, Feb. 2016, doi: 10.1016/J.JMB.2015.09.014.
- [90] C. Dominguez, R. Boelens, and A. M. J. J. Bonvin, “HADDOCK: A protein-protein docking approach based on biochemical or biophysical information,” *J Am Chem Soc*, vol. 125, no. 7, pp. 1731–1737, Feb. 2003, doi: 10.1021/JA026939X/SUPPL_FILE/JA026939XSI20021128_085857.TXT.
- [91] V. Venkatraman, Y. D. Yang, L. Sael, and D. Kihara, “Protein-protein docking using region-based 3D Zernike descriptors,” *BMC Bioinformatics*, vol. 10, 2009, doi: 10.1186/1471-2105-10-407.
- [92] K. A. Porter, I. Desta, D. Kozakov, and S. Vajda, “What method to use for protein–protein docking?,” *Curr Opin Struct Biol*, vol. 55, pp. 1–7, 2019, doi: 10.1016/j.sbi.2018.12.010.
- [93] D. Van Der Spoel, E. Lindahl, B. Hess, G. Groenhof, A. E. Mark, and H. J. C. Berendsen, “GROMACS: Fast, flexible, and free,” *J Comput Chem*, vol. 26, no. 16, pp. 1701–1718, Dec. 2005, doi: 10.1002/JCC.20291.
- [94] M. J. Robertson, J. Tirado-Rives, and W. L. Jorgensen, “Improved Peptide and Protein Torsional Energetics with the OPLS-AA Force Field,” *J Chem Theory Comput*, vol. 11, no. 7, pp. 3499–3509, 2015, doi: 10.1021/acs.jctc.5b00356.
- [95] H. M. Berman *et al.*, “The Protein Data Bank,” 2000. doi: 10.1093/nar/28.1.235.
- [96] G. Kurisu, “Fifty years of Protein Data Bank in the Journal of Biochemistry,” 2022. doi: 10.1093/jb/mvab133.
- [97] J. R. Morris, N. H. Keep, and E. Solomon, “Identification of residues required for the interaction of BARD1 with BRCA1,” *Journal of Biological Chemistry*, vol. 277, no. 11, 2002, doi: 10.1074/jbc.M109249200.
- [98] R. C. Benirschke *et al.*, “Molecular basis for the association of human E4B U box ubiquitin ligase with E2-conjugating enzymes UbcH5c and Ubc4,” *Structure*, vol. 18, no. 8, 2010, doi: 10.1016/j.str.2010.04.017.
- [99] Y. Moriwaki *et al.*, “Solution structure of the isolated histone H2A-H2B heterodimer,” *Sci Rep*, vol. 6, 2016, doi: 10.1038/srep24999.
- [100] A. M. Stern *et al.*, “Abundant A β fibrils in ultracentrifugal supernatants of aqueous extracts from Alzheimer’s disease brains,” *Neuron*, vol. 111, no. 13, 2023, doi: 10.1016/j.neuron.2023.04.007.
- [101] H. Ai *et al.*, “Synthetic E2-Ub-nucleosome conjugates for studying nucleosome ubiquitination,” *Chem*, vol. 9, no. 5, 2023, doi: 10.1016/j.chempr.2023.01.012.
- [102] J. C. Obenauer, L. C. Cantley, and M. B. Yaffe, “Scansite 2.0: Proteome-wide prediction of cell signalling interactions using short sequence motifs,” *Nucleic Acids Res*, vol. 31, no. 13, 2003, doi: 10.1093/nar/gkg584.
- [103] T. Goldberg *et al.*, “LocTree3 prediction of localization,” *Nucleic Acids Res*, vol. 42, no. W1, 2014, doi: 10.1093/nar/gku396.

- [104] M. Varadi *et al.*, “PDBE-KB: A community-driven resource for structural and functional annotations,” *Nucleic Acids Res*, vol. 48, 2020, doi: 10.1093/nar/gkz853.
- [105] J. Jumper *et al.*, “Highly accurate protein structure prediction with AlphaFold,” *Nature* 2021 596:7873, vol. 596, no. 7873, pp. 583–589, Jul. 2021, doi: 10.1038/s41586-021-03819-2.
- [106] M. Varadi *et al.*, “AlphaFold Protein Structure Database: Massively expanding the structural coverage of protein-sequence space with high-accuracy models,” *Nucleic Acids Res*, vol. 50, no. D1, 2022, doi: 10.1093/nar/gkab1061.
- [107] H. Ashkenazy *et al.*, “ConSurf 2016: an improved methodology to estimate and visualize evolutionary conservation in macromolecules,” *Nucleic Acids Res*, vol. 44, no. Web Server issue, p. W344, Jul. 2016, doi: 10.1093/NAR/GKW408.
- [108] F. Madeira *et al.*, “Search and sequence analysis tools services from EMBL-EBI in 2022,” *Nucleic Acids Res*, vol. 50, no. W1, 2022, doi: 10.1093/nar/gkac240.
- [109] P. C. Ng and S. Henikoff, “Predicting deleterious amino acid substitutions,” *Genome Res*, vol. 11, no. 5, 2001, doi: 10.1101/gr.176601.
- [110] M. F. Rogers, H. A. Shihab, M. Mort, D. N. Cooper, T. R. Gaunt, and C. Campbell, “FATHMM-XF: Accurate prediction of pathogenic point mutations via extended features,” *Bioinformatics*, vol. 34, no. 3, 2018, doi: 10.1093/bioinformatics/btx536.
- [111] I. A. Adzhubei *et al.*, “A method and server for predicting damaging missense mutations,” 2010. doi: 10.1038/nmeth0410-248.
- [112] I. Adzhubei, D. M. Jordan, and S. R. Sunyaev, “Predicting functional effect of human missense mutations using PolyPhen-2,” *Curr Protoc Hum Genet*, no. SUPPL.76, 2013, doi: 10.1002/0471142905.hg0720s76.
- [113] J. Cheng, A. Randall, and P. Baldi, “Prediction of protein stability changes for single-site mutations using support vector machines,” *Proteins*, vol. 62, no. 4, pp. 1125–1132, Mar. 2006, doi: 10.1002/PROT.20810.
- [114] G. Li, S. K. Panday, and E. Alexov, “Saafec-seq: A sequence-based method for predicting the effect of single point mutations on protein thermodynamic stability,” *Int J Mol Sci*, vol. 22, no. 2, 2021, doi: 10.3390/ijms22020606.
- [115] E. Capriotti, P. Fariselli, and R. Casadio, “I-Mutant2.0: predicting stability changes upon mutation from the protein sequence or structure,” *Nucleic Acids Res*, vol. 33, no. Web Server issue, p. W306, Jul. 2005, doi: 10.1093/NAR/GKI375.
- [116] G. Madhavi Sastry, M. Adzhigirey, T. Day, R. Annabhimoju, and W. Sherman, “Protein and ligand preparation: Parameters, protocols, and influence on virtual screening enrichments,” *J Comput Aided Mol Des*, vol. 27, no. 3, 2013, doi: 10.1007/s10822-013-9644-8.
- [117] L. Jendele, R. Krivak, P. Skoda, M. Novotny, and D. Hoksza, “PrankWeb: a web server for ligand binding site prediction and visualization,” *Nucleic Acids Res*, vol. 47, no. W1, 2019, doi: 10.1093/nar/gkz424.
- [118] R. Krivák and D. Hoksza, “P2Rank: machine learning based tool for rapid and accurate prediction of ligand binding sites from protein structure,” *J Cheminform*, vol. 10, no. 1, 2018, doi: 10.1186/s13321-018-0285-8.
- [119] G. Macindoe, L. Mavridis, V. Venkatraman, M. D. Devignes, and D. W. Ritchie, “HexServer: An FFT-based protein docking server powered by graphics processors,” *Nucleic Acids Res*, vol. 38, no. SUPPL. 2, 2010, doi: 10.1093/nar/gkq311.

- [120] D. Ritchie, “Hex 6.3 User Manual,” *Molecules*, 2010.
- [121] M. Kurcinski, A. Badaczewska-Dawid, M. Kolinski, A. Kolinski, and S. Kmiecik, “Flexible docking of peptides to proteins using CABS-dock,” *Protein Science*, vol. 29, no. 1, 2020, doi: 10.1002/pro.3771.
- [122] M. Blaszczyk *et al.*, “Modeling of protein-peptide interactions using the CABS-dock web server for binding site search and flexible docking,” *Methods*, vol. 93, 2016, doi: 10.1016/j.ymeth.2015.07.004.
- [123] G. C. P. van Zundert and A. M. J. J. Bonvin, “Modeling protein–protein complexes using the HADDOCK webserver ‘modeling protein complexes with HADDOCK,’” *Methods in Molecular Biology*, vol. 1137, 2014, doi: 10.1007/978-1-4939-0366-5_12.
- [124] C. Christoffer and D. Kihara, “Domain-Based Protein Docking with Extremely Large Conformational Changes,” *J Mol Biol*, vol. 434, no. 21, 2022, doi: 10.1016/j.jmb.2022.167820.
- [125] S. Ilaghi-Hoseini and Z. Garkani-Nejad, “Research and study of 2-((4,6 dimethyl pyrimidine-2-yl) thio)-N-phenyl acetamide derivatives as inhibitors of sirtuin 2 protein for the treatment of cancer using QSAR, molecular docking and molecular dynamic simulation,” *J Mol Model*, vol. 28, no. 11, pp. 1–20, Nov. 2022, doi: 10.1007/S00894-022-05288-4/FIGURES/6.
- [126] D. Szklarczyk *et al.*, “STRING v11: protein-protein association networks with increased coverage, supporting functional discovery in genome-wide experimental datasets,” *Nucleic Acids Res*, vol. 47, no. D1, pp. D607–D613, Jan. 2019, doi: 10.1093/NAR/GKY1131.
- [127] A. Ben Chorin *et al.*, “ConSurf-DB: An accessible repository for the evolutionary conservation patterns of the majority of PDB proteins,” *Protein Sci*, vol. 29, no. 1, pp. 258–267, Jan. 2020, doi: 10.1002/PRO.3779.
- [128] W. Zheng, C. Zhang, Y. Li, R. Pearce, E. W. Bell, and Y. Zhang, “Folding non-homologous proteins by coupling deep-learning contact maps with I-TASSER assembly simulations,” *Cell reports methods*, vol. 1, no. 3, Jul. 2021, doi: 10.1016/J.CRMETH.2021.100014.
- [129] I. Letunic, S. Khedkar, and P. Bork, “SMART: recent updates, new developments and status in 2020,” *Nucleic Acids Res*, vol. 49, no. D1, pp. D458–D460, Jan. 2021, doi: 10.1093/NAR/GKAA937.
- [130] J. Jumper *et al.*, “Highly accurate protein structure prediction with AlphaFold,” *Nature* 2021 596:7873, vol. 596, no. 7873, pp. 583–589, Jul. 2021, doi: 10.1038/s41586-021-03819-2.
- [131] H. Ashkenazy, E. Erez, E. Martz, T. Pupko, and N. Ben-Tal, “ConSurf 2010: calculating evolutionary conservation in sequence and structure of proteins and nucleic acids,” *Nucleic Acids Res*, vol. 38, no. Web Server issue, p. W529, Jul. 2010, doi: 10.1093/NAR/GKQ399.
- [132] E. Capriotti, P. Fariselli, and R. Casadio, “I-Mutant2.0: predicting stability changes upon mutation from the protein sequence or structure,” *Nucleic Acids Res*, vol. 33, no. Web Server issue, p. W306, Jul. 2005, doi: 10.1093/NAR/GKI375.
- [133] J. Cheng, A. Randall, and P. Baldi, “Prediction of protein stability changes for single-site mutations using support vector machines,” *Proteins*, vol. 62, no. 4, pp. 1125–1132, Mar. 2006, doi: 10.1002/PROT.20810.

- [134] M. Kurcinski, M. Jamroz, M. Blaszczyk, A. Kolinski, and S. Kmiecik, “CABS-dock web server for the flexible docking of peptides to proteins without prior knowledge of the binding site,” *Nucleic Acids Res*, vol. 43, no. W1, pp. W419–W424, Jul. 2015, doi: 10.1093/NAR/GKV456.
- [135] R. V. Honorato *et al.*, “Structural Biology in the Clouds: The WeNMR-EOSC Ecosystem,” *Front Mol Biosci*, vol. 8, p. 729513, Jul. 2021, doi: 10.3389/FMOLB.2021.729513/BIBTEX.
- [136] M. J. Mizianty *et al.*, “In-silico prediction of disorder content using hybrid sequence representation,” *BMC Bioinformatics*, vol. 12, Jun. 2011, doi: 10.1186/1471-2105-12-245.
- [137] A. Drozdetskiy, C. Cole, J. Procter, and G. J. Barton, “JPred4: A protein secondary structure prediction server,” *Nucleic Acids Res*, vol. 43, no. W1, pp. W389–W394, 2015, doi: 10.1093/NAR/GKV332.
- [138] S. Montgomerie, J. A. Cruz, S. Shrivastava, D. Arndt, M. Berjanskii, and D. S. Wishart, “PROTEUS2: a web server for comprehensive protein structure prediction and structure-based annotation,” *Nucleic Acids Res*, vol. 36, no. suppl_2, pp. W202–W209, Jul. 2008, doi: 10.1093/NAR/GKN255.
- [139] I. Letunic, S. Khedkar, and P. Bork, “SMART: recent updates, new developments and status in 2020,” *Nucleic Acids Res*, vol. 49, no. D1, pp. D458–D460, Jan. 2021, doi: 10.1093/NAR/GKAA937.
- [140] T. Paysan-Lafosse *et al.*, “InterPro in 2022,” *Nucleic Acids Res*, vol. 51, no. D1, pp. D418–D427, Jan. 2023, doi: 10.1093/NAR/GKAC993.
- [141] W. Tian, C. Chen, X. Lei, J. Zhao, and J. Liang, “CASTp 3.0: computed atlas of surface topography of proteins,” *Nucleic Acids Res*, vol. 46, no. W1, pp. W363–W367, Jul. 2018, doi: 10.1093/NAR/GKY473.
- [142] D. F. Thieker, J. B. Maguire, S. T. Kudlacek, A. Leaver-Fay, S. Lyskov, and B. Kuhlman, “Stabilizing proteins, simplified: A Rosetta-based webtool for predicting favorable mutations,” *Protein Sci*, vol. 31, no. 10, Oct. 2022, doi: 10.1002/PRO.4428.
- [143] O. Buß, J. Rudat, and K. Ochsenreither, “FoldX as Protein Engineering Tool: Better Than Random Based Approaches?,” *Comput Struct Biotechnol J*, vol. 16, pp. 25–33, Jan. 2018, doi: 10.1016/J.CSBJ.2018.01.002.
- [144] C. W. Chen, M. H. Lin, C. C. Liao, H. P. Chang, and Y. W. Chu, “iStable 2.0: Predicting protein thermal stability changes by integrating various characteristic modules,” *Comput Struct Biotechnol J*, vol. 18, pp. 622–630, Jan. 2020, doi: 10.1016/J.CSBJ.2020.02.021.
- [145] V. Parthiban, M. M. Gromiha, and D. Schomburg, “CUPSAT: prediction of protein stability upon point mutations,” *Nucleic Acids Res*, vol. 34, no. Web Server issue, Jul. 2006, doi: 10.1093/NAR/GKL190.
- [146] D. E. V. Pires, D. B. Ascher, and T. L. Blundell, “mCSM: predicting the effects of mutations in proteins using graph-based signatures,” *Bioinformatics*, vol. 30, no. 3, p. 335, Feb. 2014, doi: 10.1093/BIOINFORMATICS/BTT691.
- [147] G. Weng *et al.*, “PROTAC-DB 2.0: an updated database of PROTACs,” *Nucleic Acids Res*, vol. 51, no. D1, 2023, doi: 10.1093/nar/gkac946.

- [148] A. Daina, O. Michielin, and V. Zoete, “SwissADME: A free web tool to evaluate pharmacokinetics, drug-likeness and medicinal chemistry friendliness of small molecules,” *Sci Rep*, 2017, doi: 10.1038/srep42717.
- [149] J. Eberhardt, D. Santos-Martins, A. F. Tillack, and S. Forli, “AutoDock Vina 1.2.0: New Docking Methods, Expanded Force Field, and Python Bindings,” *J Chem Inf Model*, vol. 61, no. 8, 2021, doi: 10.1021/acs.jcim.1c00203.
- [150] G. Scardoni, G. Tosadori, M. Faizan, F. Spoto, F. Fabbri, and C. Laudanna, “Biological network analysis with CentiScaPe: centralities and experimental dataset integration,” *F1000Res*, vol. 3, Jul. 2014, doi: 10.12688/F1000RESEARCH.4477.2.
- [151] C. H. Chin, S. H. Chen, H. H. Wu, C. W. Ho, M. T. Ko, and C. Y. Lin, “cytoHubba: Identifying hub objects and sub-networks from complex interactome,” *BMC Syst Biol*, vol. 8, no. 4, pp. 1–7, Dec. 2014, doi: 10.1186/1752-0509-8-S4-S11/TABLES/4.
- [152] K. L. Lorick, J. P. Jensen, S. Fang, A. M. Ong, S. Hatakeyama, and A. M. Weissman, “RING fingers mediate ubiquitin-conjugating enzyme (E2)-dependent ubiquitination,” *Proc Natl Acad Sci U S A*, vol. 96, no. 20, p. 11364, Sep. 1999, doi: 10.1073/PNAS.96.20.11364.
- [153] M. Ying *et al.*, “Comprehensively Surveying Structure and Function of RING Domains from *Drosophila melanogaster*,” *PLoS One*, vol. 6, no. 9, p. e23863, Sep. 2011, doi: 10.1371/JOURNAL.PONE.0023863.
- [154] H. Ashkenazy *et al.*, “ConSurf 2016: an improved methodology to estimate and visualize evolutionary conservation in macromolecules,” *Nucleic Acids Res*, vol. 44, no. Web Server issue, p. W344, Jul. 2016, doi: 10.1093/NAR/GKW408.
- [155] V. Le Guilloux, P. Schmidtke, and P. Tuffery, “Fpocket: An open source platform for ligand pocket detection,” *BMC Bioinformatics*, vol. 10, no. 1, pp. 1–11, May 2009, doi: 10.1186/1471-2105-10-168/TABLES/1.
- [156] K. S. Hsu and H. Y. Kao, “PML: Regulation and multifaceted function beyond tumor suppression,” *Cell & Bioscience 2018 8:1*, vol. 8, no. 1, pp. 1–21, Jan. 2018, doi: 10.1186/S13578-018-0204-8.
- [157] S. Tessier *et al.*, “Exploration of nuclear body-enhanced sumoylation reveals that PML represses 2-cell features of embryonic stem cells,” *Nature Communications 2022 13:1*, vol. 13, no. 1, pp. 1–15, Sep. 2022, doi: 10.1038/s41467-022-33147-6.
- [158] L. Ivanschitz, H. De Thé, and M. Le Bras, “PML, SUMOylation, and Senescence,” *Front Oncol*, vol. 3, 2013, doi: 10.3389/FONC.2013.00171.
- [159] A. Rabellino and P. P. Scaglioni, “PML degradation: Multiple ways to eliminate PML,” *Front Oncol*, vol. 3 MAR, p. 60, Mar. 2013, doi: 10.3389/FONC.2013.00060/BIBTEX.
- [160] S. L. Clark, A. M. Rodriguez, R. R. Snyder, G. D. V. Hankins, and D. Boehning, “Structure-Function of the Tumor Suppressor BRCA1,” *Comput Struct Biotechnol J*, vol. 1, no. 1, p. e201204005, 2012, doi: 10.5936/CSBJ.201204005.
- [161] P. Chatterjee, R. Karn, · I Arnold Emerson, and · Satarupa Banerjee, “Docking and Molecular Dynamics Simulation Revealed the Potential Inhibitory Activity of Amygdalin in Triple-Negative Breast Cancer Therapeutics Targeting the BRCT Domain of BARD1 Receptor,” *Molecular Biotechnology 2023*, pp. 1–19, Feb. 2023, doi: 10.1007/S12033-023-00680-8.

- [162] C. Gouveia, J. Peña-Guerrero, C. Fernández-Rubio, A. T. García-Sosa, and P. A. Nguewa, “BRCT Domains: Structure, Functions, and Implications in Disease—New Therapeutic Targets for Innovative Drug Discovery against Infections,” *Pharmaceutics* 2023, Vol. 15, Page 1839, vol. 15, no. 7, p. 1839, Jun. 2023, doi: 10.3390/PHARMACEUTICS15071839.
- [163] S. R. Witus, M. D. Stewart, and R. E. Klevit, “The BRCA1/BARD1 ubiquitin ligase and its substrates,” *Biochem J*, vol. 478, no. 18, p. 3467, Sep. 2021, doi: 10.1042/BCJ20200864.
- [164] V. Pejaver *et al.*, “Inferring the molecular and phenotypic impact of amino acid variants with MutPred2,” *Nature Communications* 2020 11:1, vol. 11, no. 1, pp. 1–13, Nov. 2020, doi: 10.1038/s41467-020-19669-x.
- [165] W. Wu, A. Koike, T. Takeshita, and T. Ohta, “The ubiquitin E3 ligase activity of BRCA1 and its biological functions,” *Cell Div*, vol. 3, no. 1, pp. 1–10, Jan. 2008, doi: 10.1186/1747-1028-3-1/FIGURES/2.
- [166] D. E. Christensen, P. S. Brzovic, and R. E. Klevit, “E2–BRCA1 RING interactions dictate synthesis of mono- or specific polyubiquitin chain linkages,” *Nature Structural & Molecular Biology* 2007 14:10, vol. 14, no. 10, pp. 941–948, Sep. 2007, doi: 10.1038/nsmb1295.
- [167] “New partners for BRCA1,” *Nature Structural & Molecular Biology* 2007 14:10, vol. 14, no. 10, pp. 879–879, Oct. 2007, doi: 10.1038/nsmb1007-879.
- [168] N. Merkley and G. S. Shaw, “Solution structure of the flexible class II ubiquitin-conjugating enzyme Ubc1 provides insights for polyubiquitin chain assembly,” *J Biol Chem*, vol. 279, no. 45, pp. 47139–47147, Nov. 2004, doi: 10.1074/JBC.M409576200.
- [169] A. J. Middleton, J. Teyra, J. Zhu, S. S. Sidhu, and C. L. Day, “Identification of Ubiquitin Variants That Inhibit the E2 Ubiquitin Conjugating Enzyme, Ube2k,” *ACS Chem Biol*, vol. 16, no. 9, pp. 1745–1756, Sep. 2021, doi: 10.1021/ACSCHEMBIO.1C00445/ASSET/IMAGES/LARGE/CB1C00445_0006.JPG.
- [170] M. A. Kalchman *et al.*, “Huntingtin is ubiquitinated and interacts with a specific ubiquitin-conjugating enzyme,” *J Biol Chem*, vol. 271, no. 32, pp. 19385–19394, 1996, doi: 10.1074/JBC.271.32.19385.
- [171] R. de Pril, D. F. Fischer, R. A. C. Roos, and F. W. van Leeuwen, “Ubiquitin-conjugating enzyme E2-25K increases aggregate formation and cell death in polyglutamine diseases,” *Mol Cell Neurosci*, vol. 34, no. 1, pp. 10–19, Jan. 2007, doi: 10.1016/J.MCN.2006.09.006.
- [172] H. Meiklejohn *et al.*, “Blood and brain protein levels of ubiquitin-conjugating enzyme E2K (UBE2K) are elevated in individuals with schizophrenia,” *J Psychiatr Res*, vol. 113, pp. 51–57, Jun. 2019, doi: 10.1016/J.JPSYCHIRES.2019.03.005.
- [173] S. Song *et al.*, “Essential role of E2-25K/Hip-2 in mediating amyloid-beta neurotoxicity,” *Mol Cell*, vol. 12, no. 3, pp. 553–563, Sep. 2003, doi: 10.1016/J.MOLCEL.2003.08.005.
- [174] J. Su *et al.*, “Reduction of HIP2 expression causes motor function impairment and increased vulnerability to dopaminergic degeneration in Parkinson’s disease models,” *Cell Death Dis*, vol. 9, no. 10, Oct. 2018, doi: 10.1038/S41419-018-1066-Z.

- [175] Q. Hu, M. V. Botuyan, D. Zhao, G. Cui, E. Mer, and G. Mer, “Mechanisms of BRCA1–BARD1 nucleosome recognition and ubiquitylation,” *Nature*, vol. 596, no. 7872, 2021, doi: 10.1038/s41586-021-03716-8.
- [176] F. Wu-Baer, K. Lagazon, W. Yuan, and R. Baer, “The BRCA1/BARD1 heterodimer assembles polyubiquitin chains through an unconventional linkage involving lysine residue K6 of ubiquitin,” *Journal of Biological Chemistry*, vol. 278, no. 37, 2003, doi: 10.1074/jbc.C300249200.
- [177] J. Kelliher, G. Ghosal, and J. W. C. Leung, “New answers to the old RIDDLE: RNF168 and the DNA damage response pathway,” *FEBS J*, vol. 289, no. 9, pp. 2467–2480, May 2022, doi: 10.1111/FEBS.15857.
- [178] R. Gupta, M. Sahu, D. Srivastava, S. Tiwari, R. K. Ambasta, and P. Kumar, “Post-translational modifications: Regulators of neurodegenerative proteinopathies,” Jul. 01, 2021, *Elsevier Ireland Ltd*. doi: 10.1016/j.arr.2021.101336.
- [179] W. Liu *et al.*, “The Ubiquitin Conjugating Enzyme: An Important Ubiquitin Transfer Platform in Ubiquitin-Proteasome System,” *Int J Mol Sci*, vol. 21, no. 8, Apr. 2020, doi: 10.3390/IJMS21082894.
- [180] P. Radivojac *et al.*, “Identification, analysis, and prediction of protein ubiquitination sites,” *Proteins: Structure, Function, and Bioinformatics*, vol. 78, no. 2, pp. 365–380, Feb. 2010, doi: 10.1002/PROT.22555.
- [181] R. H. Chen, Y. R. Lee, and W. C. Yuan, “The role of PML ubiquitination in human malignancies,” *J Biomed Sci*, vol. 19, no. 1, p. 81, Aug. 2012, doi: 10.1186/1423-0127-19-81/FIGURES/1.
- [182] K. Miyahara *et al.*, “BRCA1 degradation in response to mitochondrial damage in breast cancer cells,” *Scientific Reports 2021 11:1*, vol. 11, no. 1, pp. 1–13, Apr. 2021, doi: 10.1038/s41598-021-87698-7.
- [183] M. Kurihara, T. Mano, Y. Saito, S. Murayama, T. Toda, and A. Iwata, “Colocalization of BRCA1 with Tau Aggregates in Human Tauopathies,” *Brain Sci*, vol. 10, no. 1, Jan. 2020, doi: 10.3390/BRAINSCI10010007.
- [184] K. A. Clark *et al.*, “Comprehensive evaluation and efficient classification of BRCA1 RING domain missense substitutions,” *Am J Hum Genet*, vol. 109, no. 6, p. 1153, Jun. 2022, doi: 10.1016/J.AJHG.2022.05.004.
- [185] P. S. Brzovic, J. E. Meza, M. C. King, and R. E. Klevit, “BRCA1 RING domain cancer-predisposing mutations. Structural consequences and effects on protein-protein interactions,” *J Biol Chem*, vol. 276, no. 44, pp. 41399–41406, Nov. 2001, doi: 10.1074/JBC.M106551200.
- [186] M. Wezyk and C. Zekanowski, “Role of BRCA1 in Neuronal Death in Alzheimer’s Disease,” 2018, doi: 10.1021/acschemneuro.8b00149.
- [187] E. Leung and L. N. Hazrati, “Breast cancer type 1 and neurodegeneration: consequences of deficient DNA repair,” *Brain Commun*, vol. 3, no. 2, 2021, doi: 10.1093/BRAINCOMMS/FCAB117.
- [188] E. Suberbielle *et al.*, “DNA repair factor BRCA1 depletion occurs in Alzheimer brains and impairs cognitive function in mice,” *Nat Commun*, vol. 6, 2015, doi: 10.1038/ncomms9897.

- [189] L. Cao, W. Li, S. Kim, S. G. Brodie, and C. X. Deng, “Senescence, aging, and malignant transformation mediated by p53 in mice lacking the *brca1* full-length isoform,” *Genes Dev*, vol. 17, no. 2, 2003, doi: 10.1101/gad.1050003.
- [190] E. Suberbielle *et al.*, “Physiologic brain activity causes DNA double-strand breaks in neurons, with exacerbation by amyloid- β ,” *Nat Neurosci*, vol. 16, no. 5, 2013, doi: 10.1038/nn.3356.
- [191] M. Nakamura, S. Kaneko, D. W. Dickson, and H. Kusaka, “Aberrant accumulation of BRCA1 in Alzheimer disease and other tauopathies,” *J Neuropathol Exp Neurol*, vol. 79, no. 1, 2020, doi: 10.1093/jnen/nlz107.
- [192] H. N. Noristani *et al.*, “*Brca1* is expressed in human microglia and is dysregulated in human and animal model of ALS,” *Mol Neurodegener*, vol. 10, no. 1, 2015, doi: 10.1186/s13024-015-0023-x.
- [193] K. Kiewhuo, L. Priyadarsinee, H. Sarma, and G. N. Sastry, “Molecular dynamics simulations reveal the effect of mutations in the RING domains of BRCA1-BARD1 complex and its relevance to the prognosis of breast cancer,” *J Biomol Struct Dyn*, vol. 41, no. 22, pp. 12734–12752, 2023, doi: 10.1080/07391102.2023.2175383.
- [194] H. Sarma, K. Kiewhuo, E. Jamir, and G. N. Sastry, “In silico investigation on the mutational analysis of BRCA1-BARD1 RING domains and its effect on nucleosome recognition and ubiquitination,” *Biophys Chem*, vol. 300, Sep. 2023, doi: 10.1016/J.BPC.2023.107070.
- [195] D. Thirumal Kumar *et al.*, “Computational structural assessment of BREast CAncer type 1 susceptibility protein (BRCA1) and BRCA1-Associated Ring Domain protein 1 (BARD1) mutations on the protein-protein interface,” *Adv Protein Chem Struct Biol*, vol. 130, pp. 375–397, Jan. 2022, doi: 10.1016/BS.APCSB.2022.02.003.
- [196] M. Sahu, N. Rani, and P. Kumar, “Simulation and Computational Study of RING Domain Mutants of BRCA1 and Ube2k in AD/PD Pathophysiology,” *Mol Biotechnol*, pp. 1–21, Jan. 2024, doi: 10.1007/S12033-023-01006-4/METRICS.
- [197] M. Wezyk and C. Zekanowski, “Role of BRCA1 in Neuronal Death in Alzheimer’s Disease,” *ACS Chem Neurosci*, vol. 9, no. 5, pp. 870–872, May 2018, doi: 10.1021/ACSCHENNEURO.8B00149/ASSET/IMAGES/LARGE/CN-2018-00149N_0001.JPEG.

LIST OF PUBLICATIONS

Cumulative Impact Factor

Cumulative impact factor of all publications = 86.1

h-index and i-10 index = 7 and 5

Cumulative citation index = 1084

PUBLICATIONS FROM THESIS

1. **Sahu, M.**, Rani, N., & Kumar, P. (2024). Simulation and Computational Study of RING Domain Mutants of BRCA1 and Ube2k in AD/PD Pathophysiology. *Molecular Biotechnology*, 1–21. <https://doi.org/10.1007/S12033-023-01006-4/METRICS> [SCIE, IF: 2.4]
2. **Sahu, M.**, Gupta, R., Ambasta, R. K., & Kumar, P. (2024). IoT-driven augmented reality and virtual reality systems in neurological sciences. *Internet of Things*, 25, 101098. <https://doi.org/10.1016/J.IOT.2024.101098> [SCIE, IF: 6.0]
3. **Sahu, M.**, Ambasta, R. K., Das R. S, Mishra K. M., Shanker A., & Kumar, P. (2024). Harnessing Brainwave Entrainment: A Non-Invasive Strategy to Alleviate Neurological Disorder Symptoms. *Ageing Research Reviews*, 102547. <https://doi.org/10.1016/j.arr.2024.102547> [SCIE, IF: 12.5]
4. **Sahu, M.**, Tripathi, R., Jha, N. K., Jha, S. K., Ambasta, R. K., & Kumar, P. (2022). Cross talk mechanism of disturbed sleep patterns in neurological and psychological disorders. *Neuroscience & Biobehavioral Reviews*, 140, 104767. <https://doi.org/10.1016/J.NEUBIOREV.2022.104767> [SCIE, IF: 7.5]
5. **Sahu, M.**, Vashishth, S., Kukreti, N., Gulia, A., Russell, A., Ambasta, R. K., & Kumar, P. (2024). Synergizing drug repurposing and target identification for neurodegenerative diseases. *Progress in Molecular Biology and Translational Science*, 205, 111–169. <https://doi.org/10.1016/BS.PMBTS.2024.03.023> [IF: 3.6]
6. **Sahu, M.**, Gupta, R., Ambasta, R. K., & Kumar, P. (2022). Artificial intelligence and machine learning in precision medicine: A paradigm shift in big data analysis. *Progress in Molecular Biology and Translational Science*. <https://doi.org/10.1016/BS.PMBTS.2022.03.002> [IF: 3.6]
7. **Sahu, M.**, & Kumar, P. (2023a). E3 ligase activity of RNF168 at stake on ring domain mutation. *Journal of the Neurological Sciences*, 455, 121447. <https://doi.org/10.1016/j.jns.2023.121447> [SCIE, IF: 3.6]
8. **Sahu, M.**, & Kumar, P. (2023b). RING Domain Mutation Hinders the E3 Ligase Activity of RNF8 and Affects UBE2N Binding. 2023 International Conference on Network, Multimedia and Information Technology, NMITCON 2023. <https://doi.org/10.1109/NMITCON58196.2023.10276155>

OTHER PUBLICATIONS

1. Rani, N., **Sahu, M.**, Ambasta, R. K., & Kumar, P. (2024). Triaging between post-translational modification of cell cycle regulators and their therapeutics in neurodegenerative diseases. *Ageing Research Reviews*, 94, 102174. <https://doi.org/10.1016/J.ARR.2023.102174> [SCIE, IF: 12.5]
2. Gupta, R., **Sahu, M.**, Srivastava, D., Tiwari, S., Ambasta, R. K., & Kumar, P. (2021). Post-translational modifications: Regulators of neurodegenerative proteinopathies. In *Ageing Research Reviews* (Vol. 68). Elsevier Ireland Ltd. <https://doi.org/10.1016/j.arr.2021.101336> [SCIE, IF: 12.5]
3. Gupta, R., **Sahu, M.**, Tripathi, R., Ambasta, R. K., & Kumar, P. (2022). Protein S-sulphydration: Unraveling the prospective of hydrogen sulfide in the brain, vasculature and neurological manifestations. *Ageing Research Reviews*, 76, 101579. <https://doi.org/10.1016/J.ARR.2022.101579> [SCIE, IF: 12.5]
4. Gupta, R., Srivastava, D., **Sahu, M.**, Tiwari, S., Ambasta, R. K., & Kumar, P. (2021). Artificial intelligence to deep learning: machine intelligence approach for drug discovery. *Molecular Diversity*. <https://doi.org/10.1007/s11030-021-10217-3> [SCIE, IF: 3.9]
5. Tripathi, R., Gupta, R., **Sahu, M.**, Srivastava, D., Das, A., Ambasta, R. K., & Kumar, P. (2021). Free radical biology in neurological manifestations: mechanisms to therapeutics interventions. *Environmental Science and Pollution Research* 2021, 1–48. <https://doi.org/10.1007/S11356-021-16693-2> [SCIE]

CONFERENCES

Sahu, M., Kumar, P., 2023. RING Domain Mutation Hinders the E3 Ligase Activity of RNF8 and Affects UBE2N Binding. 2023 International Conference on Network, Multimedia and Information Technology, NMITCON 2023. <https://doi.org/10.1109/NMITCON58196.2023.10276155> [Oral presentation, IEEE conference]

Sahu, M., Kumar, P., 2023. E3 ligase activity of RNF168 at stake on ring domain mutation. *J Neurol Sci* 455, 121447. <https://doi.org/10.1016/j.jns.2023.121447> [Oral presentation, WCN conference]

Sahu, M., Kumar, P., 2024. Interplay Between AMR Susceptibility Testing Using and Deep Learning: Implication for Drug Development. Third International Conference on Antimicrobial Resistance, Novel Drug Discovery and Vaccine Development: Challenges and Opportunities. SRM University [Oral & Poster presentation, Young Scientist Award]

MEHAR SAHUmeharsahu@gmail.comRohini, Sector-16 • New Delhi, India 110089, +91-9810330403

CURRENT STATUS**DELHI TECHNOLOGICAL UNIVERSITY**

New Delhi, India

Ph.D. Scholar, Neurobiology

2021-Present

- Ubiquitination biology in neurodegenerative diseases
- Research Excellence Award 2023

EDUCATION**DELHI TECHNOLOGICAL UNIVERSITY**

New Delhi, India

Masters of Technology (M.Tech.), Biomedical Engineering

2019-2021

- Vice Chancellor's Gold Medallist
- 2nd University Rank Holder
- Research Excellence Award 2022

AMITY UNIVERSITY

Noida, India

Bachelor of Technology (B.Tech.), Biotechnology

2015-2019

PRAYAG SANGEET SAMITI

New Delhi, India

Bachelor of Arts (B.A.), Kathak

2004-Present

- Junior Diploma Completed
- Senior Diploma Completed
- Kathak Level 6 - Sangit Prabhakar (First Division)

RESEARCH EXPERIENCE**UNIVERSITY COLLEGE OF MEDICAL SCIENCES & GURU TEG BAHADUR HOSPITAL, MULTI-DISCIPLINARY RESEARCH UNIT, DELHI UNIVERSITY**New Delhi, India
September 2023**Trainee**

Cell Culture Techniques

- Hands-on training on isolation and cell viability assessment of PBMCs
- Experience in neuronal cell line revival, passaging, and cryopreservation

JAMIA HAMDARD

New Delhi, India

Trainee

December 2022

Understanding Neurological Disorders: Technical Approaches and Advancements

- Hands-on training on animal model surgery (Brain Haemorrhage, Ischemia, Alzheimer's Disease, and Traumatic Brain Injury)
- Exposure to neurobehavioral studies
- Experienced Western blotting, RT-PCR, Fluorimetry and Perfusion

JAMIA HAMDARD

New Delhi, India

Trainee

March 2022

Synergistic training program utilizing the scientific and technological infrastructure

- Hands-on training on *Drosophila melanogaster*, *Caenorhabditis elegans*, Chick embryo, and Cell culture
- Exposure to TEM and NMR facility

DELHI TECHNOLOGICAL UNIVERSITY

Project Intern

New Delhi, India
Jan-Jul 2021

Computational analysis of post-translational modifications in the pathogenesis of Alzheimer's Disease (M.Tech Dissertation)

- Studied the involvement of acetylation and ubiquitination in DEGs that contribute to the pathogenesis of AD
- Assessed the impact of lysine mutation on acetylation and ubiquitination of YWHAZ
- Identified the impact of a drug molecule on YWHAZ

INMAS, Defence Research and Development Organization

Intern

New Delhi, India
Jan-Apr 2019

Effect of EDTA on pathogenicity of *E. coli*-an in vitro study (B.Tech Dissertation)

- Evaluated the anti-microbial effect of EDTA on *E. coli*
- Identified minimum inhibitory concentration
- Analysed adjuvant activity of EDTA in combination with standard antibiotics
- Observed the effect of EDTA on microbial cellular membrane

INMAS, Defence Research and Development Organization

Summer Intern

New Delhi, India
May-Jul 2018

Effect of sub-lethal dose of ionizing radiation on hematopoietic system of Swiss-albino mice

- Performed mice and rat dissection
- Observed after-effects of 2 Gy ionizing radiation on mice
- Analysed TLC and DLC of irradiated mice by Hemocytometer chamber or Neubauer's slide

AMITY UNIVERSITY

Trainee

Noida, India
May-Jul 2017

Detection of Plant Pigments using Chromatography

- Separated and identified different plant pigments in spinach, coriander, and mint

AMITY UNIVERSITY

Summer Intern

Noida, India
May-Jul 2016

Alzheimer's Disease Pathophysiology

- Studied different stages and hallmark features of AD
- Studied disease progression and different treatment options available

SKILLS & TECHNIQUES

- Isolation of DNA, RNA, and protein
- Agarose gel electrophoresis and SDS PAGE

- Fluorescence microscopy
- Immunoprecipitation of complexes for identification by Mass Spectrometry
- Chromatin immunoprecipitation and analysis on microarrays by quantitative PCR
- Microbiology – Gram staining, growth kinetics, antibiotic susceptibility test, time-kill assay, cell viability assay, and protein quantification
- Mice and rat handling and dissection
- Tissue processing, embedding, and sectioning for histology
- Computational Skills – MD Simulation, molecular docking, visualization, and python

LEADERSHIP EXPERIENCE

DELHI TECHNOLOGICAL UNIVERSITY

Teaching Assistant (Sole Subject) – Analytical Techniques Laboratory (MSBT107)

- Assisted in preparation and execution of laboratory section, namely, validation of Henderson-Hasselbalch equation, Beer-Lambert law, ELISA, and PCR

Teaching Assistant – Functional Genomics and Proteomics (BIO505)

- Assisted in preparation and execution of laboratory section, namely, protein and DNA extraction, immunoprecipitation, SDS PAGE, Blotting techniques, and signal quantification

Teaching Assistant – Genetic Engineering Laboratory (MSBT106)

- Assisted in preparation and execution of laboratory section, namely competent and transformed cell preparation, DNA and RNA isolation, DNA gel electrophoresis, RNA gel electrophoresis, and polymerase chain reaction (PCR)

Teaching Assistant – Advanced Proteomics Laboratory (BIO503)

- Assisted in preparation and execution of laboratory section, namely Protein preparation and estimation, SDS PAGE, Western Blotting, Staining and Destaining, Chip-on-Chip, and usage of Bioinformatics tools

Class Representative

- CR for 2 consecutive years (2019-2021)

Mentored and guided numerous national and international students during their lab internships, providing hands-on training and support in various research projects.

HANSRAJ MODEL SCHOOL

Student Council Member - Music Head

- Played Santoor, Violin, and Harmonica in International Youth Meet, Delhi
- Assisted 6 grand orchestras

PUBLICATIONS

Sahu, M., Ambasta, R. K., Das R. S, Mishra K. M., Shanker A., & Kumar, P. (2024). Harnessing Brainwave Entrainment: A Non-Invasive Strategy to Alleviate Neurological Disorder Symptoms. Ageing Research Reviews, 102547. <https://doi.org/10.1016/j.arr.2024.102547>

Sahu, M., Rani, N., & Kumar, P. (2024). Simulation and Computational Study of RING Domain Mutants of BRCA1 and Ube2k in AD/PD Pathophysiology. Molecular Biotechnology, 1–21. <https://doi.org/10.1007/S12033-023-01006-4/METRICS>

Sahu, M., Gupta, R., Ambasta, R. K., & Kumar, P. (2024). IoT-driven augmented reality and virtual reality systems in neurological sciences. Internet of Things, 25, 101098. <https://doi.org/10.1016/J.IOT.2024.101098>

Sahu, M., Tripathi, R., Jha, N. K., Jha, S. K., Ambasta, R. K., & Kumar, P. (2022). Cross talk mechanism of disturbed sleep patterns in neurological and psychological disorders. *Neuroscience & Biobehavioral Reviews*, 140, 104767. <https://doi.org/10.1016/J.NEUBIOREV.2022.104767>

Sahu, M., Vashishth, S., Kukreti, N., Gulia, A., Russell, A., Ambasta, R. K., & Kumar, P. (2024). Synergizing drug repurposing and target identification for neurodegenerative diseases. *Progress in Molecular Biology and Translational Science*, 205, 111–169. <https://doi.org/10.1016/BS.PMBTS.2024.03.023>

Sahu, M., Gupta, R., Ambasta, R. K., & Kumar, P. (2022). Artificial intelligence and machine learning in precision medicine: A paradigm shift in big data analysis. *Progress in Molecular Biology and Translational Science*. <https://doi.org/10.1016/BS.PMBTS.2022.03.002>

Sahu, M., & Kumar, P. (2023a). E3 ligase activity of RNF168 at stake on ring domain mutation. *Journal of the Neurological Sciences*, 455, 121447. <https://doi.org/10.1016/j.jns.2023.121447>

Sahu, M., & Kumar, P. (2023b). RING Domain Mutation Hinders the E3 Ligase Activity of RNF8 and Affects UBE2N Binding. 2023 International Conference on Network, Multimedia and Information Technology, NMITCON 2023. <https://doi.org/10.1109/NMITCON58196.2023.10276155>

Rani, N., **Sahu, M.**, Ambasta, R. K., & Kumar, P. (2024). Triaging between post-translational modification of cell cycle regulators and their therapeutics in neurodegenerative diseases. *Ageing Research Reviews*, 94, 102174. <https://doi.org/10.1016/J.ARR.2023.102174>

Gupta, R., **Sahu, M.**, Srivastava, D., Tiwari, S., Ambasta, R. K., & Kumar, P. (2021). Post-translational modifications: Regulators of neurodegenerative proteinopathies. In *Ageing Research Reviews* (Vol. 68). Elsevier Ireland Ltd. <https://doi.org/10.1016/j.arr.2021.101336>

Gupta, R., **Sahu, M.**, Tripathi, R., Ambasta, R. K., & Kumar, P. (2022). Protein S-sulfhydration: Unraveling the prospective of hydrogen sulfide in the brain, vasculature and neurological manifestations. *Ageing Research Reviews*, 76, 101579. <https://doi.org/10.1016/J.ARR.2022.101579>

Gupta, R., Srivastava, D., **Sahu, M.**, Tiwari, S., Ambasta, R. K., & Kumar, P. (2021). Artificial intelligence to deep learning: machine intelligence approach for drug discovery. *Molecular Diversity*. <https://doi.org/10.1007/s11030-021-10217-3>

Tripathi, R., Gupta, R., **Sahu, M.**, Srivastava, D., Das, A., Ambasta, R. K., & Kumar, P. (2021). Free radical biology in neurological manifestations: mechanisms to therapeutics interventions. *Environmental Science and Pollution Research* 2021, 1–48. <https://doi.org/10.1007/S11356-021-16693-2>

CONFERENCES

Accepted Paper

Sahu, M., Kumar, P., 2023. RING Domain Mutation Hinders the E3 Ligase Activity of RNF8 and Affects UBE2N Binding. 2023 International Conference on Network, Multimedia and Information Technology, NMITCON 2023. <https://doi.org/10.1109/NMITCON58196.2023.10276155>. **[Oral Presentation]**

Accepted Abstract

Sahu, M., Kumar, P., 2023b. E3 ligase activity of RNF168 at stake on ring domain mutation. J Neurol Sci 455, 121447. <https://doi.org/10.1016/j.jns.2023.121447>.
[Poster Presentation]

Accepted Abstract

Sahu, M., Kumar, P., 2024. Interplay Between AMR Susceptibility Testing Using and Deep Learning: Implication for Drug Development. 3rd International Conference on Antimicrobial Resistance, Novel Drug Discovery and Vaccine Development: Challenges and Opportunities. SRM University. [Oral & Poster presentation, Young Scientist Award]

REFERENCES**1. Prof. Pravir Kumar, PhD**

Dean, International Affairs

Professor and former Head, Department of Biotechnology

Molecular Neuroscience and Functional Genomics Laboratory

Delhi Technological University (Formerly Delhi College of Engineering), Delhi
110042

Email: pravirkumar@dtu.ac.in; kpravir@gmail.com

2. Dr. Rashmi Ambasta

Research Assistant Professor in the Department of Medicine

Vanderbilt University Medical Center, TN 37235, United States

Associate Professor at SRM University, Delhi

Email: rashmiambasta@gmail.com

3. Dr. Vanita Gupta

Scientist D

Department of CEPIN

Institute of Nuclear Medicine & Allied Science, DRDO

Email: vanita.inmas@gov.in; vanitagupta06@gmail.com



DELHI TECHNOLOGICAL UNIVERSITY

(Formerly Delhi College of Engineering)

Shahbad Daulatpur, Main Bawana Road, Delhi-42

PLAGIARISM VERIFICATION

Title of the Thesis PROTEINOPATHIES, PROTEOTOXICITY AND TRIAGING
IN NEURODEGENERATIVE DISORDERS

Total Pages 110 Name of the Scholar MEHAR SAHU

Supervisor (s)

(1) PROF. PRAVIR KUMAR

(2) _____

(3) _____

Department BIOTECHNOLOGY

This is to report that the above thesis was scanned for similarity detection. Process and outcome is given below:

Software used: TURNITIN Similarity Index: 9%, Total Word Count: 30984

Date: 18/10/2024


Candidate's Signature


21/10/2024
Signature of Supervisor(s)

PAPER NAME

THESIS - MEHAR SAHU.docx

AUTHOR

Mehar Sahu

WORD COUNT

30984 Words

CHARACTER COUNT

175706 Characters

PAGE COUNT

110 Pages

FILE SIZE

20.3MB

SUBMISSION DATE

Oct 2, 2024 8:24 PM GMT+5:30

REPORT DATE

Oct 2, 2024 8:27 PM GMT+5:30

● 9% Overall Similarity

Mehar Sahu

Ph
21/10/2024

The combined total of all matches, including overlapping sources, for each database.

- 6% Internet database
- 6% Publications database
- Crossref database
- Crossref Posted Content database
- 4% Submitted Works database

● Excluded from Similarity Report

- Bibliographic material
- Quoted material
- Cited material
- Small Matches (Less than 10 words)
- Manually excluded sources

● 9% Overall Similarity

Janet

Top sources found in the following databases:

- 6% Internet database
- 6% Publications database
- Crossref database
- Crossref Posted Content database
- 4% Submitted Works database

TOP SOURCES

The sources with the highest number of matches within the submission. Overlapping sources will not be displayed.

1	mdpi.com Internet	<1%
2	discovery.researcher.life Internet	<1%
3	frontiersin.org Internet	<1%
4	M. Wezyk, C. Zekanowski. "Role of BRCA1 in Neuronal Death in Alzhei... Crossref	<1%
5	nature.com Internet	<1%
6	hindawi.com Internet	<1%
7	medrxiv.org Internet	<1%
8	academic.oup.com Internet	<1%

- 9 Li-Li Zheng, Li-Ting Wang, Ye-Wei Pang, Li-Ping Sun, Lei Shi. "Recent a... <1%
Crossref
- 10 Nam Soo Lee, Soomi Kim, Yong Woo Jung, Hongtae Kim. "Eukaryotic D... <1%
Crossref
- 11 **escholarship.org** <1%
Internet
- 12 **moam.info** <1%
Internet
- 13 **University of Arizona on 2014-02-11** <1%
Submitted works
- 14 **mdpi-res.com** <1%
Internet
- 15 Kathryn A Porter, Israel Desta, Dima Kozakov, Sandor Vajda. "What met... <1%
Crossref
- 16 Shuvo Chandra Das, Md. Anisur Rahman, Shipan Das Gupta. "In-silico a... <1%
Crossref
- 17 **docslib.org** <1%
Internet
- 18 **Roehampton University on 2021-05-10** <1%
Submitted works
- 19 **ia804504.us.archive.org** <1%
Internet
- 20 **tandfonline.com** <1%
Internet

21	pubmed.ncbi.nlm.nih.gov Internet	<1%
22	swissmodel.expasy.org Internet	<1%
23	digital.lib.washington.edu Internet	<1%
24	ncbi.nlm.nih.gov Internet	<1%
25	Swinburne University of Technology on 2024-05-17 Submitted works	<1%
26	coek.info Internet	<1%
27	molecularneurodegeneration.biomedcentral.com Internet	<1%
28	Rinske Drost, Peter Bouwman, Sven Rottenberg, Ute Boon et al. "BRCA... Crossref	<1%
29	VIT University on 2014-05-06 Submitted works	<1%
30	assets-eu.researchsquare.com Internet	<1%
31	iris.unict.it Internet	<1%
32	Cardiff University on 2016-09-05 Submitted works	<1%

- 33 **Tianyuan Xie, Hai Qin, Zhengdong Yuan, Yiwen Zhang, Xiaoman Li, Luf...** <1%
Crossref
- 34 **"Computational Protein Design", Springer Science and Business Media ...** <1%
Crossref
- 35 **King Saud bin Abdulaziz University for Health Sciences on 2014-03-17** <1%
Submitted works
- 36 **healthunlocked.com** <1%
Internet
- 37 **University of Liverpool on 2016-06-13** <1%
Submitted works
- 38 **cellandbioscience.biomedcentral.com** <1%
Internet
- 39 **Immd.ecust.edu.cn** <1%
Internet
- 40 **repository.up.ac.za** <1%
Internet
- 41 **University of Nottingham on 2017-11-16** <1%
Submitted works
- 42 **Mikaela D. Stewart, Emily D. Duncan, Ernesto Coronado, Paul A. DaRos...** <1%
Crossref
- 43 **journals.plos.org** <1%
Internet
- 44 **sites.utoronto.ca** <1%
Internet

- 45 **Dr Rajendra Central Agricultural University on 2020-08-18** <1%
Submitted works
- 46 **Gaoqi Weng, Xuanyan Cai, Dongsheng Cao, Hongyan Du, Chao Shen, Y...** <1%
Crossref
- 47 **Jan Brezovsky, Aaftaab Sethi, Bartłomiej Surpeta. "Computational Tool...** <1%
Crossref
- 48 **Sara de Mateo, Judit Castillo, Josep Maria Estanyol, José Luis Ballesc...** <1%
Crossref
- 49 **The Hong Kong Polytechnic University on 2005-12-15** <1%
Submitted works
- 50 **Wenwen Wu. "The ubiquitin E3 ligase activity of BRCA1 and its biologic...** <1%
Crossref
- 51 **en.wikipedia.org** <1%
Internet
- 52 **biomedcentral.com** <1%
Internet
- 53 **coursehero.com** <1%
Internet
- 54 **Anoop S. Chauhan, Satpal S. Jhujh, Grant S. Stewart. "E3 ligases: a ubi...** <1%
Crossref
- 55 **Nikol Baloghova, Tomas Lidak, Lukas Cermak. "Ubiquitin Ligases Invol...** <1%
Crossref
- 56 **Rainer Coelln. "Parkin-associated Parkinson's disease", Cell and Tissu...** <1%
Crossref

- 57 **Regional Centre for Biotechnology on 2024-07-12** <1%
Submitted works
- 58 **Rose Oughtred, Andrew Chatr-aryamontri, Bobby-Joe Breitzkreutz, Chris...** <1%
Crossref
- 59 **Steven Xijin Ge, Dongmin Jung, Runan Yao. "ShinyGO: a graphical gene...** <1%
Crossref
- 60 **oup.silverchair-cdn.com** <1%
Internet
- 61 **pubblicazioni.unicam.it** <1%
Internet
- 62 **Chengchen Tan, Xiaolong Yan, Xingchang Lu, Jianxiu Wang, Xinyao Yi. ...** <1%
Crossref
- 63 **Demos-Davies, Kimberly. "Neuropathologic Effects of Extracranial Radi...** <1%
Publication
- 64 **Emily Leung, Lili-Naz Hazrati. "Breast cancer type 1 and neurodegener...** <1%
Crossref
- 65 **Ikromi Rungsung, Amutha Ramaswamy. "Effects of Peutz-Jeghers syn...** <1%
Crossref
- 66 **Tamanna Sultana, Sadia Islam Mou, Dipankor Chatterjee, Md. Omar Fa...** <1%
Crossref
- 67 **UCSI University on 2021-05-20** <1%
Submitted works
- 68 **University of Teesside on 2024-08-14** <1%
Submitted works

81	binfo.ym.edu.tw Internet	<1%
82	drugs-dev02.ncats.io Internet	<1%
83	dspace.cuni.cz Internet	<1%
84	oatao.univ-toulouse.fr Internet	<1%
85	"PROTAC-Mediated Protein Degradation: A Paradigm Shift in Cancer T... Crossref	<1%
86	Amrita Vishwa Vidyapeetham on 2024-03-26 Submitted works	<1%
87	De Montfort University on 2024-03-14 Submitted works	<1%
88	Dhiraj Kumar, Md. Imtaiyaz Hassan. "Targeted protein degraders marc... Crossref	<1%
89	Fabio D'Amico, Saverio Candido, Massimo Libra. "Interaction between ... Crossref	<1%
90	Idaho State University - Division of Health Sciences on 2017-06-30 Submitted works	<1%
91	Jiajie Chen, Rongshuai Zhu, Junping Zhou, Taowei Yang, Xian Zhang, ... Crossref	<1%
92	Kayla Farrell, Timothy J. Jarome. "Is PROTAC technology really a game... Crossref	<1%

- 93 Khan, Faez Iqbal, Mohd. Shahbaaz, Krishna Bisetty, Abdul Waheed, Will... <1%
Crossref
- 94 Maria Russi, Domenico Marson, Alice Fermeglia, Suzana Aulic, Maurizi... <1%
Crossref
- 95 Marwa S. Hassan, A.A. Shaalan, M.I. Dessouky, Abdelaziz E. Abdelnaie... <1%
Crossref
- 96 Methods in Pharmacology and Toxicology, 2016. <1%
Crossref
- 97 Nastaran Namadyan, Bagher Seyedalipour, Saman Hosseinkhani, Paya... <1%
Crossref
- 98 Sidharth Saxena, Sai Achyuth B, T P Krishna Murthy, Vivek Chandramo... <1%
Crossref
- 99 The Hong Kong Polytechnic University on 2015-05-11 <1%
Submitted works
- 100 The University of the West of Scotland on 2024-03-25 <1%
Submitted works
- 101 Universita degli Studi di Milano on 2016-12-29 <1%
Submitted works
- 102 University of Wales, Bangor on 2021-05-15 <1%
Submitted works
- 103 Uttar Pradesh Technical University on 2022-03-05 <1%
Submitted works
- 104 Wageningen University on 2023-04-28 <1%
Submitted works

105	assets.researchsquare.com Internet	<1%
106	bidd.group Internet	<1%
107	d.docksci.com Internet	<1%
108	files-journal-api.frontiersin.org Internet	<1%
109	journal.frontiersin.org Internet	<1%
110	mobt3ath.com Internet	<1%
111	openscholar.dut.ac.za Internet	<1%
112	osti.gov Internet	<1%
113	plantphysiol.org Internet	<1%

● Excluded from Similarity Report

- Bibliographic material
- Cited material
- Manually excluded sources
- Quoted material
- Small Matches (Less than 10 words)

EXCLUDED SOURCES

Mehar Sahu, Neetu Rani, Pravir Kumar. "Simulation and Computational Study ... 25%

Crossref

Mehar Sahu, Pravir Kumar. "RING Domain Mutation Hinders the E3 Ligase Acti... 11%

Crossref

Mehar Sahu, Shrutikirti Vashishth, Neha Kukreti, Ashima Gulia, Ashish Russell... <1%

Crossref

dspace.dtu.ac.in:8080 <1%

Internet

Rohan Gupta, Mehar Sahu, Devesh Srivastava, Swati Tiwari, Rashmi K. Ambas... <1%

Crossref

Mehar Sahu, Pravir Kumar. "E3 ligase activity of RNF168 at stake on ring dom... <1%

Crossref







Simulation and Computational Study of RING Domain Mutants of BRCA1 and Ube2k in AD/PD Pathophysiology

Mehar Sahu¹ · Neetu Rani¹ · Pravir Kumar¹

Received: 9 June 2023 / Accepted: 27 November 2023

© The Author(s), under exclusive licence to Springer Science+Business Media, LLC, part of Springer Nature 2024

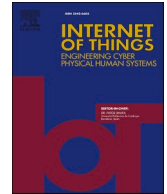
Abstract

Lysine-based post-translational modification (PTM) such as acylation, acetylation, deamination, methylation, SUMOylation, and ubiquitination has proven to be a major regulator of gene expression, chromatin structure, protein stability, protein–protein interaction, protein degradation, and cellular localization. However, besides all the PTMs, ubiquitination stands as the second most common PTM after phosphorylation that is involved in the etiology of neurodegenerative diseases (NDDs) namely, Alzheimer’s disease (AD) and Parkinson’s disease (PD). NDDs are characterized by the accumulation of misfolded protein aggregates in the brain that lead to disease-related gene mutation and irregular protein homeostasis. The ubiquitin–proteasome system (UPS) is in charge of degrading these misfolded proteins, which involve an interplay of E1, E2, E3, and deubiquitinase enzymes. Impaired UPS has been commonly observed in NDDs and E3 ligases are the key members of the UPS, thus, dysfunction of the same can accelerate the neurodegeneration process. Therefore, the aim of this study is firstly, to find E3 ligases that are common in both AD and PD through data mining. Secondly, to study the impact of mutation on its structure and function. The study deciphered 74 E3 ligases that were common in both AD and PD. Later, 10 hub genes were calculated of which protein–protein interaction, pathway enrichment, lysine site prediction, domain, and motif analysis were performed. The results predicted BRCA1, PML, and TRIM33 as the top three putative lysine-modified E3 ligases involved in AD and PD pathogenesis. However, based on structural characterization, BRCA1 was taken further to study RING domain mutation that inferred K32Y, K32L, K32C, K45V, K45Y, and K45G as potential mutants that alter the structural and functional ability of BRCA1 to interact with Ube2k, E2-conjugating enzyme. The most probable mutant observed after molecular dynamics simulation of 50 ns is K32L. Therefore, our study concludes BRCA1, a potential E3 ligase common in AD and PD, and RING domain mutation at sites K32 and K45 possibly disturbs its interaction with its E2, Ube2k.

Mehar Sahu and Neetu Rani have contributed equally to this work and also considered joint first author.

✉ Pravir Kumar
pravirkumar@dtu.ac.in; kpravir@gmail.com

¹ Molecular Neuroscience and Functional Genomics Laboratory, Department of Biotechnology, Delhi Technological University (Formerly Delhi College of Engineering), Shahbad Daultapur, Bawana Road, Delhi 110042, India



Review article

IoT-driven augmented reality and virtual reality systems in neurological sciences

Mehar Sahu^a, Rohan Gupta^{a,b}, Rashmi K. Ambasta^{a,c}, Pravir Kumar^{a,*},¹^a Molecular Neuroscience and Functional Genomic Laboratory, Department of Biotechnology, Delhi Technological University, Delhi, India^b School of Medicine, University of South Carolina, Columbia, SC, United States of America^c Department of Biotechnology and Microbiology, SRM University, Sonapat, Haryana, India

ARTICLE INFO

Keywords:

Augmented reality
Brain-computer interface
Neuromodulation
Neuroprosthetic
Neurosurgery
Virtual reality

ABSTRACT

Research in augmented and virtual reality in congregation with the Internet of Things has opened many avenues in diagnosing and treating neurological disorders. Augmented reality permits inserting virtual content in the real world, while virtual reality is a simulated experience that provides an artificial three-dimensional environment to the user. These are the game-changer technologies as they give a transformational change to existing technologies and methods. Augmented and virtual reality has come out as a significant technology in treating various mental disorders, thereby providing great applications in the field of neuroscience. In this review, we shed light on different components required for developing an augmented and virtual reality-

Abbreviations: AR, augmented reality; VR, virtual reality; HMD, head-mount display; CAVE, cave automatic virtual environment; 3D, three-dimensional; SNVs, single nucleotide variations; GWAS, genome-wide association studies; MDV, molecular dynamics visualization; HIVE, hub for immersive visualization and e-research; iMD-VR, interactive molecular dynamics in virtual reality; ARM, augmented reality microscope; AI, artificial intelligence; GUI, graphical user interface; CT, computed tomography; MRI, magnetic resonance imaging; EEVIS, enhanced electrophysiology visualization and interaction system; MR, mixed reality; GAINS, goggle augmented imaging and navigation system; EEG, electroencephalography; SLAM, simultaneous localization and mapping; GNSS, global navigation satellite system; LiDAR, light detection and ranging; RGB, red, green, blue; EKF, extended Kalman features; BCI, brain computer interface; ECoG, electrocorticogram; fMRI, functional magnetic resonance imaging; fNIRS, functional infrared spectroscopy; MEG, magnetoencephalography; PET, positron emission tomography; SMAII, spinal muscular atrophy type II; SSVEP, steady-state visual evoked potentials; ERD/ERS, (de)synchronization; ALS, amyotrophic lateral sclerosis; LED, light-emitting diode; RGS, rehabilitation gaming system; LCD, liquid-crystal display; HSV, hue, saturation, and value; TBI, traumatic brain injury; PASAT, paced auditory serial addition test; EMG, electromyography; MUPs, motor unit potential; CNN, convolutional neural network; EMG-BF, EMG biofeedback; NDDs, neurodegenerative diseases; REM, rapid eye movement; PD, Parkinson's disease; MEP, motor-evoked potential; TMS, transcranial magnetic stimulation; CST, corticospinal tract; ML, machine learning; DL, deep learning; AD, Alzheimer's disease; BEAPP, batch EEG automated processing platform; BIDS, brain imaging data structure; HAPPE, Harvard automated processing pipeline for EEG; WSBDS, wire-embedded silicon-based dry-contact sensor; WSN, wireless sensing network; IoT, Internet of Things; BS, base station; MCPS, medical cyber-physical systems; MS, multiple sclerosis; MCI, mild cognitive impairment; VMET, VR version of multiple errand test; VEPP, visual evoked potentials and fields; RNN, recurrent neural network; NLP, natural language processing; QR, quick response; RFID, radio-frequency identification; SAD, social anxiety disorders; ARET, AR exposure therapy; VRET, VR exposure therapy; LMICs, low- and middle-income countries; IGNS, image-guided neurosurgery; MR, magnetic resonance; IBIS, intraoperative brain imaging system; CTA, CT angiography; MRA, magnetic resonance angiography; DSA, digital subtraction angiography; AVM, arteriovenous malformation; VIPAR, virtual interactive presence and AR; OST-HMD, optical see-through head-mounted display; RGB-D, RGB-depth; VEGS, virtual environment grocery store; FOV, field of view; OST, optical see-through; VST, virtual studio technology.

* Corresponding author at: Professor of Biotechnology and Dean International Affairs, Delhi Technological University (Formerly Delhi College of Engineering), Molecular Neuroscience and Functional Genomics Laboratory, Shahbad Daulatpur, Bawana Road, Delhi 110042, India.

E-mail address: pravirkumar@dtu.ac.in (P. Kumar).

¹ Scopus ID: 14831447800; ISI Research ID: B-2164-2015.

<https://doi.org/10.1016/j.iot.2024.101098>

Available online 2 February 2024

2542-6605/© 2024 Elsevier B.V. All rights reserved.



Cross talk mechanism of disturbed sleep patterns in neurological and psychological disorders

Mehar Sahu^a, Rahul Tripathi^a, Niraj Kumar Jha^b, Saurabh Kumar Jha^{b,*},
Rashmi K. Ambasta^a, Pravir Kumar^{a,**}

^a Molecular Neuroscience and Functional Genomics Laboratory, Delhi Technological University (Formerly Delhi College of Engineering), Delhi, India

^b Department of Biotechnology, School of Engineering & Technology (SET) Sharda University, UP, India

ARTICLE INFO

Keywords

Sleep disorders
Neurodegenerative disorders
Neuropsychiatric disorders
Circadian rhythm
Signaling
Therapeutics
Antidepressant drugs

ABSTRACT

The incidence and prevalence of sleep disorders continue to increase in the elderly populace, particularly those suffering from neurodegenerative and neuropsychiatric disorders. This not only affects the quality of life but also accelerates the progression of the disease. There are many reasons behind sleep disturbances in such patients, for instance, medication use, nocturia, obesity, environmental factors, nocturnal motor disturbances and depressive symptoms. This review focuses on the mechanism and effects of sleep dysfunction in neurodegenerative and neuropsychiatric disorders. Wherein we discuss disturbed circadian rhythm, signaling cascade and regulation of genes during sleep deprivation. Moreover, we explain the perturbation in brainwaves during disturbed sleep and the ocular perspective of neurodegenerative and neuropsychiatric manifestations in sleep disorders. Further, as the pharmacological approach is often futile and carries side effects, therefore, the non-pharmacological

Abbreviations: AD, Alzheimer's disease; PD, Parkinson's disease; HD, Huntington's disease; OSA, Obstructive sleep apnea; SD, Sleep disorders; NDDs, Neurodegenerative disorders; NPDs, Neuropsychiatric disorders; CNS, Central Nervous System; SEM, Slow Eye Movement; REM, Rapid Eye Movement; NREM, Non-Rapid Eye Movement; SCN, Suprachiasmatic nucleus; LH, Lateral Hypothalamus; VLPO, Ventrolateral pre-optic; GABA, γ -Aminobutyric acid; SWS, Slow-Wave Sleep; EEG, Electroencephalography; SASP, Senescence-associated secretory phenotype; DDR, DNA Damage response; mGluR5, Glutamate receptors of subtype 5; BDNF, Brain-derived neurotrophic factor; APOE, Apolipoprotein E; NFTs, Neurofibrillary tangles; ICP, Intracranial pressure; IOP, Intraocular pressure; LC, Lamina cribrosa; LFPs, Local field potentials; MSA, Multiple system Atrophy; NAION, Non-arteritic anterior ischemic optic neuropathy; TED, Thyroid eye disease; FES, Floppy eyelid syndrome; DES, Dry eye syndrome; RVO, Retinal vein occlusion; CSC, central serous chorioretinopathy; DR, Diabetic Retinopathy; DME, Diabetic macular edema; VEGF, Vascular endothelial growth factor; KC, Keratoconus; OFC, Orbitofrontal Cortex; EC, Entorhinal Cortex; IP, Inferior Parietal; IT, Inferior Temporal; MTL, Medial temporal lobe; PFC, Prefrontal Cortex; PCC, Posterior cingulate cortex; CSF, Cerebrospinal fluid; MS, Multiple Sclerosis; ASD, Autism Spectrum disorder; BPSD, Behavioral and psychological symptom; MDD, Major depressive disorder; CBT-I, Cognitive behavioral therapy for insomnia; BiPAP, Bilevel positive airway pressure; TDCS, Transcranial direct current stimulation; SO, Slow oscillation; TMS, Transcranial magnetic stimulation; TCS, Transcranial current stimulation; SDB, Sleep-disordered breathing; PSG, Polysomnography; AHI, Apnea-hypopnea index; SD, Sleep deprivation; SR, Sleep restriction; RBD, REM sleep behavior disorder; TM, tuberomammillary; LDT, laterodorsal tegmental nucleus; Ach, Acetylcholine; ERK, Extracellular Signal-Regulated Kinase; MMP, matrix metalloproteinase; PGC1 α , Peroxisome proliferator-activated receptor gamma coactivator 1-alpha; PARP1, Poly [ADP-ribose] polymerase 1; SIRT1, sirtuin; GH, growth hormones; IGF-1, Insulin-like growth factor 1; mTOR, mammalian target of rapamycin; 4EBP2, 4E-binding protein 2; 4EBP2-eIF4E, Eukaryotic translation initiation factor 4E-binding protein 2; NMDA, N-methyl-D-aspartate; PRKG1, cGMP-dependent protein kinase 1; TRP, transient receptor potential; WASO, wake time after sleep onset; ISF, interstitial fluid; PET, positron emission tomography; D2, dopamine receptor 2; HTT, Huntingtin; MSN, medium spiny neurons; OPCs, oligodendrocyte precursor cells; LTP, Long-term potentiation; ADHD, Attention-Deficit/Hyperactivity Disorder; CPAP, Continuous positive airway pressure; BiPAP, bilevel positive airway pressure; SO, slow oscillations; UDP-glucose, uridine diphosphate glucose; c-Fos, proto-oncogene; NGFI-A, nerve growth factor inducible A; Stat3, signal transducer and activator of transcription 3; VGF, nerve growth factor inducible; ERP72, endoplasmic reticulum resident protein 72; HSP, Heat shock protein; GLUR2, Glutamate ionotropic receptor AMPA type subunit 2.

* Correspondence to: Department of Biotechnology, School of Engineering & Technology (SET) Sharda University, Knowledge Park III, Greater Noida, Uttar Pradesh 201310, India.

** Correspondence to: Molecular Neuroscience and Functional Genomics Laboratory, Former Dean, Delhi Technological University (Formerly Delhi College of Engineering), Room# FW4TF3, Mechanical Engineering Building, Shahbad Daultapur, Bawana Road, Delhi 110042, India.

E-mail addresses: saurabh.jha@sharda.ac.in (S.K. Jha), pravirkumar@dtu.ac.in, kpravir@gmail.com (P. Kumar).

¹ <https://orcid.org/0000-0002-7437-0755>

² ORCID: 0000-0001-7444-2344

<https://doi.org/10.1016/j.neubiorev.2022.104767>



Received 29 April 2022; Received in revised form 20 June 2022; Accepted 1 July 2022

Available online 8 July 2022




0149-7634/© 2022 Published by Elsevier Ltd.


Review Article


Harnessing Brainwave Entrainment: A Non-Invasive Strategy to Alleviate Neurological Disorder Symptoms

Mehar Sahu ^a, Rashmi K Ambasta ^b, Suman R Das ^b, Manoj K Mishra ^c, Anil Shanker ^d,
Pravir Kumar ^{a 1 2 3}  

Show more 

 Add to Mendeley  Share  Cite

<https://doi.org/10.1016/j.arr.2024.102547> 

[Get rights and content](#) 

Highlights

- Entraining impaired oscillation improves symptoms and delays the progression of neurodegenerative and neuropsychiatric disorders.
- Non-invasive brainwave entrainment techniques are safe, portable, and cost-effective.
- Brainwaves can be entrained to match the desired pattern to provide a therapeutic benefit.
- Personalized protocol depending on disease severity is more effective.



Synergizing drug repurposing and target identification for neurodegenerative diseases

Mehar Sahu^a, Shrutikirti Vashishth^a, Neha Kukreti^a,
Ashima Gulia^a, Ashish Russell^a, Rashmi K. Ambasta^b,
Pravir Kumar^{a, 1, *}

^a Molecular Neuroscience and Functional Genomics Laboratory, Department of Biotechnology, Delhi Technological University, Delhi, India

^b Department of Biotechnology and Microbiology, SRM University, Sonapat, Haryana, India

*Corresponding author: e-mail address: pravirkumar@dtu.ac.in; kpravir@gmail.com

Abstract

Despite dedicated research efforts, the absence of disease-curing remedies for neurodegenerative diseases (NDDs) continues to jeopardize human society and stands as a challenge. Drug repurposing is an attempt to find new functionality of existing drugs and take it as an opportunity to discourse the clinically unmet need to treat neurodegeneration. However, despite applying this approach to rediscover a drug, it can also be used to identify the target on which a drug could work. The primary objective of target identification is to unravel all the possibilities of detecting a new drug or repurposing an existing drug. Lately, scientists and researchers have been focusing on specific genes, a particular site in DNA, a protein, or a molecule that might be involved in the pathogenesis of the disease. However, the new era discusses directing the signaling mechanism involved in the disease progression, where receptors, ion channels, enzymes, and other carrier molecules play a huge role. This review aims to highlight how target identification can expedite the whole process of drug repurposing. Here, we first spot various target-identification methods and drug-repositioning studies, including drug-target and structure-based identification studies. Moreover, we emphasize various drug repurposing approaches in NDDs, namely, experimental-based, mechanism-based, and *in silico* approaches. Later, we draw attention to validation techniques and stress on drugs that are currently undergoing clinical trials in NDDs. Lastly, we underscore the future perspective of synergizing drug repurposing and target identification in NDDs and present an unresolved question to address the issue.

¹ ORCID ID: 0000-0001-7444-2344

Artificial intelligence and machine learning in precision medicine: A paradigm shift in big data analysis

Mehar Sahu[†], Rohan Gupta[†], Rashmi K. Ambasta,
and Pravir Kumar* 

Molecular Neuroscience and Functional Genomics Laboratory, Delhi Technological University
(Formerly Delhi College of Engineering), Shahbad Daultapur, Delhi, India

*Corresponding author: e-mail addresses: pravirkumar@dtu.ac.in; kpravir@gmail.com

Contents

1. Introduction	2
2. Artificial intelligence and big data: Changes in the landscape of precision healthcare and medicine	5
3. The emergence of AI in precision medicine	7
4. Synergies between artificial intelligence and precision medicine	8
4.1 Therapy planning	8
4.2 Risk prediction and diagnosis	11
5. Promises of implementing AI/ML in healthcare	13
5.1 Solving the human resource crisis in healthcare	13
5.2 Improving workflow and reducing medical errors	14
5.3 Enhancing healthcare delivery	15
6. The integration of nanomaterials in AI-based precision medicine	17
7. The perspective of big data analytics in precision medicine	19
8. AI and personalized medicine: A case of neurological disease	20
9. Obstacles in translating big data into healthcare	23
10. Opportunities for translating big data into healthcare	25
11. Artificial intelligence and machine learning in precision medicine: An industry perspective	26
11.1 Multi-omics profiling	26
11.2 Digital biomarkers and biomarker-based clinical trials	27
11.3 Precision dosing and safety measures	29
12. Future challenges and perspectives of artificial intelligence in precision medicine	31

[†] Equal contribution.

RING Domain Mutation Hinders the E3 Ligase Activity of RNF8 and Affects UBE2N Binding

1st Mehar Sahu

Department of Biotechnology,
Delhi Technological University,
Delhi-110042, India
meharsahu@gmail.com

2nd Pravir Kumar

Department of Biotechnology,
Delhi Technological University,
Delhi-110042, India
pravirkumar@dtu.ac.in

Abstract—A DNA damage response (DDR), particularly on double-stranded breaks (DSBs); RNF8 and RNF168 are crucial E3 ligases that are recruited first to the site of DNA damage. RNF8 initiates the conjugation of ubiquitin with H2A and H2AX, subsequently, RNF168 is employed to amplify the K-63-linked ubiquitin chain. These two E3 ligases are necessary for the downstream signaling where 53BP1 and BRCA1 are recruited. RNF168 directs 53BP1 involvement in non-homologous end joining (NHEJ) but is unable to save BRCA1 which is involved in homologous recombination (HR); therefore, it is RNF8 that plays a huge role in the recruitment of BRCA1. As recently BRCA1 has come up as a potential E3 ligase in Alzheimer's disease (AD) and damage to its heterodimeric partner BARD1 results in mislocalization of BRCA1 to cytosol that further joins tau lesion. Therefore, in this cumbersome signaling cascade, we took RNF8 to study. RNF8 and RNF168 plus UBE2N/UBC13 carry therapeutic importance, hence, this study tries to identify potential mutants that can affect the binding affinity of RNF8 with UBE2N, thereby, disturbing its E3 ligase activity.

Keywords—E3 ligase, RNF8, UBE2N, BRCA1, RNF168, Alzheimer's Disease, DNA damage response

I. INTRODUCTION

Eukaryotic cells have developed a very delicate mechanism to spot and repair different types of DNA damage, jointly known as DNA damage response (DDR). This in turn triggers cell cycle checkpoints to stop further development of cells and activate the DNA damage repair mechanism. Double-stranded breaks (DSBs) are one of the most lethal types of DNA damage. Where ATM initiates the response to DSBs which results in the phosphorylation of H2AX. Secondly, MDC1 directly interacts with γ -H2AX and amplifies the signal of DDR. Thereafter, RNF8 and RNF168 E3 ligases are recruited via MDC1. Chromatin bounded RNF8 attaches with E2 conjugating enzyme, UBE2N/UBC13 to ubiquitinate damaged chromatin. On the other hand, a ubiquitinated target X is identified by RNF168 that monoubiquitinates K13-15 on H2A [1]. Both the E3 ligases orchestrate to extend the ubiquitin chain on H2A and maintain genome integrity. However, the main purpose to target RNF8 is that it is the first E3 ligase that cooperates with UBE2N and is recruited to the site of DSB to start ubiquitination of H2AX, whereas, RNF168 recognizes the by-now ubiquitinated H2AX by RNF8. Later, RAP80 binds with the elongated chain created by RNF8 and RNF168 and forms a complex with BRCA1 (Fig. 1). Shreds of evidence suggest that BARD1 helps BRCA1 to attach with nucleosomes, however, impairment in BARD1 releases BRCA1 from the nucleosome core protein and binds with tau lesion in the cytosol which is a hallmark feature in Alzheimer's disease (AD). In this sophisticated DNA repair mechanism, a small segment of RNF 8 has been

undertaken. Here, the study highlights the impact of the point mutation on RNF8 and its binding affinity with UBE2N. Here, protein-protein interaction, network analysis, prediction of binding sites, evolutionary conservation of predicted sites, mutagenesis, and docking were performed for E3 ligase RNF8.

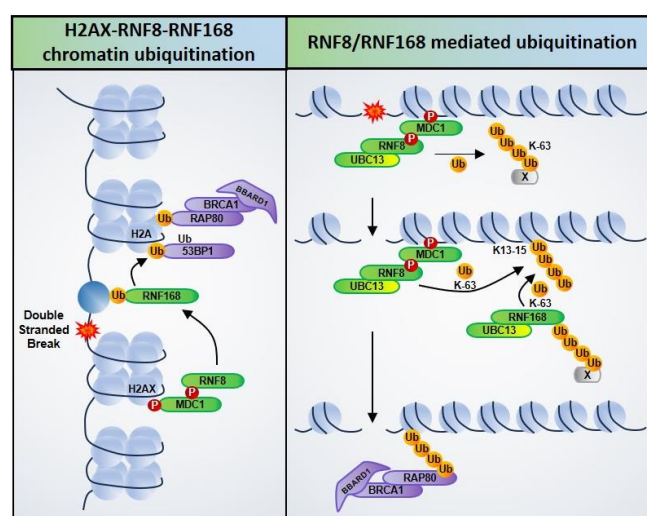


Fig. 1. RNF8 and RNF168 mediated ubiquitination at double-stranded breaks.

II. LITERATURE SURVEY

Many studies done in the past suggest that there is a strong inverse association between cancer and AD that has resulted in increased morbidity and mortality rates. Interestingly, such studies point to one common fact there is a potential link between molecular mechanisms involved in both such that in today's scenario, many anti-cancer treatments are being used against AD [2].

Breast cancer susceptibility gene 1 (BRCA1), is a tumor suppressor gene that plays a significant role in DNA damage response and many other physiological processes. However, the mutations in BRCA1 mark 80% of Breast cancer (BC) and ovarian cancer (OC) cases in females [3]. Additionally, a study also highlights increased cases of BC-AD with age in BC patients [4].

This study highlights the role of BRCA1 in regard to AD, where it has been found that BRCA1 is depleted when neuronal cultures are exposed to amyloid β (A β) and when human and transgenic mice are exposed to amyloid precursor protein (APP). The integral role of BRCA1 as E3 ligase involves the repair of DSBs and it is evident from past research that BRCA1 carries out ubiquitination of H2A and H2A variants at K125/K127/K129 residues. Nonetheless, the ubiquitination of H2A is governed by three major E3 ligases

Results

Patient 1 was a 58-year-old white woman who became unusually quiet with mild aphasia since previous year, and then developed intermittent confusion, which progressed rapidly within 2–3 months, followed by myoclonus, tremor, tactile hallucinations, and gait abnormality. Encephalography (EEG) showed diffuse slowing with occasional periodic organization and triphasic waves. Cerebral Spinal Fluid (CSF) studies were unremarkable. Patient 2 was a man who was 2 years older than patient 1. At age of 63, he developed forgetfulness and mild gait abnormality, followed by visual hallucinations and myoclonus with startle, which progressed to catastrophic cognitive decline. EEG was unremarkable. CSF showed normal 14–3-3 and cytology. Both patients' Magnet Resonance Imaging (MRI) demonstrated patterns highly suggestive of CJD. Patients died 6 and 4 months after their initial symptoms, respectively. Genetic study failed to find pathogenic mutations of the prion protein gene, and autopsy confirmed their diagnosis of sCJD MM1 and VV1–2, respectively. Both patients were born in Grand Rapids, Michigan. Patient 2 moved to Florida in teenage years, and only visited Michigan in summers. They never lived or traveled together, only met occasionally at family reunion.

Conclusions

This is the first time two biologically related individuals were diagnosed of sCJD, which warrants further investigation.

doi:10.1016/j.jns.2023.121446

121447

E3 ligase activity of RNF168 at stake on ring domain mutation

Mehar Sahu, Pravir Kumar, *Delhi Technological University, Department of Biotechnology, Delhi, India*

Background and aims

RNF8 and RNF168 are two crucial E3 ligases in DNA damage response. RNF8 tags H2A and H2AX with ubiquitin which directs RNF168 to amplify the K63-linked ubiquitin chain. Both E3 ligases are important for the recruitment of the BRCA1-A complex (BRCA1-ABRAXAS-RAP80) and BRCA1-P complex (BRCA1-PALB2-BRCA2-RAD51) for DNA repair mechanism. In Alzheimer's disease (AD), the BRCA1 level elevates upon A β burden and is aligned with tau lesions in the cytoplasm. Here, we aim to investigate the relevance of mutations in RNF168.

Methods

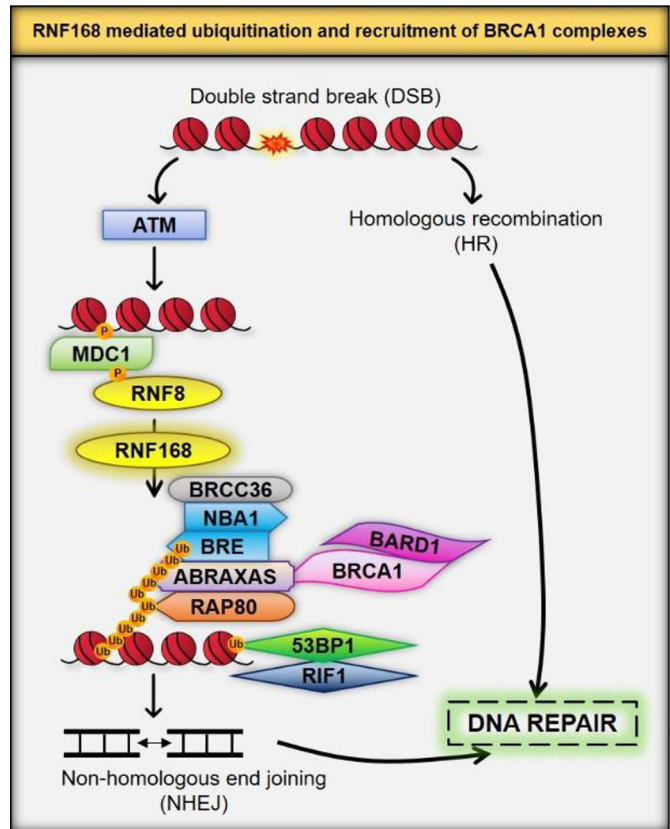
We analysed the highly conserved cysteine and histidine residues in the RING domain of RNF168 that affect E3-E2 interaction. RNF168 structure was prepared by AlphaFold, refined by Galaxy Refine, and confirmed through the Ramachandran plot. E2 enzyme, UBE2N structure was retrieved from PDB:4ONL. Protein-protein interaction, domain analysis, evolutionary conservation, mutagenesis, disease-related mutation predictions, and protein-peptide docking was performed for all putative sites.

Results

The domain structure of RNF168 (16–55 aa) carries 9 cysteine and histidine sites which are highly conserved. C16, C36, C39, C51 and C19, C31, H33, C50, C54 are buried-structural and exposed-functional respectively. Mutational studies and docking analysis suggest C19G, C19T, C31H, C36D, C36T, C51G, C51K, C51N, C54G, and C54K could be potential mutants assessed as per RMSD value.

Conclusions

We found that C36, C51, and C54 are potential active cysteine-centric sites. The top mutants C51K, C36T, and C54K disturb the binding affinity of RNF168 with UBE2N, thereby hampering its E3 ligase activity.



doi:10.1016/j.jns.2023.121447

121448

Automated AI-based volume measurement of the medial temporal lobe in early diagnosis of Alzheimer's disease

Marufjon Salokhiddinov^a, Maruf Pirnazarov^b, ^aRepublic Zangiota-2 Clinical Hospital, Tashkent Medical Academy, Neuroradiology, Tashkent, Uzbekistan, ^bNational Olympic Committee of Uzbekistan, Neuroradiology, Tashkent, Uzbekistan

Background and aims

The medial temporal lobe (MTL) is one of the first brain regions to experience neurodegeneration linked to Alzheimer's disease (AD). The need for a diagnostic tool that can accurately diagnose AD is driven by the limits of the available diagnostic biomarkers. We aim to assess a sensitivity and specificity of a recently updated convolutional neuronal network (CNN) by comparing regional volume changes in mild AD patients with matched control subjects.

Methods

Baseline 3 T MRI scans of individuals in ADNI – 3 at baseline were downloaded from ADNI database. The original scans from 37 HC (health control) and 39 mild AD patients were acquired. Total of six subregions in medial temporal lobe was taken as regions of interest. These are hippocampus (HP), parahippocampal gyrus (pH), amygdala